The Dissertation Committee for Olja Simoska Certifies that this is the approved version of the following Dissertation:

Real-time Monitoring of the Dynamic Metabolism and Responses of Pathogenic Bacteria using Electroanalytical Methods

Committee:

Jason B. Shear, Supervisor

Keith J. Stevenson, Co-Supervisor

Jennifer S. Brodbelt

Eric V. Anslyn

Adela Ben-Yakar

Richard M. Crooks

Real-time Monitoring of the Dynamic Metabolism and Responses of Pathogenic Bacteria using Electroanalytical Methods

by

Olja Simoska

Dissertation

Presented to the Faculty of the Graduate School of

The University of Texas at Austin

in Partial Fulfillment

of the Requirements

for the Degree of

Doctor of Philosophy

The University of Texas at Austin

December 2019

Dedication

This work is dedicated in loving memory of my caring grandmothers, Božana Stefanovska and Olga Simoska. Their unconditional love for me knew no bounds. My maternal grandmother, Božana, taught me valuable life lessons, passed on her enthusiasm for chemistry and encouraged me to always work hard for the things I aspire to achieve. My paternal grandmother, Olga, taught me to be a very strong woman and to focus on the positive and joyous life experiences. To my parents and brother for being my biggest sources of strength and inspiration. I love you all dearly!

Acknowledgements

Undertaking this PhD journey has been a truly life-changing experience for me. I have taken advantage of unique opportunities to become extremely independent. I have learned that scientific research is not always easy, but with hard work and perseverance, the rewards will ultimately follow. As an individual with ambitious goals, I have learned that there will be people who doubt whether I have what it takes to be successful. Yet I have been able to create new knowledge with my research. And the brightest part – the life-long professional and personal friendships I have created, which are priceless and a source to draw upon, allowing me to complete this doctoral dissertation.

First and foremost, I would like to express my deepest gratitude to my graduate advisor Prof. Keith J. Stevenson for his tremendous positive impact on my development as a scientist. Without his unwavering support, I would not be here today; I could not have asked for a better mentor. I thank him for taking a chance on me (after leaving UT) and for giving me much-needed guidance, resources, and freedom to pursue projects that greatly interest me. Committing to work with Keith has been the best decision I have made in graduate school. Keith has seen more talent within me than anyone else (myself included) and has helped bring it out of me. He is an electrochemistry mastermind as his innovate mind works in many distinct areas – this has been extremely inspiring for me. Keith has shown me that great mentoring is about mutual respect and that the opportunities are endless for a person who is driven, passionate, and good at what they do ("Procrastinate... later!"). Keith has motivated me to hold myself accountable ("your word is everything") and to be fearless in my endeavors ("take risks"). He has had ultimate confidence in me and never doubted what I am capable of accomplishing ("get 'er done"); he has lifted my spirits when I needed it the most by reminding me to accelerate my potential. Keith has taught me to take the higher road and lead by setting

an example. Perhaps the best example Keith and I have set together is to demonstrate that long-distance mentoring can be successful. For almost my entire PhD, Keith has mentored me from miles away and has been with me on this journey with every step – unprecedented and he has done a stellar job. Regardless of his physical location, Keith has always made himself available to speak with me – we have used the time zone differences to our advantage to efficiently get things done – but we are also a great team! Keith has also made personal investments in me based on his amazing intuition thereby I stick with him! While listed second as a co-advisor in this dissertation due to university formatting rules, Keith has been my main advisor and this long-winded acknowledgment is proof of it. I can hear you telling me to stop thanking you, but I promise to pay it forward, Keith! I am most lucky to know you and proud to have been your mentee! Don't forget the lyrics to our bacto song – *E. coli*, next!

I would like to thank my co-advisor Prof. Jason Shear for teaching me how to look at my data with a critical eye and for giving me a great deal of scientific freedom and space to work on projects that I am passionate about. In addition, I wish to thank Prof. Jennifer Brodbelt for recognizing my capabilities, providing valuable advice during difficult situations, and encouraging me to apply for fellowship awards when I felt very discouraged by others in the department. I also would like to thank the rest of my committee members Prof. Eric Anslyn, Prof. Adela Ben-Yakar, and Prof. Richard Crooks for their time and efforts in evaluating my dissertation.

I would like to offer my gratitude to my mass spectrometry collaborators Prof. Livia Eberlin, Marta Sans and Dr. Chris Crittenden for their engaging dialogue and active participation. I also thank my microbiology collaborators, Dr. Sophie Darch and Prof. Marvin Whiteley, for providing certain bacterial strains used in this dissertation. I would like to thank the former graduate students of the Stevenson group: Dr. Jonathon Duay, Dr. Daniel Redman, Dr. Caleb Alexander, and Dr. Robin Forslund for their

companionship, constructive criticism and feedback on my research. Jonathon Duay has done critical work in the development of the electrochemical platform that has been the basis for my PhD. I thank Caleb for his friendship and great memories from our trip to Russia – I am glad I was able to locate you at the giant airport in Moscow and safely return you back to the Texas motherland, dude (except you did manage to forget your stinky shoes at Keith's sun-palace even after consuming two bags of Russian cereal!)

To my best friend and colleague Dr. Janine Elliott, I owe a great deal of respect and gratitude to you for first introducing me to Stevenson's research and T-CUAs. Janine's mentorship and enthusiasm in electrochemistry, cell culture, and bioanalytical sensing technologies were instrumental to my progress as a scientist. She has provided support on a personal and professional level and has shown me how to survive this grad school ride. I remember our times in Keith's FNT lab space – long hours making electrodes, producing bubbly nitric oxide gas, Adventure Time-ing, bacon-ing pancakes, and consuming massive amounts of sour patch kids. Janine is a person I genuinely cannot imagine my life without – my best friend for life, always, forever. Am glad we have our very own –ioso language. I love yousiosos, my Janineioso, and you are always going to be Jake (the Dog) to my Finn (the Human)! Don't mess with us (or Texas)!

A good support system is important for surviving and staying sane in graduate school. I was lucky to be a part of a group that we like to call "Bunch of Nerds 2.0" consisting of Michelle Blemker, Joey Gurrentz, Emily Raulerson, Marta Sans Escofet, Jason Michael, Josh Pender, Dylan Boucher, Ryan Ciufo, Mason Valentine, Clara Feider, and myself. Thank you all for being wonderful and for providing the support and friendship I needed. I would like to thank Michelle Blemker for her companionship, her positive outlook and her ability to smile (or cry) despite the situation; I am so grateful we have each other and as your lovely grandfather said, our friendship is very special, indeed. Oh, and thank you, Michelle, for always correcting my pronunciation of so-

difficult-for-me th- sounds of the English language (“don't thread on me” in the “tree house”). I am thankful to my best friend Joey Gurrentz for great memories from grad school in trying to be classy, day-drinking manmosas on a Sunday, drinking Russian water on parking lots, hiking at Hamilton pool, looking for the sun, and just being so silly (“Hiiii, I am from Macedonia, hiii”). I am thankful for our high-quality conversations and am excited about our future adventures, Joey. I also wish to thank Emily Raulerson for understanding the frustrated version of myself (the one with fire flame eyes). In addition, I would like to thank my dearest roommate Marta Sans for her kindness, positive energy and for understanding the things I so desperately miss about our European/Mediterranean homelands. I thank Kanchan Aggarwal for being the sweetest, taking good care of me, and zumba-ing with me – glad to have you in my life. Am thankful for coffee breaks with Dr. Jialing Zhang who has provided great advice during challenging times.

Throughout grad school I participated in many other activities, with several people mentoring and helping me. My appreciation goes to the Council of Graduate Chemists (CGC) officers for doing respectable work and for allowing me to serve as their president. Bold Women in Chemistry (BWIC) and My Science My Life (MSML) have provided me with supportive and empowering communities for women in chemistry. I would like to thank my BWIC mentor Dr. Kate Biberdorf for her enthusiasm, passion, and sticking up for me. I am also very thankful for my MSML mentor, Dr. Jennifer Lyon Gardner, who has provided valuable advice about time management, people skills, and career options. In addition, I thank my undergraduate mentees, Jordan York and Mandy Banik, for allowing me to be their graduate student mentor. I also thank my outreach enthusiast friend Jacks Reyna for reminding me to continue inspiring others.

I would like to thank the chemistry graduate coordinator (our department mom), Betsy Hamblen for helping with everything paperwork-related, empowering me to make needed changes when I felt lost, allowing me to assist with recruitment activities, and

giving great hugs. Thanks to Danielle Nestler for her magical work in handling accounts. I thank Cory Koniezcny and Steve Moore who have greatly assisted me with moving our research labs between Welch, FNT, and NHB. Special thanks to Cory for providing the highly coveted lock and top-secret access to my very own electrochemistry room. I thank Tim Hooper for helping me fix many pieces of electronic equipment.

I consider myself fortunate to have entered graduate school with great support from my undergraduate mentors and Bard College Team Chem. I am thankful to my former college research advisor Prof. Christopher LaFratta who continues to advise me to strive for excellence, above and beyond the duties of a typical undergraduate advisor. I would also like to thank Prof. Emily McLaughlin, Prof. Craig Anderson, and Prof. Swapan Jain for their advice and following my PhD journey. In addition, I thank my closest college friends Seoyoung Kim, Dr. Leila Duman, Amanda Benowitz, Berk Atuk, Miles Lim, Anuska Shrestha and my forever-favorite seniors Dr. Madison Fletcher, Dr. Nicole Camasso, and Dr. Izzy Taylor. Mental toughness…

I greatly appreciate the funding I have received toward my PhD from Skolkovo Institute of Science and Technology, Welch Foundation, ACS Division of Analytical Chemistry Graduate Fellowship and Society of Analytical Chemists of Pittsburgh. I am extremely thankful for the KJS and SL lifetime achievement fund, as well – thanks to both Keith and Svetlana Stevenson, for their investments to support my work and me!

Of course, I would like to thank the wonderful dogs that have provided lots of support. Thanks to the most beloved mini dachshunds Hugo and Odette of my family – while miles and oceans away, your puppy eyes provided me with smiles (thanks to my mom for the dog photos). I thank my best friend's dog, Kovu, for spending hours in the Stevenson group office while Janine and I were working on experiments/papers. I also thank Stevenson's adorable Watts for being the best electrochemistry puppy and for carefully assisting Keith in editing my manuscripts.

My deep appreciation goes to my best friend back in Macedonia, Elena Kamcevska. She has been by my side since first grade and despite the over-the-Atlantic-pond distance for the past eight years, she remains one of my closest friends. Elena has provided me with valuable perspectives on the world outside of chemistry and research, and I'm thankful for that. I miss you and love you!

I finish with my beautiful country Macedonia, where the most basic source of my life energy resides: my amazing family. My family has been the community that has shaped my life's journey. I consider myself very fortunate to have been raised in a loving and nurturing home with giving parents, caring grandparents, and smiling sibling/cousins. Above all, I am sincerely grateful to my hard-working parents Maja and Svetislav, who always believed in me, inspired me to overcome my barriers, and provided me with opportunities. There are no adequate words to express how much I appreciate my parents for sacrificing their lives for my brother and myself to provide us with unconditional love, life-long support, solid advice, and endless care. I love you so very much, mom and dad. All that I am today comes back to you – thank you! My brother Simon has been one of my closest friends all my life and I love him so dearly. I thank him for being a ray of sunshine and for often reminding me to breathe/relax. I also thank my aunts, uncles, and cousins, for their love and support, especially my cousin Biljana for being like a sister to me and reminding me that we always have each other. Thanks to my beautiful nieces Katarina and Alexandra, for being most adorable. I know I always have my family to count on. This journey would have been impossible without their warm love, continued patience, and endless support. Благодарам и ве сакам најмногу!

Abstract

Real-time Monitoring of the Dynamic Metabolism and Responses of Pathogenic Bacteria using Electroanalytical Methods

Olja Simoska, Ph.D.

The University of Texas at Austin, 2019

Supervisor: Jason B. Shear

Co-Supervisor: Keith J. Stevenson

Microbial infections remain the leading cause of increased morbidity and mortality rates of patients suffering from infectious diseases. While thousands of pathogenic bacteria have been recognized, the majority of healthcare-associated infections are caused by only a few opportunistic pathogens (e.g., *Pseudomonas aeruginosa*, *Staphylococcus aureus*, *Escherichia coli*), which are associated with increased antibiotic resistance. The rapid detection, reliable identification and real-time monitoring of these pathogens remain not only a scientific problem but also a practical challenge of vast importance, especially in tailoring effective treatment strategies. Various approaches, such as conventional culturing, molecular methods and mass spectrometry techniques, have been employed to identify and quantify pathogenic agents. Yet, these procedures are costly, time-consuming, mostly qualitative, and are indirect detection methods. A great challenge is therefore to develop rapid and quantitative methods for the detection of microbes. As an alternative, electrochemical techniques have been explored as a means for the detection of infection-related biomarkers. This thesis

presents the development and application of a robust electrochemical platform using transparent carbon ultramicroelectrode arrays (T-CUAs) for the *in vitro* detection of bacterial warfare toxin, pyocyanin, and other phenazine metabolites produced by *P. aeruginosa*. This antibiotic-resistant pathogen is commonly found in chronic wounds and the lungs of cystic fibrosis patients. During early infection stages, *P. aeruginosa* produces various phenazines as virulence factors, which are highly diffusible signals that are toxic to surrounding host cells and other competing microorganisms. Although phenazines play important roles in cellular functions, very little is known about how their concentrations fluctuate and influence cellular behaviors and population-dependent responses (quorum sensing) during infection and growth. Therefore, quantitative, real-time electrochemical monitoring of distinct redox-active phenazine metabolites from *P. aeruginosa* in simulated growth media is demonstrated using T-CUAs. Moreover, electrochemical monitoring of the influence of polymicrobial infections on *P. aeruginosa* phenazine production is presented. In addition to quantifying phenazine concentrations in complex environments, changes in phenazine dynamics are observed in the biosynthetic route for pyocyanin production. Finally, desorption electrospray ionization and nanoelectrospray ionization mass spectrometry are used to identify phenazines observed with our electrochemical devices.

.

Table of Contents

List of Tables

List of Figures

Chapter 1: Introduction[1]

The development and spread of pathogenic infections remain the leading causes for increased morbidity and mortality rates affecting over 250 million people worldwide.[1-5] These infections commonly occur through water and food contaminations and/or various bodily fluids. Additionally, severe diseases spread in clinical facilities where immune-compromised host patients come in contact with pathogenic bacteria heavily populating hospital surfaces. These infections are typically initiated by only a few clinically relevant microbial species, including *Pseudomonas aeruginosa*, *Staphylococcus aureus*, *Escherichia coli*, *Enterococcus faecium*, *Klebsiella pneumoniae*, and *Acinetobacter baumannii*, which lead to deleterious consequences as they are majorly responsible for disease progress by rapidly developing antimicrobial resistance mechanisms.[6] Therefore, the advancement of methodologies for detection, identification, and monitoring of pathogens is necessary for selecting the most effective treatment and intervention strategies.[7]

The design and development of rapid, reliable, cost-efficient, specific and sensitive methods remain challenging, however, as pathogen detection still heavily relies on the standard microbiology tests and diagnostic schemes.[8] Specifically, the major conventional methods used to identify pathogenic species and determine resistance are: (1) selective cell culturing, (2) molecular methods and (3) mass spectrometry, some of which can be relatively time-consuming and/or can require technically trained personnel and regular maintenance.[9,10]

---

[1]Portions of this chapter were published in a review article by Simoska, O. and Stevenson, K. J. titled "Electrochemical Sensors for Rapid Diagnosis of Pathogens in Real Time" *Analyst*, **2019**, *144*, 6461–6478. This review article was an invited contribution for the themed collection "Versatile Electrochemical Approaches" in the *Analyst*. Copyright © 2019 The Royal Society of Chemistry. Simoska, O. wrote the review article. All authors contributed in editing the manuscript.

Health-care facilities typically use cell culture platforms, which involve incubation of specimens in an array of distinct growth media with varying nutrients and antibiotics. Thus, pathogen identification is determined visually based on the distinct growth patterns observed. Since they include numerous steps (e.g., selective enrichment, biochemical screening, bodily fluid confirmation), cell culturing approaches are laborious and time-costly, requiring 24–72 hours for initial results in pathogen identification.[7,11,12] Moreover, cell cultures are associated with low sensitivity and selectivity, as well as the risk of microbial contamination that could inhibit bacterial growth rates.[11]

As a result, molecular-based techniques, including polymerase chain reaction (PCR) and nucleic acid sequencing, have taken a prominent role as diagnostic methods in replacing cell culture-based techniques.[10,13,14] While they provide more sensitive, highly specific, and accurate identification of microorganisms and significantly reduce diagnosis time (1–4 h) molecular approaches have certain limitations compared to cell culture.[10] In particular, they require the most sample preparation and manipulation, in addition to expensive imaging equipment.[13] Additionally, false negatives could result due to sample cross-contamination, inhibition of amplification reaction by matrix sample compounds and/or challenges in differentiating viable from non-viable cells as nucleic acid is present in both.[10,11]

Another alternative to cell culturing approaches are mass spectrometry (MS) methods,[15-17] which provide qualitative results within minutes through the detection of a broad range of unique molecules produced by bacteria at different concentrations.[10,18-23] Various MS procedures,[16] specifically matrix-assisted laser desorption time-of-flight (MALDI-TOF), electrospray ionization (ESI), and desorption electrospray ionization (DESI), have been employed in various clinical and microbiology studies for the identification of several pathogens, including *E. coli*, *P. aeruginosa, S. aureus*, and *S.*

agalacriae.[15,19,21,22] However, in addition to requiring the use of expensive equipment, MS methods are associated with biases in sample preparation. Particularly pathogens are isolated from their natural growth environments prior to MS analysis. While being sensitive and rapid, MS-based pathogen identification requires the use of reference database libraries,[23] making the detection of potential candidate biomarkers from complex biological samples challenging.[15]

Recent research has focused on the design and development of electrochemical sensing platforms (Figure 1.1). Electrochemical sensors have emerged as a promising alternative to the traditional approaches for pathogen detection,[2,3,12] due to their ability to provide increased sensitivity, fast response times, simplicity of operation, and lower cost. Since most electrochemical-based sensors are label-free devices, their potential for direct detection of bacterial pathogens has been considered a powerful alternative to the benchmark methods. Moreover, electrochemical sensors are attractive due to the possibility of device miniaturization, combined with the ability to design and assemble low-cost, disposable, flexible, wearable and/or implantable electrochemical devices. Therefore, electrochemical strategies have been recognized as effective tools for the successful detection of whole bacteria, cellularly derived signaling molecules, bacterial metabolites and byproducts, and enzymes.[3,24-26]

The use of electrochemical sensing devices started with glucose oxidase-based biosensors, which are based on amperometric detection of glucose in the blood. In contrast to glucose biosensors, electrochemical sensors for pathogen detection have yet to enter the market as real-time monitoring devices. As a result, in the last decade, significant research has focused on improving the performance of bioelectroanalytical sensors, specifically with respect to limits of detection, sensitivity, linear dynamic ranges,

selectivity, specificity, rapid experimental analysis times (e.g., 5–7 min), and no pre-enrichment steps, which are all required for manufacturing clinical diagnosis devices.[24]

Various published literature reviews have provided an overview of fundamental sensing principals, case studies, and challenges in developing point-of-care sensors for monitoring in a clinical setting.[3,27,28] Particularly, an extensive summary of advantages and disadvantages of electrochemical sensing platforms was published by Monzó et al. in 2015.[3] Extensive emphases were given on the development of synthetic polymers and cost-efficient nanomaterials, along with the design of microarray and microfluidics devices. The authors concluded that limitations intrinsic to sample preparation steps, analysis times and sensor sensitivity are reasons for the slow-paced entrance of electrochemical sensors into the global market.[3] Additionally, Justino and co-workers in 2016 published a comprehensive review of clinical sensing platforms for detection of bacteria and physiologically relevant analytes.[28] A detailed comparison of analytical sensors performance was presented, highlighting the advantages of microfluidics and lab-on-a-chip platforms due to significant advances in reducing analysis times for pathogen detection and identification.[28] Moreover, two additional reviews have been published more recently in 2018 on electrochemical methodologies for identification of pathogenic microorganisms. Specifically, Amiri and co-workers published an overview of biosensors for the detection of pathogens associated mainly with water and food contaminations, providing a summary of surface modification strategies and types of electrochemical detection schemes used.[2] Additionally, another review was published by Kuss et al. in 2018,[29] providing an extensive summary of biosensors for bacteria detection developed since 2015. The review emphasized compelling advances towards the development of portable point-of-care sensors.[29] The authors discussed future challenges in designing portable electrochemical devices that are cost-efficient, sensitive and selective.

In this chapter, a brief summary is given of the latest advances in the design and development of electrochemical sensing strategies for detection of pathogenic bacteria, with a particular focus on a major clinically relevant species, *P. aeruginosa*. While it rarely establishes persistent antibiotic-resistant infections in otherwise healthy individuals, this opportunistic human pathogen can establish chronic infections in individuals with compromised immune systems, and those suffering from conditions, such as severe burns, chronic wounds and cystic fibrosis.[30-34] During initial infection stages, *P. aeruginosa* produces various redox-active metabolites, which can have toxic effects on surrounding host cells and/or other microbes. Therefore, electrochemical methods offer rapid, direct, and sensitive detection of these redox *P. aeruginosa* metabolites, thus providing important evidence about the onset of *P. aeruginosa* infections. To prevent disease progress and determine effective treatment strategies, prompt detection, pathogen identification and real-time monitoring of early infection stages, pathogenic responses and metabolism dynamics are necessary.[34,35] Yet the development of simple, cost-efficient sensors with the necessary figures of merit (e.g., detection limits and linear ranges, fast sensor responses and rapid analysis times) remains challenging. Herein, recent advances in electrochemical devices based on *P. aeruginosa* detection via electrochemically-active biological target metabolites and byproducts are discussed, highlighting the advantages of micro- and nano-electrode array platforms.

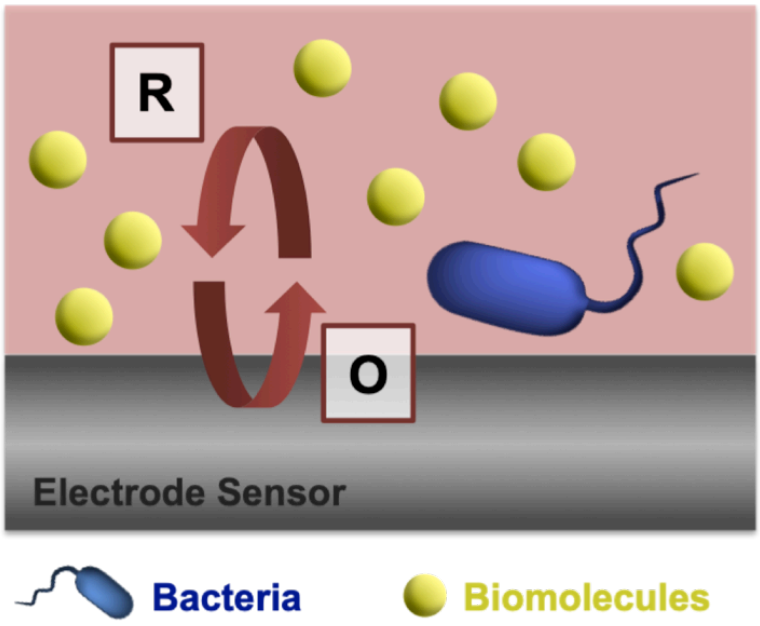

Figure 1.1: Electrochemical sensors for pathogen detection and quantification in biological, laboratory and/or clinical samples via detection of bacterial biomolecules.

1.1 Electrochemical Sensors Based On Pathogen Identification Via The Detection of Redox-active Cellular Metabolites

An extensive number of electrochemical-based devices for the detection of clinically relevant pathogens (in particular, *P. aeruginosa*) have been recently developed and reported in the literature. These sensing devices often include (1) complex electrode platforms, modified with specific nanomaterials, nanostructure, and antibodies, (2) combined multiplexed sensing systems (e.g., electrochemical lab-on-a-chip platforms), and (3) electroanalytical sensing methodologies based on the direct detection of unique cellular redox biogenic molecules at electrode surfaces. The principle of pathogen identification via direct detection of cellular biogenic metabolites on an electrode surface represents a desirable, straightforward electrochemical sensing approach, which does not require use of highly specialized materials and/or instruments. This method typically relies on the use of voltammetric methodologies to directly sense *P. aeruginosa* metabolites and byproducts. The electrochemical detection of bacterial toxins has recently received attention because of its applicability for biodiagnosis in healthcare settings. Various bacterial toxins and exotoxins secreted by *P. aeruginosa* have been recently detected via electrochemical methods,[25,37-41] thereby making these approaches applicable in wound diagnostics and biosensing technologies.[42] Additionally, electrochemical sensors for the detection of siderophores and virulence factors produced by *P. aeruginosa* strains have been recently described.[43,44] An overview of recent literature of these electrochemical sensors is provided, emphasizing the advantages of micro- and nano-electrode arrays, for the real-time, quantitative detection of *P. aeruginosa* target metabolites and intermediates. Table 1.1 provides a detailed summary of the literature on electrochemical sensors for the detection of cellular *P. aeruginosa* biogenic metabolites and intermediates.

Cernat et al. reported the design of a nanohybrid electrode platform based on graphene, polypyrrole and gold nanoparticles for the detection of biomarker, pyoverdine, secreted by *P. aeruginosa*.[43] The developed composite material demonstrated catalytic activity for electron transfer rate and enhanced surface area. Using differential pulse voltammetry (DPV), the authors examined the sensor's selectivity in the presence of common interferences found in biological samples and hospital settings and obtained excellent recovery rates. Finally, the sensor performance was successfully tested for detection of pyoverdine from real biological samples, including human serum and saliva, with a total analysis time of 165 s.[43] Similarly, in a more recent example, Gandouzi and co-workers developed an electrochemical sensor for sensitive and selective detection of pyoverdine.[44] This sensing platform used graphene/graphite-modified screen-printed electrodes, which were electrochemically reduced and decorated with gold nanoparticles. The limit of detection (LOD) and linear dynamic range (LDR) for pyoverdine detection achieved on these sensors were 66.9 nM and 1–100 μM, respectively. In optimizing sensor performance, the authors showed the detection of pyoverdine in serum, saliva, and tap water using DPV. Thus, these sensing platforms for pyoverdine detection show an effective principle for early diagnosis of *P. aeruginosa* species.

In addition to electrochemical sensors for the detection of pyoverdine, a significant amount of research has been devoted to the development of biodiagnostic devices based on the electrochemical conversion of pyocyanin (PYO). Redox-active PYO is exclusively secreted by *P. aeruginosa*, hence making it a unique diagnostic biomarker for detecting *P. aeruginosa* infections.[45] Consequently, several electroanalytical systems for the detection and quantification of PYO have been reported, using voltammetry,[38,46-49] amperometry,[37] and scanning electrochemical microscopy.[50,51] In recent studies, Alatraktchi et al. have demonstrated use of disposable, screen-printed gold electrodes,[37,46]

as well as carbon paper-based sensors,[46] for PYO detection, achieving LODs in the micromolar range and LDRs up to 100 μM. Additionally, carbon disk electrodes and carbon-based, disposable electrodes have been employed by Sismaet et al. and Santiveri et al., respectively,[48,49] for *P. aeruginosa* recognition via square-wave voltammetric detection of PYO. Most recently, Jarosŏva et al. demonstrated the use of inkjet-printed carbon nanotube electrodes as small, flexible and disposable sensors[52] for the electrochemical detection of both PYO and uric acid from *P. aeruginosa* in would-like fluid stimulated media.[40] Furthermore, Buzid et al. developed boron-doped diamond electrodes, which were optimized and successfully used for the simultaneous detection of three *P. aeruginosa* biomarkers, PYO, 2-heptyl-3-hydroxy-4-quinolone (PQS) and 2-heptyl-4-hydroxyquinoline (HHQ).[53,54] The authors utilized cationic surfactant hexadecyltrimethylammonium bromide to improve effectiveness of unmodified boron-doped diamond electrodes for direct detection of PYO, PQS, and HHQ from *P. aeruginosa* cell cultures and biological samples. Using DPV, Buzid and co-workers determined the LODs to fall in the nanomolar range for all three cellularly derived biomolecules.[54] While these boron-doped diamond electrodes allow for simultaneous detection of three biological metabolites, they are quite costly compared to other low-cost carbon electrodes for PYO detection.[55]

In addition to the aforementioned electrochemical methods based on voltammetric detection of *P. aeruginosa* pathogens via the redox conversion of PYO, Bellin et al. have shown miniaturization and arrangement of multiplex electrochemical devices into high-density arrays. The chip-based system allowed the authors to image colonies based on spatial, voltammetric, quantitative measurements of *P. aeruginosa* phenazine metabolites.[56,57] Phenazines are small, redox-active, nitrogen-containing heterocyclic compounds, which engage in redox processes in the presence of molecular oxygen.

Produced during early *P. aeruginosa* infection stages, phenazines play key roles in altering metabolism, modify immune responses and damage host tissue.[58-61] Using square wave voltammetry (SWV) measurements, phenazine concentrations as low as 2.6 μM were detected by Buzid and co-workers. In earlier work, the authors' designed system consisted of an array of 60 gold electrodes in 5 channels, containing integrated trans-impedance amplifiers organized in 12 working electrodes.[56] This integrated circuit device allowed spatially resolved electrochemical imaging of redox-active phenazine metabolites from wild-type and mutant *P. aeruginosa* colonies and biofilms. In more recent research, the authors improved the sensor design by dramatically increasing the working electrode array and the number of parallel output channels via a complementary metal-oxide semiconductor (CMOS) process.[57] This facilitated electrochemical imaging of whole-colony *P. aeruginosa* biofilms for the first time, however, the device may bias the time-dependent analysis of spatially resolved results. Although the authors demonstrated imaging of phenazine signals at various time points, this method takes up to 10 minutes to acquire information from all integrated electrodes in the array.[57] Additionally, in this electrochemical camera chip, bacterial colonies were grown on <15-μM thick agar-soaked membranes placed directly on top of the integrated chip. This sensor design raises a question about real-time measurements of *P. aeruginosa* phenazine production as transport parameters are neither quantified nor reported. While the device allows for simultaneous, spatially resolved detection of redox phenazine metabolites from *P. aeruginosa*, this approach could involve quite costly and highly specialized equipment and skills to perform a simple, rapid, quantitative analysis in a clinical facility.

Therefore, bacterial products and secreted metabolites are motivating targets for the direct detection of *P. aeruginosa* strains and their biomarkers. The electrochemical conversions of *P. aeruginosa*'s biogenic molecules allow for fairly simple

electrochemical sensor design. The electroanalytical sensors summarized in this section do not require sample pretreatments before quantitative analysis and pathogen detection, which is desirable in sensor design for detection of pathogens.

1.2 CARBON MICROELECTRODE ARRAYS

Research in the 1980s demonstrated that microelectrodes (electrodes with a diameter of 25 μm or less) have several advantages relative to typical macroelectrodes.[62-64] Generally, the diameter of microelectrodes is at least one dimension smaller than the thickness of the diffusion layer for an electrochemically active species.[62-64] The radial diffusion at microelectrodes permit for enhanced, fast steady state diffusional profiles.[65] As a result of their small sizes, microelectrodes have low non-faradaic background currents, small ohmic (resistive) drops, and reduced double layer capacitance.[62] Thereby, microelectrodes can detect low analyte concentrations with small capacitive currents and display large current densities; however, the absolute signal at the microelectrode is extremely low (picoamperes to nanoamperes range).[66,67] This drawback can be bypassed by using an array consisting of tens to hundreds to thousands of microelectrodes, where the current increases proportionally with the number of electrodes within the array;[65,68,69] making the resulting current outputs of microelectrode arrays are up to several orders of magnitude larger than those of a single microelectrode.[65,68,69]

For microelectrode arrays, the voltammetric responses are directly related to the geometric features of the arrays (e.g., average radius of microelectrode, average inter-electrode distance) and the scan rate.[65-69] Thereby, the diffusion profiles of individual microelectrodes within the array dependent on the size and distance between each microelectrode in the array. For equal scan rates, microelectrode arrays with smaller inter-electrode diameter result in voltammetric responses similar to those of

macroelectrodes, while microelectrodes with larger inter-electrode distances display true microelectrode behaviors.

While there are many options in terms of electrode materials, carbon-based substrates are primarily used due to their inertness, hardness, low cost, and high biocompatibility. As a result of their outstanding analytical qualities, carbon microelectrode arrays have received a significant amount of interest in various bioanalytical sensing applications.[38,66,67,69-79] In particular, they have been widely used to measure oxygen and nitric oxide levels from fibroblast cells,[80] nucleic acids,[81] and release of neurotransmitters.[82,83] Additionally, cellular functions, including release and/or consumption of chemicals (e.g., oxygen, glucose) and enzymatic activities, can be monitored using microelectrode arrays.[73,74]

1.3 TRANSPARENT CARBON ULTRAMICROELECTRODE ARRAYS

P. aeruginosa identification based on the detection of redox biogenic molecules secreted from cells can be also achieved with microelectrode array devices.[72-74] The Stevenson research group recently reported a low-cost, facile, and versatile fabrication of transparent carbon ultramicroelectrode arrays (T-CUAs) and their characterization.[38,70,71] Preparation of T-CUA electrodes used throughout studies in this dissertation follows a microsphere lithography process where micrometer-diameter (here, 1.54 μm) polystyrene spheres (PSS) are drop cast onto a conductive carbon pyrolized photoresist film electrode followed by atomic layer deposition of an insulating metal oxide layer (Al_2O_3), which enables the thickness to be controlled precisely (here, 10 nm). Upon removal of PSS, disk-shaped carbon areas remain where the PSS were in contact with carbon film, thus forming an array of microelectrodes. The steps of T-CUA electrode fabrication process are illustrated in Figure 1.2.[70]

The T-CUA platform offers various benefits relative to other electrochemical detection methods. Specifically, in addition to the aforementioned advantages of microelectrodes, T-CUAs provide an additional benefit of amplified currents resulting from individual microelectrodes in the array functioning in a parallel circuit.[70] Their nanometer-scale sizes permit analytical measurements on smaller samples in biological environments with fast response times.[70,84] Additionally, the small electroactive area allows for lower non-faradaic background currents, thereby resulting in improved signal-to-noise (*S/N*) ratios and enhanced limits of detection with large linear dynamic ranges. Moreover, the electroactive material of T-CUAs, pyrolized photoresist film, is similar to glassy carbon, thus it is chemically stable, extremely conductive, and highly biocompatible.

The complex environments in which cells interact can have diverse cellular populations and be susceptible to changes that influence cellular survival, division, differentiation, and virulence. Such dynamic responses are often mediated, at least in part, by changes in the concentrations of signaling biomolecules. Hence, the *in vitro* electrochemical detection of cellular biogenic species allows real-time monitoring of cellular communication in mono- and poly-microbial environments, thus providing information about chemically and environmentally dependent bacterial responses. In a previous study, members of the Stevenson research group characterized analytical responses of T-CUAs to hydrogen peroxide (H_2O_2),[38,70,71] a biogenic metabolite produced by various pathogenic bacteria, such as *Streptococcus gordonii*. Additionally, we have shown successful modification of T-CUAs for the detection of cellularly derived nitric oxide ($NO^{\bullet}$), a biogenic signaling molecule produced by immune host cells such as macrophages.[84]

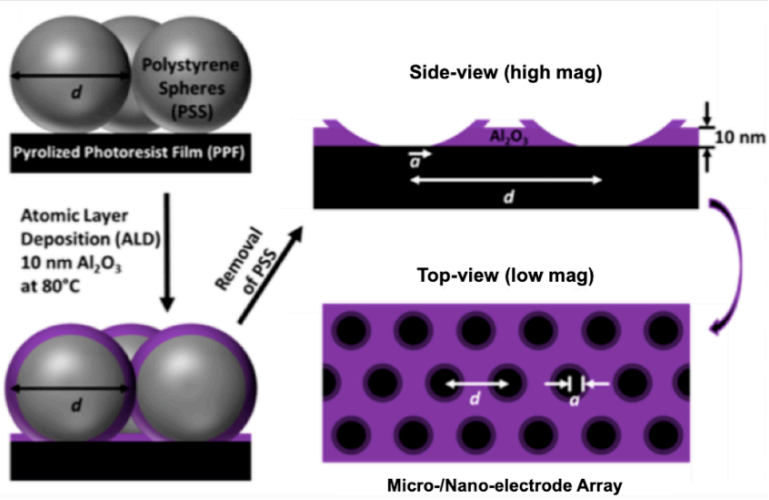

Figure 1.2: Schematic of fabrication steps of transparent carbon ultramicroelectrode arrays (T-CUAs).

Polystyrene spheres (PSS) are drop-cast on a pyrolized photoresist film, followed by atomic layer deposition of 10 nm Al_2O_3 layer, after which PSS are removed by sonication and chemical dissolution steps to give an array of ultramicroelectrodes (side and top-view illustrated). Figure courtesy of Dr. Jonathon Duay of the Stevenson research group. (Reprinted with permission from ref. 70. Copyright 2014 American Chemical Society).

1.4 OUTLINE OF CHAPTERS

This dissertation describes the development, optimization and application of T-CUAs for the *in vitro*, temporal, rapid, and highly sensitive detection of bacterial warfare toxin, pyocyanin, and various other phenazine metabolites produced by the opportunistic human pathogen *P. aeruginosa*. This antibiotic-resistant pathogen causes various hospital-acquired infections, and is most commonly found in chronic wound infections and in lungs of cystic fibrosis patients. During early infection stages, *P. aeruginosa* produces phenazines as virulence factors, which are highly diffusible chemical signals that are toxic to surrounding mammalian host cells and other competing microorganisms. Therefore the detection of these metabolites is of high importance as it could provide insights regarding *P. aeruginosa* virulence mechanisms. Although phenazines are known to play important roles in cellular functions, very little is known about how their concentrations fluctuate and influence cellular behaviors over the course of infection and growth.

Herein, this collective body of work reports the use of easily assembled, low-cost T-CUAs as electrochemical sensors providing rapid response times, improved sensitivity and high reproducibility for the real-time, simultaneous detection and monitoring of phenazine metabolites from *P. aeruginosa*, which has not been previously demonstrated. In comparison with other carbon-based sensors described previously (Table 1.1), T-CUAs have enhanced sensitivity due to their nanometer sizes, thus allowing for simultaneous detection and quantification not only of PYO, but also of multiple other phenazine molecules. Additionally, the fast response times of T-CUAs allow readouts to be obtained in approximately 15 s only from all ultramicroelectrodes in the array. Contrary to other aforementioned approaches, T-CUAs do not require use of 'permselective' membranes due to their high degree of biological compatibility, allowing

to sense *P. aeruginosa* markers in complex biological environments. Finally, optical imaging of *P. aeruginosa* cells on T-CUAs can be performed in tandem with electrochemical analysis, which allows for simultaneous determination of bacterial growth rates from correlated optical density measurements.

This dissertation is organized into five chapters, with Chapter 1 providing a broad overview of the motivation and scope of this work, as well as providing a detailed summary of electrochemical-based sensors developed for the detection of *P. aeruginosa*. Additionally, the design and advantages of T-CUA electrodes, developed by the Stevenson research group, are described. The remaining four chapters outline the application of T-CUAs as an electrochemical sensing platform for rapid, sensitive, diagnostic, quantitative and real-time monitoring of *P. aeruginosa* metabolism dynamics.

Chapter 2 describes the characterization and optimization of T-CUAs analytical figures of merit for the electrochemical detection of *P. aeruginosa* redox-active, virulence metabolite, PYO, from solutions with pathogenic bacteria. Square wave voltammetry was used to quantify PYO concentrations on T-CUAs with and without chitosan gold nanoparticles (CS/GNP) and planar transparent macroelectrodes (T-Macro). The response time (RT), limit of detection (LOD) and linear dynamic range (LDR) differ for each electrode type due to subtle influences in how the detectable signal varies in relation to the charging time and resistive and capacitive noise. The determined LODs and LDRs fall within the range of PYO concentrations for a variety of *in vitro* and *in vivo* cellular environments and offer promise of the application of T-CUAs for the quantitative study of biotoxins, quorum sensing and pathogenesis. Successful use of T-CUAs for the electrochemical detection of PYO secreted from *P. aeruginosa* strains while optically imaging the cells is demonstrated.

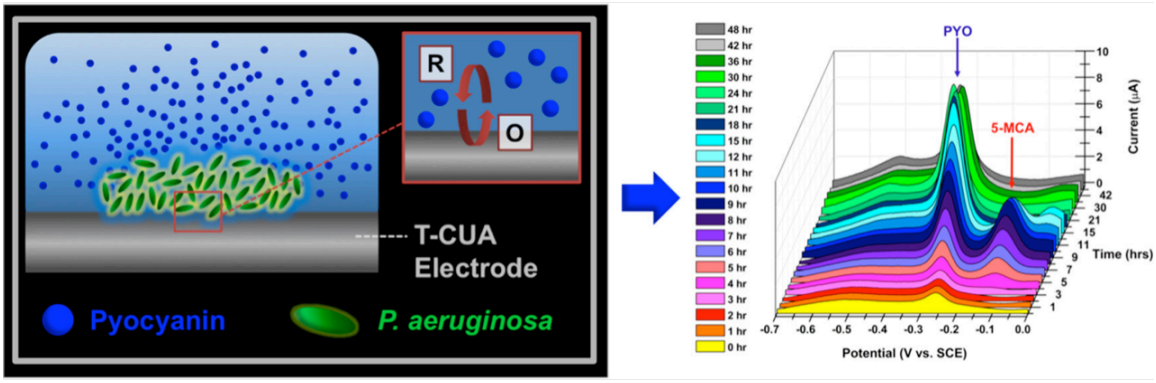

Figure 1.3: Application of T-CUAs for the real-time electrochemical detection of *P. aeruginosa* phenazine metabolites.

Specifically, PYO, 5-MCA, OHPHZ and an unknown biomolecule are electrochemically detected from living unperturbed cell cultures in simulated growth media.

Chapter 3 discusses the application of T-CUAs for the *in vitro*, simultaneous detection of various redox-active phenazine metabolites, including PYO, an extremely reactive species, 5-methylphenazine-1-carboxylic acid (5-MCA), and the side-product 1-hydroxyphenazine (OHPHZ), from a highly virulent *P. aeruginosa* PA14 strain in simulated growth media (Figure 1.3). In addition to quantifying phenazine metabolite concentrations over 48 hours, changes in phenazine dynamics are observed in the biosynthetic route for the production of PYO. Additionally, environmental effects on phenazine dynamics and PYO concentrations in two growth media, tryptic soy broth (TSB) and lysogeny broth (LB), are explored. Finally, desorption electrospray ionization (DESI) and nano-electrospray ionization (nano-ESI) mass spectrometry are used to confirm the detection and identification of reactive phenazine metabolites.

Chapter 4 details the electrochemical monitoring of the impact of polymicrobial infections on *P. aeruginosa* and growth dependent medium, where the differences in *P. aeruginosa* phenazine production and dynamics in polymicrobial communities are investigated (Figure 1.4). Specifically, *P. aeruginosa* is co-cultured with two pathogens of clinical relevance, *S. aureus* and *E. coli*, which typically populate infection sites with *P. aeruginosa*. Phenazine production rates and biosynthesis dynamics are electrochemically monitored during a 48-h period using T-CUAs. Moreover, the effect on phenazine production rates and dynamics is explored in two growth media, LB and TSB. The concentrations of PYO and highly reactive 5-MCA are determined in different polymicrobial culture samples in both media. The results demonstrate that other bacterial pathogens noticeably influence *P. aeruginosa* phenazine production and dynamics. Conclusively, the media type significantly influences phenazine product distribution, especially in polymicrobial co-cultures, signifying the need for analytical standardization of simulation media in the study of polymicrobial communities.

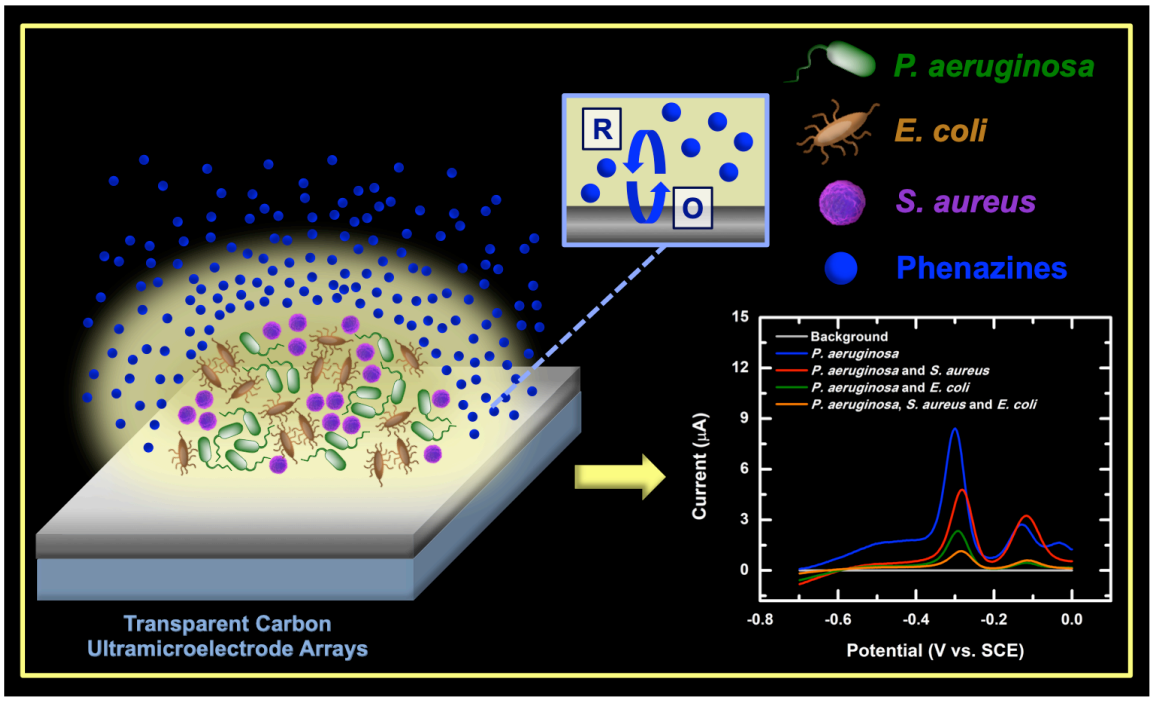

Figure 1.4: T-CUAs for the real-time electrochemical detection of *P. aeruginosa* phenazines in polymicrobial samples as a function of growth dependent medium.

Chapter 5 presents a summary of initial studies performed for future work. Using T-CUAs, temporal electrochemical detection of PYO from *P. aeruginosa* grown in a synthetic cystic fibrosis sputum medium, SCFM2 (developed by the Whiteley lab) is evaluated while simultaneously performing confocal microscopy imaging of cellular aggregates. The characterization of PYO diffusion coefficients and the viscoelastic properties of SCFM2 are described. Additionally, the interaction between two biogenic species of importance, specifically pathogenic PYO and immunological nitric oxide ($NO^{\bullet}$), is investigated on T-CUA sensors. The *in vitro* detection of these cellular species will enable real-time monitoring of pathogen-host responses.

Table 1.1: Summary of published work overviewed in detail and referenced in this dissertation chapter.

Target Pathogen	Sensing Strategy and Methods	Electrode Type/Material	LOD	LDR	Analysis Time	Ref.
P. aeruginosa	Detection of the electrochemical conversion of PYO using CV	Commercially available, disposable, screen-printed Au electrodes	2 μM	2–100 μM	Not stated	37
P. aeruginosa	Detection of the electrochemical conversion of PYO using SWV	Transparent Carbon Ultramicroelectrode Arrays	1.0 μM	1–250 μM	15 sec	38
P. aeruginosa	Detection of the electrochemical conversion of PYO and other phenazine metabolites using SWV	Transparent Carbon Ultramicroelectrode Arrays	1.0 μM	1–250 μM	15 sec	39, 85
P. aeruginosa	Detection of electrochemical conversion of PYO and uric acid using CV and SWV	Inkjet-printed Carbon Nanotube Electrodes	0.1 μM (PYO), not specified for uric acid	0.1–100 μM (PYO) 100–1000 μM (uric acid)	Not stated	40
P. aeruginosa	Electrochemical detection of PYO using *in situ* spectroelectrochemical setup and CV	Au electrode	Not specified	Not specified	Not stated	41

Table 1.1 (continued)

Target Pathogen	Sensing Strategy and Methods	Electrode Type/Material	LOD	LDR	Analysis Time	Ref.
P. aeruginosa	Detection of pyoverdine using DPV	Nanohybrid based on graphene, carboxylic polypyrrole and AuNPs on screen printed electrode	0.33 µM	1–100 µM	165 s	43
P. aeruginosa	Detection of pyoverdine using DPV	Graphene/graphite-modified screen-printed electrode modified with AuNPs	66.9 nM	0.5–100 µM	Not stated	44
P. aeruginosa	Detection of the electrochemical conversion of PYO using amperometry	Screen printed Au electrode	2.5 µM	1–100 µM	Not stated	46
P. aeruginosa	Detection of the electrochemical conversion of PYO using CV and SWV	Carbon paper-based screen printed electrodes	95 nM	1–100 µM	Not stated	47
P. aeruginosa	Detection of electrochemical conversion of PYO using SWV	Disposable, screen-printed, carbon-based electrode	Not specified	0–100 µM	Not stated	48
P. aeruginosa	Detection of electrochemical conversion of PYO using SWV	Carbon-based disk electrode	Not specified	Not specified	Not stated	49

Table 1.1 (continued)

Target Pathogen	Sensing Strategy and Methods	Electrode Type/Material	LOD	LDR	Analysis Time	Ref.
P. aeruginosa	Detection of electrochemical conversion of PYO and phenazine metabolites using SWV	Electrochemical camera chip with integrated electrodes and membrane	Not specified	Not specified	480 sec	57
P. aeruginosa	Detection of electrochemical conversion of metabolites (PYO, PQS, HHQ) using DPV	Thin film BDD electrode	2.06 µM (PYO), 3.61 µM (HHQ) and 4.85 µM (PQS)	5–50 µM	Not stated	53
P. aeruginosa	Detection of electrochemical conversion of microbial metabolites (PYO, PQS, HHQ) using DPV	BDD electrode	50 nM (PYO), 250 nM (HHQ) and 250 nM (PQS)	2–100 µM (PYO), 2–75 µM (HHQ) and 2–100 µM (PQS)	Not stated	54

Table 1.1 Acronyms: LOD – limit of detection; LDR – linear dynamic range; PYO – pyocyanin; Au – gold; CV – cyclic voltammetry; SWV – square wave voltammetry; DPV – differential pulse voltammetry; AuNPs – gold nanoparticles; PQS – 2-heptyl-3-hydroxy-4-quinolone (Pseudomonas Quinolone Signal); HHQ – 2-heptyl-4-hydroxyquinoline; BDD – boron doped diamond; *P. aeruginosa* – *Pseudomonas aeruginosa*

1.5 REFERENCES

(1) Ventola, C. L. *P T*, **2015**, *40*, 344–352.

(2) Amiri, M.; Bezaatpour, A.; Jafari, H.; Boukherroub, R.; Szunerits, S. *ACS Sensors* **2018**, *3*, 1069–1086.

(3) Monzó, J.; Insua, I.; Fernandez-Trillo, F.; Rodriguez, P. *Analyst* **2015**, *140*, 7116–7128.

(4) Boucher, H. W.; Talbot, G. H.; Bradley, J. S.; Edwards, J. E.; Gilbert, D.; Rice, L. B.; Scheld, M.; Spellberg, B.; Bartlett, J. *Clin. Infect. Dis.* **2009**, *48*, 1–12.

(5) Dye, C. *Philos. Trans. R. Soc. Lond., B, Biol. Sci.* **2014**, *369*, 20130426–20130435.

(6) Pogue, J. M.; Kaye, K. S.; Cohen, D. A.; Marchaim, D. *Clin. Microbiol. Infect.* **2015**, *21*, 302–312.

(7) Hudu, S. A.; Alshrari, A. S.; Syahida, A.; Sekawi, Z. *J Clin Diagn Res* **2016**, *10*, DE01–DE05.

(8) Swaminathan, B.; Feng, P. *Annu. Rev. Microbiol.* **1994**, *48*, 401–426.

(9) Lazcka, O.; Campo, F. J. D.; Muñoz, F. X. *Biosens. Bioelectron.* **2007**, *22*, 1205–1217.

(10) Buchan, B. W.; Ledeboer, N. A. *Clinical Microbiology Reviews* **2014**, *27*, 783–822.

(11) Paniel, N.; Baudart, J.; Hayat, A.; Barthelmebs, L. *Methods* **2013**, *64*, 229–240.

(12) Goluch, E. D. *Trends Biotechnol* **2017**, *35*, 1125–1128.

(13) Douterelo, I.; Jackson, M.; Solomon, C.; Boxall, J. *Appl Microbiol Biotechnol* **2015**, *100*, 3301–3311.

(14) Cho, J. C.; Tiedje, J. M. *Applied and Environmental Microbiology* **2001**, *67*, 3677–3682.

(15) Ho, Y. P.; Reddy, P. M. *Clinical Chemistry* **2010**, *56*, 525–536.

(16) Krásný, L.; Hynek, R.; Hochel, I. *Int. J. Mass Spectrom.* **2013**, *353*, 67–79.

(17) Hou, T.-Y.; Chiang-Ni, C.; Teng, S.-H. *J Food Drug Anal* **2019**, *27*, 404–414.

(18) Emonet, S.; Shah, H. N.; Cherkaoui, A.; Schrenzel, J. *Clinical Microbiology and Infection* **2010**, *16*, 1604–1613.

(19) Phelan, V. V.; Fang, J.; Dorrestein, P. C. *J. Am. Soc. Mass Spectrom.* **2015**, *26*, 873–877.

(20) Watrous, J. D.; Dorrestein, P. C. *Nature Rev. Microbiol.* **2011**, *9*, 683–694.

(21) Watrous, J.; Roach, P.; Alexandrov, T.; Heath, B. S.; Yang, J. Y.; Kersten, R. D.; van der Voort, M.; Pogliano, K.; Gross, H.; Raaijmakers, J. M.; Moore, B. S.; Laskin, J.; Bandeira, N.; Dorrestein, P. C. *Proc Natl Acad Sci USA* **2012**, *109*, E1743–E1752.

(22) Ge, M.-C.; Kuo, A.-J.; Liu, K.-L.; Wen, Y.-H.; Chia, J.-H.; Chang, P.-Y.; Lee, M.-H.; Wu, T.-L.; Chang, S.-C.; Lu, J.-J. *J Microbiol Immunol Infect* **2017**, *50*, 662–668.

(23) Angeletti, S. *J. Microbiol. Methods* **2017**, *138*, 20–29.

(24) Ivnitski, D.; Hamid, I. A.; Atanasov, P.; Wilkins, E.; Stricker, S. *Electroanalysis* **2000**, *12*, 317–325.

(25) Tang, Y.; Ali, Z.; Zou, J.; Jin, G.; Zhu, J.; Yang, J.; Dai, J. *RSC Adv.* **2017**, *7*, 51789–51800.

(26) Shahdordizadeh, M.; Taghdisi, S. M.; Ansari, N.; Langroodi, F. A.; Abnous, K.; Ramezani, M. *Sensor Actuat B-Chemical* **2017**, *241*, 619–635.

(27) Kokkinos, C.; Economou, A.; Prodromidis, M. I. *Trends in Analytical Chemistry* **2016**, *79*, 88–105.

(28) Justino, C. I. L.; Duarte, A. C.; Rocha-Santos, T. A. P. *Trends in Analytical Chemistry* **2016**, *85*, 36–60.

(29) Kuss, S.; Amin, H. M. A.; Compton, R. G. *Chem. Asian J.* **2018**, *13*, 2758–2769.

(30) Ringen, L. M.; Drake, C. H. *J. Bacteriol.* **1952**, *64*, 841–845.

(31) Walker, T. S. *Plant Physiol.* **2004**, *134*, 320–331.

(32) Fetzer, A. F.; Werner, A. S.; Hagstrom, J. W. *Am. Rev. Respir. Dis.* **1967**, *96*, 1121–1130.

(33) Bedrossian, C. W. M.; Greenberg, S. D.; Singer, D. B.; Hansen, J. J.; Rosenberg, H. S. *Hum. Pathol.* **1976**, *7*, 195−204.

(34) Fick, R. B. *Chest.* **1989**, *96*, 158–164.

(35) Magill, S. S.; Edwards, J. R.; Bamberg, W.; Beldavs, Z. G.; Dumyati, G.; Kainer, M. A.; Lynfield, R.; Maloney, M.; McAllister-Hollod, L.; Nadle, J.; Ray, S. M.; Thompson, D. L.; Wilson, L. E.; Fridkin, S. K. *N Engl J Med* **2014**, *370*, 1198–1208.

(36) Bowler, P. G.; Duerden, B. I.; Armstrong, D. G. *Clinical Microbiology Reviews* **2001**, *14*, 244–269.

(37) Alatraktchi, F.; Breum Andersen, S.; Krogh Johansen, H.; Molin, S.; Svendsen, W. *Sensors* **2016**, *16*, 408–410.

(38) Elliott, J.; Simoska, O.; Karasik, S.; Shear, J. B.; Stevenson, K. J. *Anal. Chem.* **2017**, *89*, 6285–6289.

(39) Simoska, O.; Sans, M.; Fitzpatrick, M. D.; Crittenden, C. M.; Eberlin, L. S.; Shear, J. B.; Stevenson, K. J. *ACS Sensors* **2019**, *4*, 170–179.

(40) Jarošová, R.; Mcclure, S. E.; Gajda, M.; Jović, M.; Girault, H. H.; Lesch, A.; Maiden, M.; Waters, C.; Swain, G. M. *Anal. Chem.* **2019**, *91*, 8835–8844.

(41) Do, H.; Kwon, S.-R.; Fu, K.; Morales-Soto, N.; Shrout, J. D.; Bohn, P. W. *Langmuir* **2019**, *35*, 7043–7049.

(42) McLister, A.; McHugh, J.; Cundell, J.; Davis, J. *Adv. Mater.* **2016**, *28*, 5732–5737.

(43) Cernat, A.; Tertis, M.; Gandouzi, I.; Bakhrouf, A.; Suciu, M.; Cristea, C. *Electrochemistry Communications* **2018**, *88*, 5–9.

(44) Gandouzi, I.; Tertis, M.; Cernat, A.; Saidane-Mosbahi, D.; Ilea, A.; Cristea, C. *Materials* **2019**, *12*, 1180–1193.

(45) Dietrich, L. E. P.; Price-Whelan, A.; Petersen, A.; Whiteley, M.; Newman, D. K. *Mol. Microbiol.* **2006**, *61*, 1308–1321.

(46) Alatraktchi, F. A.; Johansen, H. K.; Molin, S.; Svendsen, W. E. *Nanomedicine* **2016**, *11*, 2185–2195.

(47) Alatraktchi, F. A.; Noori, J. S.; Tanev, G. P.; Mortensen, J.; Dimaki, M.; Johansen, H. K.; Madsen, J.; Molin, S.; Svendsen, W. E. *PLoS ONE* **2018**, *13*, e0194157–e0194159.

(48) Santiveri, C. R.; Sismaet, H. J.; Kimani, M.; Goluch, E. D. *ChemistrySelect* **2018**, *3*, 2926–2930.

(49) Sismaet, H. J.; Pinto, A. J.; Goluch, E. D. *Biosens. Bioelectron.* **2017**, *97*, 65–69.

(50) Koley, D.; Ramsey, M. M.; Bard, A. J.; Whiteley, M. *Proc. Natl. Acad. Sci. U.S.A.* **2011**, *108*, 19996–20001.

(51) Connell, J. L.; Kim, J.; Shear, J. B.; Bard, A. J.; Whiteley, M. *Proc Natl Acad Sci USA* **2014**, *111*, 18255–18260.

(52) Moya, A.; Gabriel, G.; Villa, R.; del Campo, F. J. *Current Opinion in Electrochemistry* **2017**, *3*, 29–39.

(53) Buzid, A.; Reen, F. J.; Langsi, V. K.; Muimhneacháin, E. Ó.; O'Gara, F.; McGlacken, G. P.; Luong, J. H. T.; Glennon, J. D. *ChemElectroChem* **2017**, *4*, 533–541.

(54) Buzid, A.; Shang, F.; Reen, F. J.; Muimhneacháin, E. Ó.; Clarke, S. L.; Zhou, L.; Luong, J. H. T.; O'Gara, F.; McGlacken, G. P.; Glennon, J. D. *Sci. Rep.* **2016**, *6*, 1–9.

(55) Takahashi, Y.; Zhou, Y.; Fukuma, T. *Current Opinion in Electrochemistry* **2017**, *5*, 121–125.

(56) Bellin, D. L.; Sakhtah, H.; Rosenstein, J. K.; Levine, P. M.; Thimot, J.; Emmett, K.; Dietrich, L. E. P.; Shepard, K. L. *Nat. Commun.* **2014**, *5*, 3256–3265.

(57) Bellin, D. L.; Sakhtah, H.; Zhang, Y.; Price-Whelan, A.; Dietrich, L. E. P.; Shepard, K. L. *Nat. Commun.* **2016**, *7*, 10535–10544.

(58) Mavrodi, D. V.; Blankenfeldt, W.; Thomashow, L. S. *Annu. Rev. Phytopathol.* **2006**, *44*, 417–445.

(59) Pierson, L. S.; Pierson, E. A. *Appl Microbiol Biotechnol* **2010**, *86*, 1659–1670.

(60) Glasser, N. R.; Kern, S. E.; Newman, D. K. *Mol. Microbiol.* **2014**, *92*, 399–412.

(61) Hendiani, S.; Pornour, M.; Kashef, N. *Photodiagnosis and Photodynamic Therapy* **2019**, *26*, 8–12.

(62) Wightman, R. *Anal. Chem.* **1981**, *53*, 1125A–1134A.

(63) Pons, S.; Fleischmann, M. *Anal. Chem.* **1987**, *59*, 1391A–1399A.

(64) Bard, A. J.; Faulkner, L. R. *Electrochemical Methods Fundamentals and Applications*, 2nd ed.; Harris, D., Ed.; John Wiley & Sons, Inc., 2001; pp 1–850.

(65) Chen, R.; Li, Y.; Huo, K.; Chu, P. K. *RSC Adv.* **2013**, *3*, 18698–18716.

(66) Hood, S. J.; Kampouris, D. K.; Kadara, R. O.; Jenkinson, N.; del Campo, F. J.; Muñoz, F. X.; Banks, C. E. *Analyst* **2009**, *134*, 2301–2305.

(67) Arrigan, D. W. M. *Analyst* **2004**, *129*, 1157–1165.

(68) Koehne, J. E.; Marsh, M.; Boakye, A.; Douglas, B.; Kim, I. Y.; Chang, S.-Y.; Jang, D.-P.; Bennet, K. E.; Kimble, C.; Andrews, R.; Meyyappan, M.; Lee, K. H. *Analyst* **2011**, *136*, 1802–1805.

(69) Guo, J.; Lindner, E. *Anal. Chem.* **2009**, *81*, 130–138.

(70) Duay, J.; Goran, J. M.; Stevenson, K. J. *Anal. Chem.* **2014**, *86*, 11528–11532.

(71) Duay, J.; Elliott, J.; Shear, J. B.; Stevenson, K. J. *Anal. Chem.* **2015**, *87*, 10109–10116.

(72) Ino, K.; Shiku, H.; Matsue, T. *Current Opinion in Electrochemistry* **2017**, *5*, 146–151.

(73) Ino, K.; Yamada, Y.; Kanno, Y.; Imai, S.; Shiku, H.; Matsue, T. *Sensor Actuat B-Chemical* **2016**, *234*, 201–208.

(74) Kurosawa, H.; Utsunomiya, H.; Shiga, N.; Takahashi, A.; Ihara, M.; Ishibashi, M.; Nishimoto, M.; Watanabe, Z.; Abe, H.; Kumagai, J.; Terada, Y.; Igarashi, H.; Takahashi, T.; Fukui, A.; Suganuma, R.; Tachibana, M.; Yaegashi, N. *Hum. Reprod.* **2016**, *31*, 2321–2330.

(75) Gardner, R. D.; Zhou, A.; Zufelt, N. A. *Sensor Actuat B-Chemical* **2009**, *136*, 177–185.

(76) Orozco, J.; Fernández-Sánchez, C.; Jiménez-Jorquera, C. *Sensors* **2010**, *10*, 475–490.

(77) Feeney, R.; Kounaves, S. P. *Electroanalysis* **2000**, *12*, 677–684.

(78) Albers, J.; Grunwald, T.; Nebling, E.; Piechotta, G.; Hintsche, R. *Anal Bioanal Chem* **2003**, *377*, 521–527.

(79) Nebling, E.; Grunwald, T.; Albers, J.; Schäfer, P.; Hintsche, R. *Anal. Chem.* **2004**, *76*, 689–696.

(80) Patel, B. A.; Arundell, M.; Quek, R. G. W.; Harvey, S. L. R.; Ellis, I. R.; Florence, M. M.; Cass, A. E. G.; Schor, A. M.; O'Hare, D. *Anal Bioanal Chem* **2008**, *390*, 1379–1387.

(81) Arumugam, P. U.; Yu, E.; Riviere, R.; Meyyappan, M. *Chemical Physics Letters* **2010**, *499*, 241–246.

(82) Yakushenko, A.; Schnitker, J.; Wolfrum, B. *Anal. Chem.* **2012**, *84*, 4613–4617.

(83) McKnight, T. E.; Melechko, A. V.; Fletcher, B. L.; Jones, S. W.; Hensley, D. K.; Peckys, D. B.; Griffin, G. D.; Simpson, M. L.; Ericson, M. N. *J. Phys. Chem. B* **2006**, *110*, 15317–15327.

(84) Elliott, J.; Duay, J.; Simoska, O.; Shear, J. B.; Stevenson, K. J. *Anal. Chem.* **2017**, *89*, 1267–1274.

(85) Simoska, O.; Sans, M.; Eberlin, L. S.; Shear, J. B.; Stevenson, K. J. *Biosens. Bioelectron.* **2019**, *142*, 111538.

Chapter 2: Electrochemical Detection of a Bacterial Warfare Toxin, Pyocyanin, using Transparent Carbon Ultramicroelectrode Arrays[2]

2.1 INTRODUCTION

Numerous infectious diseases are easily spread through hospitals when patients are exposed to pathogenic bacteria contaminating heavily trafficked hospital surfaces, in some instances having established dense, antibiotic-resistant biofilm communities. The opportunistic pathogen, *Pseudomonas aeruginosa*, is responsible for various severe hospital-contracted infections.[1,2] While it rarely establishes persistent infections in otherwise healthy individuals, this microorganism can establish chronic infections in individuals with compromised immune systems, and suffering from other conditions, such as severe burns (and other wounds) and cystic fibrosis.[3-7]

P. aeruginosa secretes several biotoxins as virulence factors that cause infections in host organisms to thrive.[8,9] One of these factors is pyocyanin (PYO), a blue pigment, redox-active nitrogen-containing aromatic compound in the family of phenazine compounds.[10-12] It is exclusively secreted as a secondary metabolite by quorum sensing (a population-dependent response to diffusible signals) *P. aeruginosa* bacteria, which makes this molecule an effective diagnostic marker for identifying developing infections.[13] PYO has been isolated and detected within *in vivo* environments in the low- to mid-micromolar range.[14-16] It readily reacts with cellular metabolites to generate reactive oxygen species (ROS) that damage host tissue.[10] PYO is also involved in quorum sensing (QS), a cell-to-cell communication process allowing bacteria to regulate gene expression based on the

[2]Adapted with permission from Simoska, O.; Elliott, J.; Karashik, S.; Shear, J. B.; Stevenson, K. J. Transparent Ultramicroelectrode Arrays for the Electrochemical Detection of Bacterial Warfare Toxin, Pyocyanin. *Anal. Chem.* **2017**, *89*, 6285–6289. Copyright © 2017 American Chemical Society. Elliott, J. and Simoska, O. contributed equally to the work both in taking the data and writing the manuscript. All authors contributed in editing the manuscript.

effective cell density.[13,17] Therefore, detecting and quantifying PYO could provide a better understanding of *P. aeruginosa*'s pathogenesis.

PYO is most commonly detected using spectrophotometric methods,[18,19] which typically require time-consuming sample pre-treatments. Using ultraviolet absorption, PYO has been detected at concentrations ranging from 12–38 μM.[18] Additionally, high performance liquid chromatography (HPLC) in combination with mass spectrometry is a frequently employed approach for detecting PYO.[20,21] Although such methods generally yield good analytical sensitivities, they require time-consuming preparative steps, large sample volumes and relatively costly equipment. Unlike these conventional procedures, electrochemical approaches have been demonstrated to be low cost, rapid, sensitive, and direct methods for detection of PYO.[22-25] Hence, they are becoming increasingly popular alternatives to standard optical or separation based analytical methods.

Previous studies have successfully used voltammetric techniques for the detection and quantification of PYO from *P. aeruginosa* strains and from human fluid samples.[22-24,26] Additionally, a recent study reported on an amperometric method for the selective detection and quantification of PYO[27] and scanning electrochemical microscopy (SECM) has been employed to examine PYO at the surface of biofilms with high spatial resolution.[28,29] However, none of the aforementioned electroanalytical techniques have demonstrated the use of optically transparent ultramicroelectrode arrays for the detection of PYO. In addition to easy fabrication, low cost, and simple modification procedures, the optical transparency of these electrodes provides a means to analyze *P. aeruginosa* cells on electrode surfaces while simultaneously monitoring changes in electrochemical signals of cellularly derived PYO. Thus, this electrode platform has the potential to provide simultaneous optical information about cell modulation in addition to real-time, continuous electrochemical analyses of cellular PYO.

The Stevenson research group has previously reported a facile, low-cost, versatile approach for the fabrication of transparent carbon ultramicroelectrode arrays (T-CUAs).[30] These electrodes offer several advantages relative to typical bulk electrodes. Their small size allows for the use of less supporting electrolyte, thus achieving enhanced mass transport and fast steady state responses.[30] T-CUAs retain the benefits of microelectrodes, but have the additional advantage of amplified currents because the individual electrodes in the array function in parallel.[30] In addition, these electrodes achieve lower background current due to their small electroactive areas, which result in higher signal-to-noise (S/N) ratios and lower limits of detection (LODs).[30] The active electrode material of T-CUAs is a pyrolyzed photoresist film (PPF), which provides advantages similar to glassy carbon: inert, highly conductive, chemically stable, and biocompatible. We have recently characterized T-CUA analytical response to hydrogen peroxide (H_2O_2), a biogenic metabolite produced by various types of cells.[31] Using cyclic voltammetry, the LOD was determined to be in the nanomolar range (~35 nM).[31] In addition, we recently employed T-CUAs for the detection of another biogenic ROS, nitric oxide ($NO^{\bullet}$), achieving an LOD of 0.2 ± 0.1 μM using square wave voltammetry (SWV).[32] The optical transparency of the electrodes allows for the bright-field imaging of cells as well as the ability to perform fluorescence experiments on cells. Furthermore, the T-CUA and T-Macro electrodes' biocompatibilities are comparable to glass, deeming them extremely biocompatible surfaces.

Herein, we demonstrate use of T-CUAs for the detection of PYO with the goal of incorporating this device with biological systems for the electrochemical detection of PYO secreted by cells. We evaluated PYO responses at different electrodes using square wave voltammetry to determine respective LODs and LDRs. The LODs determined fall within the micromolar ranges for PYO detection from *P. aeruginosa* infected sputum

samples and biofilm aggregates, indicating that our approach could be useful for measuring PYO concentration in *in vitro* and/or *in vivo* biological environments. Finally, as a proof-of-concept study, T-CUAs were used as a sensing platform to detect PYO from bacterial strains, while concurrently performing bright-field imaging of the cells.

2.2 EXPERIMENTAL METHODS

2.2.1 General

All chemicals were used as received. Photoresist AZ 1518 was purchased from Microchemicals. Potassium chloride, acetic acid, cyclohexanone, isopropanol, and nitric acid were acquired from Sigma-Aldrich Co. Polystyrene spheres (Polybead®) with a diameter of 1.54 μm were purchased from Polysciences, Inc. Pyocyanin was purchased from Cayman Chemical Company. Ethanol, Monosodium phosphate, disodium phosphate were purchased from Thermo Fisher Scientific Inc.

2.2.2 Fabrication of T-Macro and T-CUA Electrodes

Preparation of the T-CUAs and T-Macro follows a previously described procedures.[30,31] Quartz microscopic slides (6.45 cm^2 and 1 mm thick, Technical Glass Products) were treated with piranha (3:1 H_2SO_4: 30% H_2O_2) to remove any organic contaminants. A 1:3 dilution of AZ 1518 photoresist with PGMEA (1-methoxy-1-propanol acetate) was spun onto the piranha cleaned quartz slides at 6000 rpm for 60 s. Following spin coating, the photoresist slides were soft baked at 90 °C for 10 min and then transferred to a tube furnace. After 15 min of purging with 5% H_2: 95% N_2 (~100 mL/min), the photoresist slides were pyrolized by heating to 1000 °C at 5 °C/min and holding at that temp for 1 h before allowing them to cool slowly back to room temperature at 5°C/min. The pyrolized photoresist film (PPF) slides were then removed

from the furnace and stored for 3 days prior to use to allow for the oxide layer to stabilize. T-CUAs fabrication involved a lithography method using polystyrene microspheres (PSS) with a diameter of 1.54 μm, which were drop cast from a 5.4 wt % methanol suspension onto the conductive PPF electrodes. The organization of the spheres is that of a hexagonal close-packed two-dimensional ordered network. After this microsphere lithography step, 10 nm of Al_2O_3 layer was deposited via atomic layer deposition (ALD) technique at 80 °C. The ALD process was calibrated by the manufacturer (Cambridge Nanotech Savannah 100) to deposit 0.089 nm conformal Al_2O_3 layer per cycle. Thus, cycling this process for 112 times formed a 10 nm ALD layer. This ALD step is then followed by removal of PSS via sonication with methanol, acetone, isopropanol and water. Disk-shaped carbon areas remained where the PSS made contact with the PPF, thus forming a carbon ultramicroelectrode array. T-Macro refers to the planar carbon electrode where no PSS were used during the fabrication process to create an array of electrodes. Details on characterization of T-CUA electrodes have been reported in previous research studies from our group.[30,31]

2.2.3 Preparation of Chitosan-Gold Nanoparticles (CS/GNP)

The CS/GNP solution was prepared according to modified procedures described in previous literature.[32,33] Briefly, a 10.00 mg/mL solution of chitosan (CS) in 0.05 M acetic acid and a 3.76×10^{-3} M solution of chloroauric acid ($HAuCl_4$) were prepared and mixed in a 20:1 (v/v) ratio, respectively. The mixture was well-shaken and placed in a heated sonic bath for 1 h until the solution color went from cloudy white to pink, indicating gold nanoparticles (GNP) formation. The solution pH is adjusted to 2.0 using nitric acid (HNO_3) to dissolve the CS.

2.2.4 Preparation of CS/GNP Modified T-CUA Electrodes

The CS/GNP film was electrodeposited on the T-CUA and T-Macro electrodes using chronoamperometry by holding a potential at –1.00 V vs SCE for 60 s in the aforementioned CS/GNP solution. The selected potential and time for the deposition was previously determined by Wang et al.[33] Upon the electrodeposition step, the T-CUA and T-Macro electrodes were rinsed with deionized water and gently dried with N_2 gas.

2.2.5 Preparation of Standard Pyocyanin Solutions

A 2 mM PYO stock solution was prepared in ethanol and was diluted to make a 500 μM stock solution in sodium phosphate buffer solution (SPB, 7.0 pH). From the 500 μM stock solution the respective PYO standard solutions were prepared having the following concentrations: 0.5 μM, 1 μM, 5 μM, 10 μM, 25 μM, 50 μM, 100 μM, and 250 μM, in SPB.

2.2.6 Electrochemical Measurements

The electrochemical measurements were done using a three-electrode cell system. Electrochemical experiments, including square wave voltammetry (SWV) and cyclic voltammetry (CV), were performed using an Autolab PGSTAT30 potentiostat. T-CUA or T-Macro was the working electrode with a total exposed geometric area of 0.495 cm^2, defined by the electrode area exposed to a solution in a homemade Teflon electrochemical well. A platinum mesh was used as the counter electrode and a saturated calomel electrode (SCE) was used as the reference electrode. CV experiments were performed at scan rates of 2.5, 25, and 50 mV s^{-1}. SWV measurements were performed using a current of 5 μA, 3 mV step potential, and a frequency of 15 Hz. The potential ranged from –0.3 or –0.4 to (–0.1) V vs SCE. The background solution used was sodium

phosphate buffer solution (SPB, 7.0 pH). After a background CV or SWV curve was collected using SPB, subsequent PYO measurements were obtained.

2.2.7 Bacterial Strains Cell Culture and Optical Imaging

Wild-type PA14 and a clinically relevant PA11 LESB58 (SED11)[34] *P. aeruginosa* strains were used in these studies. The growth medium for these experiments was a 1:15 (vol/vol) mixture of lysogeny broth (LB) (5 g/L yeast extract, 10 g/L NaCl, and 10 g/L tryptone) buffered to pH of 7.2 with sodium succinate (20 mM) as the carbon source. Cultures were grown aerobically overnight at 37 °C. Cells were diluted with sodium phosphate buffer (SPB, pH 7.0) for electrochemical measurements. Using UV-Vis spectrometry (Agilent Instrument 8453 UV−vis−NIR spectrometer), the ODs at 600 nm were measured to be 0.763 and 1.628 for PA11 and PA14 in 1:3 (v/v) LB:SPB, respectively. The ODs at 600 nm were measured to be 1.674 and 0.934 for Pa11 and Pa14 in 1:1 (v/v) LB:SPB, respectively. Images of bacterial strains on T-CUAs were obtained using bright-field illumination settings using an Olympus PlanApo 60×, 1.40 N.A. oil- immersion objective on an inverted microscope (Zeiss; Axiovert). An ORCA-Flash 2.8 scientific-grade complementary metal oxide semiconductor camera (Hamamatsu) controlled by HCImage Live software (Hamamatsu) was used.

2.3 Results and Discussion

2.3.1 Evaluation of Electrochemical Behavior of PYO at T-CUA and T-Macro Electrodes

Cyclic voltammetry (CV) was employed to evaluate the electrochemical activity of pyocyanin (PYO) at the T-CUA and T-Macro electrodes. The structural half-reactions of PYO are shown in Figure 2.1a. Figure 2.1b depicts a quasi-reversible, CV response with an anodic peak at −0.21 V and cathodic peak at −0.28 V with $E_{1/2}$ = −0.245 V vs

SCE. In addition, a non-reversible phenolic oxidation[24] of pyocyanin (I−III) occurs at +0.89 V (Figure 2.1b), which is responsible for the polymerization of PYO. The product of the polymerization, III, undergoes a reversible conversion to IV. This transformation occurs at the same redox potential as PYO in solution. The conversion of soluble PYO to its polymerized form as well as the cycling between III and IV causes an increase in the reversible peak heights (Figure 2.1b).[24] This polymerization can be avoided by reducing the scan range to a range of −0.4 to −0.1 vs SCE (Figure 2.1c). Within this potential window, the redox couple observed is exclusively caused from the conversion between soluble, monomeric forms of PYO, I and II (Figure 2.1a). To allow a comparison, cyclic voltammograms, under the same conditions, for the other two electrode configurations used in this work (T-Macro and CS/GNP modified T-CUA) are shown in Figure 2.2.

The electrochemical behavior of PYO observed at the T-Macro and T-CUA is not a purely reversible outer-sphere electron transfer reaction, as it undergoes a quasi-reversible redox mechanism with $E_p > 59$ mV/n that is scan rate dependent. Figure 2.1c shows that at a very slow scan rate of 2.5 mV s^{-1} PYO experiences an irreversible reduction. At faster scan rates (>25 mV s^{-1}) the reversibility of the current-potential response improves, which is corroborated by the presence of an anodic peak. Therefore the reduced chemical product is stable on the time scale of CV experiments at or below a scan rate of 2.5 mV s^{-1}. The observation of chemical reversibility is related to how fast the voltammetric experiment is conducted. Being that the pKa of PYO is 4.95, the reduced product is re-oxidizes in the solution with pH 7.4.

A particular redox couple may appear chemically irreversible when voltammetric experiments are performed on a slow time scale. Whereas during the acquisition of a faster measurement, the rate of reversible electron transfer is faster than the rate of formation for the stable, reduced chemical product achieving chemical reversibility for

the system. To further illustrate the quasi-reversible nature of PYO redox, peak anodic (i_a) and peak cathodic (i_c) current responses were plotted as a function of the square root of the scan rates at T-CUA electrodes (Figure 2.3a). As described by the Randles-Sevcik equation i_a does equal i_c for a purely reversible couple,[35] which does not hold true here. Consequently, the ratio of peak anodic current to peak cathodic current does not equal 1 (Figure 2.3b, Table 2.1).

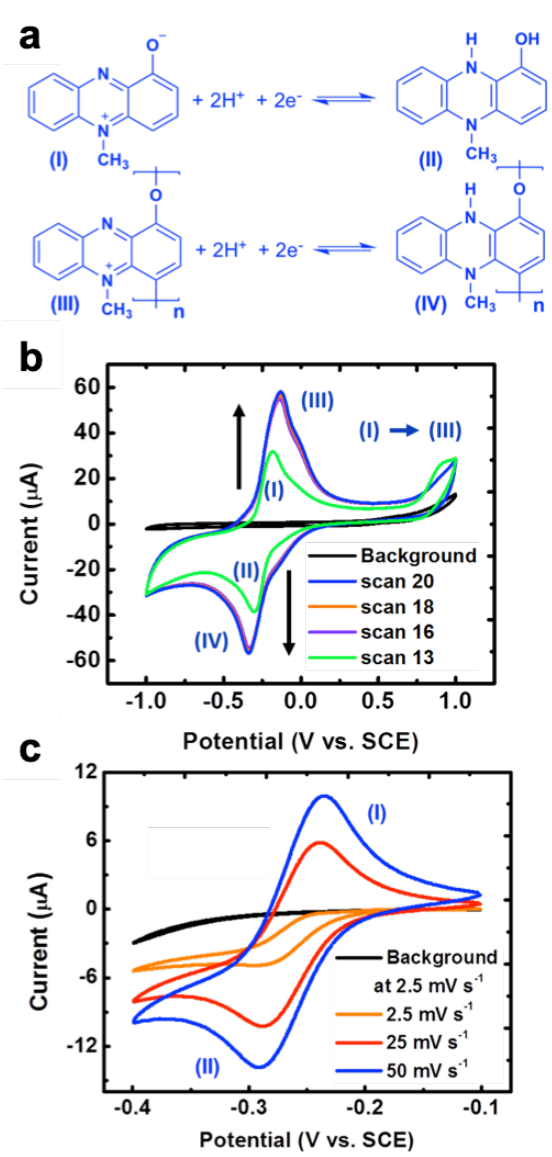

Figure 2.1: Pyocyanin (PYO) electrochemical behavior at T-CUA electrodes.

(a) PYO redox reaction for its monomeric and polymeric forms. (b) Cyclic voltammograms of PYO polymerization due to high anodic potentials at different scans, with 100 μM PYO, at T-CUA electrode, scan rate of 100 mV s^{-1}. (c) Cyclic voltammetric current responses of PYO at scan rates of 2.5, 25 and 50 mV s^{-1}, as indicated, with 100 μM PYO, at T-CUA electrode. The limited scan range from – 0.40 V to – 0.10 V prevents PYO polymerization.

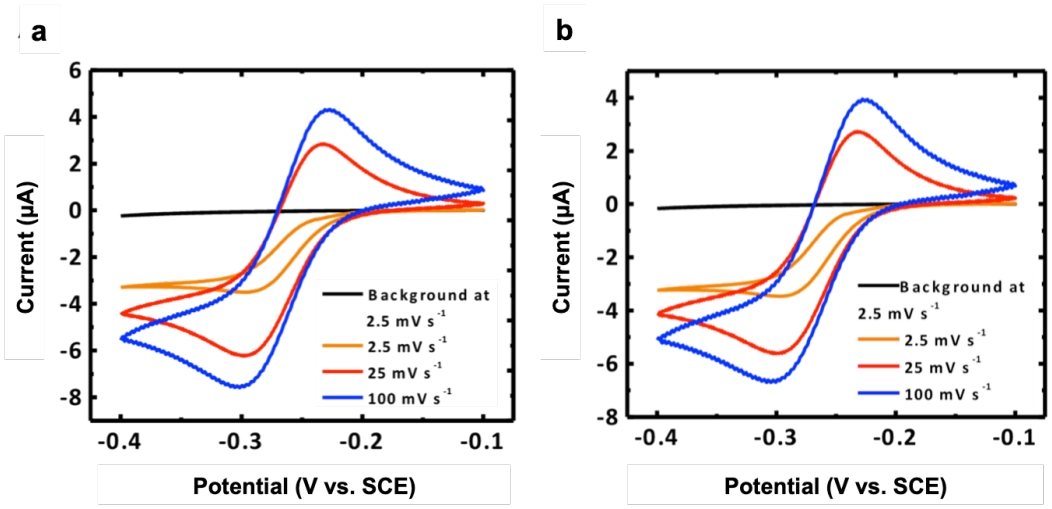

Figure 2.2: PYO electrochemical behavior at T-Macro and CS/GNP modified T-CUA electrodes.

Cyclic voltammetry response curves of PYO at scan rates of 2.5, 25 and 50 mV s^{-1}, as indicated, with 100 μM PYO, at (a) T-Macro, and (B) CS/GNP modified T-CUA electrodes. The limited scan range from – 0.40 V to – 0.10 V prevents PYO polymerization.

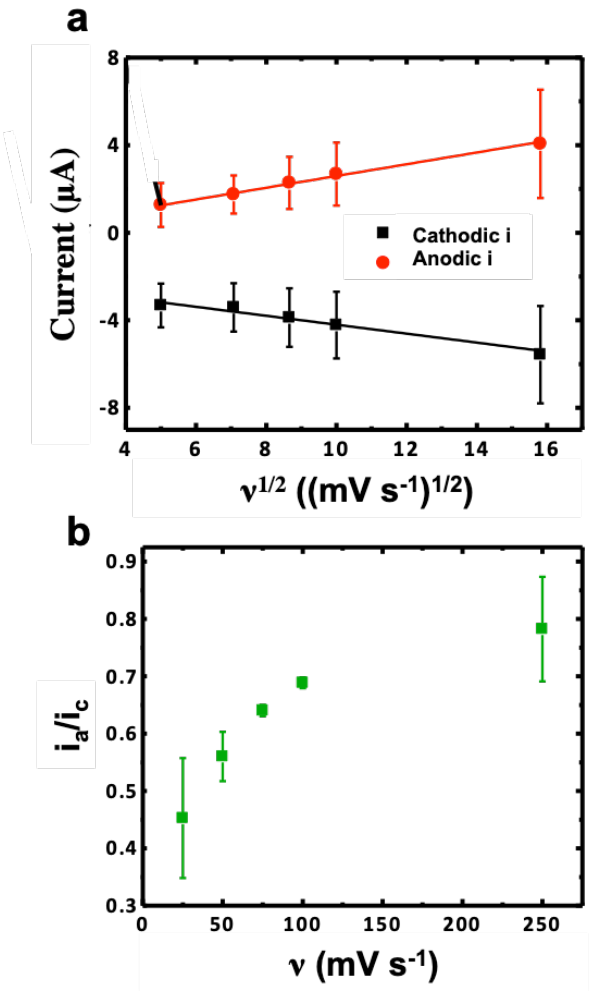

Figure 2.3: Reversibility of PYO redox.

(a) Plot of current responses obtained from cyclic voltammograms as a function of the square root of the scan rate for peak anodic and peak cathodic currents for PYO redox at T-CUA electrode. (b) Ratio of anodic to cathodic currents (i_a/i_c) as a function of corresponding scan rates. This is also depicted in Table 2.1.

ν (mV s^{-1})	i_a/i_c
25	0.4 ± 0.1
50	0.56 ± 0.04
75	0.64 ± 0.01
100	0.69 ± 0.01
250	0.78 ± 0.09

Table 2.1: The scan rate, ν, and corresponding anodic to cathodic current (i_a/i_c) ratio of PYO redox at T- CUA electrode.

2.3.2 Figures of Merit and Electrochemical Characterization of PYO at T-CUA and T-Macro Electrodes

The T-Macro, T-CUA, and CS/GNP T-CUA electrodes were used to detect pyocyanin using SWV (Figure 2.4). Figure 2.4b shows SWV current-potential curves and the corresponding calibration curve (Figure 2.4e) for the T-CUA electrode. The LOD was calculated as 3σ/slope of our calibration curve, utilizing standard approach 1 (SA1).[36] The LDR and LOD for PYO differ for each type of electrode. The determined LOD for the T-Macro is 0.51 μM with a linear range of 0.75– 25 μM, respectively (Figure 2.4a and Figure 2.4d). The LOD for the CS/GNP modified T-CUA is 1.6 μM with a LDR of 1–100 μM, and the LOD of the T-CUA with a LDR of 1–250 μM is 1.0 μM, respectively (Figure 2.4c and Figure 2.4f). The maximum level of pyocyanin produced by wild-type biofilm aggregates is ~2.7 μM.[28,29,37] The concentration of pyocyanin in the sol phase (colloidal solution) of sputa from infected patients has been reported to be in the range of 0.2 to 27.3 μg/ml (1–130 μM) with a median value 1.7 μg/ml (8.1 μM).[14,26,38] Therefore our detection limits are in the range to detect PYO from individual *P. aeruginosa* biofilm aggregates and from the sputa of infected patients. To demonstrate this, we performed *in vitro* studies to probe PYO responses from two different *P. aeruginosa* strains, PA11 and

PA14 (Figure 2.6) using T-CUA electrodes as sensing detectors. The PA14 strain is a wild-type highly virulent *P. aeruginosa* strain,[39] while the PA11 (CEB11) strain is a clinically significant *P. aeruginosa* strain, isolated from cystic fibrosis patient sputum sample.[34] Our results show that after 24 hours of growing cultures at 37 °C, concentrations of secreted PYO were measured to be 50 ± 4 μM and 45 ± 5 μM from PA11 clinical strain, and 6 ± 6 μM and 3 ± 2 μM from wild-type PA14 strain (Figure 2.7a-b, Table 2.2). Furthermore, while performing the electrochemical analyses, we also performed optical bright-field imaging of the two *P. aeruginosa* strains (Figure 2.7c-d) on T-CUA electrodes. These results indicate that we can successfully detect secreted PYO while optically imaging the cells.

The linear range differs between the T-Macro and the T-CUA series. This divergence is primarily related to the varying RC time constants and subsequent response times[40,41] of the electrodes to the PYO redox mechanism. For these electrodes, the inherent response times are predicated upon the resistive and capacitive components of the electrodes. Since all electrodes examined here are constructed from the same electroactive material, PPF, they inherently share the same sheet resistance. Additional solution resistance results from the charge transfer process through the thin carbon film to and from the solution. Thus, increases in carbon area exposed to the solution cause an increase in overall resistance. As a consequence, electrodes with greater exposed carbon (T-Macro electrodes) have higher overall resistance and greater response times than electrodes with less exposed carbon (T-CUA electrodes).[31,32]

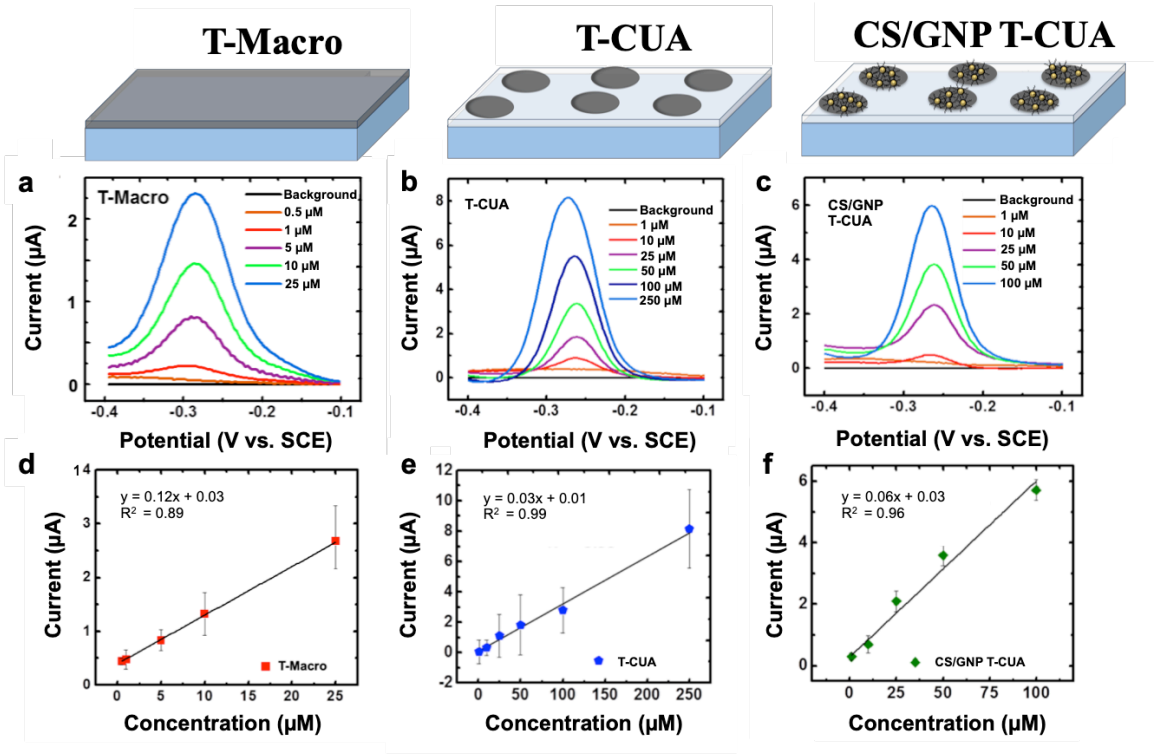

Figure 2.4: Square wave voltammograms and calibration curves for PYO at T-CUA electrodes.

The graphs in the top row depict background corrected square wave voltammetric response curves for various different concentrations of PYO at: (a) T-Macro, (b) T-CUA, and (c) CS/GNP T-CUA electrodes. The bottom row (d–f) shows the corresponding calibration curves.

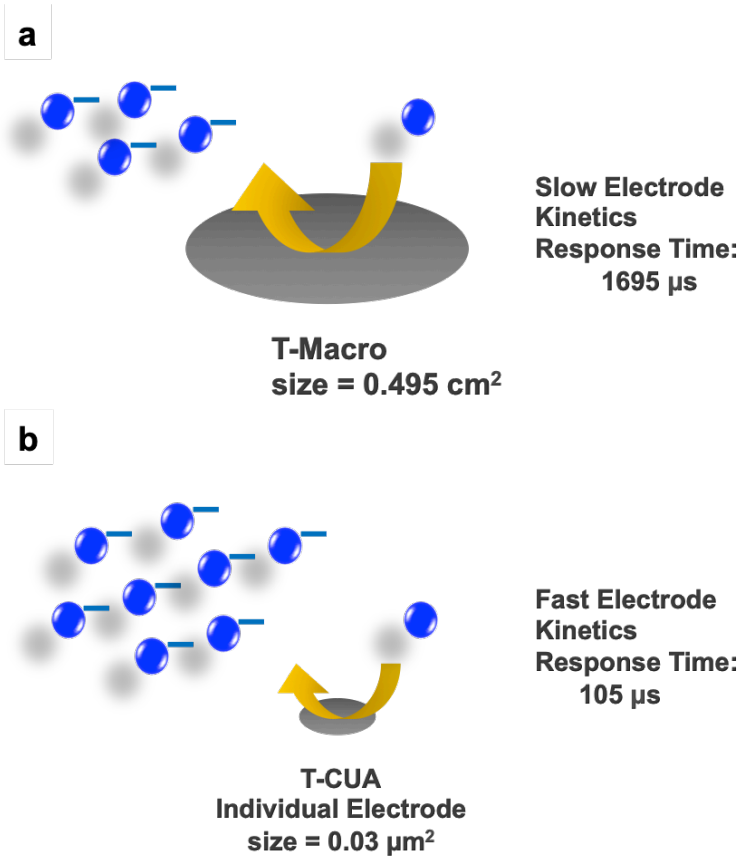

Figure 2.5: Response times at (a) T-Macro and (b) T-CUA relating with linear dynamic range.

Furthermore, the capacitance is correspondingly related to the electroactive area, which is responsible for producing the double layer capacitance. Essential to the RC time constant, the capacitive component plays a prominent role in determining the response time (Figure 2.5).[40,41] As a potential is applied to the electrode, molecules within the solution organize and distribute by charge to create a capacitive double layer. The double layer capacitance increases the thermodynamic barrier consequentially increasing the energy required to transfer charge between analyte and electrode, thus increasing the response time. It follows that as the electroactive area increases the greater the double layer capacitance and the slower the kinetics of charge transfer with the electrode. The faster kinetics permitted at the T-CUA series facilitates a faster conversion of analyte to product at the electrode, increasing the amount of analyte reacting at the electrode over a given amount of time. Therefore, higher concentrations of PYO can be determined by the T-CUA electrode series than the T-Macro, accounting for a larger LDR (Figure 2.4).

The observed linear range of the T-CUA is diminished by the CS/GNP modification, an effect that appears counterintuitive given numerous reports examining the ability of GNPs to enhance the rate of electron transfer.[33] GNPs have been shown to be biocompatible and catalytically selective for biogenic species. Gold is relatively inert activity when in its bulk form; however, when distributed in the form of fine particles with sizes below 10 nm, its catalytic activity increases. This enhancement is associated with the high concentrations of low coordinated active sites on the small nanoparticles surface, allowing GNPs to efficiently facilitate the rate of electron transfer. The method we presently use to modify our electrodes involves the electropolymerization of chitosan, which is a biocompatible polymer with anti-interference character, around GNPs. Chitosan assists the formation of CS/GNPs film on the electrodes by acting as a metal-complexing agent, encapsulating and homogeneously distributing the GNPs on the

electrode surface. Thus, we expected to observe an enriching effect and improved LODs by introducing CS/GNPs modification to the electrodes. However, PYO is a quasi-reversible redox active molecule whose redox mechanism is not entirely dependent on an electron transfer step and involves a chemical intermediates. Therefore the mechanistic ability of GNPs to provide catalytic enhancement as the overall response is limited by bimolecular chemical steps and not electron transfer rates. The CS acts as an insulating layer and the GNPs restore and facilitate the electron transfer to the electrode, but it does not influence the rate of the chemical step or rate-limiting step. Upon modification, the residual electroactive area of the electrode is further decreased to a point at which the rate of electrochemical conversion for PYO is not fast enough to compete with the flux of PYO to the electrode (CS/GNP surface), saturating the electrode and effectively decreasing the linear range. It should be noted that T-CUA geometry does not show the expected improved analytical response and thus a lower LOD compared to the T-Macro. We have previously characterized and determined the critical scan rate of T-CUA using Electrochemical Impedance Spectroscopy (ESI),[30] to be 22 Hz, below which semi-infinite linear diffusion regimes are observed identical to that of T-Macro electrodes. Here, we used a scan rate below the T-CUA critical scan rate, thus T-CUAs do not demonstrate pure ultramicroelectrode behavior. As a result, the LOD of T-CUA is marginally higher compared to T-Macro. It should also be mentioned that the benefit of T-CUA relative to T-Macro also depends on the resistive and capacitive effects introduced by the alumina layer at the T-CUA.[31]

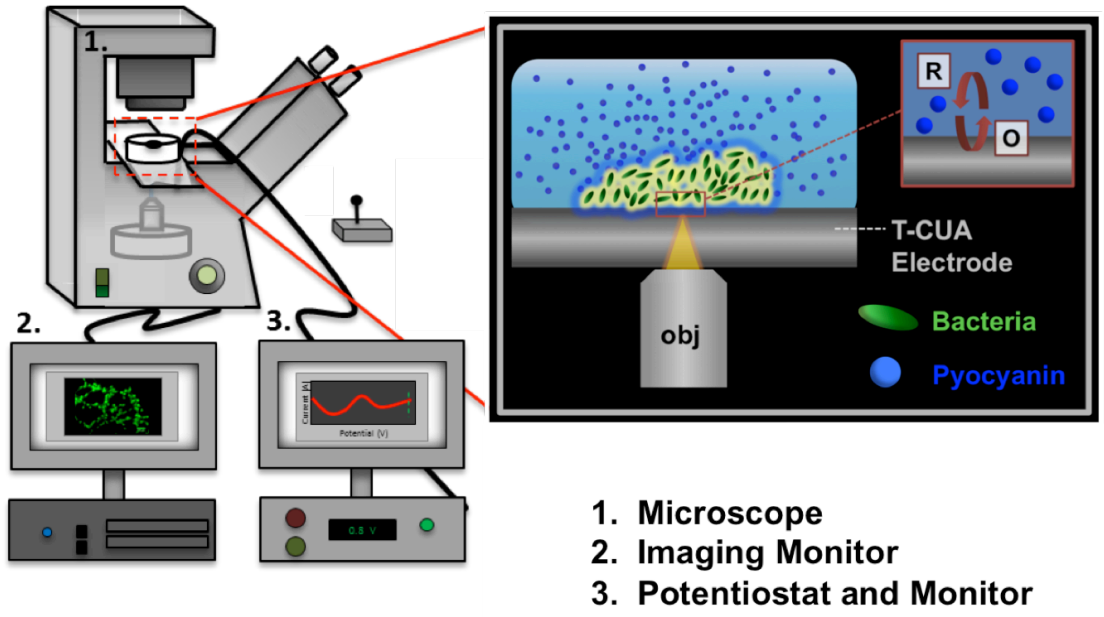

Figure 2.6: Setup of the *in vitro* T-CUA device implementation.

Electrochemical detection of cellularly derived PYO from *P. aeruginosa* strains while concurrently imaging bacterial cells through T-CUA electrodes.

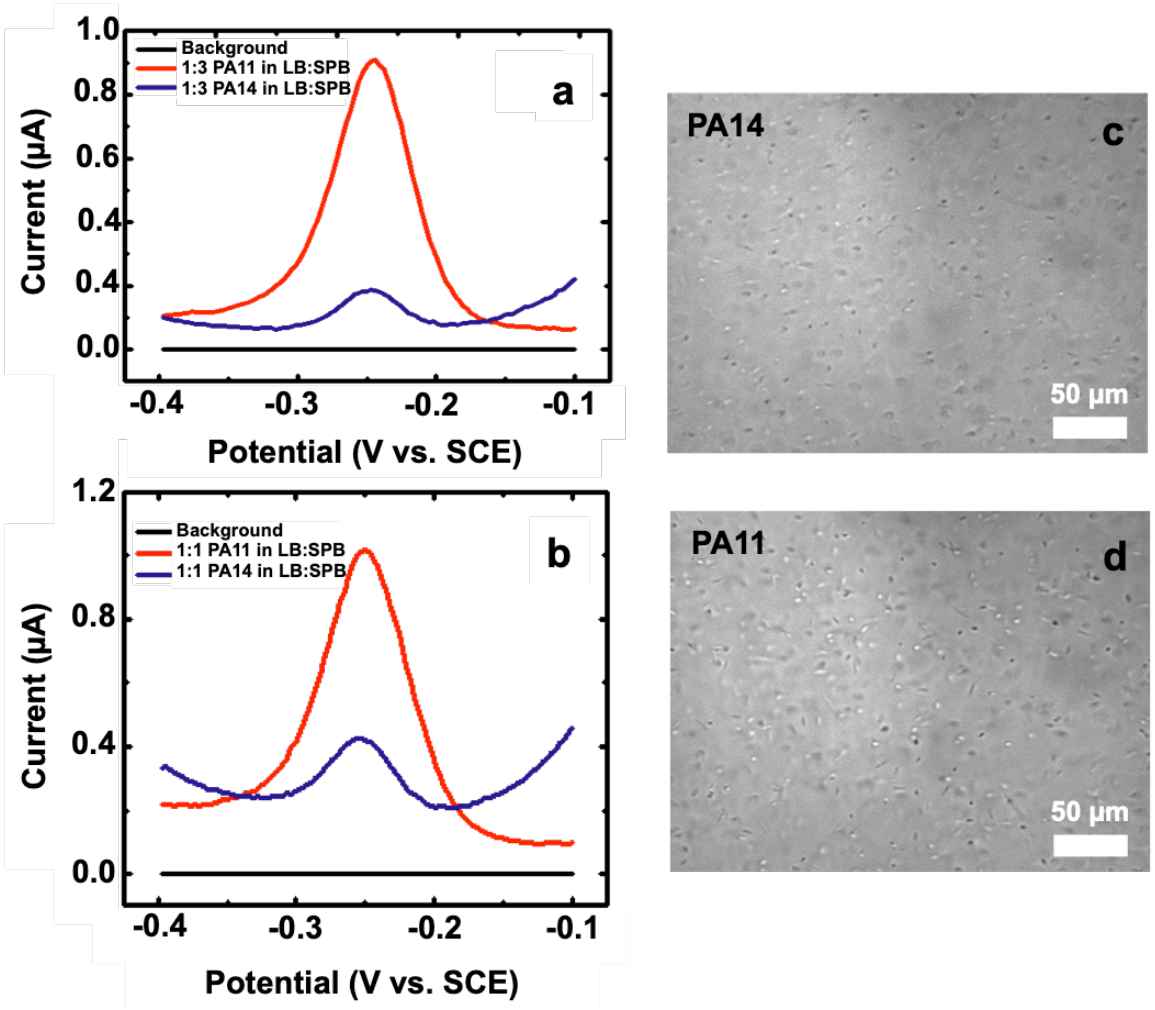

Figure 2.7: Electrochemical detection of cellular PYO from clinical and laboratory bacterial strains while simultaneously imaging cells on T-CUAs.

Background corrected square wave voltammetric responses for cellular PYO from two *P. aeruginosa* strains PA11 and PA14 in (a) 1:3 (v/v) lysogeny broth (LB) to sodium phosphate buffer (SPB) and (b) 1:1 (v/v) LB:SPB. The quantitatively determined PYO concentrations are displayed in Table 2.2. Optical bright-field images of (c) PA14 bacterial strain and (d) PA11 bacterial strain obtained through T-CUA electrodes.

Table 2.3 compares the present work's figures of merit to the previous reported values in the literature. The current LODs and LDRs are compare favorable to those reported using previous PYO detection schemes. T-CUAs have the greatest LDR of all current electrochemical detection schemes. In addition, the electrochemical platform reported here represents a low-cost alternative compared to the other electrochemical methods referenced in Table 2.3, in particular platinum and boron-doped diamond electrodes. Finally, the electrode sensors for PYO here are transparent and planar, enabling concurrent optical studies of cells that will be key to acquiring contextual information for appropriate interpretation of electrochemical data (Figure 2.7).

Bacterial Strain	**PA11**	**PA14**
Pyocyanin concentration in 1:3 (v/v) LB:SPB (μM)	45 ± 5	3 ± 2
Pyocyanin concentration in 1:3 (v/v) LB:SPB (μM)	50 ± 4	6 ± 6

Table 2.2: Concentrations of pyocyanin secreted from *P. aeruginosa* PA11 and PA14 bacterial strains measured using T-CUA electrodes.

Working Electrode	Electrochemical Technique	LDR (µM)	LODs (µM)	Ref.
T-Macro$^{\delta, \varphi}$	SWV	0.75–25	0.75 ± 0.09	This Work
T-CUA$^{\delta, \varphi}$	SWV	1–250	1.0 ± 0.3	
CS/GNP T-CUA$^{\delta, \varphi}$	SWV	1–100	1.6 ± 0.2	
Au$^{\Psi,\varphi}$	SWV	1–100	0.597	[22]
Carbon Fibre tow laminate$^{¥, \varphi}$	SWV	1–100	0.03	[24]
Boron Doped Diamond $^{¥,\varphi}$	DPV	2–100	0.05	[25]
Disposable screen printed electrode, Au$^{\psi,ŧ}$	CV	0–100	2	[23]
Disposable screen printed electrode, Au$^{\psi,ŧ}$	Amperometry	0–90	0.125	[27]

¥ - Ag/AgCl reference electrode, ψ - Ag quasi-reference electrode,
φ - Pt counter electrode, ŧ - Au counter electrode,
Ψ- palladium hydride (PdH) reference electrode, δ- SCE reference electrode

Table 2.3: Comparison of limits of detection (LODs) and linear dynamic ranges (LDRs) of PYO using T-CUAs in comparison to other electrochemical tools used for the electrochemical detection of PYO.

2.4 CONCLUSIONS

The possibility of using transparent carbon ultramicroelectrode arrays (T-CUAs) as an electroanalytical sensing platform for the electrochemical detection of PYO was investigated. The redox activity of PYO at T-Macro and T-CUA electrodes was examined using CV. Using SWV, the detection of PYO at these electrodes was evaluated and LODs and LDRs were determined at each electrode type. The LOD for the T-Macro was determined to be 0.75 ± 0.09 μM with a linear range of 0.75–25 μM. The LOD for the CS/GNP modified T-CUA was 1.6 ± 0.2 μM with a LDR of 1–100 μM, while the LOD for the T-CUA electrode was 1.0 ± 0.3 μM with a LDR of 1–250 μM. Additionally, the determined LDR at the T-CUA electrode was larger than previously reported linear ranges, allowing for detection of higher PYO concentrations. Although our LODs are comparable to other electrodes previously used for the detection of PYO,[22,23,27] they fall within the low- to mid-micromolar range for PYO detection from *P. aeruginosa* organized within individual biofilm aggregates and from infected cystic fibrosis sputum samples.[22-24,26] Thus, this work presents an electrochemical sensing platform that could be useful for monitoring PYO concentrations in *in vitro* and *in vivo* environments, a subject of further investigation. Finally, our method has an additional benefit compared to other electrochemical detection techniques; the T-CUA electrodes transparency provides a means to optically analyze *P. aeruginosa* cell modulation in tandem with electrochemical analyses of cellularly derived PYO, in real time.

2.5 REFERENCES

(1) Alhede, M.; Kragh, K. N.; Qvortrup, K.; Allesen-Holm, M.; van Gennip, M.; Christensen, L. D.; Jensen, P. Ø.; Nielsen, A. K.; Parsek, M.; Wozniak, D.; Molin, S.; Tolker-Nielsen, T.; Høiby, N.; Givskov, M.; Bjarnsholt, T. *PLoS ONE* **2011**, *6*, e27943–12.

(2) Schleheck, D.; Barraud, N.; Klebensberger, J.; Webb, J. S.; McDougald, D.; Rice, S. A.; Kjelleberg, S. *PLoS ONE* **2009**, *4*, e5513–e5515.

(3) Ringen, L. M.; Drake, C. H. *J. Bacteriol.* **1952**, *64*, 841–845.

(4) Walker, T. S. *Plant Physiol.* **2004**, *134*, 320–331.

(5) Fetzer, A. F.; Werner, A. S.; Hagstrom, J. W. *Am. Rev. Respir. Dis.* **1967**, *96*, 1121–1130.

(6) Bedrossian, C. W. M.; Greenberg, S. D.; Singer, D. B.; Hansen, J. J.; Rosenberg, H. S. *Hum. Pathol.* **1976**, *7*, 195–204.

(7) Fick, R. B. *Chest.* **1989**, *96*, 158–164.

(8) Hauser, A. R. *Nature Rev. Microbiol.* **2009**, 654–665.

(9) Woods, D. E.; Iglewski, B. H. *Rev. Infect. Dis.* **1983**, *5*, S715–S722.

(10) Hall, S.; McDermott, C.; Anoopkumar-Dukie, S.; McFarland, A.; Forbes, A.; Perkins, A.; Davey, A.; Chess-Williams, R.; Kiefel, M.; Arora, D.; Grant, G. *Toxins* **2016**, *8*, 236–14.

(11) Lau, G. W.; Hassett, D. J.; Ran, H.; Kong, F. *Trends Mol. Med.* **2004**, *10*, 599–606.

(12) Jayaseelan, S.; Ramaswamy, D.; Dharmaraj, S. *World J. Microbiol. Biotechnol.* **2014**, *30*, 1159–1168.

(13) Dietrich, L. E. P.; Price-Whelan, A.; Petersen, A.; Whiteley, M.; Newman, D. K. *Mol. Microbiol.* **2006**, *61*, 1308–1321.

(14) Wilson, R.; Sykes, D. A.; Watson, D.; Rutman, A.; Taylor, G. W.; Cole, P. J. *Infect. Immun.* **1988**, *56*, 2515–2517.

(15) Reimer, Å. *Acta Otolaryngol.* **2009**, *120*, 86–88.

(16) Cruickshank, C. N. D.; Lowbury, E. J. L. *Brit. J. Exp. Pathol.* **1953**, *34*, 1–6.

(17) Miller, M. B.; Bassler, B. L. *Annu. Rev. Microbiol.* **2003**, *55*, 165–199.

(18) Al-Ani, F. Y.; Al-Shibib, A. S.; Khammas, K. M.; Taher, R. *Folia Microbiolol.* **1986**, *31*, 215–219.

(19) Propst, C.; Lubin, L. *J. Gen. Microbiol.* **1979**, *113*, 261–266.

(20) *Pseudomonas Methods and Protocols*, 1st ed.; Filloux, A., Ramos, J.-L., Eds.; Springer New York: New York, NY, 2014; pp 1–800.

(21) Mavrodi, D. V.; Bonsall, R. F.; Delaney, S. M.; Soule, M. J.; Phillips, G.; Thomashow, L. S. *J. Bacteriol.* **2001**, *183*, 6454–6465.

(22) Webster, T. A.; Goluch, E. D. *Lab Chip* **2012**, *12*, 5195–5197.

(23) Alatraktchi, F.; Breum Andersen, S.; Krogh Johansen, H.; Molin, S.; Svendsen, W. *Sensors* **2016**, *16*, 408–410.

(24) Sharp, D.; Gladstone, P.; Smith, R. B.; Forsythe, S.; Davis, J. *Bioelectrochemistry* **2010**, *77*, 114–119.

(25) Buzid, A.; Shang, F.; Reen, F. J.; Muimhneacháin, E. Ó.; Clarke, S. L.; Zhou, L.; Luong, J. H. T.; O'Gara, F.; McGlacken, G. P.; Glennon, J. D. *Sci. Rep.* **2016**, *6*, 30001–30009.

(26) Webster, T. A.; Sismaet, H. J.; Conte, J. L.; Chan, I.-P. J.; Goluch, E. D. *Biosens. Bioelectron.* **2014**, *60*, 265–270.

(27) Alatraktchi, F. A.; Johansen, H. K.; Molin, S.; Svendsen, W. E. *Nanomedicine* **2016**, *11*, 2185–2195.

(28) Koley, D.; Ramsey, M. M.; Bard, A. J.; Whiteley, M. *Proc. Natl. Acad. Sci. U.S.A.* **2011**, *108*, 19996–20001.

(29) Connell, J. L.; Kim, J.; Shear, J. B.; Bard, A. J.; Whiteley, M. *Proc Natl Acad Sci USA* **2014**, *111*, 18255–18260.

(30) Duay, J.; Goran, J. M.; Stevenson, K. J. *Anal. Chem.* **2014**, *86*, 11528–11532.

(31) Duay, J.; Elliott, J.; Shear, J. B.; Stevenson, K. J. *Anal. Chem.* **2015**, *87*, 10109–10116.

(32) Elliott, J.; Duay, J.; Simoska, O.; Shear, J. B.; Stevenson, K. J. *Anal. Chem.* **2017**, *89*, 1267–1274.

(33) Wang, F.; Deng, X.; Wang, W.; Chen, Z. *J Solid State Electrochem* **2011**, *15*, 829–836.

(34) Darch, S. E.; McNally, A.; Harrison, F.; Corander, J.; Barr, H. L.; Paszkiewicz, K.; Holden, S.; Fogarty, A.; Crusz, S. A.; Diggle, S. P. *Sci. Rep.* **2015**, *5*, 7649–7661.

(35) Bard, A. J.; Faulkner, L. R. *Electrochemical Methods Fundamentals and Applications*, 2nd ed.; Harris, D., Ed.; John Wiley & Sons, Inc., 2001; pp 1–850.

(36) Mocak, J.; Bond, A. M.; Mitchell, S.; Scollary, G. *Pure & Appl. Chem.* **1997**, *69*, 297–328.

(37) Bellin, D. L.; Sakhtah, H.; Rosenstein, J. K.; Levine, P. M.; Thimot, J.; Emmett, K.; Dietrich, L. E. P.; Shepard, K. L. *Nat. Commun.* **2014**, *5*, 3256–3265.

(38) Muller, M. *Free Radical Biology and Medicine* **2006**, *41*, 1670–1677.

(39) Mikkelsen, H.; McMullan, R.; Filloux, A. *PLoS ONE* **2011**, *6*, e29113–e29117.

(40) Zoski, C. G. Handbook of Electrochemistry. Elsevier, **2006**.

(41) Orwiler, B. Oscilloscope Vertical Amplifier Circuit Concepts © Tektronix **1969**, 1–467.

Chapter 3: Real-time Electrochemical Detection of *Pseudomonas aeruginosa* Phenazine Metabolites using Transparent Carbon Ultramicroelectrode Arrays[3]

3.1 INTRODUCTION

The detection, identification, and monitoring of severe infectious diseases in host organisms by pathogenic bacteria remains a major challenge[1-3] as infections spread through specific entities (e.g., hospitals) when the hosts (e.g., patients) make contact with bacterial communities. One microorganism responsible for the majority of hospital-acquired infections is the opportunistic human pathogen *Pseudomonas aeruginosa*, which causes a significant increase in morbidity and mortality rates.[4-6] Although this pathogen is rarely the source of microbial diseases in healthy individuals, it successfully establishes infections in patients with compromised immune systems and suffering from conditions such as cystic fibrosis, severe burns, and chronic wounds.[7-11]

In hospital diagnosis, to confirm presence of *P. aeruginosa* in samples from patients, specimens are typically grown on agar plates with selective growth components to specifically target the bacterial strain, however, this process requires several days. As a result, patients with symptoms are treated with broad-spectrum antibiotics, which leads to increased antibiotic resistance,[12] making *P. aeruginosa* infections difficult to treat. Therefore, understanding early stages of infection is necessary as it could point to more effective treatments. To avoid time-consuming diagnostics, a variety of electrochemical sensing techniques have recently been established as popular alternatives to standard

[3]Adapted with permission from Simoska, O.; Sans, M.; Fitzpatrick, M. D.; Crittenden, C. M.; Eberlin, L. S.; Shear, J. B.; Stevenson, K. J. Real-time Electrochemical Detection of *Pseudomonas aeruginosa* Phenazine Metabolites using Transparent Ultramicroelectrode Arrays. *ACS Sensors* **2019**, *4*, 170–179. Copyright © 2019 American Chemical Society. Simoska, O. acquired the data, wrote the manuscript, and performed electrochemical measurements/characterization. Simoska, O., Crittenden. C. M., and Sans, M. performed mass spectrometry experiments. Simoska, O. and Stevenson, K. J. designed studies, planned experiments, and analyzed all data. All authors contributed in editing the manuscript.

spectrophotometric and molecular pathogen detection approaches due to their enhanced sensitivity, rapid response times, and simplicity of operation.[5,13] In addition to electrochemical sensors, several optical sensing methods have been developed for analysis of *P. aeruginosa*. Both optical and electrochemical sensors are relatively non-invasive with biological systems. While optical sensors can provide a means for spatial analysis of cells, they have several limitations. In particular, they involve the use of expressed fluorescent protein reporters,[14,15] which have time delays associated with production of detectable signal, and are limited by nonspecific reactivity. On the other hand, electrochemical sensors can directly detect and rapidly quantify critical components, including cellular signaling species and metabolites, with high sensitivity. As a result, various electrochemical methods have successfully used voltammetry[16-19] and amperometry[4] for detection and quantification of *P. aeruginosa* toxins. However, none of these methods have demonstrated *in situ*, real-time detection of biogenic species from true, unperturbed *P. aeruginosa* cell cultures in simulated cell growth media. In addition, spatially resolved detection of phenazine metabolites from *P. aeruginosa* biofilm surfaces has been performed by very specialized techniques such as scanning electrochemical microscopy[20,21] and integrated-circuit based electrochemical chips.[22,23] However, these approaches involve quite costly and highly specialized equipment and expertise to perform quantitative studies.

Our group has recently reported a low-cost, facile and versatile method to design transparent carbon ultramicroelectrode arrays (T-CUAs),[24] which offer several advantages to other electrochemical detection methods. T-CUAs provide the benefits of microelectrodes, but have an additional advantage of amplified currents due to the individual electrodes in the array functioning in a parallel circuit.[24] Their nanometer sizes permit measurements on smaller samples in biological environments with fast response

times.[24,25] Furthermore, their small electroactive area allows for lower background currents to be achieved, thus resulting in higher signal-to-noise (S/N) ratios and lower limits of detection (LODs) with large linear dynamic ranges (LDRs).[24] Since T-CUAs are constructed of primarily glassified carbon, they are chemically stable, very conductive, and highly biocompatible.

In a previous study, we characterized T-CUAs analytical responses to hydrogen peroxide (H_2O_2),[26] a biogenic metabolite produced by pathogenic bacterium *Streptococcus gordonii*. Additionally, we have previously presented successful modification of T-CUAs for the detection of cellularly derived nitric oxide ($NO^{\bullet}$), a biogenic signaling molecule produced by host cells like macrophages.[25] Moreover, we have recently used T-CUAs to determine the figures of merit for pyocyanin (PYO),[27] a redox-active bacterial toxin, which engages in chemical warfare with the immune system (Chapter 2). PYO is secreted by 96-98% *P. aeruginosa* strains[28,29] and its redox state has important implications about its biological activity.[20,30-34] Using square wave voltammetry (SWV), the LOD was determined to be 1.0 ± 0.3 μM with the largest reported linear dynamic range (LDR) of 1–250 μM, which allows detection of higher concentrations of cellular PYO.[27] Importantly, these fall within the reported range of PYO concentrations (1–130 μM)[35] from sputa isolated from lungs of cystic fibrosis patients.[27] Additionally, we successfully used T-CUAs to detect PYO from laboratory and clinical *P. aeruginosa* strains (Chapter 2).[27]

P. aeruginosa produces biotoxins as virulence factors,[36] including various phenazine metabolites. Although phenazines play significant roles in cellular functions and *P. aeruginosa* virulence mechanisms, little is known about how their concentrations vary and direct cellular behavior over time. Here, we demonstrate use of T-CUAs for the sensitive, continual, real-time, electrochemical monitoring of phenazine metabolites

secreted from wild type *P. aeruginosa* strain (PA14), over a 48-hour period. Our results show an increase in electrochemical current responses for PYO in the first 21 h, after which the cells secrete similar levels of PYO. At intermediate stages of growth, we also observe an increase in production of 5-MCA, an extremely reactive phenazine species[37] and a precursor to PYO.[38] Additionally, the metabolism dynamics in different growth media are quite distinct, which is reflective of the heavy influence of various broth components. Therefore, distinctive PYO concentration fluctuations at different time points are observed. In addition to changes in current responses of PYO, we observed dynamic changes in the detection of 5-MCA. While the electrochemical signature of 5-MCA has been previously detected from wild type and mutant PA14 strains, its identity has only been speculated due to its reactive nature.[22,23,39] Here, we used nano-electrospray ionization tandem mass spectrometry (nano-ESI MS/MS) to confirm its detection and identity. Additionally, we performed desorption electrospray ionization mass spectrometry imaging (DESI-MSI) in tandem with electrochemical measurements at various time points, which show correlations between levels of cellular PYO.

3.2 Experimental Methods

3.2.1 General

All chemicals were used as received. Photoresist AZ 1518 was purchased from Microchemicals. Polystyrene spheres (Polybead®) with a diameter of 1.54 μm were purchased from Polysciences, Inc. Pyocyanin (PYO) was purchased from Cayman Chemical Company. Ethanol and Lysogeny Broth (LB) Lennox were purchased from Thermo Fisher Scientific Inc. Acetone, 2-Propanol, and Carbenicillin Sodium Salt, were acquired from Sigma-Aldrich Co. Bacto Tryptic Soy Broth (TSB) and Tryptic Soy Agar

(TSA) were purchased from Becton, Dickinson, and Company and from Remel, respectively.

3.2.2 Cell Culture and Optical Density

Wild-type *Pseudomonas aeruginosa* strain PA14 was used, carrying pMRP9-1, a constitutive green fluorescent protein (GFP) expressing plasmid. PA14 was cultured from a freezer stock on TSA plates containing 10 μg/mL carbenicillin sodium salt (carb10) to maintain the plasmid. Using PA14 cells initially grown on TSA agar plates, overnight liquid cultures were prepared by inoculating 75 cm^2 tissue culture flasks with vented caps filled to a volume of 75 mL with LB and TSB, respectively, using sterile wooden dowels. These samples were left to shake in a 37 °C incubator for 18 h at 150 rpm. The optical densities (ODs) of these solutions were then determined using an Agilent Instrument 8453 UV–vis–NIR spectrophotometer by recording the absorbance at 600 nm. These samples were subsequently diluted into 250 mL Erlenmeyer flasks to achieve an OD of 0.15 at 600 nm with a volume of 125 mL with TSB and LB, respectively. Cell cultures were shaken for another 2 h at 37 °C to achieve exponential phase, which is indicated as t=0 h. OD measurements were performed alongside electrochemical square wave voltammetry (SWV) measurements for 48 h starting at 0 h. All ODs were set to standard method at 600 nm. Blanks were taken using either TSB or LB and for each of the two cultures, three cuvettes were sampled from the main flask at each time point against the appropriate blank. Flasks were removed from the 37 °C shaker for only the brief time needed to transfer liquid culture into the cuvettes to minimize disruption of cell growth. Finally, pH measurements were taken at each time point using a pH electrode connected to a portable pH meter (VWR Scientific pH Meter Model 8005).

3.2.3 Fabrication of T-CUA Electrodes

Preparation of transparent carbon ultramicroelectrode arrays (T-CUAs) follows previously described procedures.[24–27] Quartz microscopic slides (6.45 cm^2 and 1 mm thick, Technical Glass Products) were treated with piranha (3:1 H_2SO_4: 30% H_2O_2) to remove any organic contaminants. A 1:3 dilution of AZ 1518 photoresist with PGMEA (1-methoxy-1-propanol acetate) was spun onto the piranha cleaned quartz slides at 6000 rpm for 60 s. Following spin coating, the photoresist slides were soft baked at 90 °C for 10 min and then transferred to a tube furnace. After 15 min of purging with 5% H_2: 95% N_2 (~100 mL/min), the photoresist slides were pyrolized by heating to 1000 °C at 5 °C/min and holding at that temp for 1 h before allowing them to cool slowly back to room temperature at 5°C/min. The pyrolized photoresist film (PPF) slides were then removed from the furnace and stored for 3 days prior to use to allow for the oxide layer to stabilize. T-CUAs fabrication involved a lithography method using polystyrene microspheres (PSS) with a diameter of 1.54 μm, which were drop cast from a 5.4 wt % methanol suspension onto the conductive PPF electrodes. The organization of the spheres is that of a hexagonal close-packed two-dimensional ordered network. After this microsphere lithography step, 10 nm of Al_2O_3 layer was deposited via atomic layer deposition (ALD) technique at 80 °C. The ALD process was calibrated by the manufacturer (Cambridge Nanotech Savannah 100) to deposit 0.089 nm conformal Al_2O_3 layer per cycle. Thus, cycling this process for 112 times formed a 10 nm ALD layer. This ALD step is then followed by removal of PSS via sonication with methanol, acetone, isopropanol and water. Disk-shaped carbon areas remained where the PSS made contact with the PPF, thus forming a carbon ultramicroelectrode array. Details on characterization of T-CUA electrodes have been reported in previous research studies from our group.[24–27]

3.2.4 Preparation of Standard Pyocyanin Solutions

For calibration curves of PYO in TSB and LB, a 2 mM PYO stock solution was prepared in ethanol and was then diluted to make a 500 μM stock solution in either TSB or LB broth. From the 500 μM stock solution respective PYO standard solutions were prepared to have the following concentrations: 1 μM, 5 μM, 10 μM, 25 μM, 50 μM, 75 μM, 100 μM, 150 μM and 250 μM, in either LB or TSB.

3.2.5 Electrochemical Measurements

Electrochemical measurements were performed using a three-electrode cell system. Electrochemical experiments including square wave voltammetry (SWV) and cyclic voltammetry (CV) were performed using an Autolab PGSTAT30 potentiostat. T-CUA was used as the working electrode with a total geometric area of 0.495 cm^2, defined by the electrode area exposed to a solution in a homemade Teflon electrochemical well. A gold wire electrode was used as the counter electrode and saturated calomel electrode (SCE) was used as the reference electrode. SWV measurements were performed using a current sensitivity of 5 μA, 3 mV step potential and a frequency of 15 Hz. The potential window ranged from –0.7 to 0.0 V vs SCE. CVs were carried at scan rates of 25, 50 and 100 mV s^{-1} to check for PYO polymerization on T-CUA. The background solutions used were TSB and LB. After a background SWV or CV curve was collected using a total of 20 scans, subsequent PYO measurements were obtained. For the real-time electrochemical detection of PYO from PA14 in LB and TSB growth media, all liquid-batch cell samples were incubated at 37 °C and shaken at 150 rpm for the duration of the experiments (48 h). For each electrochemical measurement, 800 μL of each liquid culture were placed onto T-CUA electrodes to immediately perform SWV measurement, detecting PYO from *P. aeruginosa* at different time points. For the first 12 h of

experiments, SWV measurements were taken every hour, followed by every three hours until 24 h, and finally followed by every six hours until 48 h of bacterial growth.

3.2.6 Mass Spectrometry for Identification of 5-methylphenazine-1-cabocylic acid (5-MCA)

Mass spectrometry (MS) analysis was used to confirm identity of 5-MCA phenazine species. Samples were prepared from PA14 cell cultures in LB and TSB grown to 6 hr. At 6 h, 1 mL of each cell culture, in LB and TSB, was placed in a centrifuge tube equipped with 0.2 μm pore filters to separate cells from growth media. Electrochemical measurements, as described previously, were carried using the growth media separated from cells to confirm the presence of PYO and 5-MCA in samples before MS analysis. Samples were then infused into a Thermo Scientific Velos Pro dual linear ion trap mass spectrometer (San Jose, CA) via a pulled borosilicate glass emitter coated in Au/Pd with an outer diameter of 1.2 mm and a tip of less than 1 μm in diameter. A source voltage of 1.2 kV (both in the positive and negative polarity) was applied and the capillary temperature was held at 275 °C for optimal spray stability. To further characterize the sample, tandem mass spectrometry (MS/MS) was performed on the precursor ion to confidently assign structure. Collisional-induced dissociation (CID) was performed with normalized collision energy (NCE) of 20-30% with a *q*-value of 0.25 and an isolation width of 1.5 *m/z*. A maximum ion injection time of 100 ms was utilized and the automated gain control (AGC) target for the MS^2 experiments was held at 1×10^4.

3.2.7 Desorption Ionization Mass Spectrometry Imaging (DESI-MSI)

For DESI-MSI experiments, a 20 μL drop of bacterial growth broth was allowed to dry on air for about an hour. Media and cell aliquots (10-20 μL) were deposited onto well microscope slides and allowed to dry for 50 to 90 minutes in the fume hood prior to

analysis. Note that drying time was dependent on sample volume. Cells grown in LB and TSB media were analyzed at various different growth times. A 2D Omni Spray (Prosolia Inc.) coupled to an LTQ-Orbitrap Elite was utilized for the DESI-MS imaging experiments. Both negative and positive ion modes were used from *m/z* 100 to 400, using a hybrid mass spectrometer that allows for tandem MS experiments using both CID and HCD methods, high mass accuracy (<5 ppm mass error), and high mass resolution (60,000 resolving power) measurements. A spatial resolution of 200 μm was used and ion images were assembled using Biomap software. A 1:1 (v/v) mixture of acetonitrile (ACN) and dimethylformamide (DMF) was used for negative ion mode analysis, at a flow rate of 2 μL/min. For positive ion mode analysis, pure ACN was used, at a flow rate of 5 μL/min. The N_2 pressure was set to 185 psi.

3.3 Results and Discussion

3.3.1 Biosynthetic Route of Phenazine Metabolites in *P. aeruginosa*

The opportunistic human pathogen *P. aeruginosa* secretes small redox-active metabolites known as phenazines, which are nitrogen−containing heterocyclic pigments.[38,40,41] These metabolites are known for their ability to engage in redox cycling processes in the presence of molecular oxygen and reducing agents, such as NADH and NADPH, causing generation of reactive oxygen species (ROS), including toxic hydrogen peroxide and superoxide in host organisms and tissue.[38,41] Due to their small sizes and similar physiological properties, phenazine species facilitate electron transfer and cross cell membranes, transferring content from inside the cell to the extracellular environment.[42] In addition, phenazines act as signals that regulate gene expression, contributing to survival of pathogenic species. In *P. aeruginosa*, the core biosynthetic genes encode various terminal-modifying enzymes, resulting in production of phenazine

derivatives.[41] Wild type *P. aeruginosa* PA14 produces various phenazine derivatives, including phenazine-1-carboxylic acid (PCA), pyocyanin (PYO) and 5-methylphenazine-1-carboxylic acid (5-MCA).[38] Among these species, cellular PYO is essential for generation of disease symptoms,[43] therefore, previous studies have explored its biosynthetic pathway.[38] As shown in Figure 3.1a, the synthetic pathway begins with chorismic acid, which yields PCA via the phenazine biosynthetic enzymes PhzA-G. The following step involves the N-methylation of enzyme PhzM, which then converts PCA to 5-MCA, a highly reactive and unstable intermediate.[37] Finally, 5-MCA is converted to PYO by monooxygenase PhzS. The minor differences between functional groups surrounding the core phenazine structure have an effect on chemical properties and redox activity of each species (Figure 3.1b). Previous studies have made efforts in examining steps of this biosynthetic route, however little is known about the dynamics of the conversion process from PCA to PYO.[44] In this study, we show the use of T-CUAs for simultaneous electrochemical detection of two phenazine species, 5-MCA and PYO, from wild type *P. aeruginosa* PA14 liquid-batch cultures and provide temporal evidence about metabolite dynamics of phenazine biosynthesis.

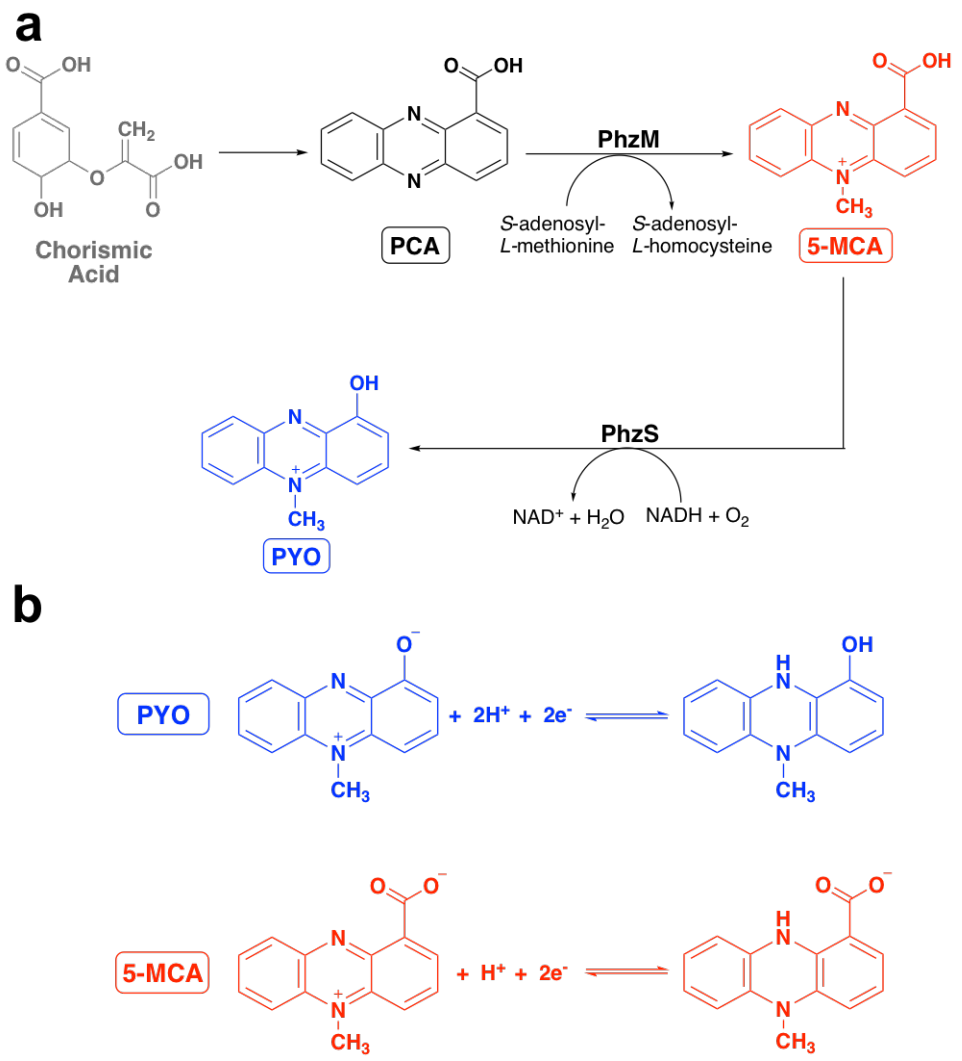

Figure 3.1: Representation of the biosynthetic *P. aeruginosa* phenazine pathway.

(a) Biosynthesis and signaling pathway of PYO. The arrows are marked with the enzymes acting as catalysts for the shown conversion reactions. (b) Redox reactions for PYO and 5-MCA.

3.3.2 T-CUAs for the Electrochemical Detection of PYO in Biologically Relevant Media

Previously, we have reported T-CUAs analytical figures of merit and for PYO,[27] however, these studies were performed in a simple buffer with no growth media. While the direct detection of PYO in buffer solutions is significant, detection of cellular PYO in biologically relevant growth media is key as bacterial species are exposed to a plethora of compounds (e.g., sugars and proteins) that could adsorb onto the working electrode surface and possibly hinder the detection, identification, and quantification of certain metabolites of *P. aeruginosa*. In order to quantify secreted PYO levels from wild type PA14 on T-CUAs, we constructed calibration curves using square wave voltammetry and various PYO concentrations in two biological growth media, tryptic soy broth (TSB) and lysogeny broth (LB). TSB and LB are both nutritionally rich liquid media, which support the growth of various microbial species, in particular, common aerobic bacteria such as *P. aeruginosa*. Figure 3.2 shows background subtracted square wave current-potential curves for biological concentrations of PYO in TSB and LB (Figure 3.2a,b) and corresponding calibration curves (Figure 3.2c,d). Using standard approach 1 (SA1),[45] LODs were determined as 3σ/slope from calibration curves to be 1.0 ± 0.8 μM and 1.0 ± 0.3 μM for PYO in TSB and LB, respectively. The LODs (Table 3.1) determined in these biologically relevant environments are in agreement with our previously reported LODs in sodium phosphate buffer,[27] indicating good sensitivity and resistance to biofouling on T-CUA electrode surfaces that can significantly affect quantification. Additionally, our previously reported linear dynamic range (LDR) remains the same,[27] ranging from 1–250 μM, in both LB and TBS. This LDR is the largest compared to those of other electrochemical sensing platforms reported to date[27] and falls within the determined micromolar range for PYO concentrations from *in vitro* cellular environments.[46]

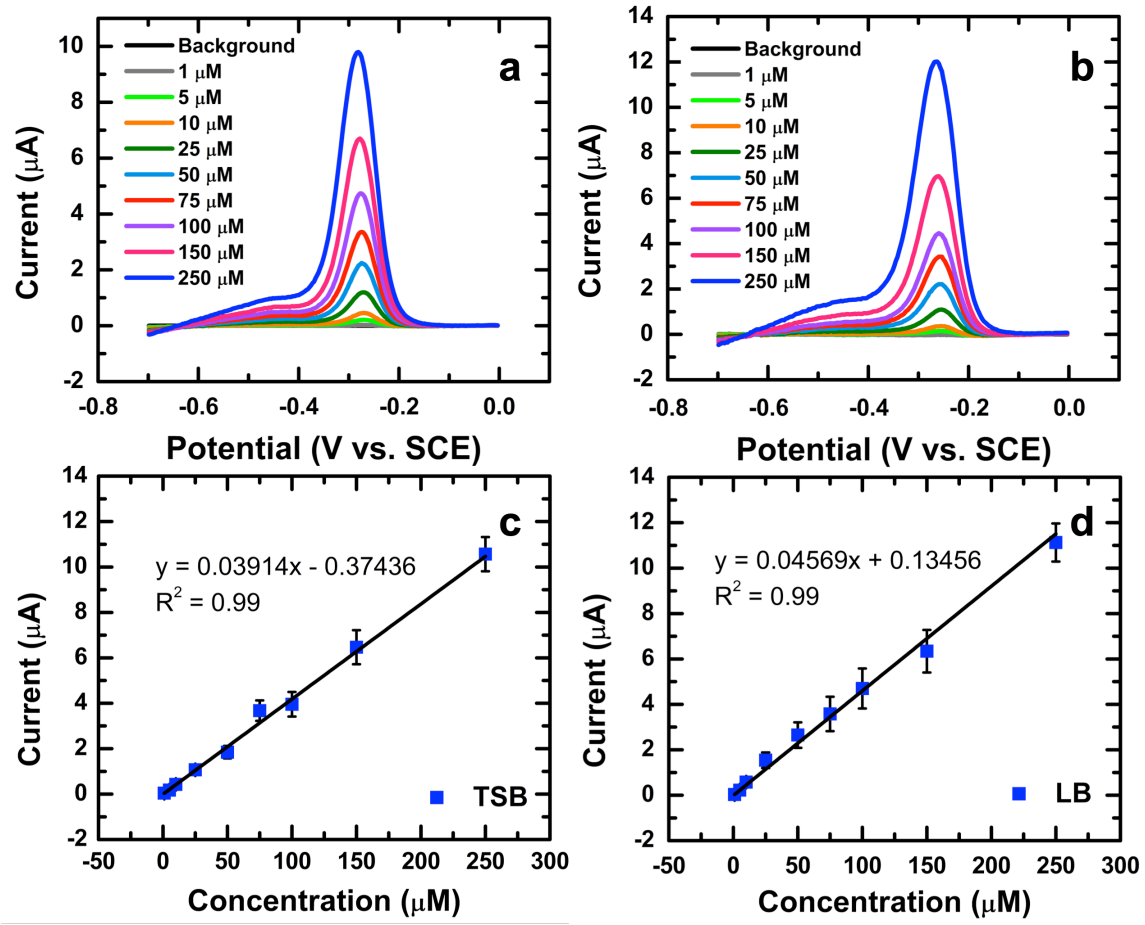

Figure 3.2: Square wave voltammetric responses and calibration curves for PYO in TSB and LB growth media.

Square wave voltammetric studies (background corrected) for various concentrations of PYO in (a) TSB growth media, and (b) LB growth media. Corresponding calibration curves, shown in (c) and (d), are used to quantify concentrations of PYO secreted from P. aeruginosa cell cultures.

Biological Sample	Sensitivity (nA/μM)	LOD (μM)
Tryptic soy broth (TSB)	39 ± 2	1.0 ± 0.8
Lysogeny broth (LB)	46 ± 4	1.0 ± 0.3

Table 3.1: PYO detection in biological growth media using T-CUAs.

Different from our previous study (Chapter 2), here, we extended the potential window (−0.7 to 0.0 V vs SCE) for PYO detection in order to observe changes in other phenazine derivatives from *P. aeruginosa*. PYO is known to undergo a non-reversible phenolic oxidation, forming a polymerization product that can influence the detection and quantification of PYO. We have previously shown that this polymerization process can be avoided by reducing the potential window to −0.4 to −0.1 V vs SCE.[27] Using cyclic voltammetry, we performed tests in both TSB and LB and successfully confirmed that no PYO polymerization reaction takes place in this new potential window (Figure A1.4), and the redox couple detected is entirely due to conversions between soluble, monomeric species of PYO. Additionally, we determined that it takes a total of 20 background scans, in both TSB and LB, to establish a consistent double layer capacitance on T-CUAs (Figure A1.5). Moreover, T-CUA electrode surfaces are comparable to glass, thus they are extremely biocompatible (Figure A1.6) and are not prone to biofouling. These results indicate that PYO production can be quantitatively detected, in real time, with T-CUAs in complex growth media of biological significance.

3.3.3 Real-time Electrochemical Monitoring of *P. aeruginosa*

The major aim of this study was to use T-CUAs as bioanalytical sensing platforms for the time-based, continual electrochemical detection of cellularly derived phenazine metabolites from *P. aeruginosa* in TSB and LB growth media, monitored over a 48-hour period. Among these phenazine species is PYO, which is exclusively secreted by *P. aeruginosa* during early stages of infection,[40] and as such it has been considered an effective diagnostic biomarker for infections caused by this microorganism.[30] Consequently, there has been a significant amount of research dedicated to designing sensors for the detection of this biogenic species of interest,[4,16,17,27,47-49] however, no studies to date have explored how the relative concentrations of cellular PYO change at numerous points during a longer time-frame. The real-time, *in vitro* detection of PYO enables us to monitor *P. aeruginosa* virulence, thus providing fundamental information about pathogenic responses to environmental factors, such as levels of molecular oxygen.

A major concern with use of electrochemical sensors is the working electrode's ability to differentiate phenazine species from interferents. In this application, components in the growth media and cellularly derived species (e.g., glucose, NAD, NADH, NADP, NADPH, pyoverdine) could interfere with the sensor's response in potential window where phenazine redox peaks are observed. Previous research showed that these common interferents have positive redox potentials,[4] which fall outside of the potential window used. Additionally we tested 100 μM solutions of glucose, gluconic acid, NADH, NAD, NADP, NADPH, and H_2O_2 in LB, which confirmed that these interferents do not show redox activity in potential range (−0.7 to 0.0 V vs SCE). Our results in Figure 3.3 demonstrate that the notable electroactive peaks result from phenazine metabolites, which we confirm with mass spectrometry analyses.

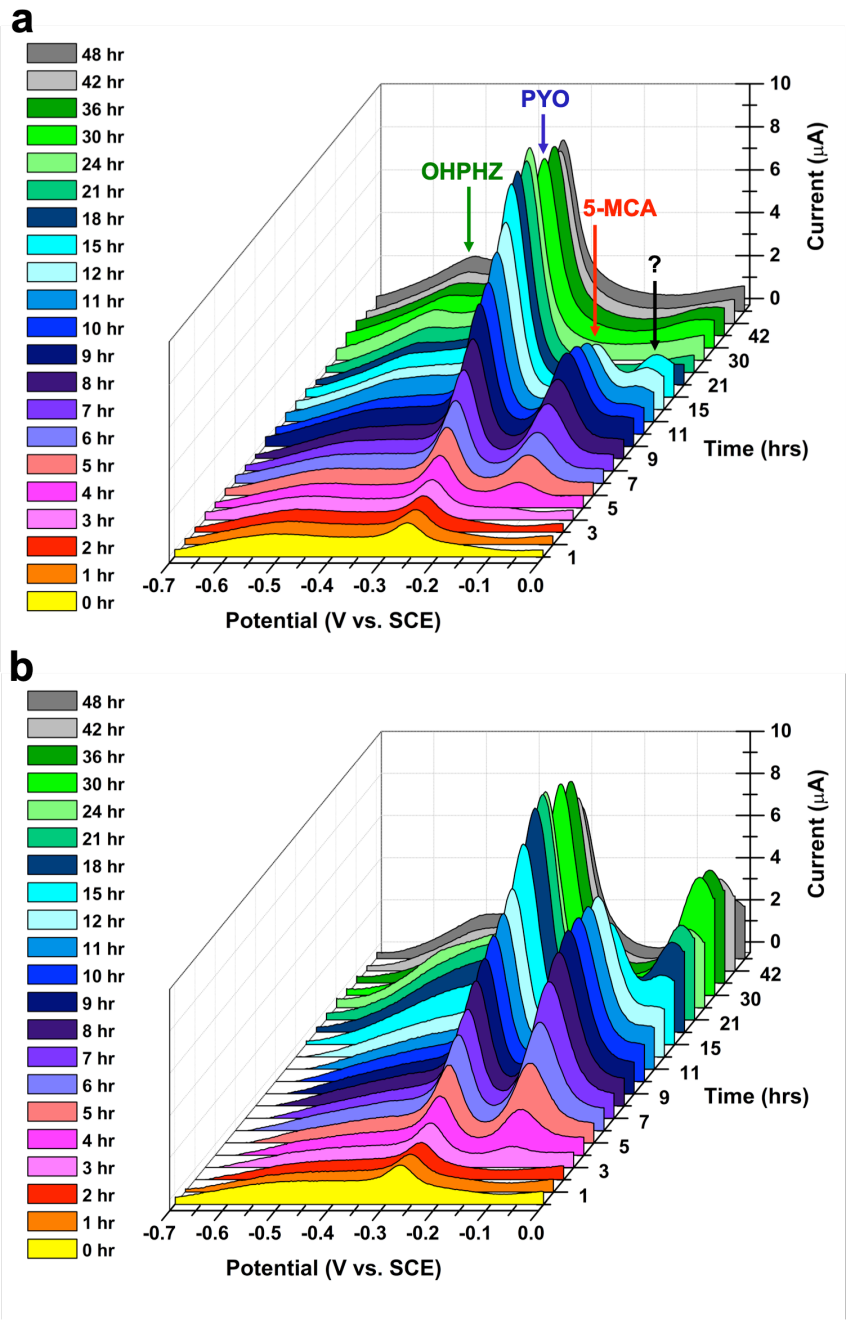

Figure 3.3: Time-dependent square wave voltammetric studies conducted for 0–48 h in (a) LB growth media and (b) TSB growth media. The peak at −0.256 V vs SCE is due to PYO oxidation, while the emerging peak at a more positive potential (−0.115 V vs SCE) is due to 5-MCA phenazine oxidation.

Liquid-batch cultures of wild type *P. aeruginosa* PA14 in TSB and LB were grown at 37 °C and 150 rpm over the course of two days, during which concentrations of cellular PYO were monitored (Figure 3.3). Using square wave voltammetry, the production of PYO was monitored directly from bacterial cultures every hour during the first 12 h of bacterial growth, then every three hours for the next 12 h, followed by every six hours until 48 h. The data were analyzed using background-subtraction (background was either TSB or LB) to determine the concentration of PYO in each growth media (Figure 3.2b, Table S1) using the respective calibration curves (Figure 3.2). The redox-active peak around −0.256 V vs SCE identifies the presence of PYO (Figure 3.3, Figure 3.1). To demonstrate reproducibility, real-time electrochemical measurements of cellularly derived PYO were made a total of nine times in each growth media, thus error bars reported represent standard deviation between nine samples (Figure 3.4). Contrary to other carbon electrodes, which require the use of a fresh electrode for each measurement, T-CUAs can be reused for numerous measurements. Note that for each 48-hour electrochemical measurement, the same T-CUA sensor was used to constantly monitor cellular PYO for the entire duration of each experiment. Additionally, T-CUAs utilized in 48-hour tests can be successfully used again because the SWV background current responses are nearly identical pre- and post-48-hr studies (Figure A1.5).

While performing electrochemical detection, we also acquired optical density measurements (absorbance at 600 nm) of samples to monitor growth stages of bacteria in TSB and LB. Figure 3.4a shows the bacterial growth curves during the 48-h period, which have a fairly sigmoidal character. Briefly, during the first 4 hours (0–3 h), bacteria are in exponential phase, followed by the stationary phase where the curves start to plateau. During the stationary phase, the number of viable bacteria remains unchanged, which means that the rate of bacterial growth equals the rate of bacterial death. Bacteria

grown in LB media show marginally higher optical densities compared to those in TSB for the first 12 h, after which optical densities of cells in TSB are higher than those in LB.

Figure 3.3 displays resulting square wave voltammetry current–potential responses as a function of time. The determined PYO concentrations at different time points in both TSB and LB are summarized in Table A1.1. During the exponential phase of bacterial growth (0–3 h), the concentrations of PYO remain fairly constant. During this growth phase, concentrations secreted in LB media are almost twice as high compared to TSB. Once in stationary phase, PA14 start producing higher levels of PYO, which increase over time until 21 h, after which PYO levels slightly decrease and plateau in both media. At 21 h, PA14 strains produce maximum PYO concentrations of 190 ± 5 μM and 150 ± 1 μM in TSB and LB, respectively. Note that from 4–12 h, there is not a significant difference in PYO concentrations when comparing TSB and LB media. Yet after 15 h, PYO concentrations in TSB are approximately 1.3 times higher than those in LB (Figure 3.4b, Table A1.1). These differences are likely the result of distinctive composition of media (Figure A1.8, Table A1.3, Table A1.4) and changes in phenazine production dynamics, which is discussed in detail in the next sections. These results show an increase in PYO production rates in two media during the first 21 h, which is likely due to increased intercellular communication during the exponential phase of bacterial growth. After 21 h, PYO levels slightly decrease, indicating a decrease in virulence factor production after prolonged growth in the stationary phase.

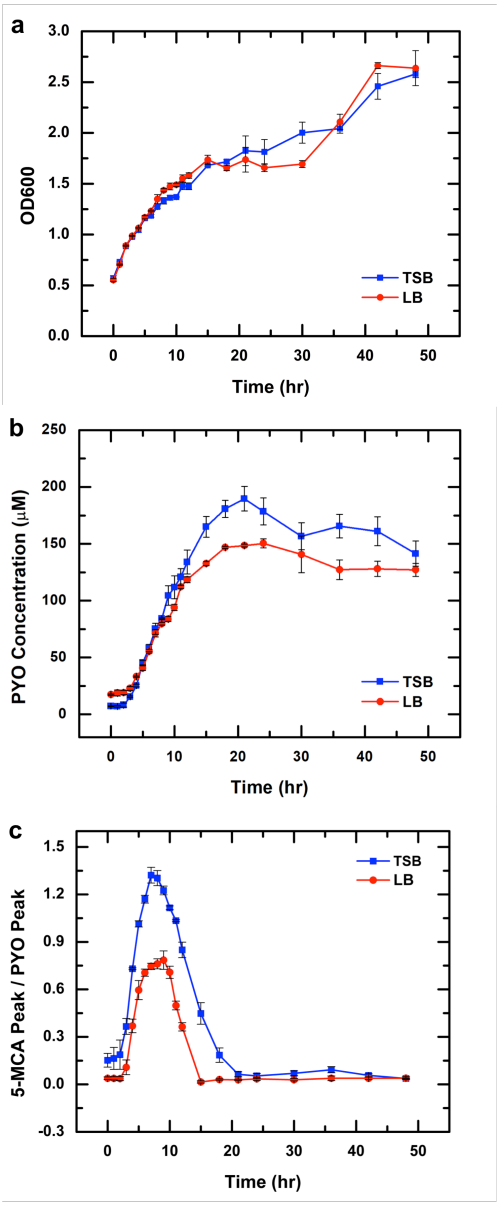

Figure 3.4: Time-dependent optical densities, PYO concentrations, and 5-MCA/PYO Dynamics.

(a) *P. aeruginosa* optical density at 600 nm (OD600) determined over time in TSB and LB media. (b) PYO concentrations secreted from cells *P. aeruginosa* over time in TSB and LB media. (c) Phenazine synthesis kinetics between PYO and 5-MCA as a function of time in TSB and LB. Error bars are plotted to represent standard deviation between nine samples.

PYO from *P. aeruginosa* liquid cultures shows its electrochemical fingerprint around −0.256 V vs SCE, but when bacteria enter stationary phase, we observe the appearance of an additional redox peak at a more positive potential of −0.115 V vs SCE (Figure 3.3). A few previous studies[22,23,39] have attributed redox activity at this potential to production of 5-MCA (Figure 3.1), a highly reactive phenazine that is a precursor to PYO in the biosynthetic pathway (Figure 3.1). While a previous electrochemical study has speculated on the detection of 5-MCA,[22] that earlier study was not able to confirm its identity due to its extremely unstable nature. In these studies, nano-ESI MS/MS was used to corroborate the identity of this *P. aeruginosa* reactive intermediate, which is further elaborated on in a subsequent subsection.

Square wave voltammograms in Figure 3.3 at later time points show that the PYO redox peak shifts slightly to more negative potentials (Figure A1.3a), likely due to increasing pH values in growth media.[50] To demonstrate this, time-based pH readings were recorded, showing an increase in pH over time (Figure A1.3). The resulting peak potential shifts were plotted as a function of pH, showing that the pH dependence of PYO is almost completely Nernstian (Figure A1.3) and shift by ~60 mV per pH unit change.

3.3.4 Biosynthetic Route of Phenazine Metabolites in *P. aeruginosa*

In addition to quantifying the concentration of cellular PYO, the dynamics of phenazine biosynthesis was monitored in a time-based fashion, which enabled the detection of reactive intermediates. The results shown in Figure 3.3 demonstrate noteworthy differences in 5-MCA production, suggesting variations in the dynamics of biosynthesis processes, which appear to be dependent on growth media that has not heretofore been observed nor reported in quantitative detail. Initially, when *P. aeruginosa* are in exponential phase (0–3 h), 5-MCA cannot be detected in either media. Yet once the

cells enter stationary phase, the production of 5-MCA increases, then decreases after 12 h. 5-MCA is no longer detected after 21 h, indicating that PA14 no longer produces this metabolite or that some other process leads to rapid diminishment such as cross reaction with oxygen. These data show that initially there is a build-up of 5-MCA, which later decreases. This is likely associated with environmental factors, suggesting that cells might be O_2-starved.

The square wave voltammetric currents for 5-MCA in TSB are higher compared to LB (Figure 3.3). Additionally, at various time points (5–11 h), 5-MCA concentrations are higher than those of PYO in TSB, which is not the case in LB. To better illustrate differences between the two media, a plot of the ratio of peak currents between 5-MCA to PYO was constructed as a function of time, which assuming equal diffusion coefficients (Table A1.2), is equal to the ratio of concentrations (Figure 3.4c). The ratio of currents of 5-MCA to PYO is an important parameter, relating to kinetics, as the standard heterogeneous electron transfer rate constant is a function of current ratio and frequency in square wave voltammetry.[51,52] The ratio of 5-MCA to PYO peak currents in TSB is significantly higher relative to LB, which suggests that the media composition influences the dynamics of phenazine synthesis. Consequently, the difference in dynamics between two growth environments likely contributes to the variance in PYO production rates and determined concentrations (Figure 3.4b, Table A1.1).

The two growth media used in this study are known to be composed of different peptides, casein peptones, various vitamins, minerals and trace elements such as N, S, and Mg. To better understand the differences in media composition, DESI MS/MS analyses were performed. A detailed summary of identified species from acquired mass spectra is provided in supporting information (Figure A1.8, Table A1.3, A1.4), which shows the presence of small species such as peptides and amino acids. In the positive ion

mode, choline (*m/z* 104.107) was detected at a higher relative abundance in TSB compared to LB. Choline is a water-soluble vitamin, which bacteria consume as a nutrient to produce toxins. In the negative ion mode, a higher relative abundance of deprotonated and chlorinated hexose species (simple six-carbon sugars, such as glucose) was detected in TSB compared to LB. These differences in media composition, such as the higher abundance of choline and hexose species in TSB relative to LB, might be catalyzing the production of higher levels of 5-MCA, and consequently higher amounts of PYO at later stages of bacterial growth. A previous research study has shown that the nutrient sources, in particular, carbon sources, have a significant effect on PYO production rates.[28,53] Supplementary DESI-MS experiments performed at various time points of cell growth (3, 21 and 48 h) in TSB media provided the detection of hexose (glucose), hexonic acid (gluconic acid) and keto-hexonic acid (keto-gluconic acid). These results suggest that *P. aeruginosa* metabolizes glucose to gluconic and keto-gluconic acids. Interestingly, these species were also detected in LB media, but at lower relative abundances. Figure A1.7 shows that as growth time increases, the abundance of hexose species and ratios of gluconic acid to keto-gluconic acid decrease over time. These differences in media composition observed from DESI-MS data can aid in understanding the distinct dynamics of 5-MCA and PYO in LB and TSB. Finally, PYO levels secreted from *P. aeruginosa* cultures appear to depend on several parameters, such as nutrient availability, temperature, and oxygenation of cultures.

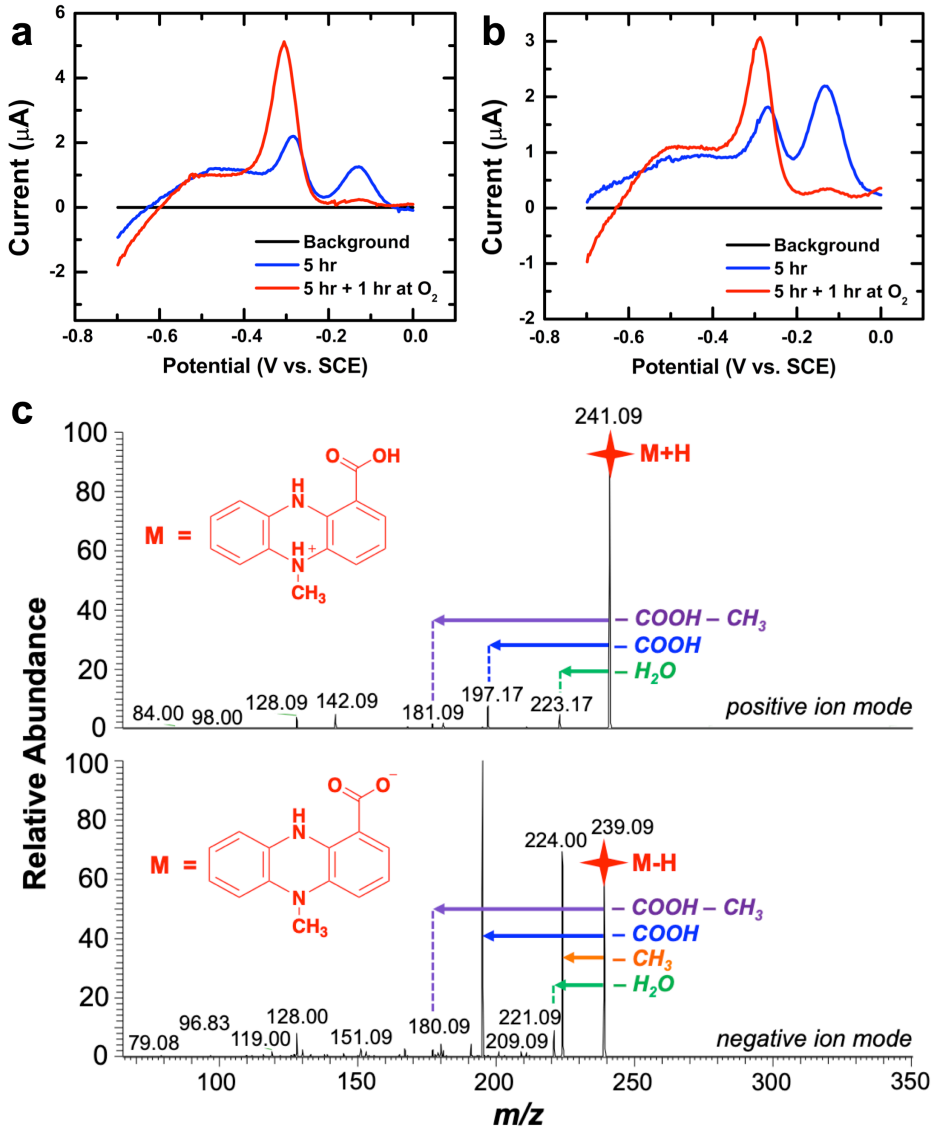

Figure 3.5: Stability and identification of 5-MCA phenazine species.

Square wave voltammograms showing 5-MCA's highly reactive nature after 1 hour of air (O2) exposure in (a) LB and (b) TSB, media. (c) nano-ESI MS/MS spectra of 5-MCA species in the positive ion mode (top) and negative ion mode (bottom).

The conversion of 5-MCA to PYO (Figure 3.1), involves NADH and molecular O_2, thus this reaction will proceed as long as there is molecular oxygen present. To confirm this and examine the reactive nature of 5-MCA, we performed electroanalytical tests using square wave voltammetry (Figure 3.5a,b). At 5 h of bacterial growth, liquid cultures were centrifuged and the media supernatant was separated from *P. aeruginosa* cells. Immediately after separation, square wave voltammograms were recorded using LB and TSB supernatants (Figure 3.5b), both showing the presence of PYO and 5-MCA. The supernatant samples were then exposed to air (O_2) for one hour, after which current responses were recorded again. The current-potential curves shown in red (Figure 3.5a,b) revealed that the 5-MCA peak current decreases and almost completely diminishes, while the PYO peaks increase. These results demonstrate that the conversion of 5-MCA to PYO is highly oxygen-dependent, indicating that environmental parameters comparatively regulate phenazine synthesis. In future studies, we plan to investigate the effects on phenazine dynamics with cells grown under anaerobic (O_2-free) conditions, which are very difficult to achieve.

Previously, Bellin and co-workers explored the effects of anaerobic conditions on *P. aeruginosa* PA14 biofilms by growing cells on nitrate, which confirmed that conversion of 5-MCA to PYO depends on the availability of molecular oxygen.[23] However, their reported results indicate that 5-MCA is concentrated at the edges of *P. aeruginosa* biofilm colonies, where the O_2 levels would be highest,[23] which contradicts our evidence of 5-MCA reacting quickly in presence of oxygen to generate PYO. In their study, researchers used an electrochemical chip with integrated electrodes arrays to detect phenazine metabolites,[23] which may bias the time dependent analysis of spatially resolved results. While Bellin et al. can image phenazine signals at specific time points we note that this method takes on the order of approximately 5 minutes to obtain a

readout of all electrodes in the array.[23] In contrast, our sensing platform using T-CUAs provides high sensitivity and very rapid response times, thus allowing us to obtain responses in roughly 15 seconds from all ultramicroelectrodes in the array. Additionally, as part of Bellin and co-workers' sensor design, bacterial colonies are grown on agar membranes placed directly on top of the integrated chip,[23] which raises a question about measuring real-time concentrations of phenazine production since transport parameters are not quantified. Contrary to other approaches, our method does not require the use of a "permselective" membrane and is demonstrated to be biologically compatible which should not interfere with quantitative measurements (Figure A1.5, Figure A1.6). Finally, compared to other carbon-based, macro-sized electrodes,[4,16,39,48] T-CUAs have enhanced sensitivity due to their nano-scale features.[24] This allows for simultaneous monitoring and quantification of dynamics of multiple phenazine species (Figure 3.2), which has not been previously demonstrated with carbon electrodes.

3.3.5 Detection and Characterization of *P. aeruginosa* Phenazines

Various mass spectrometry (MS) techniques were used to confirm the identity of the 5-MCA metabolite. Originally, DESI-MS at various time points was used when 5-MCA was electrochemically observed. Since 5-MCA rapidly converts to PYO in the presence of O_2 (Figure 3.5a,b), DESI-MSI was not a suitable technique for this analysis. Additionally, LC-MS with supernatant samples at 5 h of growth was employed. However, with this method, neither 5-MCA nor PYO was detected possibly due to the presence of many other interfering species in media (Figure A1.8).

The best approach relied upon nano-ESI MS/MS by directly injecting separated supernatant samples into the mass spectrometer. The identity of 5-MCA was confirmed (Figure 3.5c) based on the observed collision-induced fragmentation pattern in both the

positive and negative ion modes. The mass spectrum in the negative ion mode shows the precursor ion of *m/z* 239.09; the resulting fragment ions of *m/z* 224.00, *m/z* 221.09, *m/z* 195.09, and *m/z* 180.09 correspond to the loss of CH_3, H_2O, COOH, and (COOH+CH_3) groups, respectively, thus confirming the identity of 5-MCA phenazine. To the best of our knowledge, for the first time, the identity of this reactive metabolite was confirmed directly from bacterial populations since prior electrochemistry studies were only able to speculate the identity of 5-MCA.[22]

As previously discussed, the observed shifts in PYO peak potentials in square wave voltammograms with increasing pH over time follow the predicted Nerstian dependence upon pH. To further investigate that observed peak shift is not due to presence of other phenazine derivatives, in tandem with electrochemical measurements, DESI-MSI analyses were preformed at a number of different time points, which confirmed that PYO is the phenazine species present (Figure 3.6). Figure 3.6a illustrates mass spectrometry (MS) ion images of PYO in LB and TSB at different time stages of bacterial growth, showing an increase in ion abundance of *m/z* 211.086, identified as PYO, over time. During initial hours of growth, qualitative MS ion images show higher amounts of PYO in LB relative to TSB, which is in agreement with trends in the electrochemical results (Figure 3.4b). Figure 3.6b includes a DESI MS/MS spectrum of PYO. Fragment ions at *m/z* 196.063, *m/z* 183.092, and *m/z* 168.068 correspond to loss of CH_3, CO and (CH_3+CO) groups, respectively. Figure 3.6c displays representative mass spectra of LB and TSB media only compared to LB and TSB media with cells present. The mass spectra obtained from cell samples were mostly characterized by high relative abundance of PYO, which was not detected (S/N<3) in the mass spectra of media alone. Other signaling molecules from *P. aeruginosa* detected using DESI-MS, such as 4-

hydroxy-2-heptylquinoline (HHQ) and 2-nonyl-4-hydroxy-quinoline (NHQ), (Figure 3.6c) are detailed in Table A1.5.

In addition, the only other phenazine species detected, using DESI-MS, in trace amounts at late time points (21 h) was 1-hydroxyphenazine (OHPHZ) (Figure A1.9). OHPHZ is a redox-active phenazine metabolite, which is a degradation product of PYO, where PYO coverts to OHPHZ under basic conditions.[18] Previous research has shown that OHPHZ oxidizes at more negative potentials than PYO.[18] Note that at later time points (21 h) in square wave voltammograms (Figure 3.3), a small shoulder peak around –0.512 V vs SCE is observed, in particular in LB media, which is likely due to OHPHZ. However, this OHPHZ redox potential needs to be confirmed in the future using a commercially available OHPHZ standard. Additionally, at later stages of bacterial growth, the detection of a new species at a more positive potential (–0.0122 V vs SCE) is seen that has previously not been detected and identified. Although there are various species that oxidize at higher potentials, speculatively this may be a short-lived derivative of 5-MCA due to its high reactivity. Studies have shown that 5-MCA can undergo extracellular modification by free amine-compounds.[54] Presently, however, the identification of this species remains elusive. Future work will focus on enhancing MS methods to enable the identification of this new metabolite or degradation species.

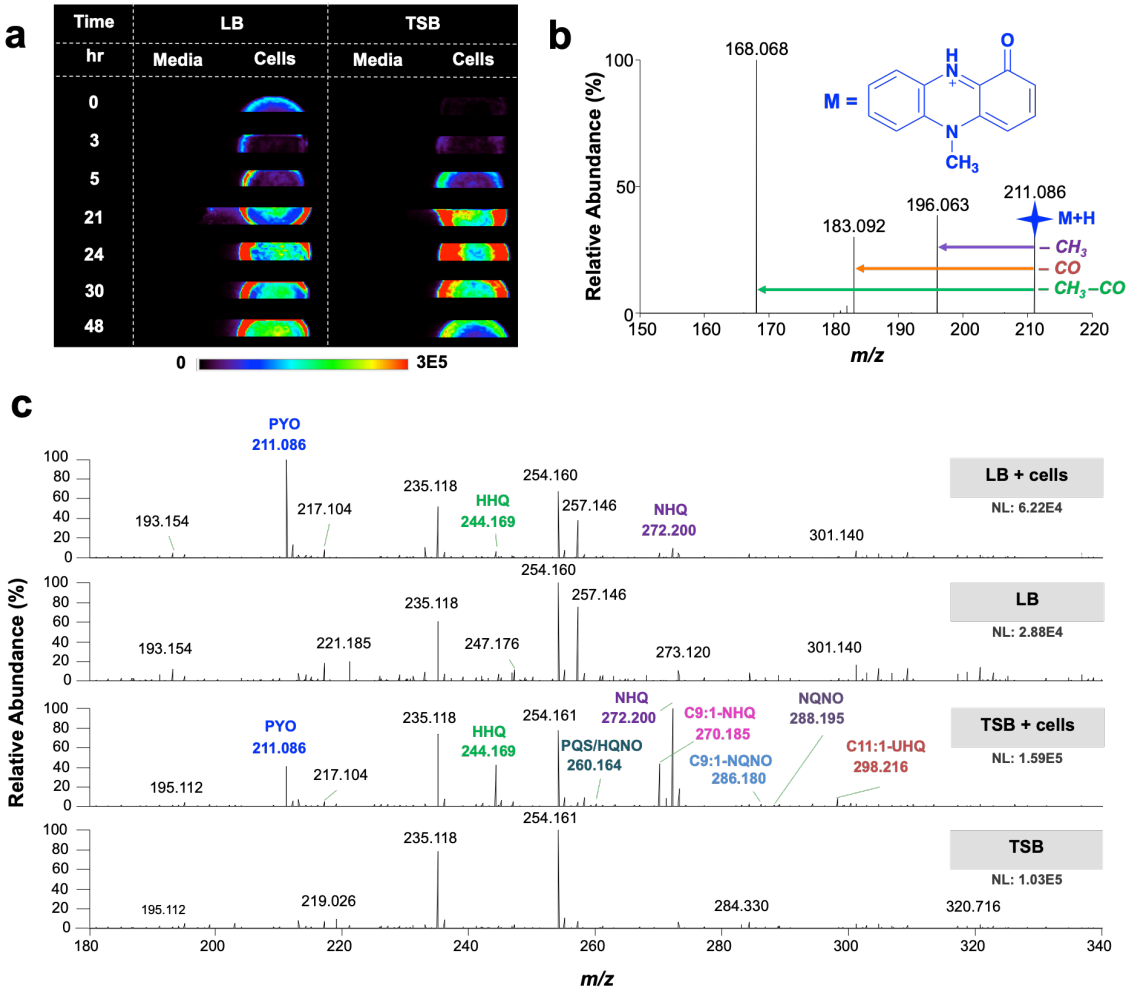

Figure 3.6: DESI-MSI of PYO at different time points – the relative abundance increases over time in accordance with electrochemical data.

(a) DESI-MSI ion images at various time points from PA14 cell cultures in LB and TSB growth media. Initially, relative abundance of PYO is lower in TSB compared to LB, which is in agreement with electrochemical quantitative data. (b) DESI MS/MS spectra of PYO (positive ion mode). (c) DESI-MS spectra of cells + media compared to media only. Note that cells are secreting PYO. No other phenazine species were identified using this method. NL directly correlates to ion current (ion abundance).

Our electrochemical method comprising T-CUAs is capable of simultaneously sensing several redox-active phenazine metabolites from *P. aeruginosa* in liquid-batch cultures thereby enabling the *in situ* detection of cellular metabolites from undisturbed bacterial populations. Furthermore, this method is capable of quantifying the concentration of these species, which is presently not achievable with most MS techniques.[55] Because our platform allows for continual, *in situ* sensing of cellular phenazine metabolites, it provides fundamental information about the metabolic dynamics of *P. aeruginosa* phenazines biosynthesis. In follow-on work T-CUAs will be used to characterize redox phenazines in microbial cultures and monitor their interactions in realistic environments. Furthermore, T-CUAs offer great promise as electrochemical devices in diagnostics and real-time monitoring of *P. aeruginosa* in healthcare settings. This platform provides impetus for the elucidation of the metabolite dynamics including detection, identification, and monitoring of infection state and quorum sensing variables such as oxygen availability, antibiotics and presence of additional pathogenic bacteria and/or host cells.

3.4 CONCLUSIONS

In summary, we demonstrated a quantitative, real-time sensing platform using T-CUAs as electrochemical sensors, to detect, identify and monitor the production of phenazine metabolites from wild type *P. aeruginosa* PA14 liquid cultures in two different media. This study shows continual monitoring of the dynamics of *P. aeruginosa* phenazine biosynthesis by sensing not only PYO but also its highly reactive precursor, 5-MCA. The real-time quantitative analyses show an increase of cellular concentrations of PYO during the first 21 h of bacterial growth, which then plateau. Using square wave voltammetry, we determined the maximum concentrations of cellularly secreted PYO to

be 190 ± 5 μM and 150 ± 1 μM TSB and LB, respectively. Additionally, the media type has an effect not only on rates of PYO production but also on amount of secondary phenazine derivatives, which directly correlate to presence of different nutrients, media concentrations, and components. Furthermore, MS analysis, including nano-ESI and DESI-MSI, confirmed the identity of phenazine species observed in our electrochemical measurements.

While previous research has focused on developing an electrochemical sensing device to monitor PYO, this is the first time that this approach has been used to detect, identify and monitor the dynamics of phenazine biosynthesis. Future work will focus on performing real-time electrochemical studies using *P. aeruginosa* strains of clinical relevance. Additionally, the effects on PYO production rates and phenazine dynamics in the presence of polymicrobial communities need to be investigated. Finally, effects on phenazine biosynthetic dynamics and PYO concentrations should be examined in other media (e.g., buffered yeast extract broth, nutrient broth, Mueller-Hinton broth, MOPS)[53] and growth environments, such as artificial cystic fibrosis sputum,[56] that resemble key attributes of *in vivo* environments.

3.5 ADDITIONAL INFROMATION

Details on additional experimental methods, quantitatively determined pyocyanin concentrations from real-time electrochemical data, time-dependent square wave voltammograms for pyocyanin detection on T-CUAs in LB and TSB, pH and peak potential changes as a function of time, PYO polymerization tests, T-CUA biocompatibility data and images, pyocyanin diffusion coefficients, DESI-MS/MS mass spectra of TSB and LB media contents, DESI-MS data of cellular species detected from *P. aeruginosa*, Tables A1.1–A1.5, and Figures A1.1–A1.10 are provided in Appendix 1.

3.6 REFERENCES

(1) Henke, J. M.; Bassler, B. L. *Trends in Cell Biology* **2004**, *14*, 648–656.

(2) Bassler, B. L.; Losick, R. *Cell* **2006**, *125*, 237–246.

(3) Stevens, A. M.; Schuster, M.; Rumbaugh, K. P. *J. Bacteriol.* **2012**, *194*, 2131–2141.

(4) Alatraktchi, F. A.; Johansen, H. K.; Molin, S.; Svendsen, W. E. *Nanomedicine* **2016**, *11*, 2185–2195.

(5) Monzó, J.; Insua, I.; Fernandez-Trillo, F.; Rodriguez, P. *Analyst* **2015**, *140*, 7116–7128.

(6) Boucher, H. W.; Talbot, G. H.; Bradley, J. S.; Edwards, J. E.; Gilbert, D.; Rice, L. B.; Scheld, M.; Spellberg, B.; Bartlett, J. *Clin. Infect. Dis.* **2009**, *48*, 1–12.

(7) Fick, R. B. *Chest.* **1989**, *96*, 158–164.

(8) Fetzer, A. F.; Werner, A. S.; Hagstrom, J. W. *Am. Rev. Respir. Dis.* **1967**, *96*, 1121–1130.

(9) Bedrossian, C. W. M.; Greenberg, S. D.; Singer, D. B.; Hansen, J. J.; Rosenberg, H. S. *Hum. Pathol.* **1976**, *7*, 195–204.

(10) Ringen, L. M.; Drake, C. H. *J. Bacteriol.* **1952**, *64*, 841–845.

(11) Walker, T. S. *Plant Physiol.* **2004**, *134*, 320–331.

(12) Llor, C.; Bjerrum, L. *Ther Adv Drug Saf* **2014**, *5*, 229–241.

(13) Amiri, M.; Bezaatpour, A.; Jafari, H.; Boukherroub, R.; Szunerits, S. *ACS Sensors* **2018**, *3*, 1069–1086.

(14) Sullivan, N. L.; Tzeranis, D. S.; Wang, Y.; So, P. T. C.; Newman, D. *ACS Chem. Biol.* **2011**, *6*, 893–899.

(15) O'Malley, Y. Q.; Reszka, K. J.; Britigan, B. E. *Free Radical Biology and Medicine* **2004**, *36*, 90–100.

(16) Alatraktchi, F.; Breum Andersen, S.; Krogh Johansen, H.; Molin, S.; Svendsen, W. *Sensors* **2016**, *16*, 408–410.

(17) Buzid, A.; Shang, F.; Reen, F. J.; Muimhneacháin, E. Ó.; Clarke, S. L.; Zhou, L.; Luong, J. H. T.; O'Gara, F.; McGlacken, G. P.; Glennon, J. D. *Sci. Rep.* **2016**, *6*, 30001–30009.

(18) Sismaet, H. J.; Pinto, A. J.; Goluch, E. D. *Biosens. Bioelectron.* **2017**, *97*, 65–69.

(19) Webster, T. A.; Sismaet, H. J.; Conte, J. L.; Chan, I.-P. J.; Goluch, E. D. *Biosens. Bioelectron.* **2014**, *60*, 265–270.

(20) Koley, D.; Ramsey, M. M.; Bard, A. J.; Whiteley, M. *Proc. Natl. Acad. Sci. U.S.A.* **2011**, *108*, 19996–20001.

(21) Connell, J. L.; Kim, J.; Shear, J. B.; Bard, A. J.; Whiteley, M. *Proc Natl Acad Sci USA* **2014**, *111*, 18255–18260.

(22) Bellin, D. L.; Sakhtah, H.; Rosenstein, J. K.; Levine, P. M.; Thimot, J.; Emmett, K.; Dietrich, L. E. P.; Shepard, K. L. *Nat. Commun.* **2014**, *5*, 3256–3265.

(23) Bellin, D. L.; Sakhtah, H.; Zhang, Y.; Price-Whelan, A.; Dietrich, L. E. P.; Shepard, K. L. *Nat. Commun.* **2016**, *7*, 10535–10544.

(24) Duay, J.; Goran, J. M.; Stevenson, K. J. *Anal. Chem.* **2014**, *86*, 11528–11532.

(25) Elliott, J.; Duay, J.; Simoska, O.; Shear, J. B.; Stevenson, K. J. *Anal. Chem.* **2017**, *89*, 1267–1274.

(26) Duay, J.; Elliott, J.; Shear, J. B.; Stevenson, K. J. *Anal. Chem.* **2015**, *87*, 10109–10116.

(27) Elliott, J.; Simoska, O.; Karasik, S.; Shear, J. B.; Stevenson, K. J. *Anal. Chem.* **2017**, *89*, 6285–6289.

(28) Jayaseelan, S.; Ramaswamy, D.; Dharmaraj, S. *World J. Microbiol. Biotechnol.* **2013**, *30*, 1159–1168.

(29) Reyes, E. A. P.; Bale, M. J.; Cannon, W. H.; Matsen, J. M. *J Clin Microbiol* **1981**, *13*, 456–458.

(30) Dietrich, L. E. P.; Price-Whelan, A.; Petersen, A.; Whiteley, M.; Newman, D. K. *Mol. Microbiol.* **2006**, *6*, 1308–1321.

(31) Lau, G. W.; Hassett, D. J.; Ran, H.; Kong, F. *Trends Mol. Med.* **2004**, *10*, 599–606.

(32) Bergen, G. A.; Shelhamer, J. H. *Infect Dis Clin North Am* **1996**, *10*, 297–325.

(33) Fergie, J. E.; Shema, S. J.; Lott, L.; Crawford, R.; Patrick, C. C. *Clin Infect Dis* **1994**, *18*, 390–394.

(34) Hall, S.; McDermott, C.; Anoopkumar-Dukie, S.; McFarland, A.; Forbes, A.; Perkins, A.; Davey, A.; Chess-Williams, R.; Kiefel, M.; Arora, D.; Grant, G. *Toxins* **2016**, *8*, 236–14.

(35) Wilson, R.; Sykes, D. A.; Watson, D.; Rutman, A.; Taylor, G. W.; Cole, P. J. *Infect. Immun.* **1988**, *56*, 2515–1517.

(36) Hauser, A. R. *Nature Rev. Microbiol.* **2009**, 654–665.

(37) Hansford, G. S.; Holliman, F. G.; Herbert, R. B. *J. Chem. Soc., Perkin Trans. 1* **1972**, 103–105.

(38) Mavrodi, D. V.; Blankenfeldt, W.; Thomashow, L. S. *Annu. Rev. Phytopathol.* **2006**, *44*, 417–445.

(39) Santiveri, C. R.; Sismaet, H. J.; Kimani, M.; Goluch, E. D. *ChemistrySelect* **2018**, *3*, 2926–2930.

(40) Mavrodi, D. V.; Peever, T. L.; Mavrodi, O. V.; Parejko, J. A.; Raaijmakers, J. M.; Lemanceau, P.; Mazurier, S.; Heide, L.; Blankenfeldt, W.; Weller, D. M.; Thomashow, L. S. *Applied and Environmental Microbiology* **2010**, *76*, 866–879.

(41) Pierson, L. S.; Pierson, E. A. *Appl Microbiol Biotechnol* **2010**, *86*, 1659–1670.

(42) Glasser, N. R.; Kern, S. E.; Newman, D. K. *Mol. Microbiol.* **2014**, *92*, 399–412.

(43) Mavrodi, D. V.; Bonsall, R. F.; Delaney, S. M.; Soule, M. J.; Phillips, G.; Thomashow, L. S. *J. Bacteriol.* **2001**, *183*, 6454–6465.

(44) Parsons, J. F.; Greenhagen, B. T.; Shi, K.; Calabrese, K.; Robinson, H.; Ladner, J. E. *Biochemistry* **2007**, *46*, 1821–1828.

(45) Mocak, J.; Bond, A. M.; Mitchell, S.; Scollary, G. *Pure & Appl. Chem.* **1997**, *69*, 297–328.

(46) Wilson, R.; Pitt, T.; Taylor, G.; Watson, D.; MacDermot, J.; Sykes, D.; Roberts, D.; Cole, P. *J. Clin. Invest.* **1987**, *79*, 221–229.

(47) Webster, T. A.; Goluch, E. D. *Lab Chip* **2012**, *12*, 5195–5197.

(48) Alatraktchi, F. A.; Noori, J. S.; Tanev, G. P.; Mortensen, J.; Dimaki, M.; Johansen, H. K.; Madsen, J.; Molin, S.; Svendsen, W. E. *PLoS ONE* **2018**, *13*, e0194157–e0194159.

(49) Sharp, D.; Gladstone, P.; Smith, R. B.; Forsythe, S.; Davis, J. *Bioelectrochemistry* **2010**, *77*, 114–119.

(50) Shah, A.; Ullah, A.; Nosheen, E.; Rana, U. A.; Shakir, I.; Badshah, A.; Rehman, Z. U.; Hussain, H. *Journal of the Electrochemical Society* **2013**, *160*, H765–H769.

(51) Mirceski, V.; Laborda, E.; Guziejewski, D.; Compton, R. G. *Anal. Chem.* **2013**, *85*, 5586–5594.

(52) Dauphin-Ducharme, P.; Arroyo-Currás, N.; Kurnik, M.; Ortega, G.; Li, H.; Plaxco, K. W. *Langmuir* **2017**, *33*, 4407–4413.

(53) Li, S.; Mou, Q.; Feng, N.; Leung, P. H. M. *Int. J. Electrochem. Sci.* **2018**, *13*, 3789–3798.

(54) Morales, D. K.; Jacobs, N. J.; Rajamani, S.; Krishnamurthy, M.; Cubillos-Ruiz, J. R.; Hogan, D. A. *Mol. Microbiol.* **2010**, *78*, 1379–1392.

(55) Watrous, J. D.; Dorrestein, P. C. *Nature Rev. Microbiol.* **2011**, *9*, 683–694.

(56) Darch, S. E.; Simoska, O.; Fitzpatrick, M.; Barraza, J. P.; Stevenson, K. J.; Bonnecaze, R. T.; Shear, J. B.; Whiteley, M. *Proc Natl Acad Sci USA* **2018**, *115*, 4779–4789.

Chapter 4: Electrochemical Monitoring of the Impact of Polymicrobial Infections on *Pseudomonas aeruginosa* and Growth Dependent Medium[4]

4.1 INTRODUCTION

The development of severe microbial infections remains a challenge[1,2] in healthcare facilities as immune-compromised hosts are exposed to communities of pathogenic bacteria.[3-5] Prompt detection, identification and real-time monitoring of early stages of infectious diseases, such as pneumonia, invasive wounds, and bloodstream infections,[6,7] are essential in disease prevention and determining effective treatment strategies. Typically, these hospital-contracted infections are populated by multiple microbial species, including *Pseudomonas aeruginosa* (*Pa*), *Staphylococcus aureus* (*Sa*), *Escherichia coli* (*Ec*), *Enterococcus faecalis*, and *Staphylococcus epidermidis*.[8,9] Current hospital diagnosis methods involve use of cell-culturing platforms, which classify specimens based on growth patterns observed in different media with selective growth components and/or antibiotics. These approaches, however, often require several days before pathogen identity is known, resulting in an increased antibiotic resistance as patients undergo treatments with broad-spectrum antibiotics.[10] As an alternative to the standard techniques, various electrochemical sensor platforms have been developed, which offer rapid identification, direct detection, and quantification of pathogenic signaling metabolites and byproducts.

In previous studies, our group has reported an inexpensive, facile and adaptable electrochemical platform using transparent carbon ultramicroelectrode arrays (T-

[4]Adapted with permission from Simoska, O.; Sans, M.; Eberlin, L. S.; Shear, J. B.; Stevenson, K. J. Electrochemical Monitoring of the Impact of Polymicrobial Infections on *Pseudomonas aeruginosa* and Growth Dependent Medium. *Biosens. Bioelectron.* **2019**, *142*, 111538. Copyright © 2019 Elsevier. Simoska O. acquired the data, wrote the manuscript, and performed electrochemical measurements/characterization. Simoska, O. and Sans, M. performed mass spectrometry experiments. Simoska, O. and Stevenson, K. J. designed studies, planned experiments, and analyzed all data. All authors contributed in editing the manuscript.

CUAs).[11,12] These sensors provide advantages in contrast to other electrochemical sensing devices, including amplified current responses, fast response times, large linear dynamic ranges (LDRs), high signal-to-noise (S/N) ratios and lower limits of detection (LODs).[11-15] As their electroactive material is comparable to glassy carbon, T-CUAs are inert, highly conductive and extremely biocompatible. This electroanalytical platform has been used to rapidly detect the common opportunistic human pathogen *Pa*.[14,15] Similar to other pathogens, *Pa* readily establishes infections in hosts with compromised immune systems and in those suffering from conditions, such as chronic wounds, lung infections, and severe burns.[16-19] Using electrochemical sensors, *Pa* can be easily detected via the production of redox-active pyocyanin (PYO),[14,15,20-23] which is a bacterial warfare toxin secreted as a secondary metabolite.[23] Because it is produced uniquely by *Pa* during early infection stages,[24] PYO is considered a useful electroactive biomarker indicative of infections caused by this pathogen.[25]

Although a significant amount of research has focused on developing electrochemical platforms for the detection of PYO,[14,20,21,26-28] this is only the end product of *Pa* phenazine biosynthetic pathway.[24,29,30] PYO is synthesized through a cascade of complex metabolic reactions involving various genes. In addition to PYO, *Pa* produces several phenazine derivatives in this biosynthetic route, including a side product, 1-hydroxyphenazine (OHPHZ), and a short-lived, reactive precursor, 5-methylphenazine-1-carboxylic acid (5-MCA).[30] Phenazines are small, redox-active, nitrogen-containing heterocyclic molecules, which engage in reduction and oxidation processes in the presence of molecular oxygen. Thus, they play key roles in altering metabolism, modify immune responses and damage host tissue.[29-32] Additionally, a recent study reported that phenazines interact with antibiotics, thus influencing treatment of *Pa* infections.[33] Detection and examination of their relative quantities produced during various growth

stages could provide a better understanding of phenazine functions in *Pa* virulence mechanisms.

In a recent study, described in Chapter 3 herein, we have demonstrated use of T-CUAs for the real-time monitoring of phenazine production and metabolism dynamics from *Pa* cell cultures in simulated growth media.[15] Our previous work increased knowledge about phenazine biosynthesis in *Pa* monocultures, yet a follow-on study is necessary to understand the impact of polymicrobial cultures on phenazine production and dynamics, in particular when *Pa* is cultured alongside other bacterial pathogens in the same growth environments. Microorganisms seldom live in isolation as in almost all environments, multiple bacterial species inhabit diverse microbial communities in which interactions between species shape biological activities of cellular populations.[34-37] During polymicrobial infections, cellular communication within complex cellular communities can alter virulence and/or host responses.[8,36,38] As a prominent pathogen in polymicrobial infections, *Pa* often displays either synergistic or adversarial relationships with other bacteria, thus increasing disease severity.[39] Therefore, *Pa* phenazine production and biosynthesis dynamics in polymicrobial environments need to be examined, as they represent a clinically relevant problem. Although various fluorescence microscopy-based methods have been employed,[38,40,41] additional analytical tools are necessary to quantitatively study the dynamic microbe-microbe interactions, in real time.[39,42,43]

Herein, we demonstrate use of T-CUAs for the quantitative, real-time electrochemical monitoring of the impact of polymicrobial communities on *Pa* phenazine production where *Pa* is co-cultured with other clinical pathogens, *Sa* and *Ec*, in two different growth media that are predominately used for such bacterial-based cell culture studies. Our results, during 48 h bacterial growth, show distinct differences in amounts of

phenazine products and intermediates secreted by *Pa* in mono- and polymicrobial communities. Specifically, when *Pa* was co-cultured with *Ec*, the concentrations of cellular PYO were significantly reduced compared to amounts produced in monoculture samples, in both media. Yet when *Pa* was cultured alongside *Sa*, PYO concentrations were lower in only one media. These results show that the amounts of phenazine derivatives produced during growth depend on both various environmental factors in the media and presence of other microbes. These electrochemical results were confirmed by desorption electrospray ionization mass spectrometry (DESI-MS) imaging studies to determine differences in relative abundances of key growth media components and nutrients, and to identify other cellular metabolites produced in polymicrobial cultures.

4.2 EXPERIMENTAL METHODS

4.2.1 General

All chemicals were used as received. Photoresist AZ 1518 was purchased from Microchemicals. Polystyrene spheres (diameter of 1.54 μm) were purchased from Polysciences, Inc (Polybead®). Lysogeny Broth (LB) Lennox and Bacto Tryptic Soy Broth (TSB) were acquired from Thermo Fisher Scientific Inc. and from Becton, Dickinson, and Company, respectively. Tryptic Soy Agar (TSA) was obtained from Remel. Ethanol, Acetone, 2-Propanol, Methanol, Carbenicillin Sodium Salt, and Kovac's reagent for indoles were purchased from Sigma-Aldrich Co. Erythromycin was acquired from MP Biomedicals.

4.2.2 Cell Culture

The bacterial strains used for this works were the following: (1) wild-type *Pseudomonas aeruginosa* (*Pa*) PA14 strain carrying pMRP9-1 plasmid, constitutively

expressing green fluorescent protein (gfp), (2) wild-type *Staphylococcus aureus* (*Sa*) MN8 strain, carrying a pJY209 reported plasmid with expressing yellow fluorescent protein (yfp_{10B}), and (3) wild-type *Escherichia coli* (*Ec*) MC4100 strain expressing gfp. *Pa* and *Ec* strains were cultured separately from freezer stock on TSA plates containing 10 μg/mL carbenicillin sodium salt (carb10) to maintain the plasmids. *Sa* strain was cultured from freezer stock on TSA plates containing 0.5 μg/mL erythromycin to preserve the plasmid. Using *Pa*, *Sa*, and *Ec* cells initially grown on distinct TSA agar plates with either carb10 or erythromycin, overnight liquid-batch cultures of the three separate bacteria were prepared by inoculating 75 cm^2 tissue culture flasks with vented caps filled to a volume of 75 mL with either LB or TSB media, respectively, using sterile wooden dowels. Prior to co-culturing, the three separate bacterial cell cultures in either LB or TSB were left to shake in a 37 °C incubator for 16-18 hours at 150 rpm. LB and TSB media contained 10 μg/mL carb10 for overnight *Pa* and *Ec* cultures and 0.5 μg/mL erythromycin for overnight *Sa* cultures. The optical densities (ODs) of overnight cell culture solutions were then determined using an Agilent Instrument 8453 UV–vis–NIR spectrophotometer by recording the absorbance at 600 nm. The three separate cell culture samples, in either TSB or LB, were subsequently diluted into 250 mL Erlenmeyer flasks with fresh growth media to achieve the same staring optical densities of 0.1 at 600 nm for all three liquid cultures with a volume of 125 mL with TSB and LB (without carb10 or erythromycin antibiotics), respectively. Separate cell cultures in fresh media were shaken for another 2 h at 37 °C to achieve exponential phase, which is designated as 0 h. At 0 h, equal volume amounts of same initial cell densities were combined in 250 mL Erlenmeyer flasks to obtain differing polymicrobial combinations in either LB or TSB media. Cell cultures of individually grown *Pa* in both media were tested in a previous study.[1] For the two bacterial combination studies, *Pa* strain was co-cultured with either

Sa or *Ec*, in LB and TSB media. For the three bacterial combination studies, *Pa* was cultured alongside both *Sa* and *Ec* in either LB or TSB.

4.2.3 Optical Density Measurements

Optical density measurements at 600 nm (OD600) were determined using an Agilent Instrument 8453 UV–vis–NIR spectrophotometer. OD600 readings were performed alongside with electrochemical square wave voltammetry (SWV) measurements for 48 h starting at 0 h. All ODs were set to a standard method at 600 nm. Blank measurements were taken using either TSB or LB media and for each of the polymicrobial combination samples, three cuvettes were sampled from the main flask at each time point against the appropriate blank. Flasks were removed from the 37 °C shaker for only the brief time needed to transfer 1 mL liquid culture into the cuvettes to minimize disruption of cell growth.

4.2.4 Fabrication of T-CUA Electrodes

Preparation of electrode platform using transparent carbon ultramicroelectrode arrays (T-CUAs) follows detailed procedures described in our previous studies.[11-15] Quartz microscopic slides (6.45 cm^2 and 1 mm thick, Technical Glass Products) were treated with piranha (3:1 H_2SO_4: 30% H_2O_2) to remove any organic contaminants. A 1:3 dilution of AZ 1518 photoresist with PGMEA (1-methoxy-1-propanol acetate) was spun onto the piranha cleaned quartz slides at 6000 rpm for 60 s. Following spin coating, the photoresist slides were soft baked at 90 °C for 10 min and then transferred to a tube furnace. After 15 min of purging with 5% H_2: 95% N_2 (~100 mL/min), the photoresist slides were pyrolized by heating to 1000 °C at 5 °C/min and holding at that temp for 1 h before allowing them to cool slowly back to room temperature at 5°C/min. The pyrolized

photoresist film (PPF) slides were then removed from the furnace and stored for 3 days prior to use to allow for the oxide layer to stabilize. T-CUAs fabrication involved a lithography method using polystyrene microspheres (PSS) with a diameter of 1.54 μm, which were drop cast from a 5.4 wt % methanol suspension onto the conductive PPF electrodes. The organization of the spheres is that of a hexagonal close-packed two-dimensional ordered network. After this microsphere lithography step, 10 nm of Al_2O_3 layer was deposited via atomic layer deposition (ALD) technique at 80 °C. The ALD process was calibrated by the manufacturer (Cambridge Nanotech Savannah 100) to deposit 0.089 nm conformal Al_2O_3 layer per cycle. Thus, cycling this process for 112 times formed a 10 nm ALD layer. This ALD step is then followed by removal of PSS via sonication with methanol, acetone, isopropanol and water. Disk-shaped carbon areas remained where the PSS made contact with the PPF, thus forming a carbon ultramicroelectrode array. Details on characterization of T-CUA electrodes have been reported in previous research studies from our group.[11-15]

4.2.5 Pyocyanin Calibration Curves

To quantify phenazine concentrations from *Pa* cells in polymicrobial environments, calibration curves for pyocyanin (PYO) in TSB and LB media were used, reported in our previous study in Chapter 3.[15]

4.2.6 Electrochemical Measurements

All electrochemical measurements were performed using an Autolab PGSTAT30 potentiostat. Square wave voltammetry (SWV) experiments were done using a three-electrode cell system where T-CUA was used as the working electrode, saturated calomel electrode (SCE) was used as the reference electrode, and a gold wire electrode was used

as the counter electrode. T-CUA working electrode had a 0.495 cm^2 total geometric area, defined by the electrode area exposed to a solution in homemade Teflon or *Polydimethylsiloxane* (PDMS) electrochemical wells. SWV measurements were performed in a potential window ranging from –0.7 to 0.0 V vs SCE. A current sensitivity of 5 μA, a frequency of 15 Hz and a step potential of 3 mV were used. The background current responses were obtained using TSB and LB media (without bacteria) as background solutions. After collecting a background SWV curves with a total of 20 scans, subsequent real-time electrochemical detection measurements of polymicrobial samples in LB and TSB growth media were performed. All liquid-batch polymicrobial samples were incubated at 37 °C and shaken at 150 rpm for the entire 48-h duration of the experiments. For each electrochemical measurement, 800 μL aliquots of each polymicrobial liquid-batch culture were placed onto T-CUA electrodes to instantly perform SWV tests, detecting PYO and other phenazines from *Pa* at different time points of growth. For the first 12 h of the real-time experiments, SWV measurements were taken every hour, followed by SWV measurements every three hours until 24 h, and lastly followed by every six hours until 48 h of cell growth. A single SWV measurement took approximately 15 s to acquire

4.2.7 Desorption Ionization Mass Spectrometry (DESI-MS) Imaging of Metabolites in Polymicrobial Cultures

For DESI-MS experiments, 20 μL aliquots of bacterial growth media (with and without bacteria) were placed onto well microscope slides and allowed to dry for 60 minutes in a fume hood prior to mass spectrometry analysis. Polymicrobial cell samples grown in LB and TSB media were analyzed at 5 h or bacterial growth. For DESI-MS imaging tests, a 2D Omni Spray (Prosolia Inc.), coupled to an LTQ-Orbitrap Elite, was

used. Tests in both the negative and positive ion modes from *m/z* 100 to 400 were utilized, using a hybrid mass spectrometer that allows for tandem MS experiments using both collision-induced dissociation (CID) and high-energy collisional dissociation (HCD) methods, high mass accuracy (<5 ppm mass error), and high mass resolution (60,000 resolving power) measurements. The spatial resolution used was 200 μm and ion images were constructed using Biomap software. For the negative ion mode analysis, a 1:1 (v/v) mixture of acetonitrile (ACN) and dimethylformamide (DMF) was used, at a flow rate of 2 μL/min. Pure ACN was used for the positive ion mode analysis, at a flow rate of 5 μL/min. The N_2 pressure for analysis was set to 185 psi.

4.2.8 Kovac's Test for Indoles in Polymicrobial Cultures

To qualitatively investigate the presence of indoles in polymicrobial samples containing *Ec* in LB and TSB, Kovac's reagent was used. After 24 h growth in 37 °C incubator, polymicrobial samples in each media were examined by adding five drops of Kovac's reagent (~0.5 mL). Polymicrobial cultures in test tubes were then gently shaken. Samples containing *Ec* in both LB and TSB media resulted in the appearance of a red-violet-pink top layer in the cell culture tubes, thus qualitatively confirming the presence of indoles produced by *Ec*.

4.3 Results and Discussion

4.3.1 *Pa* Phenazine Biosynthetic Pathway in Polymicrobial Environments

During stationary phase, *Pa* strains actively produce phenazines, including phenazine-1-carboxylic acid (PCA), OHPHZ, 5-MCA, and PYO,[44] which are biomolecules with key functions in microbial virulence.[45,46] Due to their small sizes and minor structural variations,[40] these highly diffusible species are extremely challenging to

study and identify as they undergo redox changes.[25] The influence of polymicrobial communities on *Pa* phenazine production remains unclear,[44] thus research addressing distinct quantities and ratios of phenazine products and intermediates is necessary to understand interactions of *Pa* with other co-infecting species (here, *Sa* and *Ec*).[29] Phenazines are derived from shikimic acid pathways, where PYO production begins with the conversion of chorismic acid to PCA. Enzyme PhzM then converts PCA to highly reactive 5-MCA. In the final step, monooxygenase PhzS converts 5-MCA to PYO.[47]

4.3.2 Phenazines and Interferents in Polymicrobial Cultures

A general concern with the use of electrode-based sensors for biological applications is the device selectivity, particularly the ability of the working electrode to distinguish phenazine targets from potential interferents. As they grow in distinct multi-species environments, pathogens produce a variety of redox-active, small molecules as secondary metabolites.[48] In this specific application, species secreted by other bacteria could potentially interfere with T-CUA responses in the potential window where redox peaks of *Pa* phenazines are observed. To test potential interferences, the two bacterial pathogens used in this study, *Sa* and *Ec*, were electrochemically examined after 24 h of cell growth in lysogeny broth (LB) and tryptic soy broth (TSB). The square wave voltammograms (SWVs) in Figure 4.1 demonstrate that the distinguishable electroactive peaks are due to *Pa* phenazine species only. Specifically, redox-active metabolites, PYO, 5-MCA, and OHPHZ are produced by *Pa* in LB and TSB media at 24 h. The identities of these metabolites were confirmed using mass spectrometry methods in our previous study in Chapter 3.[15] The SWVs for *Sa* and *Ec* display nearly identical current responses compared to background currents (LB or TSB). These results confirm that *Sa* and *Ec* do not produce electrochemically active species in the potential window (−0.7 to 0.0 V vs

SCE) used. Furthermore, current responses for *Sa* and *Ec* co-cultures in TSB and LB were also recorded at 24 h growth, which demonstrate that the interaction between *Sa* and *Ec* does not produce redox-active metabolites in the potential window used here. In addition to the presence of other pathogens, several growth media components (e.g., glucose, gluconic acid, uric acid, ascorbic acid, NADH, NADPH, NAD, NADP, H_2O_2) could have interference effects, impacting electrode responses. Previous research has shown that biologically relevant concentration of these common biological interferents have redox signatures at more positive potentials, which are outside of the potential widow in this study.[15,21] Among phenazine metabolites, *Pa* secretes various other biological metabolites, including non-electrochemically active N-Acyl homoserine lactones, as well as electrochemically active species such as pyoverdine, 2-heptyl-3-hydroxy-4-quinolone (PQS) and its immediate precursor, 2-heptyl-4-hydroxyquinoline (HHQ). Previous research has shown that pyoverdine, PQS and HHQ have electrochemical signatures at more positive potentials, which fall outside of the potential window used herein.[49,50] Therefore, the redox peaks observed in Figure 4.1 are due to *Pa* phenazine metabolites, which were identified with mass spectrometry methods in our recent study.[15] Thus, using an electrochemical potential window specific to *Pa* phenazines, their production rates in polymicrobial samples were monitored on T-CUAs, in real time.

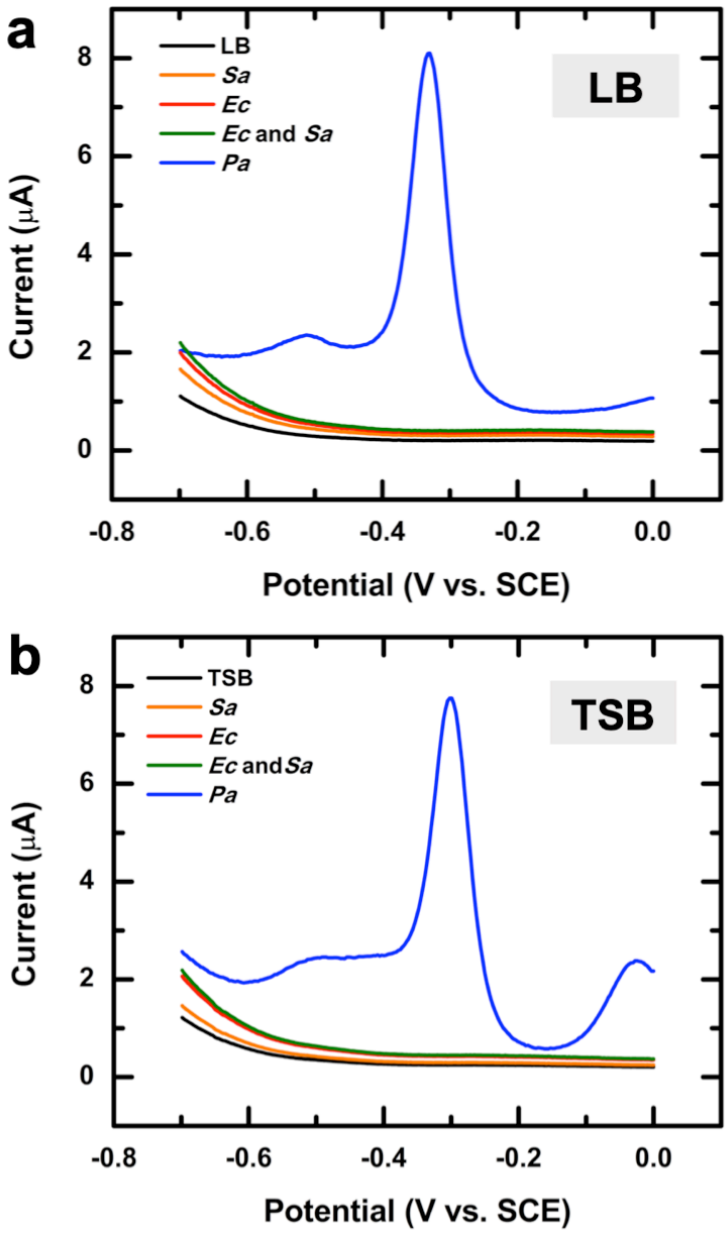

Figure 4.1: Phenazine metabolites and interferences in polymicrobial samples.

Square wave voltammograms of bacterial cultures at 24 h of growth in (a) LB and (b) TSB. The redox peaks around –0.256 V vs SCE result from PYO present in *Pa* liquid-batch cultures. No interfering redox active peaks are observed from *Sa* and *Ec* cultures in the working potential window.

4.3.3 Real-time Electrochemical Detection and Quantification of *Pa* Phenazines in Polymicrobial Cultures

Real-time, continual electrochemical monitoring, over 48 h, was performed to study the effect of polymicrobial communities' dynamics on phenazine production in two different media. Combinations of *Pa* co-cultured together with (1) *Sa*, (2) *Ec* or (3) both *Sa* and *Ec*, were prepared in either LB or TSB media to examine how other bacteria impact phenazine biosynthesis production in polymicrobial cultures. To start cell growth, individually grown liquid-batch cultures of *Pa*, *Sa* and *Ec* were diluted into fresh media to achieve identical initial optical densities. Polymicrobial samples were incubated at 37 °C and shaken at 150 rpm for a 48-h period, during which optical density (absorbance at 600 nm) measurements were performed to monitor growth stages in LB and TSB. Figure 4.2 shows fairly sigmoidal growth curves for mono- and poly-microbial samples in LB and TSB. The initial 4 h (0-3 h) represent the exponential phase, after which bacteria enter the stationary stage, as indicated by the resulting plateau in the growth curves. During the stationary phase, population size remains the same since the rate of cell growth equals the rate of cell death. When grown individually, *Pa* cells initially show higher optical densities in LB media than TSB, however, after 12 h, optical measurements are higher in TSB relative to LB. When *Pa* was co-cultured with *Sa* in LB, the time-dependent optical densities are marginally higher compared to *Pa* monoculture sample (Figure 4.2a), indicating the presence of another bacterial species. Similarly, the polymicrobial combination samples with *Ec* in LB show optical densities higher than those for *Pa* only and *Sa* sample. These higher doubling rates in combination samples containing *Ec* are likely a result of *Ec* growing faster than *Sa* and *Pa*.[43] On the other hand, all three polymicrobial combinations in TSB display higher optical densities than the control *Pa* monoculture at nearly all time points. These results suggest that media also

has an effect on bacterial growth rates as some bacteria might outgrow others in competing for resources and nutrients.[51] Although these optical density measurements show differences between mono- and poly-microbial samples in two media, this method provides no information about quantities of phenazine metabolites produced during different growth stages.

Therefore, in tandem with optical density, electrochemical measurements, using SWV, were performed in a time-based fashion to simultaneously detect various phenazines, including PYO, 5-MCA, OHPHZ, and an unknown derivative, in polymicrobial environments (Figure 4.3). Specifically, phenazine production was monitored directly from different polymicrobial samples every hour during the initial 12 h, followed by every three hours until 24 h, then every six hours till 48 h. To quantify concentrations of cellular metabolites in polymicrobial samples in LB and TSB, the data were analyzed using background current subtraction and previously constructed calibration curves.[15] In this study, real-time electrochemical measurements of cellular PYO and 5-MCA in polymicrobial cell cultures were performed six times in each media to validate high reproducibility. Thus, error bars (Figure 4.4) represent the standard deviation between the six replicates. Figure 4.3 shows the resulting SWVs for different cell combination samples in LB and TSB, where the current-potential responses are plotted as a function of time. In previous research, mass spectrometry methods, including DESI-MS and nano-electrospray ionization (nano-ESI), were used to confirm the identities of phenazine metabolites observed in our electrochemical data.[15] Specifically, cellular PYO has a redox-active peak at −0.256 V vs SCE while highly reactive 5-MCA shows its electrochemical fingerprint at −0.115 V vs SCE (Figure 4.3). Additionally, the shoulder peak observed at a more negative potential (−0.512 V vs SCE) after 21 h, is corroborated by OHPHZ, a degradation, side product of PYO.[15,52] Finally, in certain

samples, an unknown species is detected at a more positive potential of −0.0112 V vs SCE at later stages of growth. Unfortunately, the identity of this species remains elusive, but it is suspected to be a highly unstable 5-MCA derivative or a degradation species. Presently, this metabolite can only be detected using our electrochemical T-CUA platform, however, MS methods need optimization to enable its identification. The marginal shifts in PYO redox peaks in SWVs (Figure 4.3) are due to increasing pH values in liquid-batch cultures in the two media.[15,53]

The SWV responses in Figure 4.3 show the temporal changes in phenazine dynamics in the different microbial samples in LB and TSB. When *Pa* is individually cultured, concentrations of cellular PYO do not change significantly in both broths during the exponential growth phase (0–3 h). Initially, PYO concentrations in LB are approximately two times higher compared to those in TSB for *Pa* cultures. In the stationary phase, *Pa* cells produce increasing amounts of PYO until 21 h, after which PYO concentrations decrease and plateau in LB and TSB as observed in the resulting current responses. While PYO levels do not significantly differ between LB and TSB during 4–12 h, PYO amounts in TSB are 1.3 times higher than in LB broth after 15 h (Figure 4.3a–b, Table A2.1–A2.2). During 21 h growth, increasing PYO production rates correlate to increased intercellular communication.[15,33] Extended growth in the stationary stage results in a decrease in production of virulence factors. The time-dependent SWVs show different current responses when additional pathogens are cultured with *Pa* in LB and TSB. When co-cultured with *Sa* in LB, *Pa* produces PYO amounts that are twice lower than those in *Pa* sample during 0–12 h. After 15 h, levels of cellular PYO in *Pa* and *Sa* combination sample in LB are similar to those in *Pa* alone (Figure 4.3b). On the other hand, when grown with *Ec*, *Pa* produces PYO concentrations that are two times lower compared to *Pa* only, at all time points of growth (Figure 4.3c). For samples

comprised of all three microorganisms in LB, PYO concentrations are approximately five-fold lower, on average, relative to individual *Pa* culture (Figure 4.3d). These results, summarized in Figure 4.4a, show the determined PYO concentrations as a function of growth time in polymicrobial samples in LB. Similarly to LB, the presence of *Sa* and *Ec* changes phenazine production rates in TSB. PYO concentrations decrease nearly four times when *Pa* is co-cultured with *Sa* in TBS (Figure 4.3f). The presence of *Ec* in TBS significantly reduces phenazine production (Figure 4.3g–h) resulting in notably smaller quantities of PYO. These quantitative results, summarized in Figure 4.4b, illustrate PYO concentrations at different time points of growth for polymicrobial combinations in TSB. The concentrations of PYO produced by *Pa* in polymicrobial samples in LB and TSB are outlined in Tables A2.1–A2.2 in the supplementary information. For individual *Pa* cultures, the maximum PYO concentrations were determined to be 150 ± 1 μM and 190 ± 5 μM in LB and TSB, respectively, at 21 h. For polymicrobial samples in LB, *Pa* produces maximum PYO concentrations of 150 ± 1 μM in *Pa* and *Sa*, 72 ± 1 μM in *Pa* and *Ec*, and 28 ± 1 μM in *Pa*, *Sa* and *Ec* sample at 21 h growth. When cultured together with *Sa* in TSB, *Pa* produces 78 ± 2 μM as the highest PYO concentration (at 21 h). The maximum concentration of PYO for *Pa* and *Ec* sample in TSB was 9.3 ± 0.2 μM at 21 h. At 48 h, *Pa* produced a maximum PYO concentration of 8.2 ± 0.5 μM in the polymicrobial combination comprising all three pathogens in TSB.

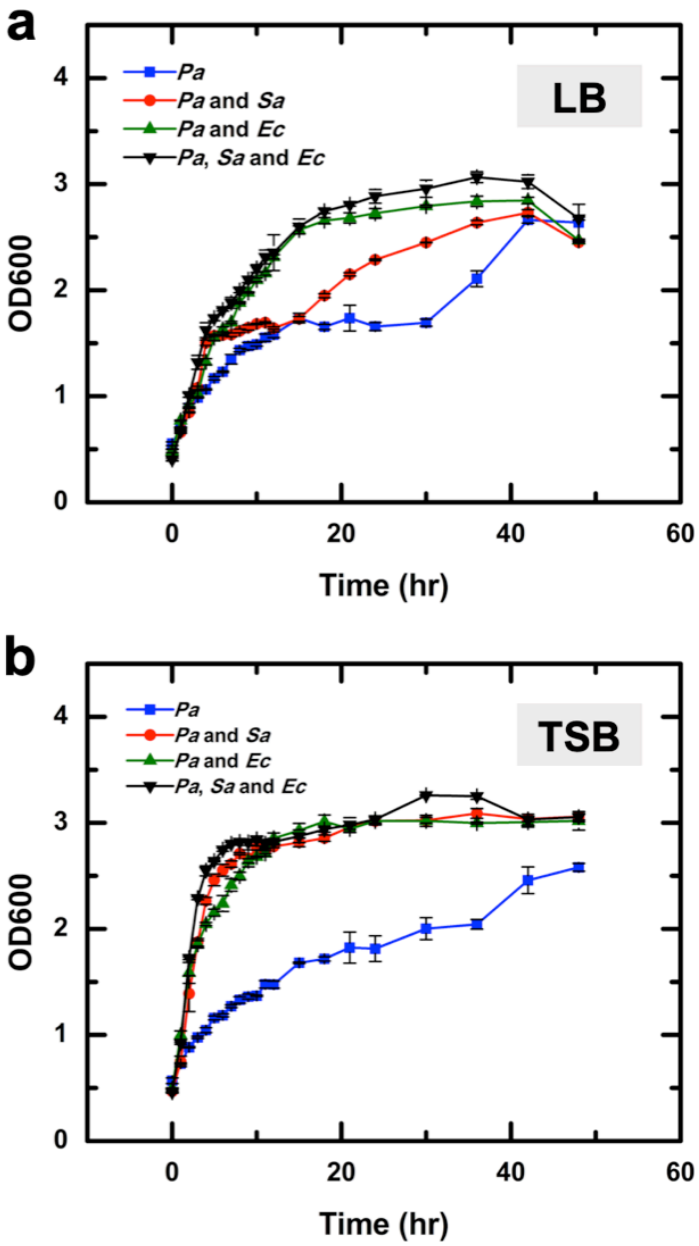

Figure 4.2: Optical density of polymicrobial co-cultures at various time points of growth in LB and TSB broth.

Optical density measurements at 600 nm (OD600) of polymicrobial co-cultures determined at various time points of growth in (a) LB and (b) TSB broth. Error bars represent the standard deviation between six samples.

These results demonstrate that in addition to other bacterial pathogens, the media composition largely impacts phenazine production rates. Briefly, the presence of *Sa* does not have a large effect on *Pa* phenazine production in LB (Figure 4.4a). The ability of PYO to inhibit *Sa* growth has been reported,[54] which might result in preferential growth of *Pa*. A previous study has shown that *Sa* promotes growth and increased aggregation of *Pa*, thus suggesting that these two pathogens can co-exist and interact in a beneficial manner.[55] Additionally, research has demonstrated *Pa* to be the dominant growing species when co-cultured with *Sa*.[34] These reports on microbial interactions potentially explain why PYO concentrations are marginally higher when *Pa* is grown with *Sa* in LB. However, this is not observed for *Pa* and *Sa* sample in TSB, suggesting the phenazine production rates greatly depend on media composition. When *Pa* is co-cultured together with *Sa* in TSB, a decrease in PYO concentrations of approximately 60% is observed (Figure 4.4b). Unlike in LB, *Pa* and *Sa* likely engage in competitive behaviors for various nutrients in TSB. The presence of *Ec* influences phenazine production in both media. Specifically, PYO amounts are approximately 50% lower in *Pa* and *Ec* sample compared to *Pa* sample in LB (Figure 4.4a). Furthermore, *Ec* considerably slows down phenazine production in TSB, as noted by approximately 95% lower PYO concentrations compared to amounts produced in *Pa* monocultures (Figure 4.4b). A previous study has shown *Ec* to not only dominate co-cultures but also hinder *Pa* growth in both nutrient-limited and enriched conditions,[56] resulting in smaller amounts of *Pa* cells compared to monocultures. Additionally, research has shown *Ec* to dominate multi-species environments, in particular, when co-cultured with either *Pa* or *Sa*,[34] suggesting that *Ec* consumes nutrients at a fast pace. In addition, *Ec* might produce unique cellular signaling molecules that can directly impact *Pa* phenazine production, which is discussed in subsequent discussion sections.

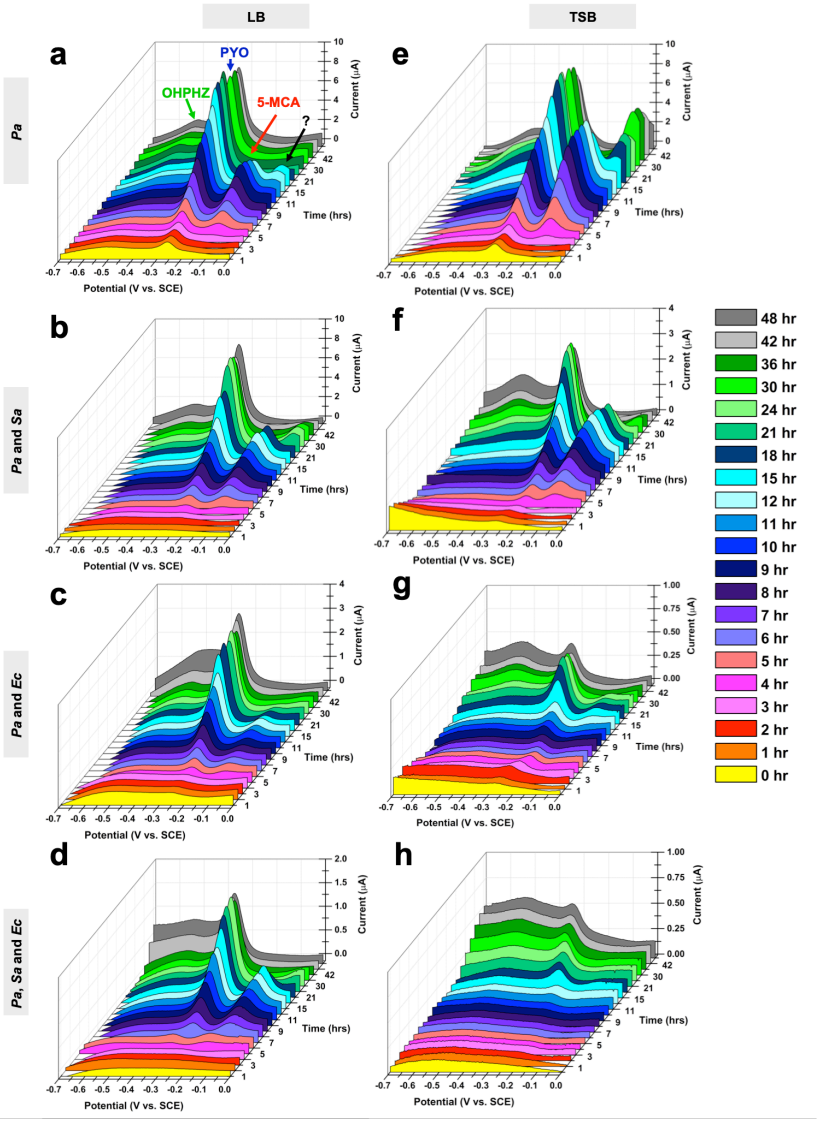

Figure 4.3: Real-time electrochemical monitoring of Pa phenazine production in polymicrobial environments

Time-dependent square wave voltammograms recorded for 0–48 h for (a) *Pa*, (b) *Pa* and *Sa*, (c) *Pa* and *Ec*, and (d) *Pa*, *Sa* and *Ec* in LB media, and (e) *Pa*, (f) *Pa* and *Sa*, (g) *Pa* and *Ec*, and (h) *Pa*, *Sa* and *Ec* in TSB media. The redox peak at –0.256 V vs SCE corresponds to PYO, while the emerging peak at a more positive potential (–0.115 V vs SCE) is due to 5-MCA. The identity of electroactive peaks at a more positive potential than 5-MCA observed in some bacterial cultures remains elusive, however, it might be a reactive derivative species of 5-MCA. Shoulder peaks observed at –0.5 V vs SCE are related to PYO side product, 1-hydroxyphenazine.

Previously, Santiveri and co-workers studied PYO production in various polymicrobial cultures in different media using another electrochemical approach.[57] Their reported results showed that the presence of additional pathogens in growth media did not affect the relative rates of PYO produced by *Pa*,[57] which contradicts our evidence. In their study, to detect and quantify PYO concentrations, researchers used a carbon, macro-size working electrode (3 mm diameter), which might not have the sensitivity, large linear dynamic ranges, and rapid response times necessary to appropriately distinguish differences in production rates not only for PYO, but also for intermediate species in polymicrobial environments. In contrast to their electrochemical platform, requiring the use of a fresh electrode for each new time-based measurement, we have shown that T-CUAs are continually used for measurements for the entire duration of 48-h experiments.[15]

4.3.4 Dynamics of Phenazine Production in Polymicrobial Environments

Along with electrochemical quantification of PYO concentrations in polymicrobial co-cultures, dynamics of the phenazine biosynthetic pathway was monitored. The current-potential responses in Figure 4.3 display remarkable distinctions in production rates of 5-MCA in polymicrobial samples in LB and TSB. These data demonstrate dissimilarities in dynamics of phenazine biosynthesis processes, suggesting a dependence on environmental factors, including other pathogens and media type, which have to date not been observed nor reported in a quantitative manner.

In LB, highly reactive 5-MCA cannot be detected during the exponential phase in any of the cell cultures (Figure 4.3a–d). During intermediate growth stages, 5-MCA production increases corroborated by increasing current responses. The time points where 5-MCA is no longer detected differ between mono- and poly-microbial combination

samples in LB. At later stages of growth, *Pa* no longer produces 5-MCA, likely due to a process leading to fast diminishment (e.g., reaction with oxygen). While there is an initial buildup of 5-MCA, current responses for this intermediate later decrease, which might be associated with factors in growth environments. Comparing polymicrobial samples in LB, the lowest 5-MCA current responses are observed in *Pa* and *Ec* sample (Figure 4.3c). Similar to these results in LB, 5-MCA does not display redox peaks during the first 4 h of growth in TSB (Figure 4.3e–h). Yet, once bacteria enter stationary growth phase, 5-MCA production rates increase in some cell cultures. In TSB-grown samples containing *Ec*, 5-MCA current responses are extremely small, particularly in the combinatorial sample containing all three pathogens (Figure 4.3h). Furthermore, the SWV responses for 5-MCA differ based on media type, where in some cases 5-MCA amounts are higher in TSB compared to LB. Additionally, OHPHZ responses are significantly higher in various polymicrobial samples, specifically those with *Ec*, suggesting increased rates of PYO decomposition in these environmental conditions. Thus, these data illustrate that both the dynamics of polymicrobial co-cultures and media composition influence the rates of phenazine production.

To illustrate the dynamics of phenazine production between polymicrobial samples in two media, the ratios of peak currents of 5-MCA to PYO were plotted as a function of time (Figure 4.5). Theoretically, assuming both metabolites have equal diffusion coefficients, the peak current ratio should be in proportion to the concentration ratio of 5-MCA to PYO. The 5-MCA/PYO current ratio is a significant parameter that reflects the standard rate constant of heterogeneous electron transfer.[58,59] For *Pa* samples, 5-MCA to PYO peak current ratio is higher in TSB relative to LB, indicating that media components impact phenazine biosynthesis. Comparing co-culture samples in LB, 5-MCA to PYO current ratio is approximately two and one half times lower when *Pa* is co-

cultured with *Ec* (Figure 4.5a). On the other hand, polymicrobial samples in TSB display 5-MCA/PYO peak current ratios that are nearly three times lower in polymicrobial samples with *Ec* (Figure 4.5b). Thus, variations in phenazine dynamics between polymicrobial samples in LB and TSB are observed, which contribute to different production rates (Figure 4.4).

Using 5-MCA to PYO peak current ratios, the concentrations of 5-MCA were determined for mono- and poly-microbial samples in LB and TSB, which are summarized in Tables A2.3–A2.4 in the supplementary information. When grown individually, *Pa* produces a maximum 5-MCA concentration of 78 ± 5 μM and 220 ± 2 μM in LB and TSB (at 9 h), respectively. For polymicrobial combinations in LB, *Pa* produces the greatest 5-MCA concentration of 56 ± 3 μM in *Pa* and *Sa* (at 12 h), 9.9 ± 0.4 μM in *Pa* and *Ec* (at 11 h), and 12 ± 2 μM in *Pa*, *Sa* and *Ec* sample (at 11 h). When cultured with *Sa* in TSB, *Pa* produces 38 ± 2 μM as the highest 5-MCA concentration, at 21 h. For *Pa* co-cultured with *Ec* in TSB, the highest amount of 5-MCA was 2.8 ± 0.5 μM at 21 h. *Pa* produces 3.3 ± 0.9 μM as the maximum concentration of 5-MCA when all three pathogens were co-cultured together in TSB. The quantified 5-MCA concentrations were plotted as a function of growth time for two media (Figure 4.4c-d). The maximum 5-MCA concentration in TSB is higher by a factor of 3 compared to LB for *Pa* samples. Yet, when cultured with *Sa*, *Pa* produces slightly higher amounts of 5-MCA in LB compared to TSB. The amounts of 5-MCA in *Pa* and *Sa* sample are marginally lower than in *Pa* culture, in LB. In contrast, 5-MCA concentrations in *Pa* and *Sa* co-culture are lower by a factor of 6 relative to the *Pa* monoculture in TSB. In both media, the presence of *Ec* results in more significant differences with notably small concentrations of 5-MCA produced.

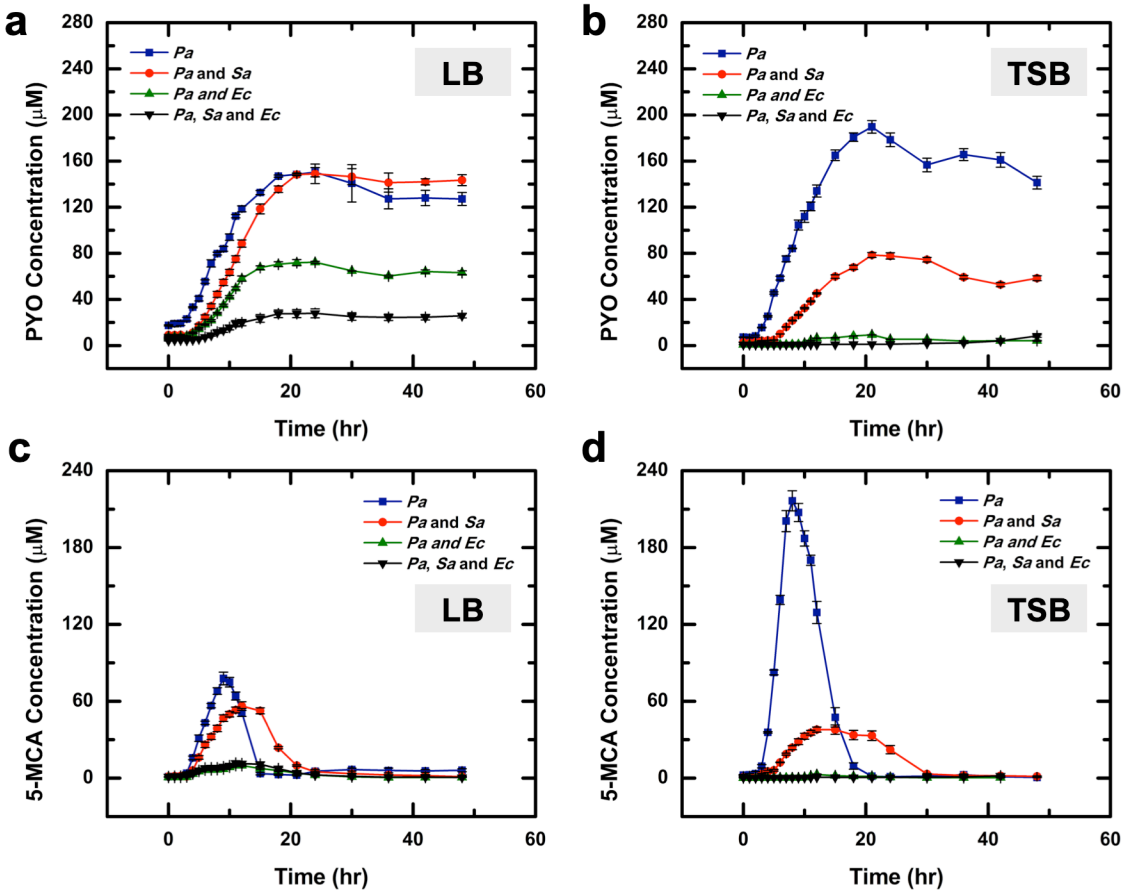

Figure 4.4: PYO and 5-MCA concentrations determined from *Pa* in different polymicrobial co-cultures in LB and TSB media as a function of time.

PYO concentrations determined from *Pa* in different microbial co-cultures in (a) LB and (b) TSB growth media, as a function of time. 5-MCA concentrations secreted from *Pa* in (c) LB and (d) TSB media, were determined from 5-MCA/PYO current peak ratios, relating to phenazine kinetics. Error bars show the standard deviation between six samples. PYO and 5-MCA concentrations are outlined in Tables A2.1–A2.4.

We note that as a highly reactive intermediate[15,60-62] 5-MCA might serve as a signaling molecule in redox balancing. The conversion of PCA to 5-MCA, and to PYO, involves additional functional groups derived from S-adenosylmethionine and molecular oxygen, respectively. The methylase PhzM is responsible for the conversion of PCA to 5-MCA. However, there is an unknown parameter that affects 5-MCA production, which needs to be examined in a future study. While 5-MCA production acts as a sink for PCA, a research study has shown that additional steps, requiring molecular oxygen, might have a significant influence on 5-MCA production.[63] As a result, 5-MCA production might not directly correlate with available PCA. This observation further suggests that environmental factors may differentially regulate synthesis of this intermediate. Our distinct results in LB and TSB further illustrate the effect of environmental factors on 5-MCA concentrations produced in polymicrobial cultures. A recent study has shown that PYO production is activated only in the presence of NADH in addition to a required interaction between PhzM and PhzS enzymes.[47] *Pa* phenazine production is growth phase dependent as metabolites are produced in the stationary phase. During this stage, oxygen is limiting, resulting in NADH accumulation and an increased intercellular $NADH/NAD^+$ ratio,[64] which is relieved by PYO redox balancing. Additionally, the growth conditions, such as nutrients, carbon and nitrogen sources, have significant effects on PYO production rates.[15,65,66]

Figure 4.4 shows distinct phenazine concentrations of PYO and 5-MCA in polymicrobial communities in each media. The presence of *Sa* in LB does not largely impact phenazine production, however, the concentrations of PYO and 5-MCA are lower by a factor of 2.5 and 4, respectively, in TSB. These results suggest that *Sa* and *Pa* compete for nutrients in TSB media, leaving far fewer nutrients available for *Pa*, which consequently decreases phenazine production. The presence of *Ec* in polymicrobial

samples in each media significantly diminishes the rates of phenazine production. In particular, large differences are observed in polymicrobial co-cultures in TSB, where extremely small amounts of both PYO and 5-MCA are produced. A previous biological study has shown initial evidence of the ability of indole produced by *Ec* to quench PYO production and facilitate growth of *Ec* in mixed cultures.[67] Produced as a signal molecule from the amino acid tryptophan by tryptophanase during stationary phase,[36,68] indole inhibits cell division, thus allowing *Ec* to thrive over other bacteria in multispecies communities. Other research has suggested that indole has the capability to decrease virulence induced production in *Pa* by altering gene expression and interfering with quorum sensing mechanisms.[36] To test for indole presence in polymicrobial samples with *Ec*, Kovac's test was performed. This qualitative procedure, which determines bacteria's ability to produce indole by deamination of tryptophan, yielded a red-violet-pink top layer in cell cultures with *Ec* in each media at various growth times (6, 18, and 24 h), confirming the presence of indole in the polymicrobial combinations.

Although a previous study has shown the *Ec* can secrete indole concentrations up to 600 μM,[36] indole production might be critically affected by several environmental factors, such as cell population, carbon sources, pH, and temperature. Therefore, indole amounts produced likely diverge in different environmental conditions thus impacting phenazine production dynamics in various ways. These results highlight the importance of identifying environmental parameters that influence metabolism dynamics in diverse microbial communities, particularly in the context of polymicrobial infections. Phenazine production rates are likely regulated on multiple environmental levels, which have to be standardized with regard to growth media to understand phenazine production dynamics.

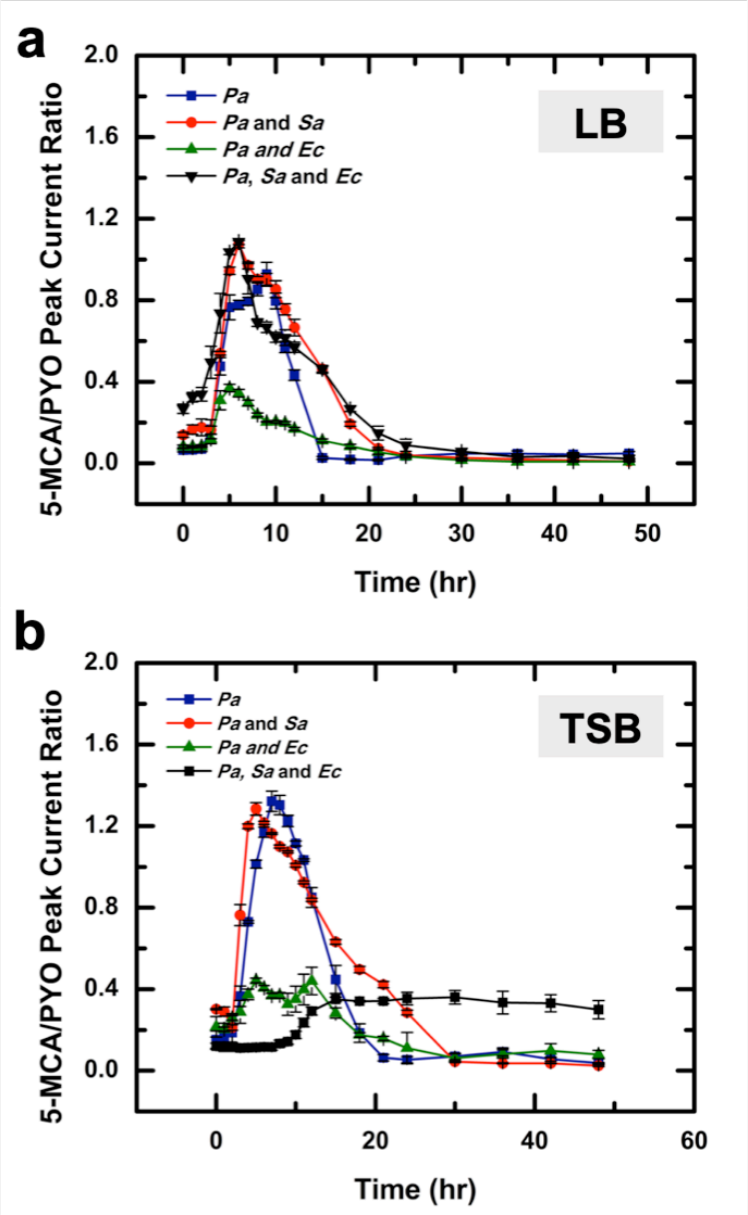

Figure 4.5: Phenazine metabolites kinetics in polymicrobial samples.

5-MCA/PYO peak currents ratios determined from *Pa* in different co-cultures in (a) LB and (b) TSB, shown as a function of time. Error bars plotted denote standard deviation between six samples.

4.3.5 Influence of Growth Media on Phenazine Production in Polymicrobial Environments

The quantitative results, shown in previous sections of this study, address how the relative phenazines production (Figure 4.4) and ratio to other intermediates (Figure 4.5) change during growth in response to various environmental factors. Most importantly changes in the dynamics are observed in the presence of other microbes, pH, and media composition. In this study, both LB and TSB liquid broths were used, which are rich with nutrients essential in supporting the growth of various microorganisms. Although there are many options when choosing growth media (e.g., phosphate buffered saline, buffered year extract broth, Mueller-Hinton broth, nutrient broth),[66] these two complex media are the most predominant in studies with *Pa* reported in the literature (Table A2.5 in Appendix 2). In particular, LB and TSB contain different casein peptones, peptides, minerals, several vitamins and trace elements (e.g., S, Mg, N). Given their complexity and richness in nutrients, TSB and LB are reasonable choices of growth media herein. In prior research,[15] described in Chapter 3, DESI-MS methods were employed to analyze differences in the composition of these media. Briefly, these results showed noteworthy distinctions between LB and TSB: (1) the relative abundance of choline (a water-soluble vitamin consumed by cells for production of toxins) at *m/z* 104.107 in the positive ion mode, and (2) the relative abundance of protonated and chlorinated hexose species (six-carbon sugars) at *m/z* 179.056 and *m/z* 215.032, respectively. Higher relative abundances for both choline and hexose species were detected in TSB relative to LB, which resulted in higher amounts of PYO produced in TSB for *Pa* monoculture.[15]

To better understand how components of each media might be contributing to observed variations in phenazine production, qualitative DESI-MS analyses were performed to compare relative abundances of choline and hexose species in

polymicrobial combinations at 5 h growth. In the positive ion mode, the relative abundances of choline at *m/z* 104.107 for three different polymicrobial cultures in LB did not notably differ between samples (Figure A2.1b), with the lowest abundance observed for the *Pa* and *Ec* sample (Figure A2.1a, A2.2). Similarly, the relative abundances of this species were comparable between the three combination samples in TSB (Figure A2.1a, A2.1c, A2.3). Higher relative abundances for choline were detected in samples in TSB compared to LB as depicted in the ion images in Figure A2.1a. When *Pa* was cultured separately in LB or TSB, significantly lower abundances of choline were detected (Figure A2.2b, A2.3b) in comparison to polymicrobial samples, suggesting high consumption of choline by individually grown *Pa*. Yet this is not observed in the polymicrobial samples, indicating that the presence of other pathogens changes choline consumption rates. In the negative ion mode, the relative abundances of hexose species did not considerably vary between three different polymicrobial combinations in LB and TSB (Figure A2.4–S2.5). For *Pa* monocultures in TSB and LB, the hexose relative abundances are qualitatively higher compared to polymicrobial samples (Figure A2.6–A2.7). Variation in the abundance of deprotonated and chlorinated hexose species are observed, likely due to possible changes occurring dependent on adduct type. These data suggest that pathogenic bacteria in these environments might compete for hexose and most likely numerous other nutrients in growth media. Consequently, growth media composition highly impacts phenazine production and dynamics in several ways as observed in our electrochemical results.

In addition to qualitatively comparing relative abundances of choline and hexose, DESI-MS analysis was performed to detect PYO and other cellular metabolites in polymicrobial samples in both growth media. Figure 4.6 provides representative mass spectra and ion images (in the positive ion mode) for cellular PYO detected at *m/z*

211.086 in polymicrobial environments in LB and TSB. Higher relative abundances of PYO were observed in polymicrobial samples in LB than in TSB (Figure 4.6a). A small decrease in PYO abundance was observed when all three pathogens were cultured together in LB (Figure 4.6b). For polymicrobial combination tests in TSB, the highest PYO abundance was detected in *Pa* and *Sa* sample while the lowest PYO abundance was found in the sample containing all three bacterial types (Figure 4.6c). Yet PYO was not detectable (S/N<3) in the mass spectra for *Pa* and *Ec* co-culture in TSB. These qualitative mass spectrometry results are in agreement with PYO trends in quantitative electrochemical data. In addition to PYO, other metabolites and enzymatic products from different polymicrobial cultures in each media were detected using DESI-MS (Figure A2.4–A2.6). Multiple changes in metabolites abundances were observed: (1) succinate at *m/z* 117.019 was less abundant in *Pa* and *Sa* samples in LB and TSB, (2) disaccharide at *m/z* 377.085 was detected in lower abundances in polymicrobial samples with *Sa* present, and (3) abundances of citrate at *m/z* 191.019 and gluconate at *m/z* 195.051 were lower in samples containing *Ec*. As summarized in Figure A2.6, metabolite distribution differs between growth media. While DESI-MS results provide useful information about media composition and additional cellular species produced in polymicrobial co-cultures, these results are only qualitative. Unlike our electrochemical method providing means for *in situ* quantitative analysis, DESI-MS measurements are associated with biases present in sampling times and sample drying effects, causing exposure to oxygen and cell death prior to analysis. Moreover, enhanced matrix and susceptibility to ion suppression associated with ambient ionization mass spectrometry methods lead to additional limitations for quantitative analysis of metabolites.

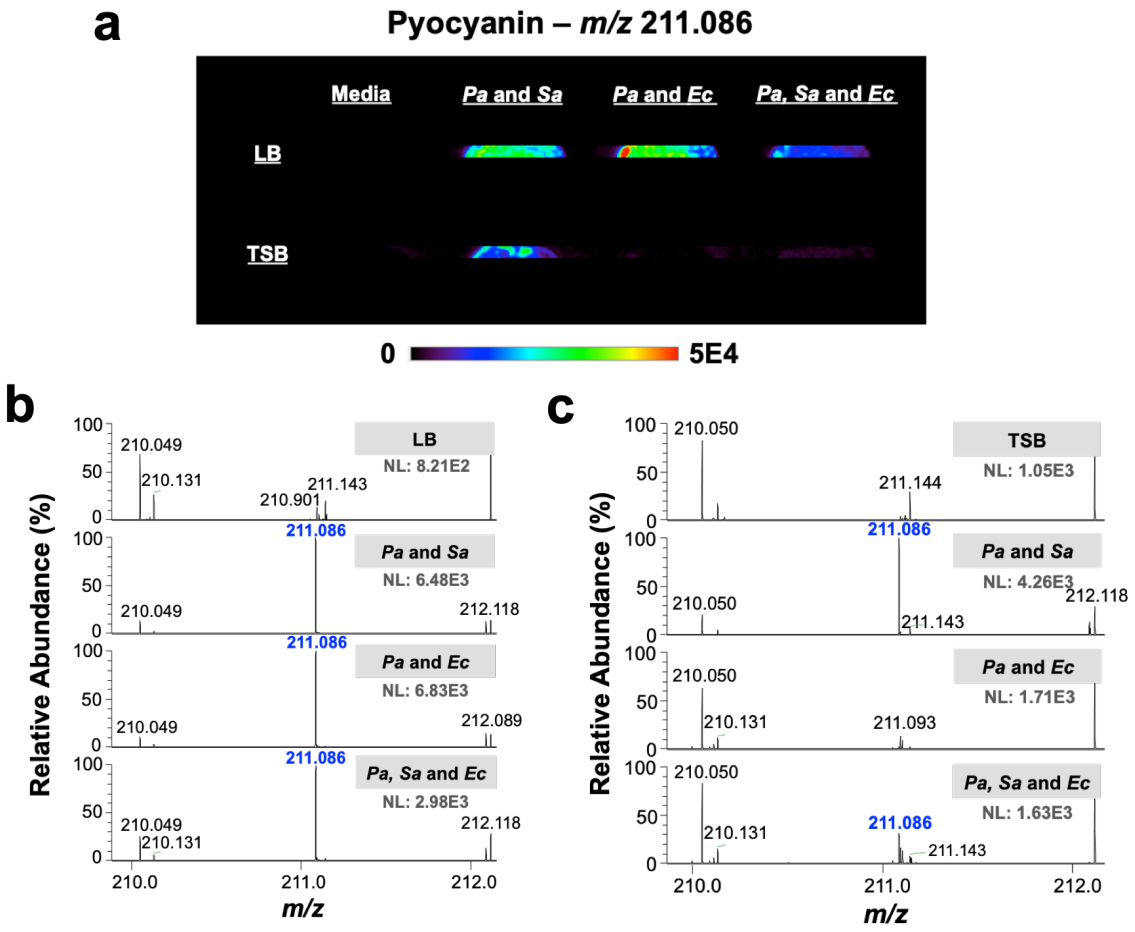

Figure 4.6: DESI-MS data of PYO at *m/z* 211.086 obtained at 5 h of growth in different polymicrobial samples in LB and TSB.

(a) DESI-MS ion images in *Pa* and *Sa*, *Pa* and *Ec*, and *Pa*, *Sa*, and *Ec* in each media. Relative abundances of PYO produced by *Pa* are higher in LB relative to TSB. Highest PYO relative abundances are observed in samples containing *Sa*. PYO relative abundances are lower in polymicrobial samples containing *Ec*, especially in TSB. These qualitative data are in agreement with electrochemical quantification of PYO. (b) DESI-MS spectra of PYO (positive ion mode) for polymicrobial samples in LB. (c) DESI-MS spectra of PYO (positive ion mode) for polymicrobial samples in TSB. PYO, secreted from *Pa*, is not detected in the DESI-MS spectra for LB and TSB only. NL represents ion abundance (ion current).

In these complex polymicrobial environments, bacteria might be feeding and competing for nutrients, and/or producing additional cellular metabolites dependent on the media type. Our results clearly demonstrate that in polymicrobial communities, the onset of infection changes drastically with respect to phenazine production rates. The presence of other bacteria significantly influences phenazine production in different ways, which is also heavily dependent on growth media. Our results call for the standardization for cell culture experiments, largely with respect to growth media components and quantities, as it is necessary to appropriately study the onset of polymicrobial infections. As summarized in Table A2.5 in Appendix 2, there are countless possibilities of growth media for culturing *Pa*, including nonstandard methods, such as synthetic cystic fibrosis sputum[69] and wound-like media.[70] Yet, with standard growth media, such as LB and TSB, the real analytical concentrations of components likely vary between batches. Future research needs to focus on optimization, standardization, and certification of growth environment standards mainly because quantitative analytical chemistry is missing from standardization of assays. Specifically, it is necessary to understand particular media components and quantities to adequately assess which contribute to differences in phenazine dynamics. To understand how complex media influences development of infections, design of certified media standards that simulate environments for cystic fibrosis, biofilms and/or wound infections is essential, which is beyond the scope of this study. Therefore, the state of polymicrobial infections needs to be reexamined for biodiagnosis of *Pa* phenazine dynamics.

Our results, showing distinct dynamics of phenazine production with regard to growth in multispecies samples, point to the need for standard methods of growth media, which have great implications towards understanding the onset of bacterial infections, antibiotic resistance, and treatments. More extensive environmental factors need to be

examined, however, our electrochemical approach provides the basis set as to the relative differences in phenazine production rates that can be quantified with high sensitivity. In follow-up work, the influence of additional factors (oxygen availability, host genetics, and antibiotics) on redox phenazine production will be monitored using T-CUAs.

3.4 CONCLUSIONS

In summary, this study shows quantitative electrochemical monitoring of the impact of polymicrobial communities on production rates of *Pa* phenazine metabolites in different growth media. Using T-CUAs as electrochemical sensors, the dynamics of phenazine biosynthesis were continually observed via detection of redox-active metabolites PYO, 5-MCA, OHPHZ, and an unknown species. These quantitative results demonstrate distinct electrochemical current responses for phenazines produced between *Pa* grown: (1) individually, and (2) in polymicrobial samples. In LB, the maximum concentrations of PYO were 150 ± 1 μM for *Pa*, 150 ± 1 μM for *Pa* and *Sa*, 72 ± 1 μM for *Pa* and *Ec,* and 28 ± 1 μM in *Pa*, *Sa* and *Ec* sample (at 21 h). In TSB, the highest PYO concentrations were 190 ± 5 μM for *Pa* (at 21 h), 78 ± 2 μM for *Pa* and *Sa* (at 21 h), 9.3 ± 0.2 μM for *Pa* and *Ec* (at 21 h), and 8.2 ± 0.5 μM in *Pa*, *Sa* and *Ec* sample (at 48 h). Additionally, the concentrations of highly reactive 5-MCA were determined. The presence of *Sa* caused a notable decrease in phenazine concentrations only in TSB while the presence of *Ec* in polymicrobial samples drastically quenched phenazine production rates in both media. These disparities likely correlate to (1) differences in nutrient consumption, and (2) other cellular metabolites produced, in polymicrobial environments. These results clearly demonstrate that presence of other bacteria dramatically impacts phenazine production rates, which also directly depends on the media type. The media type strongly influences phenazine product distribution, especially in polymicrobial co-

cultures. Therefore, these data imply the need for analytical standardization of simulation media, which represent key attributes of *in vivo* environments (e.g., wounds, cystic fibrosis lungs). Our T-CUAs electroanalytical method has the sensitivity to distinguish differences based on correlative measurements in media not only on phenazine production but also on intermediates produced in polymicrobial samples. Thus, these data support use of T-CUAs in biodiagnosis and monitoring of *Pa* infections colonized by multiple bacteria.

Future work will focus on electrochemical monitoring of *Pa* phenazine production in the presence of other relevant pathogens, such as *Enterococcus faecalis* and *Staphylococcus epidermidis*, as well as in the presence of eukaryotic, host cells (e.g., macrophages). Moreover, studies need to be performed with additional, increased co-cultures comprising of more than three pathogens. Additionally, phenazine production and dynamics need to be examined on T-CUAs with clinically relevant *Pa* strains isolated from patients, as clinical strains grow at different rates dependent on environmental conditions and composition.[71] Finally, the state of infection in these polymicrobial populations needs to be reexamined for diagnosis, specifically with respect to standardization of simulated growth media.

4.5 ADDITIONAL INFROMATION

Details on the quantitatively determined PYO and 5-MCA concentrations in polymicrobial samples in LB and TSB media from real-time electrochemical data, DESI-MS spectra in the positive and negative ion modes at 5 h of bacterial growth in polymicrobial samples TSB and LB media contents, DESI-MS data of cellular metabolites detected in polymicrobial combinations samples, summary of most

commonly used growth media for *P. aeruginosa*, Tables A2.1–A2.5, and Figures A2.1–A2.7 are provided in Appendix 2.

4.6 REFERENCES

(1) Boucher, H. W.; Talbot, G. H.; Bradley, J. S.; Edwards, J. E.; Gilbert, D.; Rice, L. B.; Scheld, M.; Spellberg, B.; Bartlett, J. *Clin. Infect. Dis.* **2009**, *48*, 1–12.

(2) Klevens, R. M.; Edwards, J. R.; Richards, C. L.; Horan, T. C.; Gaynes, R. P.; Pollock, D. A.; Cardo, D. M. *Public Health Rep* **2007**, *122*, 160–166.

(3) Henke, J. M.; Bassler, B. L. *Trends in Cell Biology* **2004**, *14*, 648–656.

(4) Bassler, B. L.; Losick, R. *Cell* **2006**, *125*, 237–246.

(5) Stevens, A. M.; Schuster, M.; Rumbaugh, K. P. *J. Bacteriol.* **2012**, *194*, 2131–2141.

(6) Magill, S. S.; Edwards, J. R.; Bamberg, W.; Beldavs, Z. G.; Dumyati, G.; Kainer, M. A.; Lynfield, R.; Maloney, M.; McAllister-Hollod, L.; Nadle, J.; Ray, S. M.; Thompson, D. L.; Wilson, L. E.; Fridkin, S. K. *N Engl J Med* **2014**, *370*, 1198–1208.

(7) Bowler, P. G.; Duerden, B. I.; Armstrong, D. G. *Clinical Microbiology Reviews* **2001**, *14*, 244–269.

(8) Bertesteanu, S.; Triaridis, S.; Stankovic, M.; Lazar, V.; Chifiriuc, M. C.; Vlad, M.; Grigore, R. *International Journal of Pharmaceutics* **2014**, *463*, 119–126.

(9) Giacometti, A.; Cirioni, O.; Schimizzi, A. M.; Del Prete, M. S.; Barchiesi, F.; D'Errico, M. M.; Petrelli, E.; Scalise, G. *J Clin Microbiol* **2000**, *38*, 918–922.

(10) Llor, C.; Bjerrum, L. *Ther Adv Drug Saf* **2014**, *5*, 229–241.

(11) Duay, J.; Goran, J. M.; Stevenson, K. J. *Anal. Chem.* **2014**, *86*, 11528–11532.

(12) Duay, J.; Elliott, J.; Shear, J. B.; Stevenson, K. J. *Anal. Chem.* **2015**, *87*, 10109–10116.

(13) Elliott, J.; Duay, J.; Simoska, O.; Shear, J. B.; Stevenson, K. J. *Anal. Chem.* **2017**, *89*, 1267–1274.

(14) Elliott, J.; Simoska, O.; Karasik, S.; Shear, J. B.; Stevenson, K. J. *Anal. Chem.* **2017**, *89*, 6285–6289.

(15) Simoska, O.; Sans, M.; Fitzpatrick, M. D.; Crittenden, C. M.; Eberlin, L. S.; Shear, J. B.; Stevenson, K. J. *ACS Sensors* **2019**, *4*, 170–179.

(16) Fetzer, A. F.; Werner, A. S.; Hagstrom, J. W. *Am. Rev. Respir. Dis.* **1967**, *96*, 1121–1130.

(17) Fick, R. B. *Chest.* **1989**, *96*, 158–164.

(18) Ringen, L. M.; Drake, C. H. *J. Bacteriol.* **1952**, *64*, 841–845.

(19) Walker, T. S. *Plant Physiol.* **2004**, *134*, 320–331.

(20) Alatraktchi, F.; Breum Andersen, S.; Krogh Johansen, H.; Molin, S.; Svendsen, W. *Sensors* **2016**, *16*, 408–410.

(21) Alatraktchi, F. A.; Johansen, H. K.; Molin, S.; Svendsen, W. E. *Nanomedicine* **2016**, *11*, 2185–2195.

(22) Webster, T. A.; Sismaet, H. J.; Conte, J. L.; Chan, I.-P. J.; Goluch, E. D. *Biosens. Bioelectron.* **2014**, *60*, 265–270.

(23) Jayaseelan, S.; Ramaswamy, D.; Dharmaraj, S. *World J. Microbiol. Biotechnol.* **2013**, *30*, 1159–1168.

(24) Mavrodi, D. V.; Peever, T. L.; Mavrodi, O. V.; Parejko, J. A.; Raaijmakers, J. M.; Lemanceau, P.; Mazurier, S.; Heide, L.; Blankenfeldt, W.; Weller, D. M.; Thomashow, L. S. *Applied and Environmental Microbiology* **2010**, *76*, 866–879.

(25) Dietrich, L. E. P.; Price-Whelan, A.; Petersen, A.; Whiteley, M.; Newman, D. K. *Mol. Microbiol.* **2006**, *61*, 1308–1321.

(26) Webster, T. A.; Goluch, E. D. *Lab Chip* **2012**, *12*, 5195–5197.

(27) Alatraktchi, F. A.; Noori, J. S.; Tanev, G. P.; Mortensen, J.; Dimaki, M.; Johansen, H. K.; Madsen, J.; Molin, S.; Svendsen, W. E. *PLoS ONE* **2018**, *13*, e0194157–e0194159.

(28) Sharp, D.; Gladstone, P.; Smith, R. B.; Forsythe, S.; Davis, J. *Bioelectrochemistry* **2010**, *77*, 114–119.

(29) Pierson, L. S.; Pierson, E. A. *Appl Microbiol Biotechnol* **2010**, *86*, 1659–1670.

(30) Mavrodi, D. V.; Blankenfeldt, W.; Thomashow, L. S. *Annu. Rev. Phytopathol.* **2006**, 417–445.

(31) Glasser, N. R.; Kern, S. E.; Newman, D. K. *Mol. Microbiol.* **2014**, *92*, 399–412.

(32) Hendiani, S.; Pornour, M.; Kashef, N. *Photodiagnosis and Photodynamic Therapy* **2019**, *26*, 8–12.

(33) Schiessl, K. T.; Hu, F.; Jo, J.; Nazia, S. Z.; Wang, B.; Price-Whelan, A.; Min, W.; Dietrich, L. E. P. *Nat. Commun.* **2019**, *10*, 762–772.

(34) Mirani, Z. A.; Fatima, A.; Urooj, S.; Aziz, M.; Khan, M. N.; Abbas, T. *Iran J Basic Med Sci* **2018**, *21*, 760–770.

(35) O'Brien, S.; Fothergill, J. L. *FEMS Microbiol Lett* **2017**, *364*, 850–860.

(36) Lee, J.-H.; Lee, J. *FEMS Microbiol Rev* **2010**, *34*, 426–444.

(37) Atkinson, S.; Williams, P. *J. R. Soc. Interface* **2009**, *6*, 959–978.

(38) Korgaonkar, A.; Trivedi, U.; Rumbaugh, K. P.; Whiteley, M. *Proc Natl Acad Sci USA* **2013**, *110*, 1059–1064.

(39) Bergeron, A. C.; Seman, B. G.; Hammond, J. H.; Archambault, L. S.; Hogan, D. A.; Wheeler, R. T. *Infect. Immun.* **2017**, *85*, 340–358.

(40) Sullivan, N. L.; Tzeranis, D. S.; Wang, Y.; So, P. T. C.; Newman, D. *ACS Chem. Biol.* **2011**, *6*, 893–899.

(41) Connell, J. L.; Ritschdorff, E. T.; Whiteley, M.; Shear, J. B. *Proc Natl Acad Sci USA* **2013**, *110*, 18380–18385.

(42) Goluch, E. D. *Trends Biotechnol* **2017**, *35*, 1125–1128.

(43) Lee, D.-H.; Koh, E.-H.; Choi, S.-R.; Kim, S. *Ann Lab Med* **2013**, *33*, 406–444.

(44) Mavrodi, D. V.; Bonsall, R. F.; Delaney, S. M.; Soule, M. J.; Phillips, G.; Thomashow, L. S. *J. Bacteriol.* **2001**, *183*, 6454–6465.

(45) Bosire, E. M.; Rosenbaum, M. A. *Front. Microbiol.* **2017**, *8*, 5026–11.

(46) Diederich, C.; Leypold, M.; Culka, M.; Weber, H. X. R.; Breinbauer, R.; Ullmann, G. M.; Blankenfeldt, W. *Sci. Rep.* **2017**, 1–13.

(47) Parsons, J. F.; Greenhagen, B. T.; Shi, K.; Calabrese, K.; Robinson, H.; Ladner, J. E. *Biochemistry* **2007**, *46*, 1821–1828.

(48) Zheng, H.; Kim, J.; Liew, M.; Yan, J. K.; Herrera, O.; Bok, J. W.; Kelleher, N. L.; Keller, N. P.; Wang, Y. *Curr Biol* **2015**, *25*, 29–37.

(49) Buzid, A.; Shang, F.; Reen, F. J.; Muimhneacháin, E. Ó.; Clarke, S. L.; Zhou, L.; Luong, J. H. T.; O'Gara, F.; McGlacken, G. P.; Glennon, J. D. *Sci. Rep.* **2016**, *6*, 30001–30009.

(50) Gandouzi, I.; Tertis, M.; Cernat, A.; Saidane-Mosbahi, D.; Ilea, A.; Cristea, C. *Materials* **2019**, *12*, 1180–1193.

(51) Rohmer, L.; Hocquet, D.; Miller, S. I. *Trends Microbiol* **2011**, *19*, 341–348.

(52) Sismaet, H. J.; Pinto, A. J.; Goluch, E. D. *Biosens. Bioelectron.* **2017**, *97*, 65–69.

(53) Shah, A.; Ullah, A.; Nosheen, E.; Rana, U. A.; Shakir, I.; Badshah, A.; Rehman, Z. U.; Hussain, H. *Journal of the Electrochemical Society* **2013**, *160*, H765–H769.

(54) Noto, M. J.; Burns, W. J.; Beavers, W. N.; Skaar, E. P. *J. Bacteriol.* **2017**, *199*, e00221-17.

(55) Alves, P. M.; Al-Badi, E.; Withycombe, C.; Jones, P. M.; Purdy, K. J.; Maddocks, S. E. *Pathogens and Disease* **2018**, *76*, 67–77.

(56) Culotti, A.; Packman, A. I. *PLoS ONE* **2014**, *9*, e107186–e107189.

(57) Santiveri, C. R.; Sismaet, H. J.; Kimani, M.; Goluch, E. D. *ChemistrySelect* **2018**, *3*, 2926–2930.

(58) Mirceski, V.; Laborda, E.; Guziejewski, D.; Compton, R. G. *Anal. Chem.* **2013**, *85*, 5586–5594.

(59) Dauphin-Ducharme, P.; Arroyo-Currás, N.; Kurnik, M.; Ortega, G.; Li, H.; Plaxco, K. W. *Langmuir* **2017**, *33*, 4407–4413.

(60) Reyes, E. A. P.; Bale, M. J.; Cannon, W. H.; Matsen, J. M. *J Clin Microbiol* **1981**, *13*, 456–458.

(61) Bellin, D. L.; Sakhtah, H.; Zhang, Y.; Price-Whelan, A.; Dietrich, L. E. P.; Shepard, K. L. *Nat. Commun.* **2016**, *7*, 10535–10544.

(62) Bellin, D. L.; Sakhtah, H.; Rosenstein, J. K.; Levine, P. M.; Thimot, J.; Emmett, K.; Dietrich, L. E. P.; Shepard, K. L. *Nat. Commun.* **2014**, *5*, 3256–3265.

(63) Xu, N.; Ahuja, E. G.; Janning, P.; Mavrodi, D. V.; Thomashow, L. S.; Blankenfeldt, W. *Acta Crystallogr. D Biol. Crystallogr.* **2013**, *69*, 1403–1413.

(64) Price-Whelan, A.; Dietrich, L. E. P.; Newman, D. K. *J. Bacteriol.* **2007**, *189*, 6372–6381.

(65) Jayaseelan, S.; Ramaswamy, D.; Dharmaraj, S. *World J. Microbiol. Biotechnol.* **2014**, *30*, 1159–1168.

(66) Li, S.; Mou, Q.; Feng, N.; Leung, P. H. M. *Int. J. Electrochem. Sci.* **2018**, *13*, 3789–3798.

(67) Chu, W.; Zere, T. R.; Weber, M. M.; Wood, T. K.; Whiteley, M.; Hidalgo-Romano, B.; Valenzuela, E., Jr.; McLean, R. J. C. *Applied and Environmental Microbiology* **2011**, *78*, 411–419.

(68) Pandey, R.; Swamy, K. V.; Khetmalas, M. B. *IJBT* **2019**, *12*, 297–310.

(69) Darch, S. E.; Simoska, O.; Fitzpatrick, M.; Barraza, J. P.; Stevenson, K. J.; Bonnecaze, R. T.; Shear, J. B.; Whiteley, M. *Proc Natl Acad Sci USA* **2018**, *115*, 4779–4789.

(70) DeLeon, S.; Clinton, A.; Fowler, H.; Everett, J.; Horswill, A. R.; Rumbaugh, K. P. *Infect. Immun.* **2014**, *82*, 4718–4728.

(71) Wu, X.; Siehnel, R. J.; Garudathri, J.; Staudinger, B. J.; Hisert, K. B.; Ozer, E. A.; Hauser, A. R.; Eng, J. K.; Manoil, C.; Singh, P. K.; Bruce, J. E. *Journal of Proteome Research* **2019**, *18*, 2601–2612.

Chapter 5: Future Directions[5]

5.1 INTRODUCTION

5.1.1 Synthetic Cystic Fibrosis Sputum as Growth Medium for *P. aeruginosa*

Cystic fibrosis is a genetic disorder associated with colonization of bacterial pathogens and accumulation of large amounts of mucus secretions (here, referred to as sputum) within the lungs, which diminishes the ability of the host to clear bacterial diseases.[1-4] The gram-negative pathogen *Pseudomonas aeruginosa* is a major bacterium causing chronic airways infections in people with cystic fibrosis (CF), causing an increase in morbidity and mortality rates.[5-9] While multicellular aggregates colonize the CF sputum during infections, *P. aeruginosa* is a major species often growing to high cell densities of 10^9 cells/mL of sputum.[2,10] Once established, *P. aeruginosa* infections in the CF lung are resistant to effective antibiotic and antimicrobial treatments as therapies fail to fully eliminate the pathogen.[9] Although the mechanisms for *P. aeruginosa* high persistence to antibiotics are not completely understood, recent studies have shown that *P. aeruginosa* adopts physiological states and evolve traits that enhance their capability to evade host responses in the CF sputum.[8,11-13] A recent study showed that airway *P. aeruginosa* strains produced higher levels of specific proteins involved in the production and transport of alginate (an exopolysaccharide involved in the formation of aggregates). The study concluded that *P. aeruginosa* grows more slowly in the CF sputum[13,14] and exhibits different metabolic provides from *in vitro* grown bacteria,[1,15-17] highlighting how

[5]Portions of this chapter were published in Darch, S. E; Simoska, O.; Fitzpatrick, M. D.; Barraza, J. P.; Stevenson, K. J.; Bonnecaze, R. T.; Shear, J. B.; Whiteley, M. Spatial Determinants of Quorum Signaling in a *Pseudomonas aeruginosa* infection model. *Proc. Natl. Acad. Sci. U.S.A.* **2018**, *5*, 4779-4789. For some data and results presented in first part of this chapter, Simoska, O. performed research; Simoska, O. and Stevenson, K. J. designed the viscosity and electrochemistry studies and analyzed the data.

standard culturing methods can provide poor models for how bacteria persist in the host.[13]

In studying bacterial infections, it is important to understand the composition of the *in vivo* growth environments (e.g., carbon source, energy from host).[1] While Garber proposed the host system as a growth medium over 50 years ago,[18] the nutritional composition of most infection sites, such as the CF lung, is not well defined and often inadequately modeled by standardized growth media used in laboratory settings. The results presented in Chapters 3 and 4 in this dissertation point to the need for analytical standard methods of simulated growth media to adequately study bacterial infections and antibiotic resistance.[19] The lack of standard methods of growth media that closely mimic *in vivo* growth environments provides significant challenges in studying the onset of *P. aeruginosa* infections. Thereby, it is critical to define the growth environment components and concentrations of infection sites (e.g., CF airway) to study the effects of environmental conditions on the production of *P. aeruginosa* virulence factors.[1]

Towards these goals, the Whiteley laboratory has previously developed a defined synthetic CF medium to closely represent key attributes of the human CF sputum (SCFM),[1,2] which has been used to study how nutritional composition impacts *P. aeruginosa* growth rates and virulence production.[20,21] In a follow-up study, the Whiteley lab further modified this growth medium via the addition of relevant levels of macromolecules found in CF sputum (mucin, DNA and lipids) to develop a second-generation CF medium (SCFM2). SCFM2 has genetic requirements similar to human sputum and closely mimics the physical properties of expectorated CF sputum.[20] Previous research has shown that SCFM2 promotes the formation of *P. aeruginosa* aggregates similar to those found in the lungs of CF patients.[3] While this growth medium is not a

standardized method of growth, it provides a relevant growth media model to study *P. aeruginosa* CF infections.[3]

In this dissertation chapter, research studies performed using SCFM2 sputum media are presented. Specifically, analyses were performed to characterize the viscoelastic properties of SCFM2 as well as to electrochemically determine the diffusion coefficients of pyocyanin (PYO) in SCFM2.[22] Additionally, we present preliminary results from time-dependent studies using transparent carbon ultramicroelectrode arrays (T-CUAs) to electrochemically monitor PYO production by *P. aeruginosa* cells grown in SCFM2 sputum in tandem with confocal microscopy imaging through T-CUAs to observe the formation of bacterial aggregates. For these studies, mutant *P. aeruginosa* strains were used, which were modified by the Whiteley laboratory to constitutively express mCherry as well as express green fluorescent protein (GFP) when quorum sensing molecules are produced. Our initial results indicate that *P. aeruginosa* grows differently in SCFM2, associated with the lower rates PYO production compared to those from *P. aeruginosa* grown in standard laboratory growth media (Chapters 3 and 4). Additionally, these preliminary results show slight correlations between electrochemical measurements of PYO concentration and data obtained confocal microscopy images of *P. aeruginosa* aggregates.

5.1.2 Pyocyanin and Nitric Oxide Interaction

The complex environments in which cells interact typically have diverse cellular populations and are susceptible to changes that influence cellular survival, division, differentiation, death, and virulence. Such dynamic responses are often mediated, at least in part, by changes in the concentrations of cellularly derived biogenic signaling molecules. Hence, the *in vitro* detection of these cellular species is pivotal to

understanding cellular communication in immunological-bacterial interactions. Microbial pathogenicity occurs in a susceptible host, which houses its microbiota while interacting with pathogenic microorganisms. Recent research findings have provided insight on how the cell signaling mechanisms are activated in host immune responses,[23] however, there is a significant lack of knowledge in understanding the interactions of signaling biogenic molecules in host-pathogen environments as infections develop.

As highly adoptable microorganism that causes infections in humans, bacteria evade host defense responses as well as antibiotic resistance mechanism. Thereby, it is important to identify and characterize complex mechanisms in which microorganisms cause chronic and persistent infections.[24] Specifically, an important strategy in developing pathogenicity and antibiotic resistance is the formation of bacterial biofilms,[24-26] which are associated with 80% of human infections and often present in the CF lungs.[27] Biofilm formation is a complex and highly regulated process, which is often an adaptation response to environmental factors, including changes in temperature, pH, nutrient limitations, and/or oxygen levels.[26] Consequently, eukaryotic, host organisms develop sophisticated defense mechanisms in response to developing antibiotic-resistant biofilms.[27] Various research studies have shown that the biogenic signaling molecule nitric oxide ($NO^{\bullet}$) to induce biofilm dispersal in many bacterial species, including *P. aeruginosa*.[28,29] $NO^{\bullet}$ is involved not only in biofilm regulation but also in mediating QS responses,[30,31] which are interconnected with biofilm formation.[32] The complex interactions between the immune system and microbes involve signaling molecules that largely vary in size, ranging from large molecules (e.g., cytokines, hormones, neurotransmitters, sugars) to very small molecules (e.g., hydrogen peroxide, PYO, nitric oxide).[27] Small molecules are most abundant and their functions include serving as intermediate metabolites, nutrients, virulence factors, and electron acceptors.[27] Therefore,

understanding the role of $NO^{\bullet}$ in *P. aeruginosa* biofilm dispersal could be fundamental in developing effective strategies in prevention and treatment of antibiotic-resistant biofilm infections. Thus, this chapter presents preliminary studies on the electrochemical monitoring of the interaction of two biogenic signaling molecules, $NO^{\bullet}$ and PYO, secreted by macrophages and *P. aeruginosa* cells, respectively. Insight into how and when *P. aeruginosa* encounter $NO^{\bullet}$ during infection progress has both clinical and physiological relevance.

As described in previous chapters in this dissertation, gram-negative, facilitative anaerobe *P. aeruginosa* is an opportunistic human pathogen responsible for a high number of hospital-acquired biofilm infections. It is the prevalent species isolated from patients with immune-compromised systems and chronic wounds as well as from the lungs of those suffering from cystic fibrosis. As part of its virulence mechanisms, *P. aeruginosa* secretes virulence factors that cause infections in host organisms to thrive.[33,34] Among these virulence factors is the blue pigment, redox-active phenazine compound, PYO.[35-37] As a highly diffusible signal, PYO is involved in quorum sensing (QS), a population-dependent cell-to-cell communication process allowing bacteria to regulate gene expression based on the effective cellular density.[38,39] Since it is uniquely produced by *P. aeruginosa* cells, PYO serves as an effective diagnostic molecule marker for identifying developing *P. aeruginosa* infections.[38] Previous studies have shown that PYO concentrations isolated and detected from various *in vivo* environments, fall in the low- to mid-micromolar range. PYO readily reacts with cellular metabolites to generate reactive oxygen species (ROS), causing damage to host tissue and surrounding microorganisms.[35] Additionally, it has a variety of pharmacological effects on both prokaryotic and eukaryotic cells.[40] PYO engages in chemical warfare with the immune system, thereby its detection could provide a better understanding of *P. aeruginosa* virulence mechanisms.

Another cellular biogenic species of interest is diatomic, cell-permeable, free radical $NO^{\bullet}$ and significant attention is garnered around its detection in biological environments.[41,42] As a major biogenic ROS, $NO^{\bullet}$ plays multiple roles in complex organisms. First, $NO^{\bullet}$ serves as a messenger molecule in neuronal communication and vasodilation, the endothelium-derived relaxing factor (EDRF), which is released by the endothelium to relax smooth muscle.[41,43-47] Second, $NO^{\bullet}$ is secreted in high concentration by immunological (eukaryotic) cells as an immunological defense mechanism in response to bacterial infections.[43,48] Three different kinds of nitric oxide synthases (NOS) are responsible for generating $NO^{\bullet}$, namely (1) endothelial nitric oxide synthase (eNOS), neuronal nitric oxide synthase (nNOS), and immunological nitric oxide synthase (iNOS),[49] where NOS converts L-arginine and oxygen (O_2) to L-citrulline and $NO^{\bullet}$. In biological organisms under physiological conditions, $NO^{\bullet}$ is present in low-micromolar concentrations.[50] $NO^{\bullet}$ is a very reactive and highly diffuse molecule, the former particularly true within complex biological systems. In the presence of oxygen, $NO^{\bullet}$ converts to reactive nitrogen species, which induce damage to biological macromolecules such as DNA, lipids, and proteins. This signaling molecule is known to regulate various physiological processes including virulence, biofilm regulation and gene expression. For instance, low, nontoxic levels of $NO^{\bullet}$ have been shown to induce biofilm dispersal in *P. aeruginosa*.[29] These biofilm dispersal mechanisms involve $NO^{\bullet}$-mediated pathways, which trigger responses based on changes in the modulation of QS.[24] While $NO^{\bullet}$ is an effective molecule in biofilm dispersal, bacterial pathogens have developed defense mechanisms against immune responses. In particular, *P. aeruginosa* initiates crosstalk to regulate not only biofilm formation and virulence, but also host immune responses.[51]

Previous research has shown the ability of PYO to inhibit ciliary functions of respiratory epithelial cells and to block EDRF $NO^{\bullet}$ release and vasorelaxation. In its

mechanism of action, PYO inhibits $NO^{\bullet}$ synthases, blocking the relaxation of smooth muscle induced by nitric oxide.[40,52] Additionally, immune cells (e.g., macrophages) produce high concentrations of $NO^{\bullet}$ in response to pathogenic infections.[43] Yet there is a lack of knowledge in understanding the *in vivo* and/or *in vitro* mechanisms in which PYO interacts with $NO^{\bullet}$. A 1990 study by Warren et al. examined the reaction between PYO and $NO^{\bullet}$.[53] The authors observed a rapid change from initial blue to pink color when $NO^{\bullet}$ was passed in a deoxygenated aqueous solution of PYO and mass spectrometry (MS) analyses of the products indicated conversion of PYO to nitrosylated species.[53] Specifically, fast atom bombardment MS showed that PYO was not present and desorption electron-impact ionization showed the presence of minor amounts of 1-methoxyphenazine and 1-hydroxyphenazine in addition to major ions at *m/z* 211 and *m/z* 193. The authors suggested that the latter ions are due to nitrosylation of PYO by nitric oxide, followed by generation of substituted oxazoline by dehydration, which was suspected to have occurred during MS analysis.[53] These results provided speculation that the interaction between PYO and $NO^{\bullet}$ could occur in patients infected with *P. aeruginosa*, thus this reaction deserves further examination.

While standard analytical methods, including fluorescence, chemiluminescence, spectrophotometry, and MS are typically used to detect both PYO and $NO^{\bullet}$,[54-58] they are either costly or time-consuming. Electrochemical detection methods have been recognized as popular alternatives for these two species as they provide low-cost, highly sensitive, responsive, robust, and direct detection methods.[19,41,57,59-66] In Chapter 2 of this dissertation, we showed the characterization of T-CUA analytical responses to PYO and the successful use of this electrode platform to detect cellular PYO from *P. aeruginosa*.[19,59,60] Additionally, the Stevenson research group has previously demonstrated promising adaptation of T-CUAs for the detection of biogenic $NO^{\bullet}$.

Specifically, two modifications were introduced to T-CUAs for detection of $NO^{\bullet}$, including (1) the addition of a cellulose acetate gas permeable membrane selective to $NO^{\bullet}$, and (2) the introduction of chitosan-gold nanoparticles (CS/GNPs) to enhance the limit of detection to $NO^{\bullet}$.[56]

Herein, we demonstrate initial experimental results on the chemical interaction between PYO and $NO^{\bullet}$ on T-CUA electrodes. To the best of our knowledge, this interaction has not been previously studied using electrochemical methods. Our preliminary electrochemical measurements performed in tandem with UV-Vis spectroscopic studies show no evidence of an interaction between PYO and $NO^{\bullet}$ at biologically relevant conditions and physiological pH 7.0. These primary observations may be important in studying other potential mechanisms in which the chemical reaction between PYO and $NO^{\bullet}$ occurs.

5.2 Experimental Methods

5.2.1 General

All chemicals were used as received. Photoresist AZ 1518 was purchased from Microchemicals. Polystyrene spheres (diameter of 1.54 μm) were purchased from Polysciences, Inc (Polybead®). All chemicals were used as received. Potassium chloride, acetic acid, cyclohexanone, isopropanol, ferrocenemethanol, nitric acid, and MOPS buffer were acquired from Sigma-Aldrich Co. Pyocyanin was purchased from Cayman Chemical Company. Ethanol, Monosodium phosphate, disodium phosphate were purchased from Thermo Fisher Scientific Inc. Carbenicillin disodium salt was purchased from Fisher BioReagents. Tryptic soy broth (TSB) was purchased from Thermo Scientific and Tryptic soy agar (TSA) was acquired from Remel.

5.2.2 Preparation of SCFM2

Parts of the studies presented in this chapter use an *in vitro* model based on chronic *P. aeruginosa* infection of the CF lung. Specifically, the studies utilize synthetic SCFM2 sputum, previously designed by the Whiteley lab,[1,2,20] to mimic the lung secretions of individuals with CF, which importantly promotes natural formation of *P. aeruginosa* aggregates.[3]

5.2.3 Viscosity Measurements of SCFM2

Viscosity measurements were performed using a Sine-wave Vibro Viscometer SV-10 and Haake temperature-controlled water bath. The SV-10 viscometer consists of two thin gold sensor plates that vibrate at a constant frequency. The electromagnetic force influencing the vibration of the sensor plates maintains constant amplitude. The magnitude of viscosity is detected as electric current necessary to resonate gold electrode plates at a selected frequency and magnitude. After performing calibration of the instrument, the viscosity of the following samples was measured with increasing temperature in 1.0°C increments ranging from 20.0 °C to 37.0 °C: (1) water, (2) SCFM, (3) SCFM2, (4) SCFM2 (mucin removed), (5) SCFM2 (DNA removed), and (6) expectorated CF sputum.

5.2.4 Electrochemical Determination of Diffusion Coefficients of Pyocyanin in SCFM2

The electrochemical measurements were done using a three-electrode cell system. All electrochemical experiments were performed at room temperature (25 °C). Electrochemical experiments including cyclic voltammetry (CV) and chronoamperometry were performed using an Autolab PGSTAT30 potentiostat. A platinum (Pt) electrode with a diameter of 5 mm (Metrohm Autolab) was used as the

working electrode. A gold mesh was used as the counter electrode and a saturated calomel electrode (SCE) was used as the reference electrode. The working electrode was polished between each run using aluminum oxide colloidal suspension with a particle size of 0.05 microns. The background solutions used were SCFM, SCFM2, SCFM2 (mucin removed), and SCFM2 (DNA removed). After collecting a background cyclic voltammogram or chronoamperogram, a 2 mM PYO stock solution (dissolved in ethanol) was added to each respective background solution to give a final concentration of 90 μM PYO. For PYO, CVs with a potential window ranging from –0.4 V to –0.1 V vs SCE at a scan rate of 50 mV s^{-1} were recorded before each chronoamperometry experiment. For ferrocene methanol (FcMeOH), CVs with a potential window ranging from –0.2 V to 0.45 V vs SCE (scan rate of 50 mV s^{-1}) were recorded before chronoamperometry experiments. The diffusion coefficients of PYO in each of the separate synthetic sputum solutions were determined via chronoamperometry by initially holding the potential at –0.20 V vs SCE for 0.5 s, then stepping the potential to –0.32 V vs SCE for 60 s in the aforementioned solutions. The diffusion coefficient of FcMeOH in synthetic SCFM2 sputum solutions was determined via chronoamperometry by holding an initial potential of 0.35 V vs SCE for 0.5 s, then stepping the potential to 0.10 V vs SCE for 60 s. Using the obtained chronoamperograms, Cottrell curves were plotted, from which the corresponding diffusion coefficients for PYO and FcMeOH were determined. For comparison studies with FcMeOH, the background solutions used were: (1) MOPS buffer, (2) SCFM2 sputum, and (3) 1:1 (v/v) MOPS:SCFM2.

5.2.5 Bacterial Strains, Plasmids, and Cell Culture Conditions

Bacterial strains used in these experiments were provided and prepared by Dr. Sophie Darch of the Whiteley lab. Specifically, *P. aeruginosa* PA14 *ΔlasIΔrhlI*

"responder" strain, containing either plasmid pSEDQS (PA14 QS) or pSEDQS2 (PA14 QS2), was used. PA14 *ΔlasIΔrhlI* pSEDQS strain constitutively expresses mCherry, and a transcriptional fusion of *rsaL:gfp*, allowing for the production of green fluorescent protein (GFP). All strains were grown from TSA plate culture and prior to use were shaken overnight at 37 °C at 200 rpm in TSB. All washing steps were performed using phosphate buffer saline (PBS, 7.0 pH).

5.2.6 Concurrent Confocal Imaging and Electrochemical Measurements

Confocal images were acquired on a Zeiss LSM 700 CLSM utilizing Zen image-capture software. Bacterial cells were pictured via mCherry with an excitation wavelength of 587 nm and an emission wavelength of 610 nm. Detection of GFP-expressing cells was performed using an excitation wavelength of 488 nm and an emission wavelength of 509 nm. Confocal images were acquired using a 63× oil-immersion objective. All data were saved as 512- by 512-pixel (0.45- by 0.45-μm pixel size) 8-bit z-stack images. Control confocal images of SCFM2 without any bacterial cells were acquired using identical settings to determine the background for image analysis. For this study, electrochemical measurements were performed using a three-electrode cell system including square wave voltammetry (SWV) and an Autolab PGSTAT30 potentiostat. T-CUA was used as the working electrode with a total geometric area of 0.495 cm^2, defined by the electrode area exposed to a solution in a homemade polydimethylsiloxane (PDMS) electrochemical well. A gold wire electrode was used as the counter electrode and SCE was used as the reference electrode. SWV measurements were performed using a current sensitivity of 5 μA, 3 mV step potential, and a frequency of 15 Hz. The potential window ranged from –0.4 to –0.1 V vs SCE. The background solution used was 1:1 (v/v) SCFM2:TSB. After a background SWV was collected using a

total of 20 scans, subsequent PYO measurements were obtained. For the real-time electrochemical detection of PYO from *P. aeruginosa* in 1:1 (v/v) SCFM2:TSB, liquid-batch cell samples were placed on T-CUA electrodes to perform SWV measurements while performing confocal microscopy imaging. PYO production was monitored during the initial 8.5 h of bacterial growth. Note that experiments were performed at room temperature due to the lack of a 37 °C chamber on the confocal microscope. Additionally, all confocal images were captured 30 min after each SWV measurement due to time delays associated with the expression of fluorescent protein reporters.

5.2.7 Pyocyanin Calibration Curves

For combined electrochemistry and confocal microscopy imagining studies, to quantify PYO concentrations from *P. aeruginosa* cells, calibration curves for PYO in TSB were used reported in our previous studies in Chapter 3.[19]

5.2.8 Pyocyanin Standard Solutions

For studies on the interaction between PYO and $NO^{\bullet}$, 100 μM of PYO in sodium phosphate buffer solution (SPB, 7.0 pH) was prepared. Initially, a 2 mM PYO stock solution was prepared in ethanol and was diluted to make a 500 μM stock solution in SPB. From the 500 μM stock solution, the respective PYO standard solution was prepared to have a concentration of 100 μM in SPB.

5.2.9 Preparation of Stock Standard $NO^{\bullet}$ Solutions

The stock $NO^{\bullet}$ solution was prepared according to a previously reported procedure with modifications.[41] 6 M sulfuric acid (H_2SO_4) was slowly added drop wise into a saturated sodium nitrate ($NaNO_2$) solution, which generated sodium sulfate and nitrous acid. Nitrous acid decomposed into nitrogen dioxide (NO_2) and $NO^{\bullet}$ gases. The

generated gases were passed through a 30% sodium hydroxide (NaOH) solution to trap the NO_2 gas, while the remaining $NO^{\bullet}$ gas was bubbled through 10 mL of 0.1 M SPB (7.0 pH) for 40 min. The $NO^{\bullet}$ concentration saturates at 2 mM at 22°C.[56,67] The entire procedure must be performed very carefully because the $NO^{\bullet}$ gas is toxic and it easily reacts with O_2 in the air. Thus, the saturated $NaNO_2$, the 30% NaOH and the SPB solutions were purified with nitrogen gas for 3 h to remove any oxygen before adding 6 M H_2SO_4 acid to generate $NO^{\bullet}$ gas. The 2 mM $NO^{\bullet}$ stock solution was used immediately upon preparation to make the standard $NO^{\bullet}$ solutions. For PYO/$NO^{\bullet}$ interaction studies, a 20 mL standard $NO^{\bullet}$ solution was prepared to have a concentration of 50 μM in SPB, by diluting from the 2 mM $NO^{\bullet}$ stock solution. Since the $NO^{\bullet}$ gas reacts highly with oxygen, the standard SPB solutions were purified with nitrogen gas for 2 h before adding any of the $NO^{\bullet}$ stock solutions.

5.2.10 Preparation of PYO/$NO^{\bullet}$ Solutions

For studies on the interaction between PYO and $NO^{\bullet}$, the solutions used were 50 μM $NO^{\bullet}$, 100 μM PYO, 1:1 (v/v) 100 μM PYO: 50 μM $NO^{\bullet}$, and 3:1 (v/v) 100 μM PYO: 50 μM $NO^{\bullet}$ in SPB (7.0 pH).

5.2.11 Fabrication of T-CUA Electrodes

Preparation of the electrode platform using transparent carbon ultramicroelectrode arrays (T-CUAs) follows detailed procedures described in our previous studies.[19,48,56,60,68] Quartz microscopic slides (6.45 cm^2 and 1 mm thick, Technical Glass Products) were treated with piranha (3:1 H_2SO_4: 30% H_2O_2) to remove any organic contaminants. A 1:3 dilution of AZ 1518 photoresist with PGMEA (1-methoxy-1-propanol acetate) was spun onto the piranha cleaned quartz slides at 6000 rpm for 60 s. Following spin coating, the

photoresist slides were soft baked at 90 °C for 10 min and then transferred to a tube furnace. After 15 min of purging with 5% H_2: 95% N_2 (~100 mL/min), the photoresist slides were pyrolized by heating to 1000 °C at 5 °C/min and holding at that temp for 1 h before allowing them to cool slowly back to room temperature at 5°C/min. The pyrolized photoresist film (PPF) slides were then removed from the furnace and stored for 3 days prior to use to allow for the oxide layer to stabilize. T-CUAs fabrication involved a lithography method using polystyrene microspheres (PSS) with a diameter of 1.54 μm, which were drop cast from a 5.4 wt % methanol suspension onto the conductive PPF electrodes. The organization of the spheres is that of a hexagonal close-packed two-dimensional ordered network. After this microsphere lithography step, 10 nm of Al_2O_3 layer was deposited via atomic layer deposition (ALD) technique at 80 °C. The ALD process was calibrated by the manufacturer (Cambridge Nanotech Savannah 100) to deposit 0.089 nm conformal Al_2O_3 layer per cycle. Thus, cycling this process for 112 times formed a 10 nm ALD layer. This ALD step is then followed by removal of PSS via sonication with methanol, acetone, isopropanol, and water. Disk-shaped carbon areas remained where the PSS made contact with the PPF, thus forming a carbon ultramicroelectrode array. Details on the characterization of T-CUA electrodes have been reported in previous research studies from our group.[19,48,56,60,68]

5.2.12 Concurrent Electrochemical and UV-Vis Measurements of PYO/NO$^{\bullet}$ Reaction

The electrochemical measurements were performed using a three-electrode cell system. Electrochemical experiments including SWV were performed using a CHI 700 potentiostat (CH Instruments Inc). The T-CUA was used as the working electrode, a steel electrode was used as the counter and a gold (Au) electrode was the reference. The T-

CUA working electrode had a total exposed geometric area of 0.495 cm^2. SWV was performed using a current of 5 A, 3 mV step potential, and a frequency of 15 Hz. The potential ranged from –0.8 V to 0.8 V vs Au. The background solution was SPB (7.0 pH), purged with argon gas for 20 min. After a background SWV curve was collected, subsequent PYO/$NO^{\bullet}$ measurements were obtained. In tandem with electrochemistry experiments, UV-Vis measurements (Agilent Instrument 8453 UV−vis−NIR spectrometer) were recorded to examine the interaction of PYO and $NO^{\bullet}$ using the solutions described in section 5.2.10. For these measurements, a homemade Teflon spectroelectrochemical well was used and contact to the working electrode was made using copper tape. To study the effects of molecular oxygen on PYO/$NO^{\bullet}$ interaction, part of these experiments were performed in a glove bag (in the absence of O_2).

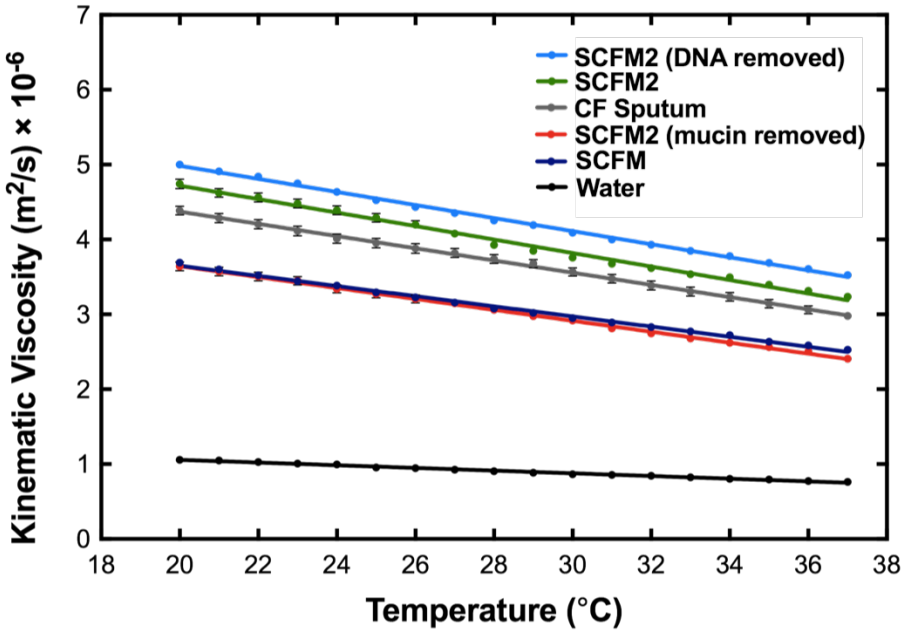

Figure 5.1: Kinematic viscosity measurements of SCFM2.

Viscosity is measured as the kinematic viscosity across a temperature range of 20–37 °C for SCFM2 (green) compared with SCFM (navy blue), SCFM2 with mucin removed (red), SCFM2 with DNA removed (blue), expectorated CF sputum (grey) and water (black). Statistical comparisons at 37 °C using a two tailed t test indicate that SCFM2 has a similar viscosity to expectorated CF sputum ($P = 0.01$), that the removal of mucin changes viscosity ($P = 0.0001$) and is more viscous than water ($P = 0.0001$). Data represent the mean value of three replicates. Error bars are too small to be seen.

5.3 Results and Discussion

5.3.1 Characterization of SCFM2 Sputum

Previous studies have attempted to determine components of CF sputum and have shown that the artificial SCFM2 sputum developed by the Whiteley lab can be used as a relevant model system to study *P. aeruginosa* chronic CF infections as it closely represents key attributes of CF sputum from patients.[1-3] The Whiteley lab developed two modulations of this medium (SCFM and SCFM2).[1,2] Originally, SCFM was designed to study how the nutritional composition of CF sputum influences the growth and virulence of *P. aeruginosa*.[1,2] SCFM2 was developed, with the addition of relevant amounts of DNA, lipids, and mucin to SCFM, to more closely represent the physical properties of human CF sputum.[3] The viscous properties of CF sputum are believed to play an important role in bacterial aggregate formation, as well as in the development of biofilms.[22,69,70] However, it remains unclear which sputum components contribute to the increased viscosity of this growth medium.

Herein, the average kinematic viscosity of four variations of SCFM2 sputum media (SCFM2, SCFM2 mucin removed, and SCFM2 DNA removed) was measured, quantified, and compared with authentic CF sputum isolated from patients, SCFM, and water (Figure 5.1). The data shows that SCFM2 and CF sputum have significantly higher average viscosities compared to SCFM and water across a range of temperatures (Figure 5.1). At 37 °C, the determined average viscosity of SCFM2 was 3.2×10^{-6} m^2/s, which was slightly more viscous than that of CF sputum with an average viscosity of 2.9×10^{-6} m^2/s (P-value=0.01). This viscosity is similar to that of the commonly used 30–40% glycerol lab solution within this range of temperatures. To determine which SCFM2 polymer components contribute to viscosity, mucin (glycoprotein constituent of mucus) or DNA

were removed from the medium. Removing mucin from SCFM2 resulted in ~25% decrease in viscosity to 2.4×10^{-6} m^2/s at 37 °C (P-value= 0.001, compared to SCFM2). These results indicate that the removal of mucin from SCFM2 gives a solution that is nearly identical to the original SCFM formulation (Figure 5.1). The data in Figure 5.1 reveal that the viscosity of SCFM2 is more similar to that of authentic CF sputum than to SCFM and that the addition of the mucin is a significant contributor to the increased viscosity. On the other hand, removal of DNA from SCFM2 resulted in higher viscosity than neat SCFM2, though they are not statistically different at 37 °C (P-value=0.02, compared to SCFM2). This increase in viscosity might be attributed to variations in different batches of SCFM2 media used in these studies, which remains a subject of further investigation.

To further characterize SCFM2 sputum and understand the significant viscosity changes observed in Figure 5.1, the apparent diffusion coefficients of PYO four variants of SCFM2 sputum (SCFM2, SCFM, SCFM2 mucin removed, and SCFM2 DNA removed) were determined using electrochemical methods (herein, chronoamperometry). Previous studies have reported the concentration levels of PYO in the sol phase (colloidal solution) of sputa from infected CF patients to fall within the range of 0.2−27.3 μg/mL (1−130 μM).[62,71,72] Consequently, a biologically relevant PYO concentration of 90 μM was used as it falls within the aforementioned range for the diffusion coefficients studies.

Initially, CV was used to determine the potential at which PYO redox occurs in each of the SCFM2 sputum solutions (Figure 5.2). Figure 5.2b displays clean, background-corrected CVs for PYO redox (Figure 5.2a) in SCFM2, SCFM, SCFM2 (mucin removed), and SCFM2 (DNA removed). The provided CVs indicate the PYO redox peak relative to the reference electrode. The reduction peak is more sensitive and shows less reversibility, which is most likely associated with a reductive radical-induced,

proton-coupled dimerization process, which is often observed for redox molecules of similar structure. According to the Randles-Sevcik equation, the peak current should be proportional to the square root of the diffusion coefficient.[73-75] However, this relationship holds true for purely reversible electron transfer processes. As demonstrated in Chapter 2, the redox reaction for PYO is a quasi-reversible outer-sphere mechanism as the redox reaction not only involves electron transfer but also slow, bimolecular steps (transfer of protons).[60] Additionally, large errors are typically associated with determining diffusion coefficients using CV; errors are significantly reduced by using chronoamperometry as it is a more sensitive technique compared to CV.[73-75]

Sputum Solution	**Diffusion coefficients (cm^2/s)**
SCFM	$(6.6\pm0.5)\times10^{-6}$
SCFM2	$(2.8\pm0.6)\times10^{-7}$
SCFM2 (mucin removed)	$(7.4\pm0.4)\times10^{-6}$
SCFM2 (DNA removed)	$(1.8\pm0.2)\times10^{-7}$

Table 5.1: Determined apparent diffusion coefficients of PYO in different sputum media. Data represent the mean of three replicates with the standard error of the mean.

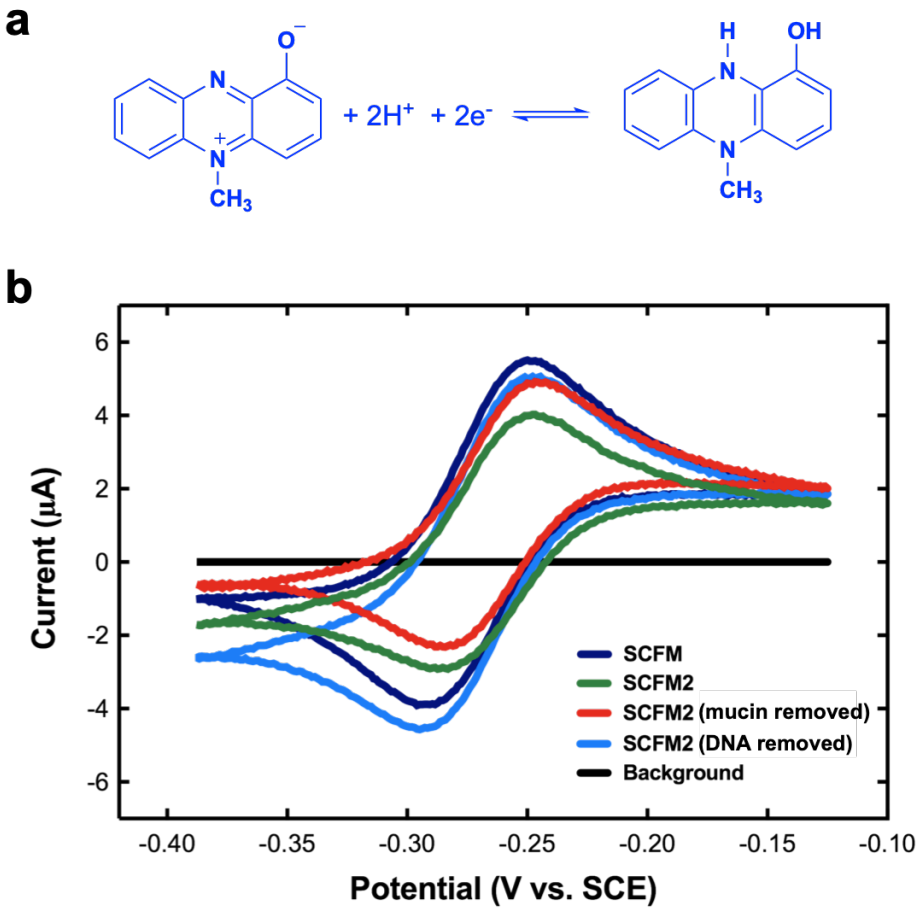

Figure 5.2: Cyclic voltammograms for PYO in SCFM2 solutions.

(a) Reduction mechanism of PYO. (b) Background subtracted cyclic voltammetry responses for 90 μM PYO in (1) SCFM2, (2) SCFM, (3) SCFM2 (mucin removed) and (4) SCFM2 (DNA removed).

To determine the diffusion coefficients of PYO in synthetic sputum media, chronoamperometry studies were performed, where the resultant current was monitored as a function of time in a controlled potential fashion. Figure 5.3a shows background-corrected chronoamperograms for four different variations of sputum media: (1) SCFM2, (2) SCFM, (3) SCFM2 (mucin removed), and (4) SCFM2 (DNA removed). Using the obtained chronoamperometry data, corresponding Cottrell curves were plotted where the resulting current was plotted as a function of the inverse square root of time (Figure 5.3b). Resultant Cottrell plot slopes (Figure 5.3b) were used to determine the apparent diffusion coefficients of PYO in SCFM2 media (Table 5.1). In the chronoamperometric measurement of diffusion coefficients for redox-active species (e.g., PYO) in solution, three distinct diffusional regimes are clearly discernable corresponding to ultrashort, short and long times. In the microsecond to second ultrashort time regime, the response is associated with instrumental responses and double layer charging of the electrochemical interface to reach the applied potential during the potential step, thus this early time is not considered. In the seconds time regime, this response is associated with semi-infinite linear diffusion associated with free diffusion of redox-active molecules to the electrode interface. This time regime is what was used to estimate apparent diffusion coefficients since they are a function of the media (pH, ionic strength, temperature, and activity effects).

The apparent diffusion coefficient of PYO in SCFM2 (2.8×10^{-7} cm^2/s) was lower compared with SCFM (6.6×10^{-6} cm^2/s), indicating that the addition of polymers to SCFM slows diffusion of quorum sensing molecules. The removal of mucin from SCFM2 resulted in a similar PYO diffusion coefficient to SCFM (7.4×10^{-6} cm^2/s) while the removal of DNA had a small but statistically significant effect (1.8×10^{-7} cm^2/s). Significant differences, using a two-tailed t-test, were determined for (1) SCFM and

SCFM2 ($P = 0.0002$), (2) SCFM2 and SCFM2 mucin removed ($P < 0.0001$), and (3) SCFM2 and SCFM2 DNA removed ($P = 0.002$). These data, in agreement with the viscosity results, indicate that mucin is likely the primary polymer impacting the diffusion of PYO in SCFM2 media. As a control, diffusion coefficients of FcMeOH and PYO were determined via chronoamperometry in (1) MOPS buffer, (2) 1:1 (v/v) MOPS:SCFM2, and (3) SCFM2. FcMeOH was chosen as a standard redox couple with a known diffusion coefficient due to its similar molecular weight to PYO. These chronoamperometric diffusion coefficients are outlined in Table 5.2.

Solution	**Diffusion coefficients (cm^2/s) for FcMeOH**	**Diffusion coefficients (cm^2/s) for PYO**
MOPS	$(3.5\pm0.3)\times10^{-5}$	$(4.0\pm0.7)\times10^{-5}$
1:1 (v/v) MOPS:SCFM2	$(1.7\pm0.6)\times10^{-6}$	$(2.7\pm0.6)\times10^{-6}$
SCFM2	$(2.1\pm0.4)\times10^{-7}$	$(2.8\pm0.6)\times10^{-7}$

Table 5.2: Determined apparent diffusion coefficients of PYO and FcMeOH in different SCFM2 sputum/buffer media. Data represent the mean of three replicates with standard error of the mean.

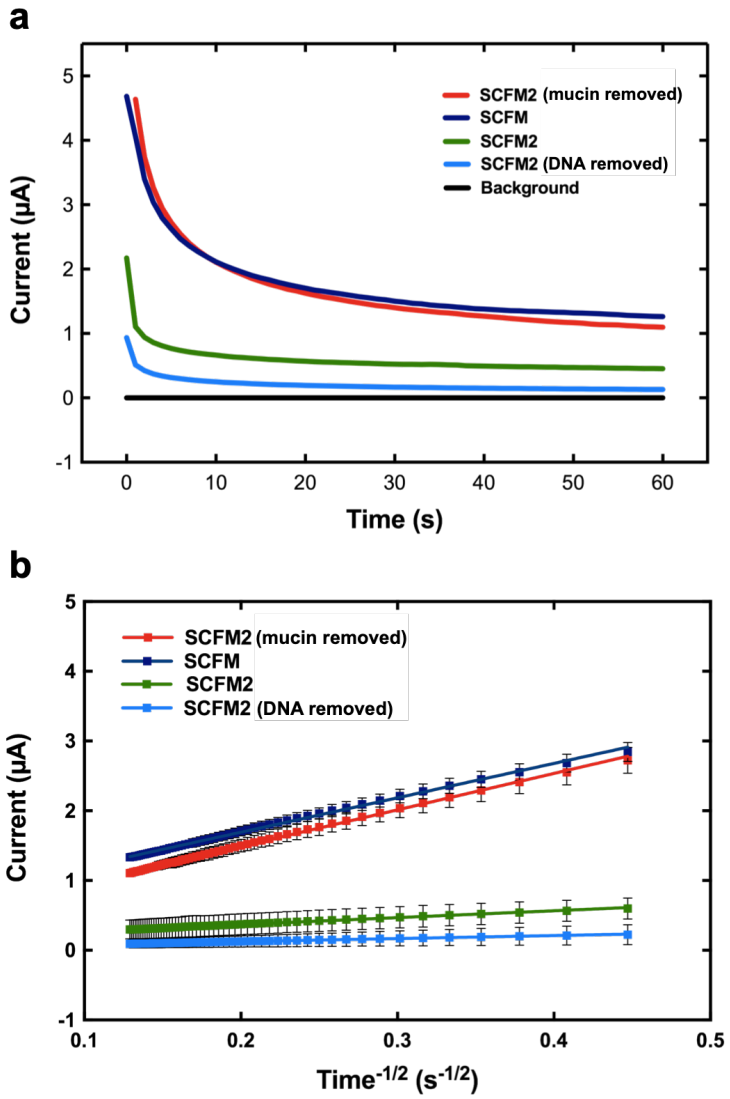

Figure 5.3: Determination of diffusion coefficients by chronoamperometry.

(a) Chronoamperometry responses for 90 μM PYO in the four different synthetic sputum media, and (b) the corresponding Cottrell plots.

5.3.2 Detection of Pyocyanin Production in Tandem with Confocal Imaging of *P. aeruginosa* Aggregates in SCFM2

In previous chapters of this dissertation, the successful application of the T-CUA platform was demonstrated for the detection and real-time monitoring of PYO and various other phenazine species from *P. aeruginosa* strains.[19,59,60] Chapters 2, 3 and 4 discussed the advantages of T-CUAs in comparison to other electrochemical sensing devices, including amplified currents, fast response times, enhanced sensitivity, large liner dynamic ranges and high degrees of biocompatibility.[19,59,60] An additional advantage of T-CUA electrodes is their planar and transparent features, which allow for electrochemical analyses to be performed concurrently with optical imaging of the bacterial cells on T-CUAs (Chapter 2).[60] As a follow-up study, herein experiments were performed, in a collaborative effort with Dr. Sophie Darch of the Whiteley lab, to electrochemically detect and quantify PYO using T-CUAs while simultaneously monitoring bacterial aggregate formation in SCFM2 via confocal microscopy. Our initial data demonstrates that we can successfully detect QS responses in developing bacterial aggregates using PA14 strains, expressing a QS reporter plasmid, in SCFM2 while also being able to detect PYO secreted from QS *P. aeruginosa* cells. These preliminary data also indicate that PYO production in SCFM2 medium differs from commonly used laboratory growth media (Chapter 4).

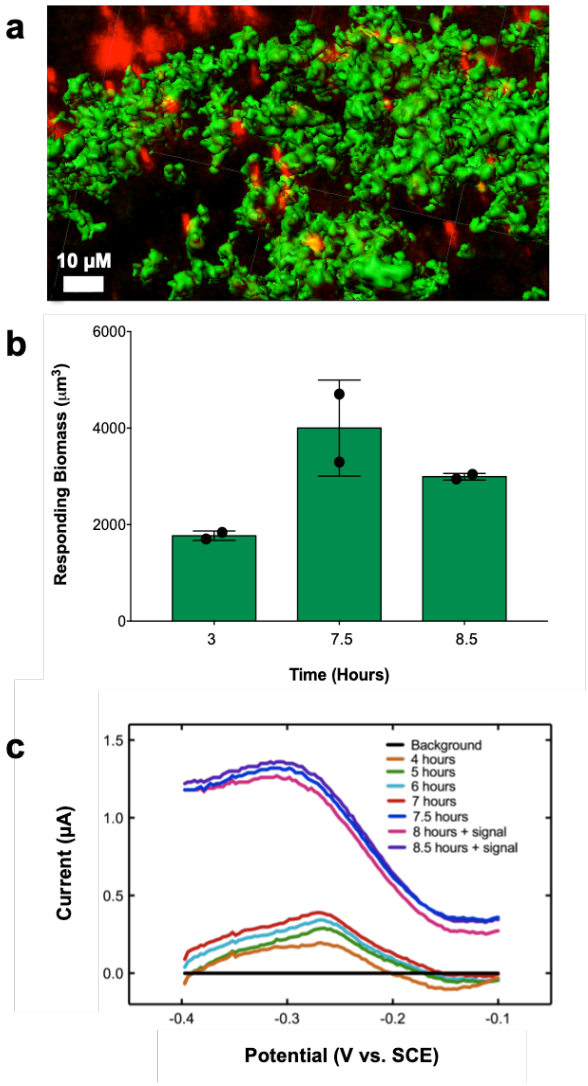

Figure 5.4: Confocal microscopy imaging of bacterial aggregates in tandem with electrochemical quantification of PYO secreted from *P. aeruginosa* in SCFM2 sputum.

(a) Confocal image of bacterial aggregates at 7.5 h of cell growth (b) Responding biomass determined GFP expression of quorum sensing bacterial cells. The confocal microscopy images and data in (a) and (b) were obtained in collaboration with the Whiteley laboratory and are a courtesy of Dr. Sophie Darch. (c) Time-dependent SWV current-potential responses of PYO secreted from *P. aeruginosa* in SCFM2 media. The peak at −0.256 V vs SCE is due to PYO redox. Quantified PYO concentrations are summarized in Table 5.3.

Liquid-batch cultures of *P. aeruginosa* PA14 *ΔlasIΔrhlI* strain were initially grown overnight at 37 °C in TSB media before re-introducing the cells into fresh SCFM2 media. Upon introducing cells to SCFM2 medium, concurrent electrochemical measurements and confocal imaging were performed during the initial 8.5 h of cellular growth. Figure 5.4a illustrates a representative confocal microscopy image at 7.5 h of bacterial growth, where GFP-expressing aggregates represent *P. aeruginosa* bacteria responding to QS signals and the mCherry-expressing species are *P. aeruginosa* cells that are not engaged in QS. Using obtained confocal images, the responding biomass (QS GFP-expressing cells) was determined at 3 h, 7.5 h, and 8.5 h of bacterial growth in SCFM2 (Figure 5.4b). In tandem with confocal imaging, PYO production was monitored from *P. aeruginosa* in SCFM2 using SWV. The confocal images data on QS bacterial aggregate formation show a certain correlation with the electrochemical quantification of PYO. The data were analyzed using background-subtraction (background was 1:1 (v/v) SCFM2:TSB) to determine PYO concentrations secreted by bacteria. Our results in Figure 5.4c demonstrate the notable electroactive PYO peak around –0.256 V vs SCE, where current-potential responses are plotted as a function of time at various time points of cell growth. The determined PYO concentrations at these time points in SCFM2 media are summarized in Table 5.3. Our results show increasing PYO concentrations during an 8-hour period, where the amounts of PYO secreted show a significant increase after 7 h bacterial growth. The maximum concentration of PYO was determined to be 36 ± 4 μM at 8.5 h growth. It should be noted that after 7 h, PYO concentrations plateau and do not change upon addition of an external QS signal, 3-oxododecanoyl homoserine lactone (30C12-HSL). Additionally, it should be noted that *P. aeruginosa* cultures in this study were kept at 25 °C for the duration of the experiments, which differs from experiments presented in Chapters 3 and 4 where cultures were grown under a physiological

temperature of 37 °C during the entire period of experiments. Compared to the findings in Chapters 3 and 4, here no other phenazine metabolites were observed when *P. aeruginosa* was grown in SCFM2, which is likely due to differences in growth media composition, as well as due to different PA14 strains used in these studies. Thereby, the quantified PYO concentrations in SCFM2 are significantly lower than those determined from cultures grown in common laboratory growth media (Chapters 3 and 4). This indicates that bacteria in SCFM2 grow at different rates that in laboratory growth media, which is in agreement with very recent discoveries.[13] Comparable to our conclusions in Chapter 4,[19] these results highlight that laboratory culturing methods can provide inadequate models of growth environments, thus making it challenging to understand how bacteria persist and develop infections in the body. Similarly, these results point to the need for analytical standardization of growth media, which could have great implications towards understanding the onset of bacterial infections, antibiotic resistance, and treatments.

Both optical imaging and electrochemical methods are relatively noninvasive with the analysis of biological systems. While optical imaging techniques proved a means for spatial analysis of bacterial cells, they have certain limitations. Specifically, they rely on the use of expressed fluorescent protein reporters,[76,77] which are linked to time delays in the production of detectable signals and are limited by nonspecific reactivity. Differently, electrochemical sensors, such as T-CUAs, provide a means to directly detect and rapidly quantify key metabolic components with high sensitivity. Our transparent electrochemical devices allow for real-time electrochemical detection of redox-active metabolites[19,59,60] to be performed together with spatial imaging of QS bacterial aggregates. Further work is necessary to examine the correlation between data obtained from confocal imaging and electrochemical measurement results.

Time (h)	PYO concentration (μM)
4	5.3 ± 0.3
5	8.1 ± 0.4
6	9.6 ± 0.5
7	11 ± 1
7.5	35 ± 2
8 + signal	33 ± 3
8.5 + signal	36 ± 4

Table 5.3: Determined concentrations of cellular PYO concentrations measured at various time points of cell growth in SCFM2 media (shown are average concentrations values from three replicas).

In future studies, more extensive environmental factors (oxygen availability, host generics, and antibiotics) need to be examined. Yet our electrochemical approach using T-CUAs provides a basis set to sensitively quantify relative differences in PYO production rates dependent on growth media composition. In a follow-up study using SCFM2 as a model, real-time electrochemical measurements will be performed using multiple wild-type and mutant *P. aeruginosa* strains, including both laboratory and clinical isolates. Additionally, quantitative electrochemical analyses, monitoring PYO production, need to be performed in synthetic sputum media variations (e.g., SCFM, SCFM2 mucin removed, SCFM2 DNA removed), as well as in expectorated CF sputum isolated from patients. Additional experiments need to be performed, including the introduction of disturbances to the biological system, to study the effects on PYO production in the presence of antimicrobial agents, as well as in more complex multi-species environments (similar to studies in Chapter 4).

5.3.3 Electrochemical Monitoring of Pyocyanin and Nitric Oxide Interaction

PYO is a low-molecular-mass biogenic species present in high concentrations of infected secretions from patients colonized with *P. aeruginosa*, thereby its reaction with $NO^{\bullet}$ could be of high importance especially in understanding host-pathogen response mechanisms. In the 1990s, evidence of the inactivation of PYO by $NO^{\bullet}$ (or vice versa) was discovered.[53] In this study, Warren and co-workers passed $NO^{\bullet}$ in a deoxygenated, aqueous solution of PYO and noted a rapid change of initial blue-pigment color to pink. Mass spectrometry (MS) methods, including fast atom bombardment and desorption electron-impact ionization, indicated the presence of trace amounts of phenazine metabolites, 1-hydroxyphenazine and 1-methoxyphenazine. Additionally, authors observed major ions of *m/z* 211 and *m/z* 193, which they suggested are due to nitrosylation of PYO by $NO^{\bullet}$, followed by dehydration step during MS analysis to form a substituted oxazoline.[53] With the exception of this study by Warren et al., no additional evidence has been reported on the interaction between the two biomolecules. Consequently, the mechanism of the reaction between $NO^{\bullet}$ and PYO is electrochemically investigated on T-CUA sensors herein. The T-CUA analytical responses to both $NO^{\bullet}$ and PYO were characterized and optimized in our previous studies.[50,56]

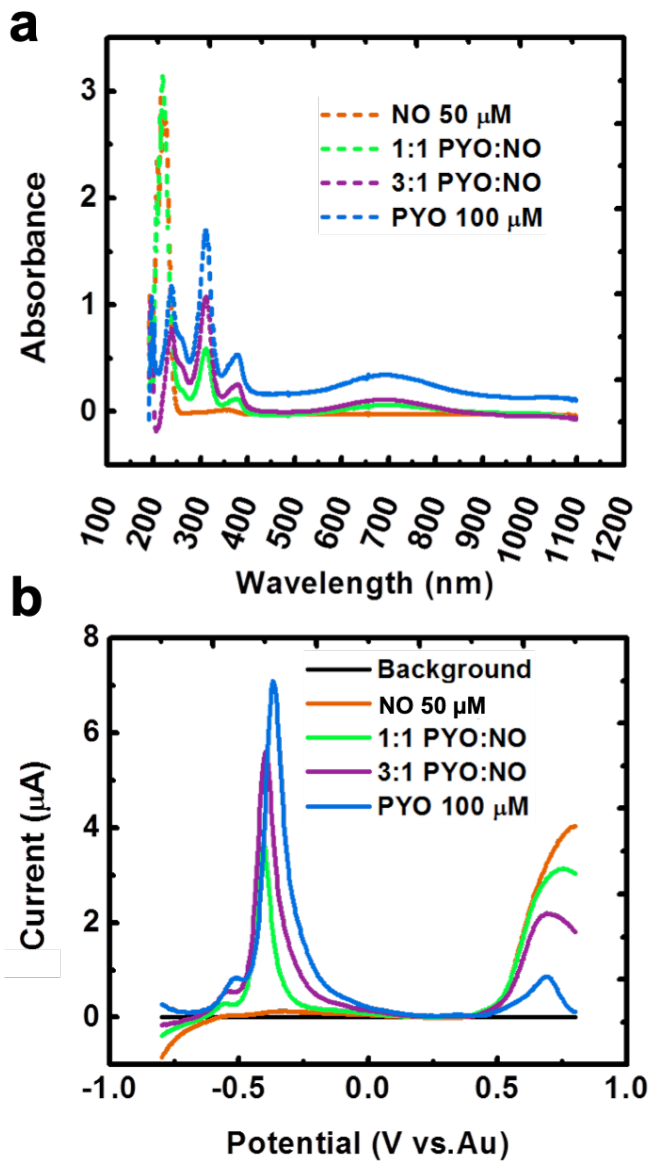

Figure 5.5: Electrochemical monitoring of PYO/NO$^{\bullet}$ interaction using T-CUAs.

(a) UV-Vis absorbance spectra and (b) square wave voltammograms for 50 μM NO$^{\bullet}$, 100 μM PYO, 1:1 (v/v) PYO:NO$^{\bullet}$, and 3:1 (v/v) PYO:NO$^{\bullet}$ recorded simultaneously.

To investigate this PYO/NO• interaction, physiologically relevant concentrations of PYO (100 μM)[71,78,79] and NO• (50 μM)[50,80] were simultaneously detected via UV-Vis spectroscopy and SWV. Figure 5.5a shows the UV-Vis spectrophotometric data of 100 μM PYO, 3:1 (v/v) 100 μM PYO: 50 μM NO•, 1:1 (v/v) 100 μM PYO: 50 μM NO•, and 50 μM NO•. The pure PYO spectrum shows characteristic peak maxima at wavelengths of 249 nm, 307 nm, 370 nm, and 697 nm, which have been observed previously.[81,82] The pure NO• spectrum shows a distinct absorption peak at 220 nm, associated with sσ, pπ, σ, and dδ transitions.[83,84] Accordingly, as the ratio of PYO to NO• increases, the absorbance of the 220 nm band disappears. Following the decrease in PYO to NO• ratio, the presence of characteristic PYO peak at 697 nm disappears, as well as an observed increase in the presence of NO• by the appearance of its absorbance maxima at 220 nm. SWV measurements were performed in parallel with UV-Vis on T-CUAs.

Figure 5.5b shows the corresponding SWV current-potential responses of pure PYO with a peak at –0.365 V vs Au and pure NO• with a peak at 0.71 V vs Au, as well as of the differing PYO/NO• ratio solutions. MS analysis of PYO/NO• solutions in the study by Warren and co-workers[53] pointed to the presence of minor amounts of two phenazine derivatives, 1-hydroxyphenazine and 1-methoxyphenazine, which have known potentials of –0.35 V and –0.42 V, respectively,[85,86] Consequently, this could explain the slight shit on PYO peak observed in the SWV responses for PYO/NO• solutions, however, it is more likely that this shift occurrence is due to the quasi-reference electrode used here. The resultant SWV data is inconsistent with the observations described by Warren et al involving an irreversible reaction between PYO and NO•. It should also be noted that no change in color (from blue to pink) was observed when nitric oxide was introduced to aqueous PYO solutions. These results indicate that PYO likely does not react with NO• at physiological pH conditions to form a nitrosylated PYO-NO• complex. Moreover, NO•

likely reacts with other species, such as molecular oxygen.[87] Specifically, $NO^{\bullet}$ converts to reactive nitrogen species in the presence of O_2 or superoxide radicals, which damage biological macromolecules (e.g., DNA, lipids, proteins).[24] Additionally, *P. aeruginosa* biofilms and PYO production are linked with oxygen availability.[24,59] Under low oxygen levels, *P. aeruginosa* switches from its aerobic to anaerobic respiratory growth to obtain energy from nitrate respiration; this denitrification pathway involves an 8-electron reduction to NO_3^- to nitrogen gas by four reductases,[88] but can also be activated by $NO^{\bullet}$.[89]

As a result, preliminary time-dependent studies were performed to examine the interaction between PYO and $NO^{\bullet}$ in the presence (Figure 5.6) and in the absence (Figure 5.7) of O_2 using the PYO/$NO^{\bullet}$ solutions. Figures 5.6 and 5.7 show SWV measurements in the presence and absence of molecular oxygen, respectively, for the two different PYO/$NO^{\bullet}$ solutions recorded when $NO^{\bullet}$ was passed into deoxygenated aqueous PYO solution at 0 h and 1 h after the solutions were allowed to react. In the presence of O_2, the PYO redox peak observed in the SWV after 1 h is broader than at 0 h for the 1:1 (v/v) PYO:$NO^{\bullet}$ solution (Figure 5.6a), which could be due to slight changes in solution pH. On the other hand, this was not observed in the O_2-present SWV curves, however, a shoulder peak at a more positive potential (–0.15 vs Au) appears (Figure 5.6b). Similarly, SWV measurements were performed for 1:1 (v/v) PYO:$NO^{\bullet}$ and 3:1 (v/v) PYO:$NO^{\bullet}$ solutions in a nitrogen glove bag, free of O_2. The resulting SWV current responses show distinct redox peaks in the region where PYO redox appears (Figure 5.7). Specifically, SWV peaks at –0.75 V and –0.46 V vs Au (Figure 5.7a) and redox peaks at –0.70 V and –0.50 V vs Au (Figure 5.7b) are observed for 1:1 (v/v) PYO:$NO^{\bullet}$ and 3:1 (v/v) PYO:$NO^{\bullet}$ solutions, respectively. Additionally, the redox peaks for nitric oxide appear wider compared to those for experiments performed in the presence of oxygen.

To better understand our preliminary electrochemical results, nanoelectrospray ionization (nano-ESI) MS experiments were performed with Dr. Christopher Crittenden of the Brodbelt research group. However, the MS studies proved to be challenging due to the use of a physiologically relevant SPB buffer (pH 7.0). Specifically, the use of nonvolatile buffers, such as SPB, is typically incompatible with MS detection as it could heavily interfere with ion generation.[90] The salt concentrations present in SPB buffers make ion formation less reproducible, thereby causing ion suppression or adduction.[91] The MS spectra in the positive ion mode for the 1:1 (v/v) PYO:NO$^{\bullet}$ solutions at 0 h and 1 h showed the characteristic precursor ion at *m/z* 211.17, indicating the presence of PYO in the solutions. On the other hand, the MS spectra in the positive ion mode for the 3:1 (v/v) PYO:NO$^{\bullet}$ solutions at 0 h and 1 h did not detect any PYO present in the solution; the formation of the PYO-NO$^{\bullet}$ complex at *m/z* 240 was also not observed.

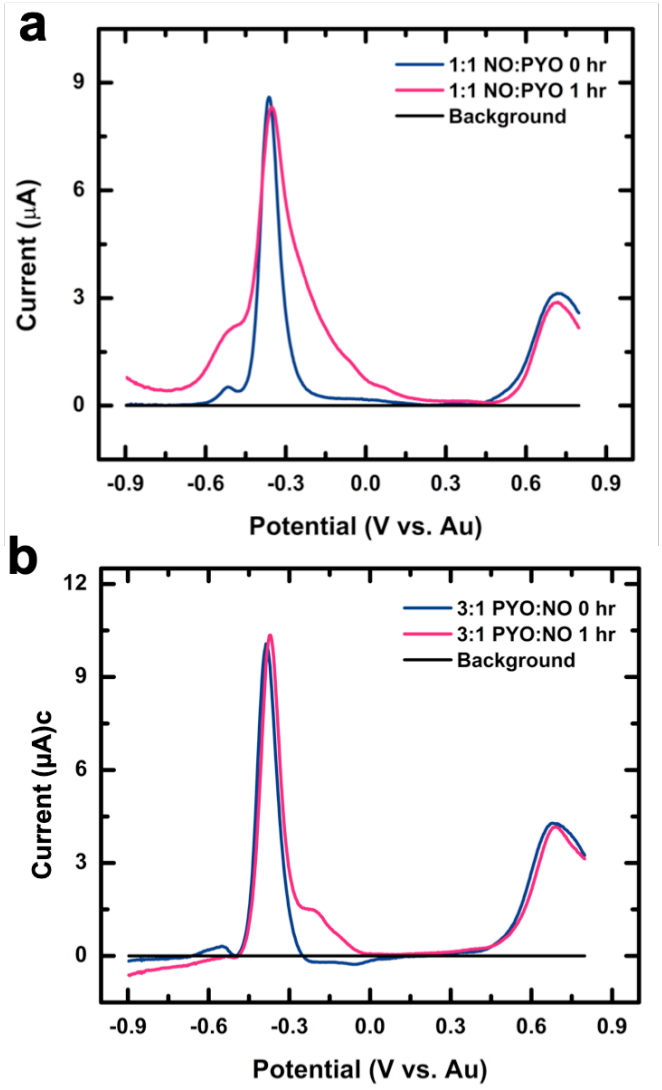

Figure 5.6: Electrochemical monitoring of PYO/$NO^{\bullet}$ interaction using T-CUAs with O_2 present.

Square wave voltammograms recorded in the presence of molecular O_2 for (a) 1:1 (v/v) PYO:$NO^{\bullet}$ solution and (b) 3:1 (v/v) PYO:$NO^{\bullet}$ solution at 0 h and 1 h after 50 μM $NO^{\bullet}$ was passed into 100 μM PYO aqueous solution.

At present, our results are inconclusive and inconsistent with the findings of Warren et al.[53] No explanation can be offered for these differences currently, especially since no immediate color changes were observed in the PYO/$NO^{\bullet}$ solutions. Future work is necessary to examine the effects of O_2 and/or other species (e.g., NADPH) that could act as limiting reagents in biological systems, which could make the PYO/$NO^{\bullet}$ interaction extremely complicated. The changes in color of PYO solutions have been observed previously with changes in pH,[40,92,93] where the immediate change in color from blue to pink was associated with a decrease in pH as protonated PYO is present. Our current results indicate that PYO is stable at pH 7.0, showing essentially no strong evidence of its reaction and/or interaction with $NO^{\bullet}$. In follow-up studies, combining UV-Vis, electrochemical and MS methods, PYO/$NO^{\bullet}$ interaction experiments need to be performed in acidic and basic buffer solutions to examine the effects of pH on this reaction mechanism. Additional research needs to address the mechanism by which nitric oxide is bubbled into aqueous buffer; in particular, studies have shown that $NO^{\bullet}$ can rapidly react with O_2 in water to generate H^+ and nitrite (NO_2^-), which could interfere with the reaction between PYO and $NO^{\bullet}$.[94-96] Finally, since redox processes are concentration-dependent, studies should be performed to examine the kinetics of this reaction. Specifically, $NO^{\bullet}$ immune responses are known to have broad concentration-dependent activity against microbes ranging from signaling molecule-like anti-biofilm to bacterial activity, [24] thereby concentration-dependent studies need to be performed.

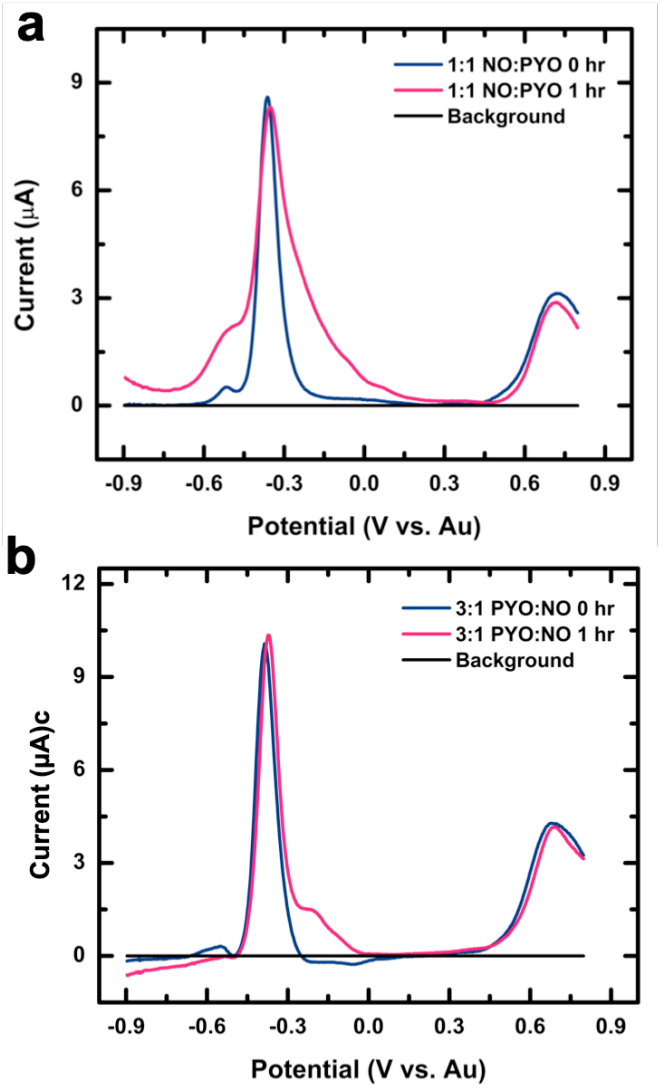

Figure 5.7: Electrochemical monitoring of PYO/NO$^{\bullet}$ interaction using T-CUAs without O_2 present.

Square wave voltammograms recorded in the absence of O_2 for (a) 1:1 (v/v) PYO:NO$^{\bullet}$ solution and (b) 3:1 (v/v) PYO:NO$^{\bullet}$ solution at 0 h and 1 h after 50 μM NO$^{\bullet}$ was passed into 100 μM PYO aqueous solution.

5.4 CONCLUSIONS

5.4.1 Electrochemical Monitoring of *P. aeruginosa* Phenazine Production in Growth Media and Samples of Clinical Relevance

The CF lung represents an immense biological landscape in which distinct multicellular populations of microbes can develop. Dynamic pathogenic responses and virulence mechanisms are highly dependent on the nutritional composition of growth environments, as demonstrated by findings in Chapters 3 and 4. Research studies presently depend on standard culturing methods and liquid-batch cultures, thus providing unsuitable models to study these pathogenic systems. Although a non-standardized method of growth media, SCFM2 sputum as media closely represents key attributes of *in vivo* environments (e.g., CF lungs). In the initial portions of this dissertation chapter, the viscosity and electrochemical apparent diffusion coefficients of PYO in SCFM2 and its variations were characterized and quantified. Specifically, the determined kinematic viscosity of SCFM2 was 3.2×10^{-6} m^2/s, which was comparable to that of CF sputum isolated from the lungs of CF patients. Additionally, the diffusion coefficient of PYO in SCFM2 was determined to be 2.8×10^{-7} cm^2/s. Removal of various key polymeric components from SCFM2 indicated that mucin is the primary polymer likely impacting both viscosity and diffusion in SCFM2 sputum. Following the characterization of SCFM2, preliminary studies were successfully performed to monitor *P. aeruginosa* PYO production while imaging the formation of bacterial aggregates in SCFM2 on T-CUA electrodes, showing a certain degree of correlation between the two methods. Importantly, the quantified PYO concentrations secreted from *P. aeruginosa* grown in SCFM2 are significantly lower than those concentrations from *P. aeruginosa* grown in typical laboratory growth media (Chapters 3 and 4). These results indicate that *P. aeruginosa* cells likely grow at slower rates in SCFM2 sputum. These findings highlight

that laboratory cell culturing methodologies provide inadequate representations of how bacteria persist in the human body. Our T-CUAs electroanalytical devices have the sensitivity to distinguish differences based on correlative measurements in SCFM2 media, laboratory media as well as polymicrobial samples. Additionally, T-CUAs are transparent which allows for imaging of bacterial cells while electrochemically quantifying PYO production from *P. aeruginosa*.

Future studies, involving both confocal imaging and electrochemical measurements, should focus on studying PYO production in SCFM2 in the presence of other clinically relevant pathogens (*Staphylococcus aureus*, *Escherichia coli*, *Staphylococcus epidermidis, Enterococcus faecalis) as well as host cells. Additional research in the future* should examine virulence factor production in *P. aeruginosa* strains and samples of clinical relevance. Finally, the state of infection needs to be reexamined for diagnosis, in particular with respect to the analytical standardization of simulated growth media.

5.4.2 Future Directions: Interaction Between Pyocyanin and Nitric Oxide

In the second part of this chapter, the interaction reaction between PYO and $NO^{\bullet}$ was investigated using T-CUAs bioanalytical devices for UV-Vis spectroscopy and electrochemical studies. Our preliminary results showed no strong evidence of PYO reacting with $NO^{\bullet}$ as no PYO-$NO^{\bullet}$ complex formation was observed via UV-Vis, electrochemical and MS methods at physiological pH 7.0. Future work should examine the effects of oxygen and/or other biological species (e.g., NADPH) on PYO/$NO^{\bullet}$ interaction. Additionally, pH- and concentration-dependent studies need to be conducted to further investigate the interaction between these two biological species. Understanding the interaction reaction between PYO and $NO^{\bullet}$ is of importance to investigators

researching pathogen-host responses and $NO^{\bullet}$ biological problems, especially to those who have attributed an effect of PYO to its chemical reaction with $NO^{\bullet}$ as suggested by a single 1990s study. Other mechanisms by which PYO could interact with $NO^{\bullet}$ include direct inhibition of NO synthase, as suggested by previous research.[97] This and other potential mechanisms, along with reaction kinetics, have to be fully examined in future experiments combining electrochemical and MS techniques.

Finally, a study showed that $NO^{\bullet}$-induced biofilm dispersal completely eliminated *P. aeruginosa* biofilms *in vitro*.[29] Additional proof-of-concept studies have shown the effectiveness of $NO^{\bullet}$-induced biofilm dispersal strategies in the treatment of chronic *P. aeruginosa* infections in CF patients,[98] where $NO^{\bullet}$ treatments resulted in the reduction of biofilm biomass in CF lungs after 5-7 days. Therefore, future work in this area needs to focus on electrochemically monitoring the role of $NO^{\bullet}$ on inducing *P. aeruginosa* biofilm dispersal. This mechanism needs to be further examined in order to understand and develop most effective treatments of chronic *P. aeruginosa* infections.

5.5 REFERENCES

(1) Palmer, K. L.; Aye, L. M.; Whiteley, M. *J. Bacteriol.* **2007**, *189*, 8079–8087.

(2) Palmer, K. L.; Brown, S. A.; Whiteley, M. *J. Bacteriol.* **2007**, *189*, 4449–4455.

(3) Darch, S. E.; Kragh, K. N.; Abbott, E. A.; Bjarnsholt, T.; Bull, J. J.; Whiteley, M. *mBio* **2017**, *8*, 277–292.

(4) Lyczak, J. B.; Cannon, C. L.; Pier, G. B. *Clinical Microbiology Reviews* **2002**, *15*, 194–222.

(5) Henke, J. M.; Bassler, B. L. *Trends in Cell Biology* **2004**, *14*, 648–656.

(6) Bassler, B. L.; Losick, R. *Cell* **2006**, *125*, 237–246.

(7) Stevens, A. M.; Schuster, M.; Rumbaugh, K. P. *J. Bacteriol.* **2012**, *194*, 2131–2141.

(8) Hauser, A. R.; Jain, M.; Bar-Meir, M.; McColley, S. A. *Clinical Microbiology Reviews* **2011**, *24*, 29–70.

(9) Jyot, J.; Sonawane, A.; Wu, W.; Ramphal, R. *Mol. Microbiol.* **2007**, *63*, 1026–1038.

(10) Jayaraman, S.; Joo, N. S.; Reitz, B.; Wine, J. J.; Verkman, A. S. *Proc Natl Acad Sci USA* **2001**, *98*, 8119–8123.

(11) Opperman, M. J.; Shachar-Hill, Y. *Metabolic Engineering* **2016**, *38*, 251–263.

(12) Smith, E. E.; Buckley, D. G.; Wu, Z.; Saenphimmachak, C.; Hoffman, L. R.; D'Argenio, D. A.; Miller, S. I.; Ramsey, B. W.; Speert, D. P.; Moskowitz, S. M.; Burns, J. L.; Kaul, R.; Olson, M. V. *Proc Natl Acad Sci USA* **2006**, *103*, 8487–8492.

(13) Wu, X.; Siehnel, R. J.; Garudathri, J.; Staudinger, B. J.; Hisert, K. B.; Ozer, E. A.; Hauser, A. R.; Eng, J. K.; Manoil, C.; Singh, P. K.; Bruce, J. E. *Journal of Proteome Research* **2019**, *18*, 2601–2612.

(14) Yang, L.; Haagensen, J. A. J.; Jelsbak, L.; Johansen, H. K.; Sternberg, C.; Hoiby, N.; Molin, S. *J. Bacteriol.* **2008**, *190*, 2767–2776.

(15) Son, M. S.; Matthews, W. J.; Kang, Y.; Nguyen, D. T.; Hoang, T. T. *Infect. Immun.* **2007**, *75*, 5313–5324.

(16) Rossi, E.; Falcone, M.; Molin, S.; Johansen, H. K. *Nat. Commun.* **2018**, *9*, 57–13.

(17) Cornforth, D. M.; Dees, J. L.; Ibberson, C. B.; Huse, H. K.; Mathiesen, I. H.; Kirketerp-Møller, K.; Wolcott, R. D.; Rumbaugh, K. P.; Bjarnsholt, T.; Whiteley, M. *Proc Natl Acad Sci USA* **2018**, *115*, E5125–E5134.

(18) Garber, E. D. *Ann. N. Y. Acad. Sci.* **1960**, *88*, 1187–1194.

(19) Simoska, O.; Sans, M.; Eberlin, L. S.; Shear, J. B.; Stevenson, K. J. *Biosens. Bioelectron.* **2019**, *142*, 111538.

(20) Turner, K. H.; Wessel, A. K.; Palmer, G. C.; Murray, J. L.; Whiteley, M. *Proc Natl Acad Sci USA* **2015**, *112*, 4110–4115.

(21) Kragh, K. N.; Alhede, M.; Jensen, P. Ø.; Moser, C.; Scheike, T.; Jacobsen, C. S.; Seier Poulsen, S.; Eickhardt-Sørensen, S. R.; Trøstrup, H.; Christoffersen, L.; Hougen, H.-P.; Rickelt, L. F.; Kühl, M.; Høiby, N.; Bjarnsholt, T. *Infect. Immun.* **2014**, *82*, 4477–4486.

(22) Darch, S. E.; Simoska, O.; Fitzpatrick, M.; Barraza, J. P.; Stevenson, K. J.; Bonnecaze, R. T.; Shear, J. B.; Whiteley, M. *Proc. Natl. Acad. Sci. U.S.A.* **2018**, *115*, 4779–4789.

(23) Bahia, D.; Satoskar, A. R.; Dussurget, O. *Front Immunol* **2018**, *9*, 221–224.

(24) Williams, D. E.; Boon, E. M. *J Innate Immun* **2018**, *11*, 205–215.

(25) Rasouly, A.; Nudler, E. *Proc Natl Acad Sci USA* **2019**, *2*, 9696–9698.

(26) O'Toole, G.; Kaplan, H. B.; Kolter, R. *Annu. Rev. Microbiol.* **2000**, *54*, 49–79.

(27) Römling, U. *J Innate Immun* **2019**, *11*, 191–192.

(28) Arora, D. P.; Hossain, S.; Xu, Y.; Boon, E. M. *Biochemistry* **2015**, *54*, 3717–3728.

(29) Barraud, N.; Hassett, D. J.; Hwang, S. H.; Rice, S. A.; Kjelleberg, S.; Webb, J. S. *J. Bacteriol.* **2006**, *188*, 7344–7353.

(30) Hossain, S.; Nisbett, L.-M.; Boon, E. M. *Acc. Chem. Res.* **2017**, *50*, 1633–1639.

(31) Nisbett, L.-M.; Boon, E. M. *Biochemistry* **2016**, *55*, 4873–4884.

(32) Li, Y.-H.; Tian, X. *Sensors* **2012**, *12*, 2519–2538.

(33) Hauser, A. R. *Nature Rev. Microbiol.* **2009**, 654–665.

(34) Woods, D. E.; Iglewski, B. H. *Rev. Infect. Dis.* **1983**, *5*, S715–S722.

(35) Hall, S.; McDermott, C.; Anoopkumar-Dukie, S.; McFarland, A.; Forbes, A.; Perkins, A.; Davey, A.; Chess-Williams, R.; Kiefel, M.; Arora, D.; Grant, G. *Toxins* **2016**, *8*, 236–14.

(36) Lau, G. W.; Hassett, D. J.; Ran, H.; Kong, F. *Trends Mol. Med.* **2004**, *10*, 599–606.

(37) Jayaseelan, S.; Ramaswamy, D.; Dharmaraj, S. *World J. Microbiol. Biotechnol.* **2013**, *30*, 1159–1168.

(38) Dietrich, L. E. P.; Price-Whelan, A.; Petersen, A.; Whiteley, M.; Newman, D. K. *Mol. Microbiol.* **2006**, *61*, 1308–1321.

(39) Miller, M. B.; Bassler, B. L. *Annu. Rev. Microbiol.* **2003**, *55*, 165–199.

(40) Vukomanovic, D. V.; Zoutman, D. E.; Stone, J. A.; Marks, G. S.; Brien, J. F.; Nakatsu, K. *Biochem. J.* **1997**, *322*, 25–29.

(41) Xu, T.; Scafa, N.; Xu, L.-P.; Su, L.; Li, C.; Zhou, S.; Liu, Y.; Zhang, X. *Electroanalysis* **2014**, *26*, 449–468.

(42) Dröge, W. *Physiol Rev* **2002**, *82*, 47–95.

(43) Zhuang, J. C.; Wogan, G. N. *Proc Natl Acad Sci USA* **1997**, *94*, 11875–11880.

(44) Garthwaite, J. *Trends in Neurosciences* **1991**, *14*, 60–67.

(45) Beckman, J. S.; Koppenol, W. H. *Am. J. Physiol.* **1996**, *271*, C1424–C1437.

(46) Bogdan, C.; Röllinghoff, M.; Diefenbach, A. *Immunological Reviews* **2000**, *173*, 17–26.

(47) Apel, K.; Hirt, H. *Annu. Rev. Plant Biol.* **2004**, *55*, 373–399.

(48) Duay, J.; Elliott, J.; Shear, J. B.; Stevenson, K. J. *Anal. Chem.* **2015**, *87*, 10109–10116.

(49) Pariente, F.; Alonso, J. L.; Abrufia, H. D. *Journal of Electroanalytical Chemistry* **1994**, *379*, 191–197.

(50) Bedioui, F.; Griveau, S. *Electroanalysis* **2012**, *25*, 587–600.

(51) Turkina, M. V.; Vikström, E. *J Innate Immun* **2019**, *11*, 263–279.

(52) Bozinovski, J.; Brien, J. F.; Marks, G. S.; Nakatsu, K. *Can. J. Physiol. Pharmacol.* **1994**, *72*, 746–752.

(53) Warren, J. B.; Rashpal, L.; Rendell, N. B.; Taylor, G. W. *Biochem. J.* **1990**, *266*, 921–923.

(54) Al-Ani, F. Y.; Al-Shibib, A. S.; Khammas, K. M.; Taher, R. *Folia Microbiolol.* **1986**, *31*, 215–219.

(55) Propst, C.; Lubin, L. *J. Gen. Microbiol.* **1979**, *113*, 261–266.

(56) Elliott, J.; Duay, J.; Simoska, O.; Shear, J. B.; Stevenson, K. J. *Anal. Chem.* **2017**, *89*, 1267–1274.

(57) Liu, Y.-C.; Zhao, J.; Wu, W.-L.; Yang, Z.-S. *Electrochimica Acta* **2007**, *52*, 4848–4852.

(58) Zhang, Y.; Huang, L. *Microchim Acta* **2011**, *176*, 463–470.

(59) Simoska, O.; Sans, M.; Fitzpatrick, M. D.; Crittenden, C. M.; Eberlin, L. S.; Shear, J. B.; Stevenson, K. J. *ACS Sensors* **2019**, *4*, 170–179.

(60) Webster, T. A.; Goluch, E. D. *Lab Chip* **2012**, *12*, 5195–5197.

(61) Webster, T. A.; Sismaet, H. J.; Conte, J. L.; Chan, I.-P. J.; Goluch, E. D. *Biosens. Bioelectron.* **2014**, *60*, 265–270.

(62) Sharp, D.; Gladstone, P.; Smith, R. B.; Forsythe, S.; Davis, J. *Bioelectrochemistry* **2010**, *77*, 114–119.

(63) Alatraktchi, F.; Breum Andersen, S.; Krogh Johansen, H.; Molin, S.; Svendsen, W. *Sensors* **2016**, *16*, 408–410.

(64) Dang, X.; Hu, H.; Wang, S.; Hu, S. *Microchim Acta* **2014**, *182*, 455–467.

(65) Griveau, S.; Bedioui, F. *Anal Bioanal Chem* **2013**, *405*, 3475–3488.

(66) Elliott, J.; Simoska, O.; Karasik, S.; Shear, J. B.; Stevenson, K. J. *Anal. Chem.* **2017**, *89*, 6285–6289.

(67) Brown, F. O.; Finnerty, N. J.; Bolger, F. B.; Millar, J.; Lowry, J. P. *Anal Bioanal Chem* **2005**, *381*, 964–971.

(68) Duay, J.; Goran, J. M.; Stevenson, K. J. *Anal. Chem.* **2014**, *86* , 11528–11532.

(69) Ryder, C.; Byrd, M.; Wozniak, D. J. *Current Opinion in Microbiology* **2007**, *10*, 644–648.

(70) Landry, R. M.; An, D.; Hupp, J. T.; Singh, P. K.; Parsek, M. R. *Mol. Microbiol.* **2006**, *59*, 142–151.

(71) Wilson, R.; Sykes, D. A.; Watson, D.; Rutman, A.; Taylor, G. W.; Cole, P. J. *Infect. Immun.* **1988**, *56*, 2515–2517.

(72) Muller, M. *Free Radical Biology and Medicine* **2006**, *41*, 1670–1677.

(73) Wightman, R. *Anal. Chem.* **1981**, *53*, 1125A–1134A.

(74) Pons, S.; Fleischmann, M. *Anal. Chem.* **1987**, *59*, 1391A–1399A.

(75) Bard, A. J.; Faulkner, L. R. *Electrochemical Methods Fundamentals and Applications*, 2nd ed.; Harris, D., Ed.; John Wiley & Sons, Inc., 2001; pp 1–850.

(76) Sullivan, N. L.; Tzeranis, D. S.; Wang, Y.; So, P. T. C.; Newman, D. *ACS Chem. Biol.* **2011**, *6*, 893–899.

(77) O'Malley, Y. Q.; Reszka, K. J.; Britigan, B. E. *Free Radical Biology and Medicine* **2004**, *36*, 90–100.

(78) Reimer, Å. *Acta Otolaryngol.* **2009**, *120*, 86–88.

(79) Cruickshank, C. N. D.; Lowbury, E. J. L. *Brit. J. Exp. Pathol.* **1953**, *34*, 1–6.

(80) Toledo, J. C., Jr.; Augusto, O. *Chem. Res. Toxicol.* **2012**, *25*, 975–989.

(81) El-Fouly, M. Z.; Sharaf, A. M.; Shahin, A. A. M.; El-Bialy, H. A.; Omara, A. M. A. *Journal of Radiation Research and Applied Sciences* **2015**, *8*, 36–48.

(82) Ohfuji, K.; Sato, N.; Hamada-Sato, N.; Kobayashi, T.; Imada, C.; Okuma, H.; Watanabe, E. *Biosens. Bioelectron.* **2004**, *19*, 1237–1244.

(83) Miescher, E. *Journal of Molecular Spectroscopy* **1978**, *69*, 281–293.

(84) Cremaschi, P. *The Journal of Chemical Physics* **1981**, *75*, 3944–3953.

(85) Shah, A.; Ullah, A.; Nosheen, E.; Rana, U. A.; Shakir, I.; Badshah, A.; Rehman, Z. U.; Hussain, H. *Journal of the Electrochemical Society* **2013**, *160*, H765–H769.

(86) Chen, W.; Liu, X.-Y.; Qian, C.; Song, X.-N.; Li, W.-W.; Yu, H.-Q. *Biosens. Bioelectron.* **2015**, *64*, 25–29.

(87) Radi, R. *Proc Natl Acad Sci USA* **2018**, *115*, 5839–5848.

(88) Yoon, S. S.; Hennigan, R. F.; Hilliard, G. M.; Ochsner, U. A.; Parvatiyar, K.; Kamani, M. C.; Allen, H. L.; DeKievit, T. R.; Gardner, P. R.; Schwab, U.; Rowe, J. J.; Iglewski, B. H.; McDermott, T. R.; Mason, R. P.; Wozniak, D. J.; Hancock, R. E. W.; Parsek, M. R.; Noah, T. L.; Boucher, R. C.; Hassett, D. J. *Dev. Cell* **2002**, *3*, 593–603.

(89) Cutruzzolà, F.; Frankenberg-Dinkel, N. *J. Bacteriol.* **2015**, *198*, 55–65.

(90) Cappiello, A.; Famiglini, G.; Rossi, L.; Magnani, M. *Anal. Chem.* **1997**, *69*, 5136–5141.

(91) Sterling, H. J.; Batchelor, J. D.; Wemmer, D. E.; Williams, E. R. *J. Am. Soc. Mass Spectrom.* **2010**, *21*, 1045–1049.

(92) Friedheim, E.; Michaelis, L. *J. Biol. Chem.* **1931**, *91*, 355–369.

(93) Zaugg, W. S. *J. Biol. Chem.* **1964**, *239*, 3964–3970.

(94) Lewis, R. S.; Deen, W. M. *Chem. Res. Toxicol.* **1994**, *7*, 568–574.

(95) Goldstein, S.; Czapski, G. *J. Am. Chem. Soc.* **1996**, *118*, 3419–3425.

(96) Ford, P. C.; Wink, D. A.; Stanbury, D. M. *FEBS Lett.* **1993**, *326*, 1–3.

(97) Hussain, A. S.; Bozinovski, J.; Maurice, D. H.; McLaughlin, B. E.; Marks, G. S.; Brien, J. F.; Nakatsu, K. *Can. J. Physiol. Pharmacol.* **1997**, *75*, 398–406.

(98) Howlin, R. P.; Cathie, K.; Hall-Stoodley, L.; Cornelius, V.; Duignan, C.; Allan, R. N.; Fernandez, B. O.; Barraud, N.; Bruce, K. D.; Jefferies, J.; Kelso, M.; Kjelleberg, S.; Rice, S. A.; Rogers, G. B.; Pink, S.; Smith, C.; Sukhtankar, P. S.; Salib, R.; Legg, J.; Carroll, M.; Daniels, T.; Feelisch, M.; Stoodley, P.; Clarke, S. C.; Connett, G.; Faust, S. N.; Webb, J. S. *Molecular Therapy* **2017**, *25*, 2104–2116.

Appendix 1: Real-time Electrochemical Detection of *Pseudomonas aeruginosa* Phenazine Metabolites using Transparent Carbon Ultramicroelectrode Arrays[6]

A1.1 Experimental Methods

A1.1.1 Electrochemical Determination of Diffusion Coefficients of Pyocyanin (PYO)

Background solutions were tryptic soy broth (TSB) and lysogeny broth (LB) growth media, while solutions of 90 μM PYO in LB and TSB were used to determine diffusion coefficients of PYO. Using double step potential chronoamperometry by initially holding the potential at −0.32 V vs SCE for 1 s, then holding the potential at −0.15 V vs SCE for 25 s, followed by stepping the potential back to −0.22 V vs SCE for another 25 s, in the aforementioned solutions. Using the obtained chronoamperograms, Cottrell plots were made, from which the corresponding diffusion coefficients for PYO in each media were determined.

A1.1.3 Cell Imaging

Images presented in electronic supporting information were acquired with a Nikon A1R confocal microscope using Nikon image-capture software. Bacterial cells PA14 were visualized via green fluorescence protein (gfp) expression utilizing appropriate filter set and v-filtering function. Images were acquired using a 20× air objective to image cells through T-CUAs.

[6]Adapted with permission from Simoska, O.; Sans, M.; Fitzpatrick, M. D.; Crittenden, C. M.; Eberlin, L. S.; Shear, J. B.; Stevenson, K. J. Real-time Electrochemical Detection of *Pseudomonas aeruginosa* Phenazine Metabolites using Transparent Ultramicroelectrode Arrays. *ACS Sensors* **2019**, *4*, 170–179. Copyright © 2019 American Chemical Society. Simoska, O. acquired the data, wrote the manuscript, and performed electrochemical measurements/characterization. Simoska, O., Crittenden. C. M., and Sans, M. performed mass spectrometry experiments. Simoska, O. and Stevenson, K. J. designed studies, planned experiments, and analyzed all data. All authors contributed in editing the manuscript.

A1.2 ADDITIONAL DATA

Growth Media	TSB	LB
Time (h)	PYO Concentration (μM)	
0	7.2 ± 0.2	17.4 ± 0.5
1	7.0 ± 0.3	18 ± 2
2	8.2 ± 0.8	19 ± 2
3	15.6 ± 0.3	22 ± 2
4	25.3 ± 0.6	33.2 ± 0.6
5	45.6 ± 0.9	41 ± 2
6	58 ± 2	55 ± 2
7	75 ± 2	71 ± 3
8	84 ± 2	79 ± 1
9	100 ± 4	84 ± 2
10	110 ± 5	94 ± 3
11	120 ± 4	110 ± 1
12	130 ± 5	120 ± 3
15	160 ± 5	130 ± 2
18	180 ± 4	150 ± 1
21	190 ± 5	150 ± 1
24	180 ± 6	150 ± 4
30	160 ± 6	141 ± 16
36	170 ± 5	130 ± 8
42	160 ± 6	130 ± 6
48	140 ± 6	130 ± 5

Table A1.1: Concentrations of PYO secreted from *P. aeruginosa* measured at each time point in both TSB and LB media (shown are average concentration values from nine replicas).

Growth Media	Diffusion coefficients (cm^2/s)
TSB	$(3.4\pm0.8)\times10^{-6}$
LB	$(5.1\pm0.1)\times10^{-6}$

Table A1.2: Determined diffusion coefficients of 90 μM PYO in TSB and LB media using double potential step chronoamperometry.

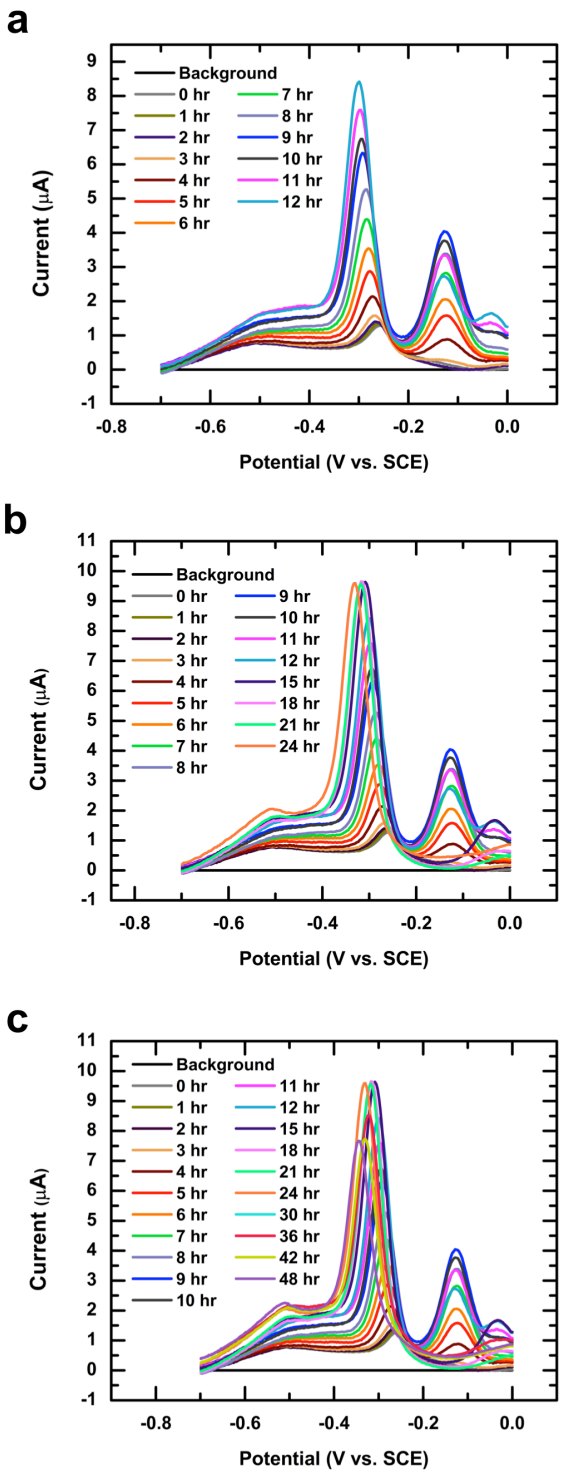

Figure A1.1: Square wave voltammograms taken over time of PA14 in LB growth media in time frames (a) 0–12 h, (b) 0–24 h, and (c) 0–48 h.

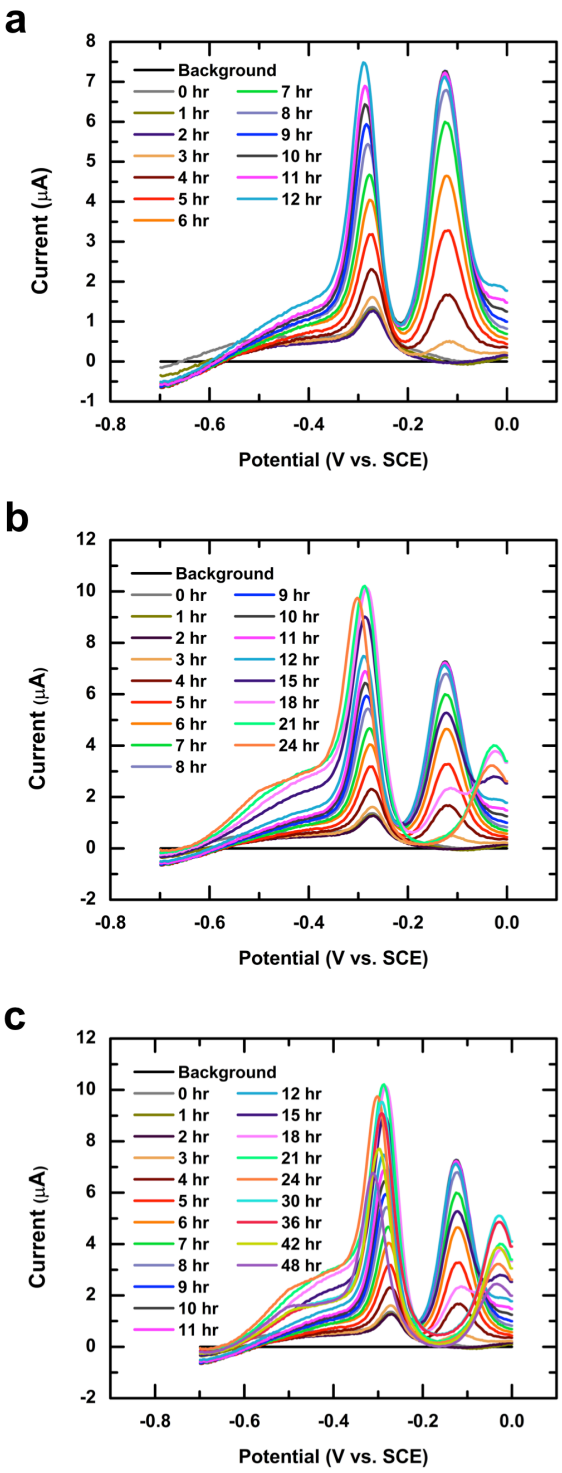

Figure A1.2: Square wave voltammograms taken over time of PA14 in TSB growth media in time frames (a) 0–12 h, (b) 0–24 h, and (c) 0–48 h.

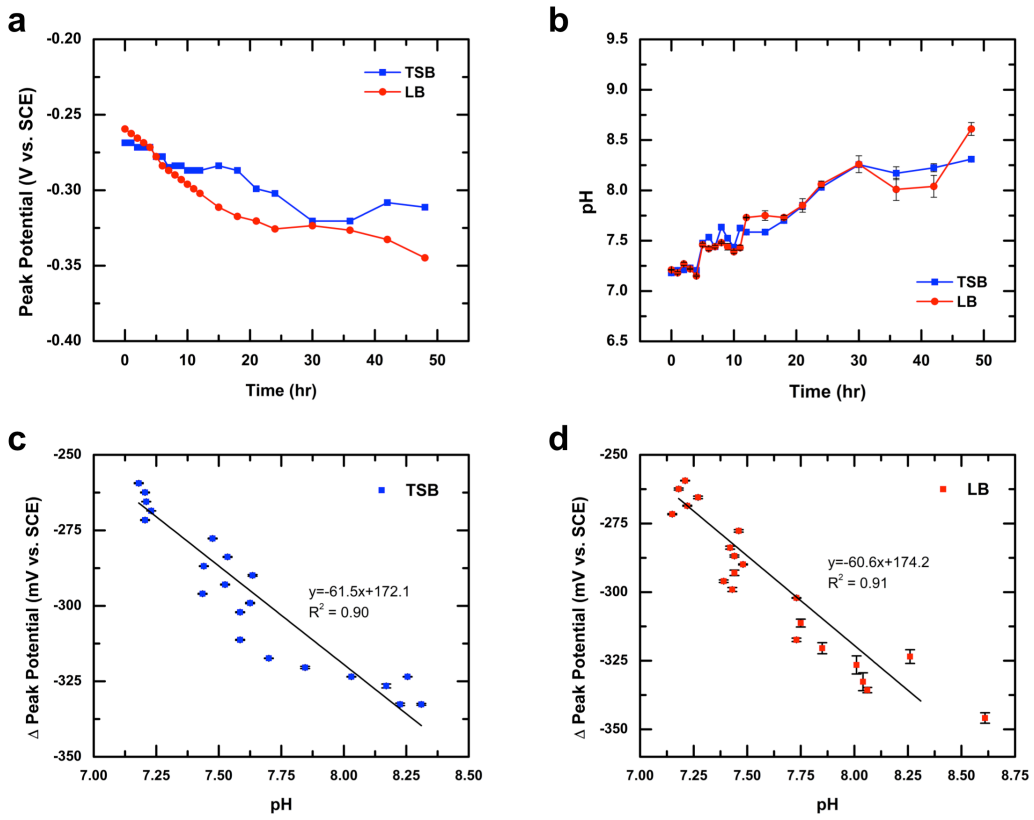

Figure A1.3: Dependence of PYO peak potential on pH.

(a) Peak potential of PYO plotted as a function of time using data shown in Figure 3.3 for TSB and LB. PYO peak potential shifts to more negative values over time, which is likely due to changes in pH of solutions. (b) Time-based measurements of pH of PA14 cultures in TSB and LB. Peak potential shifts plotted as a function of pH for (c) TSB and (d) LB, showing almost a completely Nernstian behavior with slope values close to 59 mV/pH unit. Values plotted are the mean from 3x replicated with error bars showing standard error of the mean.

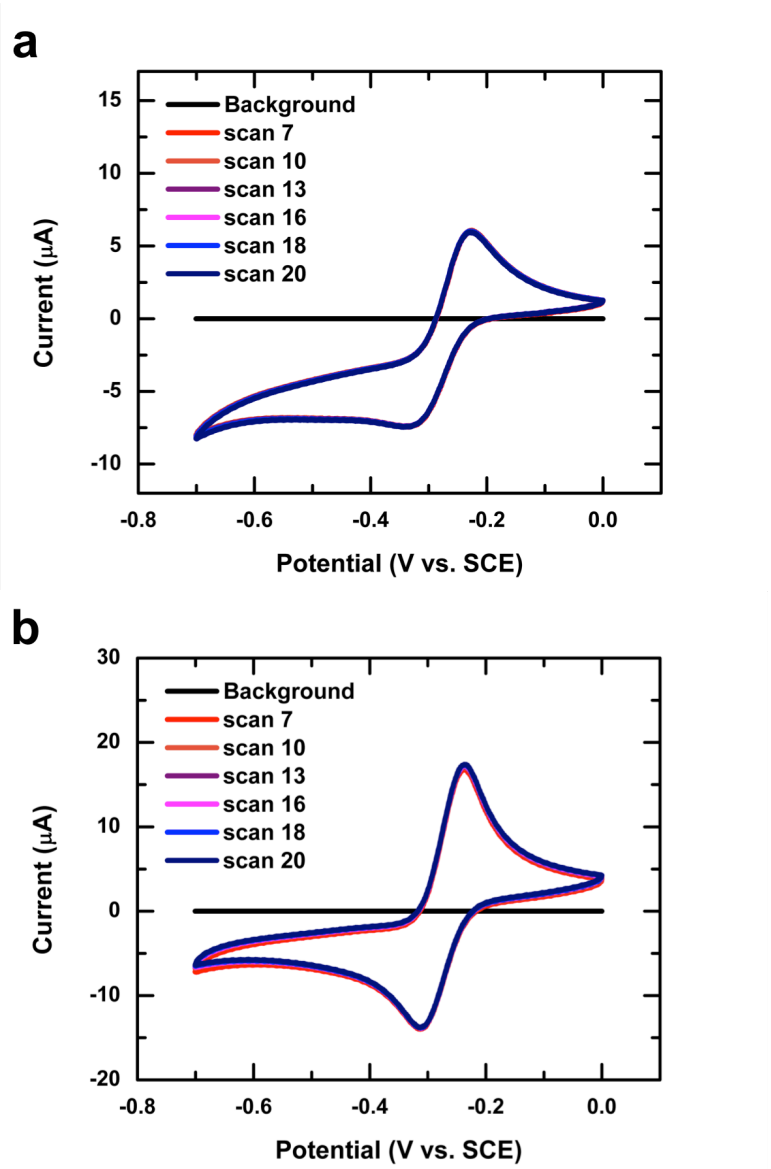

Figure A1.4: Cyclic voltammograms at different scan rates to test PYO polymerization that typically occurs at high anodic potentials.

Using 100 μM PYO on T-CUA electrodes, and a scan rate of 100 mV s^{-1}, CVs were performed in (a) LB and (b) TSB media. Note that there is no polymerization of PYO observed in this potential window.

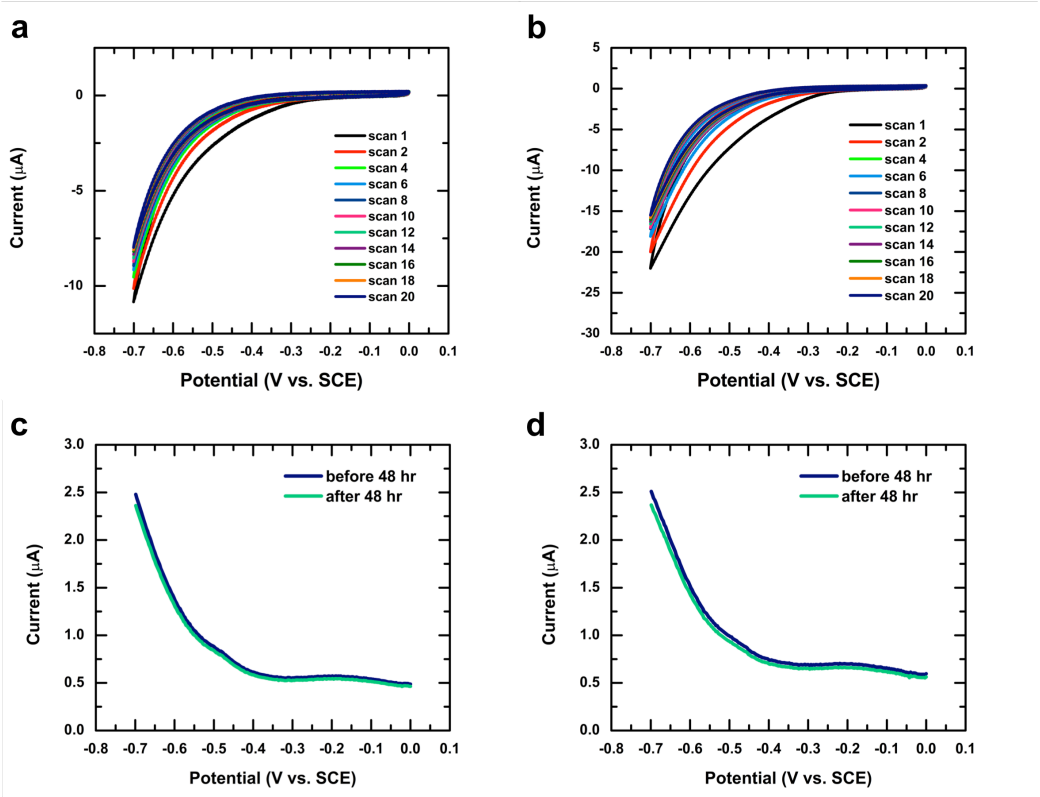

Figure A1.5: Biocompatibility of T-CUA electrodes showing that it takes 20 scans to establish double layer capacitance in biologically relevant media.

Background cyclic voltammograms at scan rate 50 mV s^{-1} using (a) LB and (b) TSB. Square wave voltammograms showing background scan 20 of T-CUAs before and after 48-hour long experiments in (c) LB and (d) TSB. These square wave curves show that we can successfully re-establish double layer capacitance after using CUAs for 48-hour continuous monitoring of PYO. These data demonstrate that T-CUAs have excellent biocompatibility.

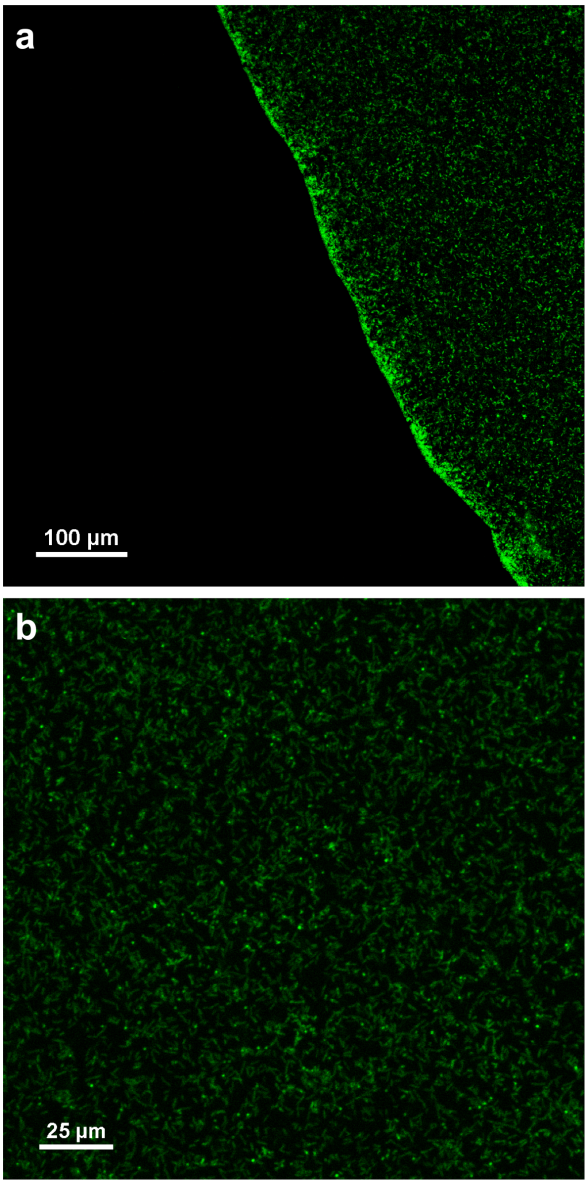

Figure A1.6: Biocompatibility of T-CUA electrode surfaces.

GFP-expressing *P. aeruginosa* PA14 in TSB imaged through T-CUAs. Confocal images of (a) an edge of a droplet of PA14 liquid culture in LB on T-CUA and (b) zoom-in view of bacterial culture shown in (a).

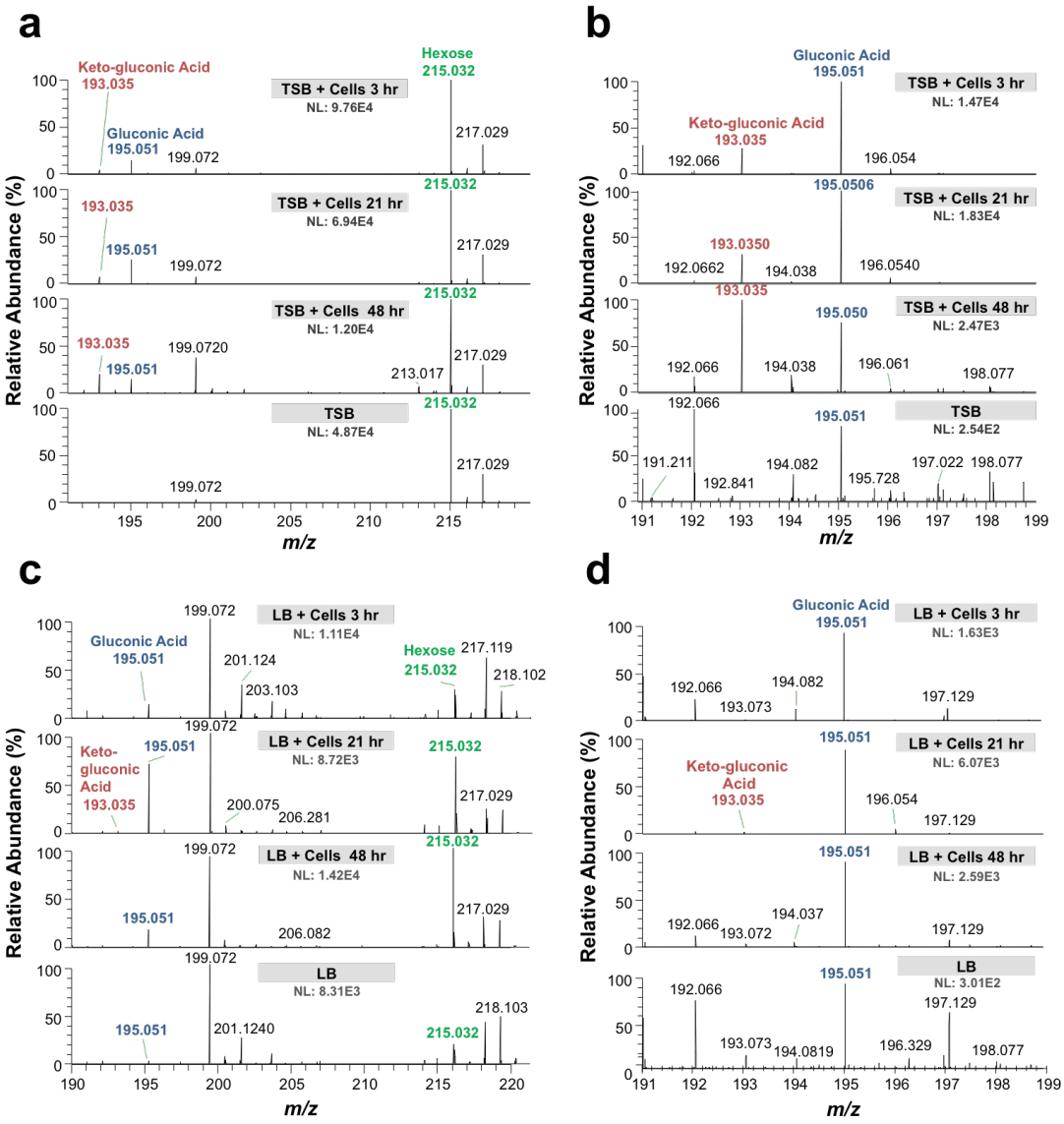

Figure A1.7: DESI-MS spectra of at various time points with changes in the relative abundances of hexose, hexonic acid and keto-hexonic acid.

DESI-MS spectra of (a) TSB and (c) LB growth media at various time points, showing changes in the relative abundances of hexose (*m/z* 215.032), hexonic acid (*m/z* 195.051) and keto-hexonic acid (*m/z* 193.035). MS spectra in the right column represent a zoomed in mass spectra from *m/z* 191 to *m/z* 199 for (b) TSB and (d) LB media. These species detected in LB media have lower the relative abundances to TSB. Data collected with the assistance of Marta Sans of the Eberlin research group.

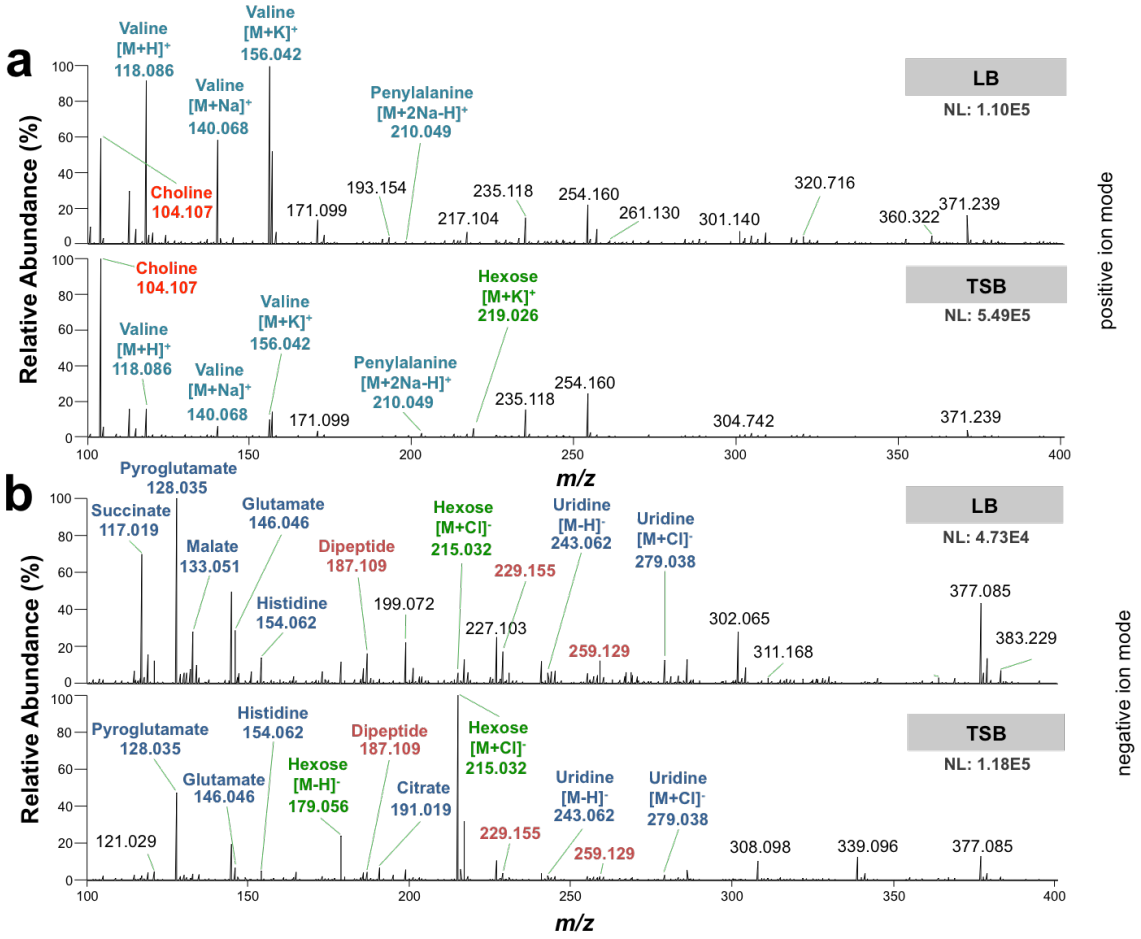

Figure A1.8: DESI MS/MS spectra of LB and TSB growth media.

DESI MS/MS spectra of LB and TSB growth media in (a) positive ion mode, and (b) negative ion mode. Note that there is a very high abundance of choline and hexose in TSB media compared to LB. Data collected with the assistance of Marta Sans of the Eberlin research group.

Detected *m/z*	Attribution	Ion	Molecular formula	Mass Error
104.107	Choline	$[M+H]^+$	$C_5H_{14}NO$	-4.8
118.086	Valine	$[M+H]^+$	$C_5H_{12}NO_2$	-4.2
140.068	Valine	$[M+Na]^+$	$C_5H_{11}NO_2Na$	-2.1
156.042	Valine	$[M+K]^+$	$C_5H_{11}NO_2K$	-1.9
166.086	Penylalanine	$[M+H]^+$	$C_9H_{12}NO_2$	-2.4
210.050	Penylalanine	$[M+2Na-H]^+$	$C_9H_{10}NO_2Na_2$	-2.9
241.997	Penylalanine	$[M+2K-H]^+$	$C_9H_{10}NO_2K_2$	-2.9
227.079	LG, GL, IG, GI	$[M+K]^+$	$C_8H_{16}N_2O_3K$	-3.5
211.105	LG, GL, IG, GI	$[M+Na]^+$	$C_8H_{16}N_2O_3Na$	-3.3
265.034	LG, GL, IG, GI	$[M+2K-H]^+$	$C_8H_{15}N_2O_3K2$	-3.4
203.138	AL, LA, AI, IA	$[M+H]^+$	$C_9H_{19}N_2O_3$	-3.0
203.052	Hexose	$[M+Na]^+$	$C_6H_{12}O_6Na$	-2.5
219.026	Hexose	$[M+K]^+$	$C_6H_{12}O_6K$	-2.7
231.170	VL, LV, VI, IV	$[M+H]^+$	$C_{11}H_{23}N_2O_3$	-2.6
245.078	Uridine	$[M+H]^+$	$C_9H_{13}N_2O_6$	3.7

Table A1.3: Contents of TSB and LB media identified using high mass accuracy and DESI MS/MS in the positive ion mode.

Species identified (Figure A1.8a) have different relative abundances in each media. Data collected with the assistance of Marta Sans of the Eberlin research group.

Detected *m/z*	Attribution	Ion	Molecular formula	Mass Error
117.019	Succinate	$[M+H]^-$	C_4H5O_4	-0.4
128.035	Pyroglutamate	$[M+H]^-$	$C_5H_6NO_3$	-0.3
133.014	Malate	$[M+H]^-$	$C_4H_5O_5$	-0.5
146.046	Glutamate	$[M+H]^-$	C_5H8NO_4	-0.3
154.062	Histidine	$[M+H]^-$	$C_6H_8N_3O_2$	-0.7
179.056	Hexose	$[M+H]^-$	$C_6H_{11}O_6$	-1.1
187.109	LG, GL, IG, GI	$[M+H]^-$	$C_8H_{15}N_2O_3$	-1.5
191.020	Citrate	$[M+H]^-$	C_6H7O7	-1.0
201.124	AL, LA, AI, IA	$[M+H]^-$	$C_9H_{17}N_2O_3$	-1.6
203.103	V-S	$[M+H]^-$	$C_8H_{15}N_2O_4$	-1.8
215.032	Hexose	$[M+Cl]^-$	$C_6H_{12}O_6Cl$	-1.5
229.155	VL, LV, VI, IV	$[M+H]^-$	$C_{11}H_{21}N_2O_3$	-2.0
243.062	Uridine	$[M+H]^-$	$C_9H_{11}N_2O_6$	-2.0
244.130	LB, BL, IB, BI, VQ, QV	$[M+H]^-$	$C_{10}H_{18}N_3O_4$	-2.0
245.114	VE, EV, DL, LD, DI, ID	$[M+H]^-$	$C_{10}H_{17}N_2O_5$	-1.9
259.129	EL, LE, EI, IE	$[M+H]^-$	$C_{11}H_{19}N_2O_5$	-1.9
267.146	HL, LH, HI, IH	$[M+H]^-$	$C_{12}H_{19}N_4O_3$	-1.9
279.038	Uridine	$[M+Cl]^-$	$C_9H_{12}N_2O_6Cl$	-1.8
377.086	Disaccharides (2Hexose)	$[M+Cl]^-$	$C_{12}H_{22}O_{11}Cl$	0.3

Table A1.4: Contents of TSB and LB media identified using high mass accuracy and DESI MS/MS in the negative ion mode.

Species identified (Figure A1.8b) have different relative abundances in each media. Data collected with the assistance of Marta Sans of the Eberlin research group.

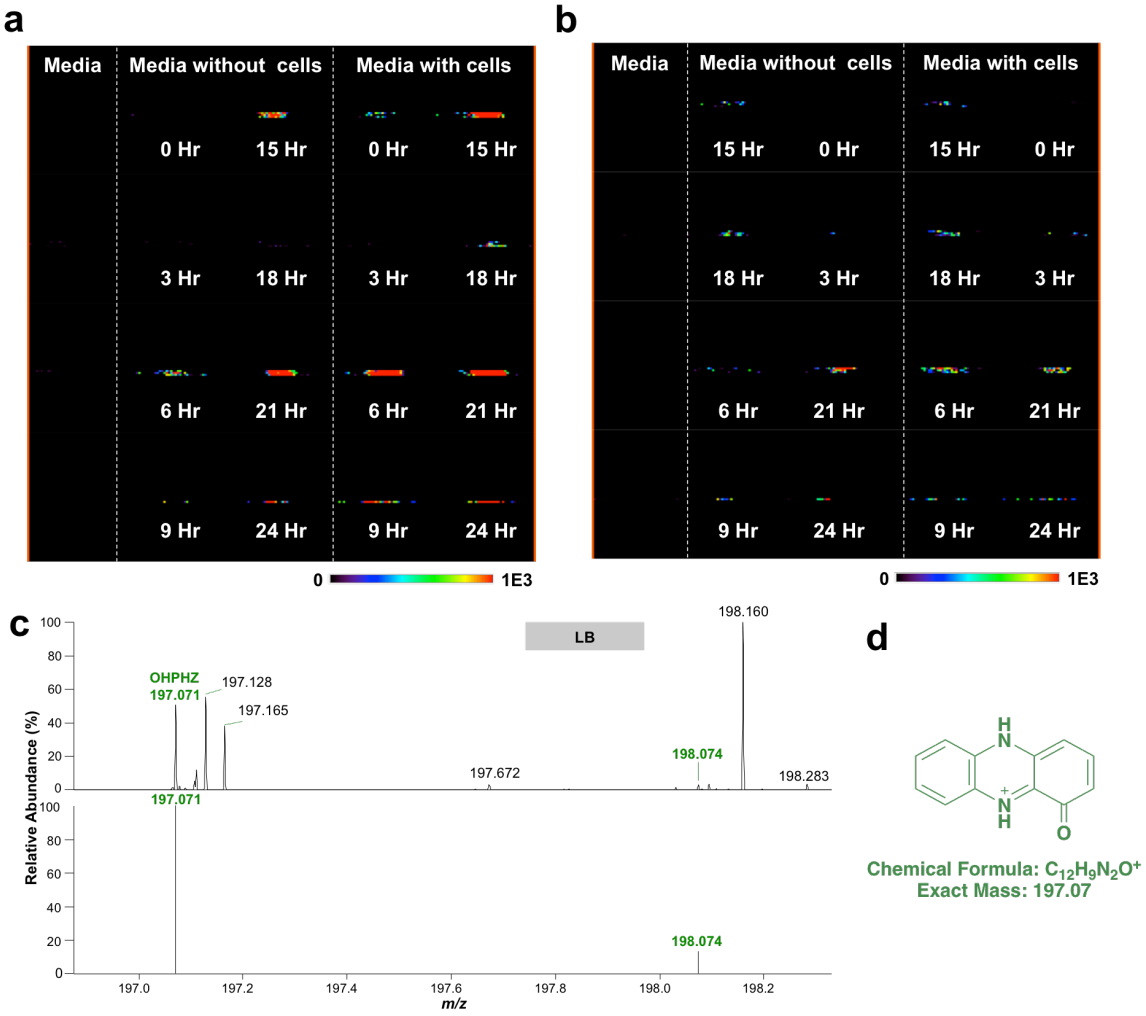

Figure A1.9: DESI-MS ion images and spectra for 1-hydroxyphenazine (OHPHZ) at various time points in LB and TSB.

DESI-MS ion images for 1-hydroxyphenazine (OHPHZ) at *m/z* 197.070 at various time points in (a) LB and (b) TSB with respective DESI-MS spectra in LB for OHPHZ shown in (c). The top DESI-MS spectra in (c) shows that species is present with highest abundance at 21 hours in LB, and the bottom shows in silico mass spectra. Note that *m/z* 197.071 and *m/z* 198.074 represent the C12 and C13 isotopes, respectively. (d) Molecular structure, formula and exact mass of OHPHZ. Data collected with the assistance of Marta Sans of the Eberlin research group.

Attribution	Molecular Formula	Detected *m/z*	Mass error (ppm)	Exact Mass
PYO	$C_{13}H_{11}O_2N$	211.0861	2.4	211.0866
HHQ	$C_{16}H_{22}ON$	244.1691	2.0	244.1696
PQS or HQNO	$C_{16}H_{22}O_2N$	260.1638	2.7	260.1645
C 9:1 - NHQ	$C_{18}H_{24}ON$	270.1848	1.5	270.1852
NHQ	$C_{18}H_{26}ON$	272.2003	2.2	272.2009
C9:1-NQNO	$C_{18}H_{24}O_2N$	286.1798	1.4	286.1802
C9-PQS or C9-NQNO	$C_{18}H_{26}O_2N$	288.1953	1.7	288.1958
C11:1-UHQ	$C_{20}H_{28}ON$	298.2160	1.7	298.2165

Table A1.5: Phenazine and quinolone species from *P. aeruginosa* detected from DESI-MS mass spectra using high mass accuracy and tandem MS measurements in the positive ion mode.

Phenazine (PYO) and quinolone species (i.e., HHQ, HQNO, NHQ, PQS) from *P. aeruginosa* detected from DESI-MS mass spectra using high mass accuracy and tandem MS measurements in the positive ion mode. Data collected with the assistance of Marta Sans of the Eberlin research group.

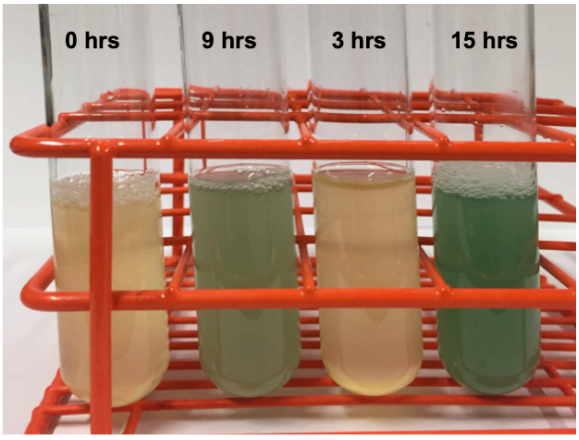

Figure A1.10: *P. aeruginosa* liquid-batch cultures in LB growth media at various time points of bacterial growth.

PYO is a blue-pigmented nitrogen-containing aromatic species, known to give a blue/green appearance to *P. aeruginosa* cultures. Due to its characteristic blue color, PYO is commonly detected using spectrophotometric approaches. While at 0 and 3 h, the bacterial cultures appear yellow and there is no blue/green color indication of presence of PYO (such as green liquid cultures in flasks at 9 and 15 h), levels of cellular PYO are electrochemically detected as demonstrated in Figure 3.4.

Appendix 2: Electrochemical Monitoring of the Impact of Polymicrobial Infections on *Pseudomonas aeruginosa* and Growth Dependent Medium[7]

A2.1 ADDITIONAL DATA

Microbial Environment	*Pa*	*Pa* and *Sa*	*Pa* and *Ec*	*Pa, Sa* and *Ec*
Time (h)	PYO Concentrations (μM) in LB			
0	17.4 ± 0.5	9.1 ± 0.5	7.5 ± 0.2	4.2 ± 0.3
1	18 ± 2	9.0 ± 0.5	7.6 ± 0.1	4.6 ± 0.1
2	19 ± 2	9.3 ± 0.3	7.9 ± 0.2	4.6 ± 0.1
3	22 ± 2	8.2 ± 0.4	8.0 ± 0.4	4.5 ± 0.1
4	33.2 ± 0.6	11 ± 1	10.5 ± 0.3	4.9 ± 0.1
5	41 ± 2	17 ± 1	14.2 ± 0.6	5.7 ± 0.1
6	55 ± 2	25 ± 2	18.3 ± 0.6	7.2 ± 0.4
7	71 ± 3	34 ± 2	21.8 ± 0.8	8.8 ± 0.7
8	79 ± 1	44 ± 3	28.1 ± 0.7	12 ± 1
9	84 ± 2	55 ± 3	35.0 ± 0.9	13 ± 2
10	94 ± 3	63 ± 3	42 ± 1	16 ± 2
11	110 ± 1	75 ± 3	50 ± 2	19 ± 3
12	120 ± 3	88 ± 3	58 ± 2	20 ± 3
15	130 ± 2	120 ± 4	68 ± 2	23 ± 3
18	150 ± 1	140 ± 3	70 ± 3	27 ± 3
21	150 ± 1	150 ± 1	72 ± 1	28 ± 3
24	150 ± 4	150 ± 8	71 ± 1	28 ± 4
30	141 ± 16	150 ± 7	65 ± 1	25 ± 3
36	130 ± 8	140 ± 8	60 ± 1	24 ± 3
42	130 ± 6	140 ± 3	64 ± 1	25 ± 2
48	130 ± 5	140 ± 5	63 ± 2	26 ± 2

Table A2.1: Pyocyanin (PYO) concentrations determined at each time point in polymicrobial samples in LB media (shown are average concentrations from 6x replicas). *Pa* for *P. aeruginosa*, *Sa* for *S. aureus*, and *Ec* for *E. coli*.

[7]Adapted with permission from Simoska, O.; Sans, M.; Eberlin, L. S.; Shear, J. B.; Stevenson, K. J. Electrochemical Monitoring of the Impact of Polymicrobial Infections on *Pseudomonas aeruginosa* and Growth Dependent Medium. *Biosens. Bioelectron.* **2019**, *142*, 111538. Copyright © 2019 Elsevier. Simoska O. acquired the data, wrote the manuscript, and performed electrochemical measurements/characterization. All authors contributed in editing the manuscript.

Microbial Environment	*Pa*	*Pa* and *Sa*	*Pa* and *Ec*	*Pa, Sa* and *Ec*
Time (h)	**PYO Concentrations (μM) in TSB**			
0	7.2 ± 0.2	2.7 ± 0.2	1.0 ± 0.1	1.0 ± 0.1
1	7.0 ± 0.3	2.3 ± 0.3	1.0 ± 0.1	1.0 ± 0.1
2	8.2 ± 0.8	2.8 ± 0.2	1.0 ± 0.1	1.0 ± 0.1
3	15.6 ± 0.3	4.1 ± 0.2	1.0 ± 0.1	1.0 ± 0.1
4	25.3 ± 0.6	4.4 ± 0.7	1.0 ± 0.1	1.0 ± 0.2
5	45.6 ± 0.9	4.8 ± 0.5	1.0 ± 0.2	1.0 ± 0.1
6	58 ± 2	10 ± 1	1.0 ± 0.1	1.0 ± 0.1
7	75 ± 2	16 ± 1	1.0 ± 0.1	1.0 ± 0.1
8	84 ± 2	22 ± 1	1.0 ± 0.1	1.0 ± 0.2
9	100 ± 4	26 ± 2	1.1 ± 0.2	1.0 ± 0.3
10	110 ± 5	32 ± 1	2.1 ± 0.2	1.0 ± 0.2
11	120 ± 4	38 ± 1	4.4 ± 0.2	1.0 ± 0.2
12	130 ± 5	45 ± 1	6.4 ± 0.1	1.0 ± 0.1
15	160 ± 5	60 ± 2	6.7 ± 0.3	1.0 ± 0.1
18	180 ± 4	68 ± 2	8.3 ± 0.2	1.0 ± 0.2
21	190 ± 5	78 ± 2	9.3 ± 0.2	1.1 ± 0.8
24	180 ± 6	78 ± 3	5.4 ± 0.1	1.2 ± 0.1
30	160 ± 6	74 ± 2	5.4 ± 0.1	1.8 ± 0.2
36	170 ± 5	59 ± 1	3.8 ± 0.1	2.3 ± 0.2
42	160 ± 6	53 ± 2	4.1 ± 0.3	4.1 ± 0.2
48	140 ± 6	58 ± 2	4.2 ± 0.4	8.2 ± 0.5

Table A2.2: PYO concentrations determined at each time point in polymicrobial environments in TSB media (shown are average concentrations from 6x replicas). *Pa* stands for *P. aeruginosa*, *Sa* for *S. aureus*, and *Ec* for *E. coli.*

Microbial Environment	*Pa*	*Pa* and *Sa*	*Pa* and *Ec*	*Pa, Sa* and *Ec*
Time (h)	**5-MCA Concentrations (μM) in LB**			
0	1.1 ± 0.2	1.3 ± 0.1	0.6 ± 0.1	1.1 ± 0.1
1	1.2 ± 0.2	1.5 ± 0.2	0.6 ± 0.1	1.5 ± 0.1
2	1.3 ± 0.2	1.6 ± 0.4	0.7 ± 0.1	1.6 ± 0.2
3	3.8 ± 0.9	1.3 ± 0.2	0.9 ± 0.2	2.2 ± 0.4
4	16 ± 1	5.9 ± 0.4	3.3 ± 0.5	3.6 ± 0.5
5	31 ± 3	16 ± 1	5.3 ± 0.3	5.9 ± 0.7
6	43 ± 1	27 ± 2	6.3 ± 0.4	7.8 ± 0.9
7	57 ± 2	32 ± 2	6.4 ± 0.4	7.9 ± 0.8
8	68 ± 3	39 ± 2	6.7 ± 0.3	8.0 ± 0.8
9	78 ± 5	47 ± 3	7.1 ± 0.2	10 ± 1
10	75 ± 4	49 ± 2	8.6 ± 0.3	10 ± 1
11	64 ± 3	53 ± 2	9.9 ± 0.4	12 ± 2
12	51 ± 3	56 ± 3	9.8 ± 0.6	11 ± 2
15	3.5 ± 0.9	52 ± 2	7.5 ± 0.6	11 ± 2
18	2.8 ± 0.9	23 ± 1	5.9 ± 0.8	7.4 ± 0.9
21	2.3 ± 0.6	10 ± 1	3.9 ± 0.6	4.1 ± 0.8
24	5.4 ± 0.9	4.9 ± 0.5	2.4 ± 0.3	2.5 ± 0.9
30	6.7 ± 0.8	3.5 ± 0.3	1.1 ± 0.1	1.5 ± 0.4
36	5.9 ± 0.7	2.5 ± 0.2	0.5 ± 0.1	1.0 ± 0.2
42	5.6 ± 0.4	2.9 ± 0.1	0.5 ± 0.1	1.0 ± 0.2
48	6.2 ± 0.7	1.2 ± 0.2	0.5 ± 0.1	1.0 ± 0.1

Table A2.3: 5-methylphenazine-1-carboxylic acid (5-MCA) concentrations determined at each time point in polymicrobial environments in LB media (shown are average concentrations from 6x replicas). *Pa* stands for *P. aeruginosa*, *Sa* for *S. aureus*, and *Ec* for *E. coli*.

Microbial Environment	*Pa*	*Pa* and *Sa*	*Pa* and *Ec*	*Pa, Sa* and *Ec*
Time (h)	**5-MCA Concentrations (μM) in TSB**			
0	2.3 ± 0.7	1.0 ± 0.2	0.15 ± 0.04	0.39 ± 0.04
1	2.6 ± 0.9	1.0 ± 0.3	0.15 ± 0.02	0.35 ± 0.05
2	3.5 ± 0.9	1.0 ± 0.2	0.19 ± 0.02	0.28 ± 0.06
3	10 ± 1	3.2 ± 0.5	0.20 ± 0.04	0.34 ± 0.07
4	36 ± 1	5.3 ± 0.8	0.27 ± 0.02	0.31 ± 0.06
5	83 ± 2	6.1 ± 0.2	0.34 ± 0.02	0.31 ± 0.05
6	140 ± 4	12 ± 1	0.32 ± 0.03	0.31 ± 0.05
7	201 ± 8	19 ± 1	0.31 ± 0.02	0.34 ± 0.04
8	220 ± 2	24 ± 2	0.36 ± 0.02	0.40 ± 0.03
9	210 ± 7	28 ± 2	0.34 ± 0.06	0.43 ± 0.03
10	190 ± 6	33 ± 2	1.0 ± 0.3	0.51 ± 0.02
11	170 ± 4	35 ± 2	1.8 ± 0.4	0.67 ± 0.05
12	130 ± 9	38 ± 2	2.8 ± 0.5	0.61 ± 0.04
15	48 ± 7	38 ± 4	1.9 ± 0.3	0.52 ± 0.02
18	10 ± 2	34 ± 4	1.5 ± 0.1	0.53 ± 0.02
21	1.5 ± 0.5	33 ± 4	1.5 ± 0.1	1.0 ± 0.1
24	1.1 ± 0.5	22 ± 3	1.0 ± 0.1	1.0 ± 0.2
30	1.6 ± 0.5	3.2 ± 0.3	0.33 ± 0.08	1.0 ± 0.4
36	2.6 ± 0.7	2.1 ± 0.3	0.31 ± 0.07	1.0 ± 0.3
42	1.1 ± 0.4	1.9 ± 0.2	0.39 ± 0.09	1.7 ± 0.3
48	1.0 ± 0.2	1.4 ± 0.3	0.33 ± 0.08	3.3 ± 0.9

Table A2.4: 5-MCA concentrations determined at each time point in polymicrobial environments in TSB media (shown are average concentrations from 6x replicas). *Pa* stands for *P. aeruginosa*, *Sa* for *S. aureus*, and *Ec* for *E. coli*.

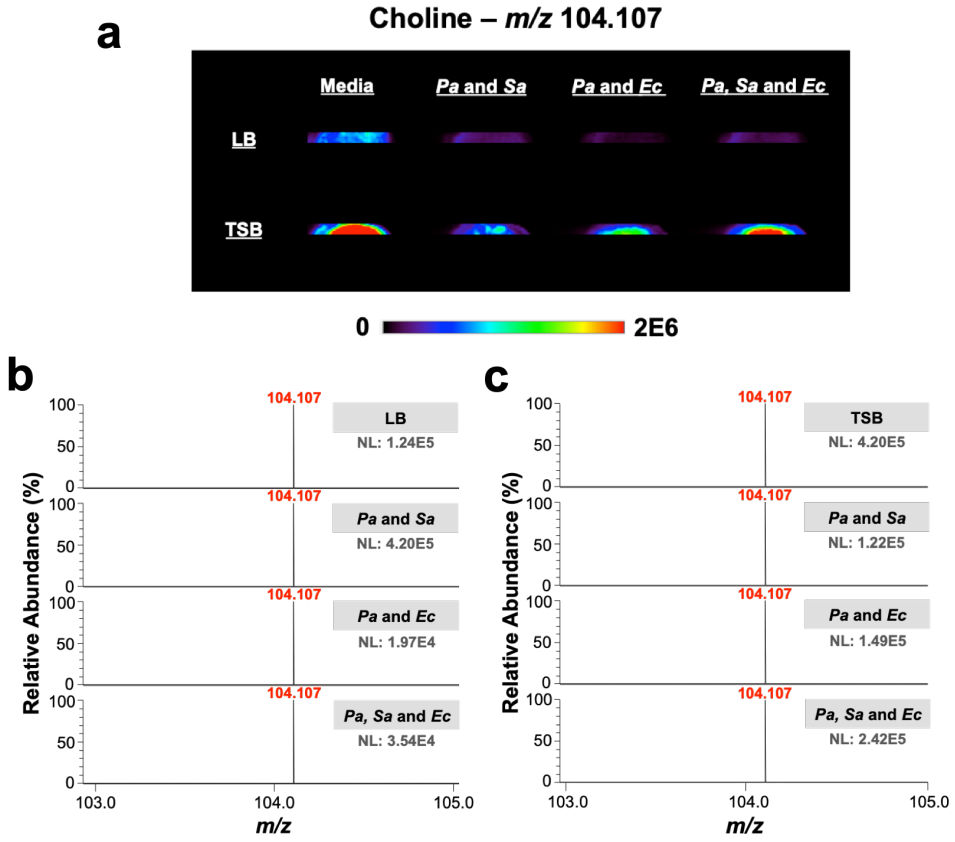

Figure A2.1: DESI-MS data of choline at *m/z* 104.107 obtained at 5 h of bacterial growth in three different polymicrobial co-cultures in LB and TSB.

(a) DESI-MS ion images for choline in (i) *Pa* and *Sa*, (ii) *Pa* and *Ec*, and (iii) *Pa*, *Sa*, and *Ec* in LB (top) and TSB (bottom). Higher abundance of choline observed in TSB relative to LB media. In LB and TSB media samples only, choline abundances are higher compared to those of samples containing cells, indicating that cells are consuming choline species present in media. (b) DESI-MS spectra of choline (positive ion mode) for LB media compared to three polymicrobial samples in LB. Similar choline abundances observed in all three co-culture samples, with lowest choline abundance in *Pa* and *Ec* sample. (c) DESI-MS spectra of choline (positive ion mode) for TSB media compared to three polymicrobial samples in TSB. In all three polymicrobial samples in TSB analyzed, choline abundances are similar, with potentially higher abundance in *Pa, Sa* and *Ec* sample. NL corresponds to the ion abundance (ion current). *Pa* stands for *P. aeruginosa*, *Sa* for *S. aureus*, and *Ec* for *E. coli*. Data collected with the assistance of Marta Sans of the Eberlin research group.

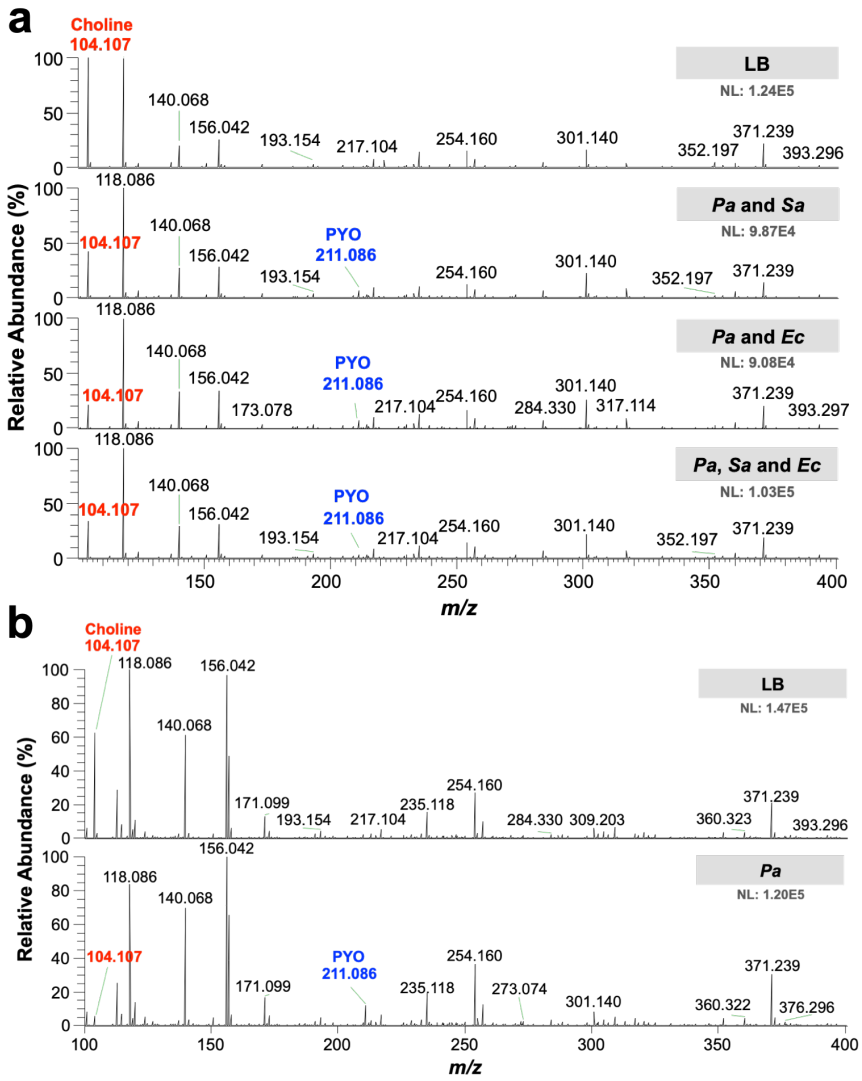

Figure A2.2: DESI-MS spectra obtained in LB media at 5 h cell growth.

(a) DESI-MS spectra (positive ion mode) for LB, *Pa* and *Sa* in LB, *Pa* and *Ec* in LS, and *Pa*, *Sa* and *Ec* in LB, and for comparison (b) DESI-MS spectra (positive ion mode) for *Pa* only in LB media. Relatively higher abundance of PYO at *m/z* 211.086 and lower abundance of choline at *m/z* 104.107 for the sample containing *Pa* cells only in TSB shown in (b) compared to three co-cultured samples in (a). NL corresponds to the ion abundance (ion current). *Pa* stands for *P. aeruginosa*, *Sa* for *S. aureus*, and *Ec* for *E. coli*. Data collected with the assistance of Marta Sans of the Eberlin research group.

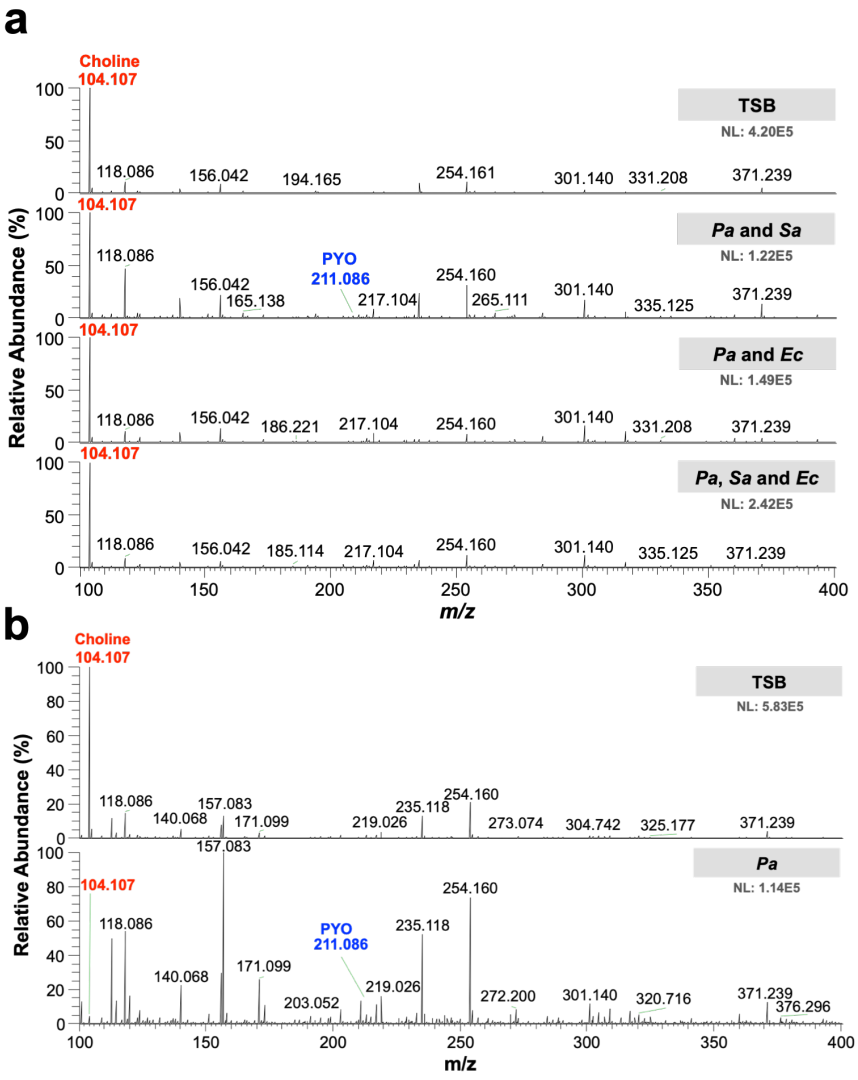

Figure A2.3: DESI-MS spectra obtained in TSB media at 5 h cell growth.

(a) DESI-MS spectra (positive ion mode) for TSB, *Pa* and *Sa* in TSB, *Pa* and *Ec* in TBS, and *Pa, Sa* and *Ec* in TSB, and for comparison (b) DESI-MS spectra (positive ion mode) for *Pa* only in TSB media. Relatively higher abundance of PYO at *m/z* 211.086 and much lower abundance of choline at *m/z* 104.107 for the sample containing *Pa* cells only in TSB shown in (b) compared to three co-cultured samples in (a). NL corresponds to the ion abundance (ion current). *Pa* stands for *P. aeruginosa*, *Sa* for *S. aureus*, and *Ec* for *E. coli.* Data collected with the assistance of Marta Sans of the Eberlin research group.

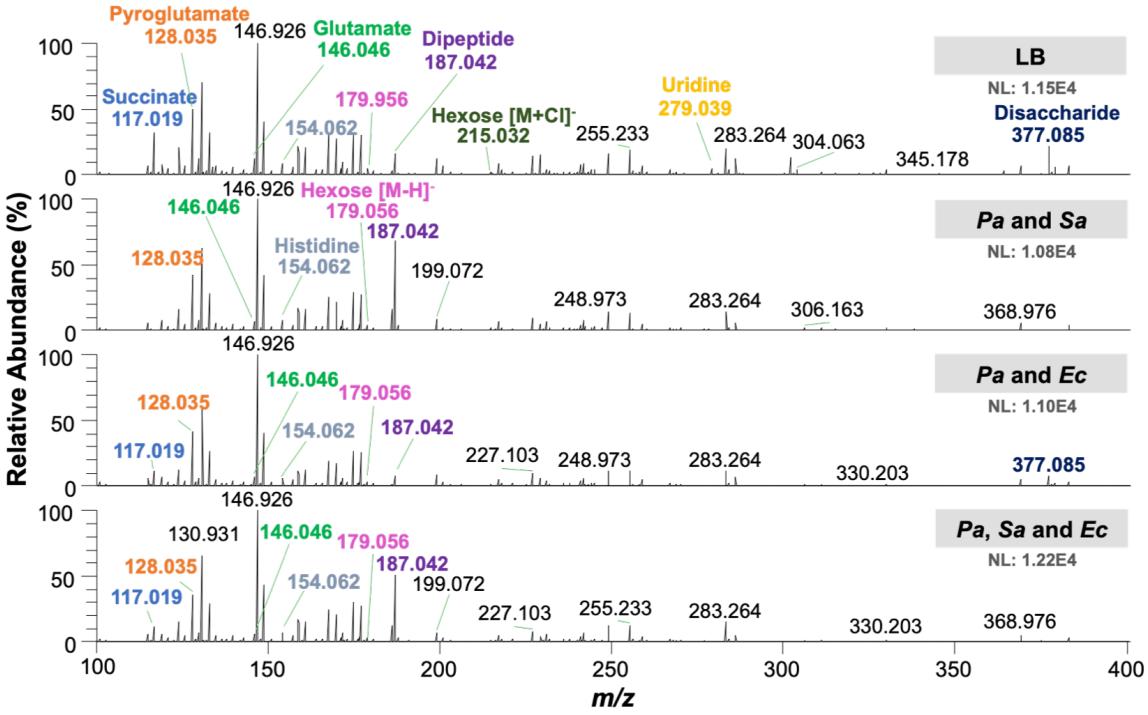

Figure A2.4: DESI-MS spectra (negative ion mode) show different species in LB media at 5 h cell growth.

Mass spectra for LB, *Pa* and *Sa* in LB, *Pa* and *Ec* in LB, and *Pa, Sa* and *Ec* in LB, shown top to bottom, respectively. Multiple species detected include succinate at *m/z* 117.019, pyroglutamate at *m/z* 128.035, glutamate at *m/z* 146.046, histidine at *m/z* 154.062, hexose $[M-H]^-$ at *m/z* 179.056, dipeptide at *m/z* 187.042, hexose $[M+Cl]^-$ at *m/z* 215.032, uridine at *m/z* 279.039, and disaccharide at *m/z* 377.085. Changes in metabolite abundances observed due to the presence of different bacterial species. Hexose abundance in LB media only is higher compared to hexose abundances in three co-cultured samples. NL represents the ion abundance (ion current). *Pa* stands for *P. aeruginosa*, *Sa* for *S. aureus*, and *Ec* for *E. coli*. Data collected with the assistance of Marta Sans of the Eberlin research group.

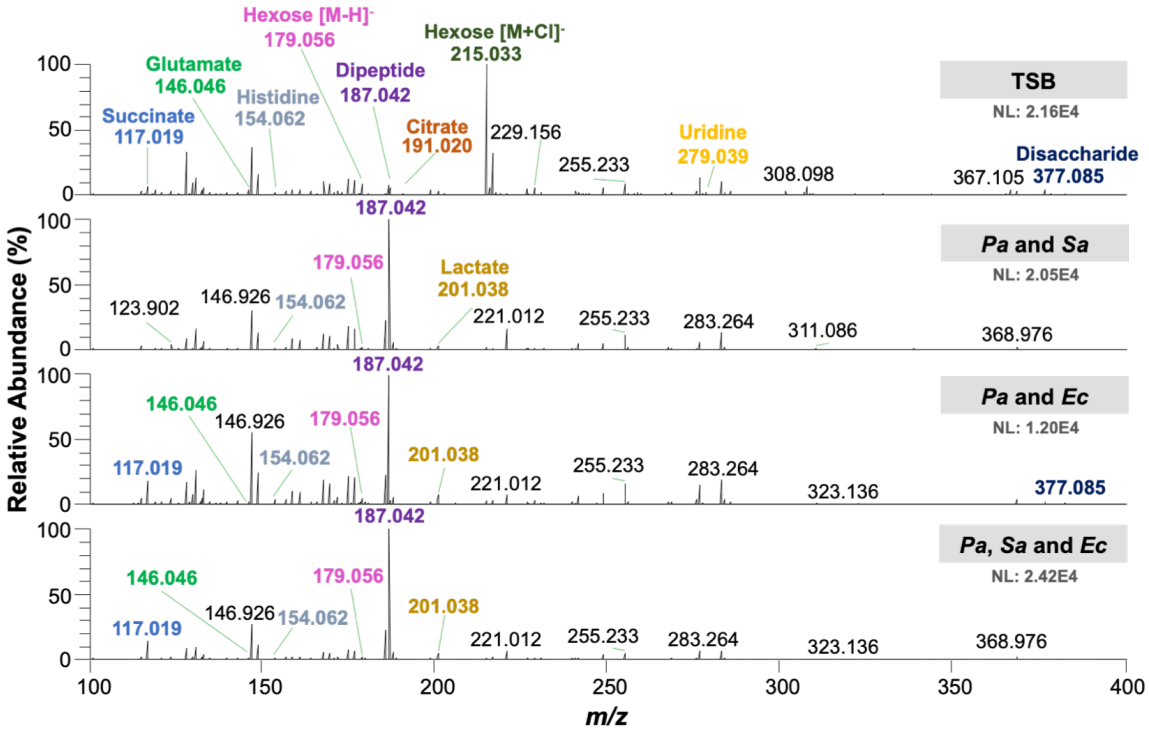

Figure A2.5: DESI-MS spectra (negative ion mode) show different species in LB media at 5 h cell growth.

Mass spectra for LB, *Pa* and *Sa* in LB, *Pa* and *Ec* in LB, and *Pa, Sa* and *Ec* in LB, shown top to bottom, respectively. Multiple species detected include succinate at *m/z* 117.019, pyroglutamate at *m/z* 128.035, glutamate at *m/z* 146.046, histidine at *m/z* 154.062, hexose $[M-H]^-$ at *m/z* 179.056, dipeptide at *m/z* 187.042, hexose $[M+Cl]^-$ at *m/z* 215.032, uridine at *m/z* 279.039, and disaccharide at *m/z* 377.085. Changes in metabolite abundances observed due to the presence of different bacterial species. Hexose abundance in LB media only is higher compared to hexose abundances in three co-cultured samples. NL represents the ion abundance (ion current). *Pa* stands for *P. aeruginosa*, *Sa* for *S. aureus*, and *Ec* for *E. coli.* Data collected with the assistance of Marta Sans of the Eberlin research group.

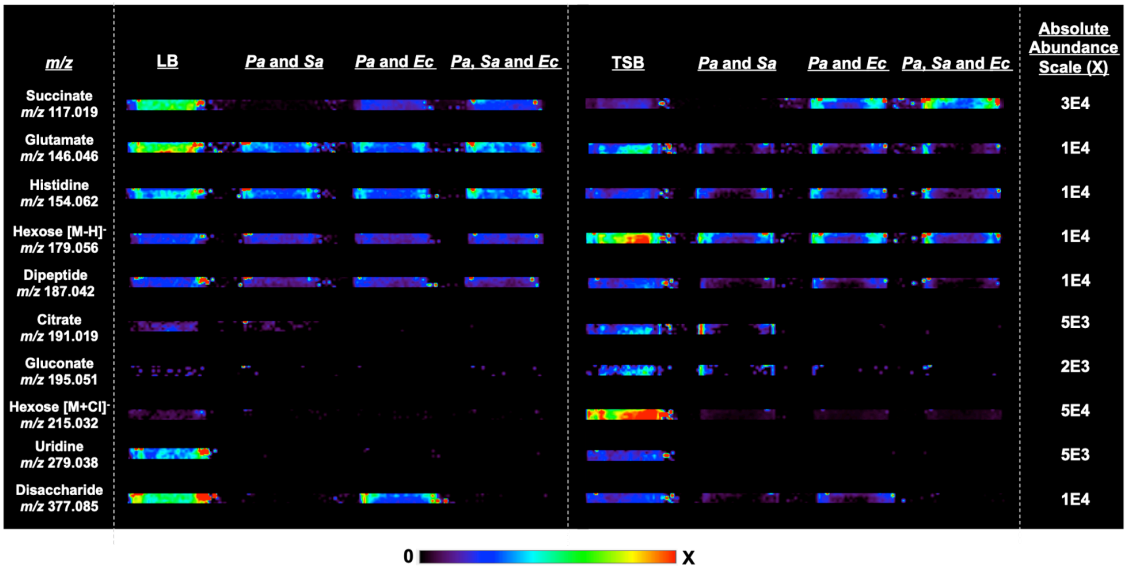

Figure A2.6: DESI-MS ion images (negative ion mode) for polymicrobial samples in LB and TSB media at 5 h cell growth.

Overall higher abundance of metabolites observed in TSB compared to LB. Differences in metabolite abundances observed in samples containing bacterial species. Succinate at *m/z* 117.019 is less abundant in *Pa* and *Sa* samples in both LB and TSB. Citrate at *m/z* 191.019 and gluconate at *m/z* 195.051, which are more abundant in TSB compared to LB, show lower abundances in *Pa* and *Ec*, and *Pa*, *Sa* and *Ec* polymicrobial samples. Disaccharide at *m/z* 377.085 is less abundant in samples containing *Sa* cells. Although the deprotonated and chlorinate hexose species should correspond to same species, the abundances of hexose $[M-H]^-$ and $[M+Cl]^-$ species are very different, likely due to changes occurring depending on the type of adduct. Abundance scale is set to the same value for species in both TSB and LB media for comparison. Corresponding DESI-MS spectra are shown in Figures A2.4 and A2.5. *Pa* stands for *P. aeruginosa*, *Sa* for *S. aureus*, and *Ec* for *E. coli*. Data collected with the assistance of Marta Sans of the Eberlin research group.

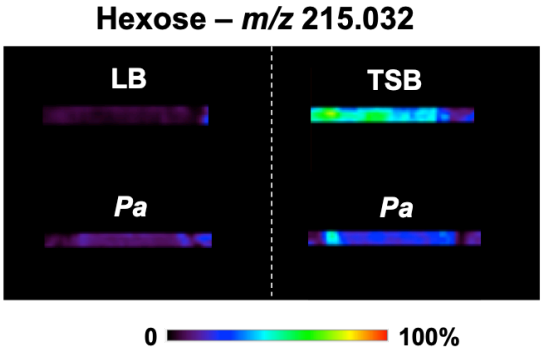

Figure A2.7: DESI-MS ion images (negative ion mode) for hexose at *m/z* 215.032 for *Pa* cells only in LB and TSB.

DESI-MS ion images (negative ion mode) for hexose at *m/z* 215.032 for *Pa* cells only in LB and TSB at 6 h cell growth for comparison to DESI-MS ion images shown in Figure A2.6. Qualitatively, the hexose abundance is higher in samples with *Pa* cells only compared to abundance observed in polymicrobial samples. *Pa* stands for *P. aeruginosa*. Data collected with the assistance of Marta Sans of the Eberlin research group.

Table A2.5: Table summary of commonly used growth media for *P. aeruginosa* reported in the literature. LB and TSB (in blue) are the most commonly used media.

Growth Media	***P. aeruginosa* strains and other pathogens**	**Used to Study Phenazines?**	**Ref.**
(1) TSB media, (2) LB media	*P. aeruginosa* PA14	Yes, PYO, 5-MCA, OHPHZ	1
TSB broth, (2) M63 minimal salts media	*P. aeruginosa* PA14	Yes, PYO	2
(1) TSB media, (2) LB media **the study uses urine, bronchial lavages, heparinized blood, and sputum, but the cells are grown in TSB and LB media and then introduced to these biological samples prior to echem measurements*	*P. aeruginosa* PA14	Yes, PYO	3
(1) TSB media	Various *P. aeruginosa* clinical isolates: hospital, mucoidal, and cystic fibrosis strains	Yes, PYO	4
(1) TSB media	NCTC 6749, NCTC 8060 and NCTC 8602 *P. aeruginosa* strains	Yes, PYO	5
Mueller-Hinton broth (MHB), (2) TSB media, (3) LB media, (4) Sabouraud dextrose broth (SDB), (5) buffered yeast extract broth (BYEB), (6) nutrient broth (NB)	*S. aureus* ATCC29213, *E. coli* ATCC25922, *P. aeruginosa* PAO1 ATCC 15692	Yes, PYO	6

Table A2.5 (continued)

Growth Media	*P. aeruginosa* strains and other pathogens	Used to Study Phenazines?	Ref.
(1) TSB media, (2) LB media	*P. aeruginosa* PA14 and PA01	Yes, PYO	7
LB media, (2) ABTG medium containing 15.1 mM $(NH_4)_2SO_4$, 33.7 mM Na_2HPO_4, 22.0 mM KH_2PO_4, 0.05 mM NaCl, 1 mM $MgCl_2 \cdot 6H_2O$, 100 µM $CaCl_2$, 1 µM $FeCl_3$, and 28 mM glucose ($C_6H_{12}O_6$)	Wild-type *P. aeruginosa* PAO1 and ΔpqsC + sPqsE mutant strains	Yes, PYO	8
(1) LB media	PA14 mutants producing different combinations of phenazines	Yes, PYO, 5-MCA, PCA depending on mutant used	9
(1) LB media	PA14 mutants producing different combinations of phenazines	Yes, PYO, 5-MCA, PCA depending on mutant used	10
(1) LB media	PA01 and various mutant strains	Yes, PYO, PCN, PCA depending on mutant used	11
(1) LB media	*P. aeruginosa* PA14	Yes, PYO, and PCA	12
(1) LB media	*P. aeruginosa* PA14 and mutant strains	No	13
(1) LB media, (2) MOPS Minimal Medium ** LB medium used for routine culturing*	*P. aeruginosa* PA14 and PA01	Yes, PYO and PCA	14

Table A2.5 (continued)

Growth Media	*P. aeruginosa* strains and other pathogens	Used to Study Phenazines?	Ref.
(1) TSB media, (2) Synthetic Cystic Fibrosis Sputum (SCFM2) **TSB used for overnight cultures; for experiments, TSB overnight cultures were diluted into SCFM2*	Wild-type *P. aeruginosa* strain PA14 and PA14 *ΔlasIΔrhlI*	No	15
(1) TSB media, (2) LB media	*P. aeruginosa* PA14, PA01, and mutants, PA clinical strains, *S. aureus* wild type, *S. aureus* mutant strains, *S. aureus* clinical strains	Yes, PYO	16
(1) LB media	*P. aeruginosa* PA14 wild-type and *DphzA-G* mutant strains	Yes, PYO	17
(1) LB media	PA01, *P. aeruginosa* and *S. aureus* isolates from CF patients	No	18
(1) Nutrient Broth	*P. aeruginosa* ATCC 9027 (NCIMB 8626) and *S. aureus* NCTC 13142	No	19
(1) Nutrient Broth	*S. aureus* ATCC 25923; *E. coli* ATCC 25922, *P. aeruginosa* ATCC 2785	No	20
(1) TSB media	Non-biofilm forming *P. aeruginosa, S. aureus, E. coli* strains	No	21

Table A2.5 (continued)

Growth Media	*P. aeruginosa* strains and other pathogens	Used to Study Phenazines?	Ref.
(1) Wound-like medium (WLM with 45% Bolton broth, 50% bovine plasma, 5% laked horse red blood cells), (2) LB media	*P. aeruginosa* PAO1 and JM2, *P. aeruginosa algD* deletion, *S. aureus* SA31 and AH1263, *S. aureus ica* deletion strain	No	22
(1) LB media and (2) morpholinepropanesulfonic acid (MOPS)-buffered defined medium	*P. aeruginosa* PA14 and the isogenic PA0601 and *nagE* transposon insertion mutants, *S. aureus* strain Mu50, *E. coli* DH5α	Yes, PYO	23
(1) LB media	*E. coli* (pEGFP) and *P. aeruginosa* (pSMC21)	No	24
(1) L broth (10% Bacto-Tryptone, 5% bacto-yeast extract, and 5% NaCl supplemented with 0.5% glucose), (2) TSY broth – 3% TSB broth and 0.5% yeast extract, (3) Succinate minimal medium (20 mM sodium succinate, 40 mM NH_3Cl, 2mM K_2SO_4, 0.4 mM $MgCl_2$, 1 µM $CaSO_4$, 1 µM $ZnCl_2$, 1 µM $FeCl_3$, 10 mM morpholinepropanesulfonic acid (MOPS), (4) Low and high-phosphate succinate media with either 0.1 or 4.0 mM potassium phosphate	*E. coli* K-12 RR1 strain, *P. aeruginosa* ATCC 27853 FRD2, PA01	No	25
(1) LB media	*P. aeruginosa* PA68 clinical isolate	No	26

Table A2.5 (continued)

Growth Media	*P. aeruginosa* strains and other pathogens	Used to Study Phenazines?	Ref.
(1) LB media, (2) Nutrient Yeast Broth	*P. aeruginosa* PA01, *P. aeruginosa* and *E. coli* clinical isolate strains	No	27
(1) LB media	*P. aeruginosa* PA01	Yes, PYO and OHPHZ	28
(1) TSB media	*P. aeruginosa* PA01 and its derivatives	No	29
(1) Yeast nitrogen base synthetic medium (YNB salts with ammonium sulfate with 10 mM glucose [Glu], 0.2% [wt/vol] amino acids from yeast synthetic dropout medium)	*P. aeruginosa* PA14 WT, PA14 Δ*phz,* PA14 *phzM*:Tn*M,* PA14 *phzS*:Tn*M*	Yes, PYO	30
(1) LB media	*E. coli* (TOP10, S17-1 K-12, AG100); *P. aeruginosa* (PAO1, PAO1 *soxR* mutant, PA14 , PA14 *phz2* mutant, PA14 *phz* mutant); *S. aureus* RN4220	Yes, PYO	31
(1) LB media, (2) TSB-DC (Chelex-treated trypticase soy broth dialysate) with glycerol and monosodium glutamate, (3) TSB-DC containing 10 % adult bovine serum, 10% adult human serum, adult human plasma, (4) Iron-sufficient medium with addition of $FeCl_3$ to TSB-DC	*P. aeruginosa* PA01 wild type and mutant strains	No	32

Table A2.5 (continued)

Growth Media	*P. aeruginosa* strains and other pathogens	Used to Study Phenazines?	Ref.
(1) LB media, (2) M9 minimal medium (BD) supplemented with 0.1 % Casamino acids and 0.5 % glucose]	*E. coli* DH5α, *P. aeruginosa (*PAO1 B36, PAO(D2593), PAO1(pUCP26), PAO1(p-qteE)	Yes, study on phenazine operons in particular	33
(1) LB media	*P. aeruginosa* PA01 and PA14, *E. coli* wild type	No	34
(1) LB media, (2) Modified MOPS (morpholinepropanesulfonic acid) smedium (50 mM MOPS at pH 7.2, 93 mM NH_4Cl, 43 mM NaCl, 2.2 mM KH_2PO_4, 1 mM $MgSO_4 \cdot 7H_2O$, and 3.6 µM $FeSO_4 \cdot 7H_2O$	*P. aeruginosa* PA14 wild-type and mutant strains	Yes, PYO	35
(1) LB media	*P. aeruginosa* PA14 wild-type and mutant strains	No	36
(1) LB media, (2) TSB-DC, chelexed trypticase soy broth dialysate containing 1% (v/v) glycerol and 0.5 M monosodium glutamate (either iron-deficient or –sufficient)	*P. aeruginosa* PA01 and mutant strains	No	37 38
(1) TSB media with 0.2% glucose, (2) Brain Heart Infusion (BHI) Broth, and (3) LB media supplemented with 2% glucose	*P. aeruginosa* PA01, PA6077 and ATCC	No	39

Table A2.5 (continued)

Growth Media	*P. aeruginosa* strains and other pathogens	Used to Study Phenazines?	Ref.
(1) Frank's medium (FM) + 1 % yeast extract, (2) FM + 0.5 % tryptone, (3) FM + 0.1 % KNO_3, (4) FM + 1 % bacto-peptone, (5) FM + 0.1 % glucose, (6) peptone, (7) nutrient broth, (8) King's Medium (20 g peptone, 1.4 g magnesium chloride, 10 g potassium sulphate, 15 g agar in 1 l of distilled water, pH 7.0 ± 0.2	*Pseudomonas* wild type and mutant strains	Yes, PYO	40
(1) LB media	*P. aeruginosa* ATCC 27853 and six clinical isolates (P1-P6) from burn wound infections	Yes, PYO	41
(1) LB media, (2) MOPS minimal medium	*P. aeruginosa* PA14 and Δ*phz* mutant strains	Yes, PCA, PYO	42

A2.2 REFERENCES

(1) Simoska, O.; Sans, M.; Fitzpatrick, M. D.; Crittenden, C. M.; Eberlin, L. S.; Shear, J. B.; Stevenson, K. J. *ACS Sensors* **2019**, *4*, 170–179.

(2) Sismaet, H. J.; Webster, T. A.; Goluch, E. D. *Analyst* **2014**, *139*, 4241–4246.

(3) Webster, T. A.; Sismaet, H. J.; Conte, J. L.; Chan, I.-P. J.; Goluch, E. D. *Biosens. Bioelectron.* **2014**, *60*, 265–270.

(4) Sismaet, H. J.; Pinto, A. J.; Goluch, E. D. *Biosens. Bioelectron.* **2017**, *97*, 65–69.

(5) Sharp, D.; Gladstone, P.; Smith, R. B.; Forsythe, S.; Davis, J. *Bioelectrochemistry* **2010**, *77*, 114–119.

(6) Li, S.; Mou, Q.; Feng, N.; Leung, P. H. M. *Int. J. Electrochem. Sci.* **2018**, *13*, 3789–3798.

(7) Santiveri, C. R.; Sismaet, H. J.; Kimani, M.; Goluch, E. D. *ChemistrySelect* **2018**, *3*, 2926–2930.

(8) Seviour, T.; Doyle, L. E.; Lauw, S. J. L.; Hinks, J.; Rice, S. A.; Nesatyy, V. J.; Webster, R. D.; Kjelleberg, S.; Marsili, E. *Chem Comm* **2015**, *51*, 3789–3792.

(9) Bellin, D. L.; Sakhtah, H.; Zhang, Y.; Price-Whelan, A.; Dietrich, L. E. P.; Shepard, K. L. *Nat. Commun.* **2016**, *7*, 10535–10545.

(10) Bellin, D. L.; Sakhtah, H.; Rosenstein, J. K.; Levine, P. M.; Thimot, J.; Emmett, K.; Dietrich, L. E. P.; Shepard, K. L. *Nat. Commun.* **2014**, *5*, 3256–3266.

(11) Mavrodi, D. V.; Bonsall, R. F.; Delaney, S. M.; Soule, M. J.; Phillips, G.; Thomashow, L. S. *J. Bacteriol.* **2001**, *183*, 6454–6465.

(12) Hunter, R. C.; Klepac-Ceraj, V.; Lorenzi, M. M.; Grotzinger, H.; Martin, T. R.; Newman, D. K. *Am J Respir Cell Mol Biol* **2012**, *47*, 738–745.

(13) Glasser, N. R.; Kern, S. E.; Newman, D. K. *Mol. Microbiol.* **2014**, *92*, 399–412.

(14) Dietrich, L. E. P.; Price-Whelan, A.; Petersen, A.; Whiteley, M.; Newman, D. K. *Mol. Microbiol.* **2006**, *61*, 1308–1321.

(15) Darch, S. E.; Simoska, O.; Fitzpatrick, M.; Barraza, J. P.; Stevenson, K. J.; Bonnecaze, R. T.; Shear, J. B.; Whiteley, M. *Proc Natl Acad Sci USA* **2018**, *5*, 4779–4789.

(16) Orazi, G.; O'Toole, G. A. *mBio* **2017**, *8*, 3–17.

(17) Das, T.; Kutty, S. K.; Tavallaie, R.; Ibugo, A. I.; Panchompoo, J.; Sehar, S.; Aldous, L.; Yeung, A. W. S.; Thomas, S. R.; Kumar, N.; Gooding, J. J.; Manefield, M. *Sci. Rep.* **2015**, *5*, 71–79.

(18) Beaudoin, T.; Yau, Y. C. W.; Stapleton, P. J.; Gong, Y.; Wang, P. W.; Guttman, D. S.; Waters, V. *npj Biofilms and Microbiomes* **2017**, *3*, 25–34.

(19) Alves, P. M.; Al-Badi, E.; Withycombe, C.; Jones, P. M.; Purdy, K. J.; Maddocks, S. E. *Pathogens and Disease* **2018**, *76*, 67–77.

(20) Sultana, S.; Shahidullah, A. H.; Islam, M. M.; Wasey, A. F. S. A.; Nahar, S. *Malays. J. Med. Biol. Res.* **2015**, *2*, 89–100.

(21) Mirani, Z. A.; Fatima, A.; Urooj, S.; Aziz, M.; Khan, M. N.; Abbas, T. *Iran J Basic Med Sci* **2018**, *21*, 760–770.

(22) DeLeon, S.; Clinton, A.; Fowler, H.; Everett, J.; Horswill, A. R.; Rumbaugh, K. P. *Infect. Immun.* **2014**, *82*, 4718–4728.

(23) Korgaonkar, A.; Trivedi, U.; Rumbaugh, K. P.; Whiteley, M. *Proc Natl Acad Sci USA* **2013**, *110*, 1059–1064.

(24) Banning, N.; Toze, S.; Mee, B. J. *Microbiology* **2003**, *149*, 47–55.

(25) Hassett, D. J.; Charniga, L.; Bean, K.; Ohman, D. E.; Cohen, M. S. *Infect. Immun.* **1992**, *60*, 328–336.

(26) Xu, H.; Lin, W.; Xia, H.; Xu, S.; Li, Y.; Yao, H.; Bai, F.; Zhang, X.; Bai, Y.; Saris, P.; Qiao, M. *FEMS Microbiol Lett* **2006**, *253*, 103–109.

(27) Denervaud, V.; TuQuoc, P.; Blanc, D.; Favre-Bonte, S.; Krishnapillai, V.; Reimmann, C.; Haas, D.; van Delden, C. *J Clin Microbiol* **2004**, *42*, 554–562.

(28) Chen, W.; Liu, X.-Y.; Qian, C.; Song, X.-N.; Li, W.-W.; Yu, H.-Q. *Biosens. Bioelectron.* **2015**, *64*, 25–29.

(29) Werner, E.; Roe, F.; Bugnicourt, A.; Franklin, M. J.; Heydorn, A.; Molin, S.; Pitts, B.; Stewart, P. S. *Applied and Environmental Microbiology* **2004**, *70*, 6188–6196.

(30) Morales, D. K.; Grahl, N.; Okegbe, C.; Dietrich, L. E. P.; Jacobs, N. J.; Hogan, D. A. *mBio* **2013**, *4*, e00526–e00538.

(31) Möker, N.; Dean, C. R.; Tao, J. *J. Bacteriol.* **2010**, *192*, 1946–1955.

(32) Kruczek, C.; Wachtel, M.; Alabady, M. S.; Payton, P. R.; Colmer-Hamood, J. A.; Hamood, A. N. *Microbiology* **2012**, *158*, 353–367.

(33) Liang, H.; Duan, J.; Sibley, C. D.; Surette, M. G.; Duan, K. *J. Med. Microbiol.* **2011**, *60*, 22–34.

(34) Meadows, J. A.; Wargo, M. J. *Applied and Environmental Microbiology* **2013**, *79*, 3355–3363.

(35) Price-Whelan, A.; Dietrich, L. E. P.; Newman, D. K. *J. Bacteriol.* **2007**, *189*, 6372–6381.

(36) Recinos, D. A.; Sekedat, M. D.; Hernandez, A.; Cohen, T. S.; Sakhtah, H.; Prince, A. S.; Price-Whelan, A.; Dietrich, L. E. P. *Proc. Natl. Acad. Sci. USA* **2012**, *109*, 19420–19425.

(37) Gaines, J. M. *Microbiology* **2005**, *151*, 2263–2275.

(38) Gaines, J. M.; Carty, N. L.; Tiburzi, F.; Davinic, M.; Visca, P.; Colmer-Hamood, J. A.; Hamood, A. N. *Microbiology* **2007**, *153*, 4219–4233.

(39) *ImQuest BioSciences*. September 19, 2016, pp 1–6.

(40) Jayaseelan, S.; Ramaswamy, D.; Dharmaraj, S. *World J. Microbiol. Biotechnol.* **2014**, *30*, 1159–1168.

(41) Hendiani, S.; Pornour, M.; Kashef, N. *Photodiagnosis and Photodynamic Therapy* **2019**, *26*, 8–12.

(42) Schiessl, K. T.; Hu, F.; Jo, J.; Nazia, S. Z.; Wang, B.; Price-Whelan, A.; Min, W.; Dietrich, L. E. P. *Nat. Commun.* **2019**, *10*, 762–772.

Bibliography

(1) Al-Ani, F. Y.; Al-Shibib, A. S.; Khammas, K. M.; Taher, R. Folia *Microbiolol*. **1986**, *31*, 215–219.

(2) Alatraktchi, F. A.; Johansen, H. K.; Molin, S.; Svendsen, W. E. *Nanomedicine* **2016**, *11*, 2185–2195.

(3) Alatraktchi, F. A.; Noori, J. S.; Tanev, G. P.; Mortensen, J.; Dimaki, M.; Johansen, H. K.; Madsen, J.; Molin, S.; Svendsen, W. E. *PLoS ONE* **2018**, *13*, e0194157–e0194159.

(4) Alatraktchi, F.; Breum Andersen, S.; Krogh Johansen, H.; Molin, S.; Svendsen, W. *Sensors* **2016,** *16*, 408–410.

(5) Albers, J.; Grunwald, T.; Nebling, E.; Piechotta, G.; Hintsche, R. *Anal. Bioanal. Chem.* **2003**, *377*, 521–527.

(6) Alhede, M.; Kragh, K. N.; Qvortrup, K.; Allesen-Holm, M.; van Gennip, M.; Christensen, L. D.; Jensen, P. Ø.; Nielsen, A. K.; Parsek, M.; Wozniak, D.; Molin, S.; Tolker-Nielsen, T.; Høiby, N.; Givskov, M.; Bjarnsholt, T. *PLoS ONE* **2011**, *6*, e27943–12.

(7) Alves, P. M.; Al-Badi, E.; Withycombe, C.; Jones, P. M.; Purdy, K. J.; Maddocks, S. E. *Pathogens and Disease* **2018**, *76*, 67–77.

(8) Amiri, M.; Bezaatpour, A.; Jafari, H.; Boukherroub, R.; Szunerits, S. *ACS Sensors* **2018**, *3*, 1069–1086.

(9) Angeletti, S. J. *Microbiol. Methods* **2017**, *138*, 20–29.

(10) Apel, K.; Hirt, H. *Annu. Rev. Plant Biol*. **2004**, *55*, 373–399.

(11) Arora, D. P.; Hossain, S.; Xu, Y.; Boon, E. M. *Biochemistry* **2015**, *54*, 3717–3728.

(12) Arrigan, D. W. M. *Analyst* **2004**, *129*, 1157–1165.

(13) Arumugam, P. U.; Yu, E.; Riviere, R.; Meyyappan, M. *Chemical Physics Letters* **2010**, *499*, 241–246.

(14) Atkinson, S.; Williams, P. J. *R. Soc. Interface* **2009**, *6*, 959–978.

(15) Bahia, D.; Satoskar, A. R.; Dussurget, O. *Front Immunol* **2018,** *9*, 221–224.

(16) Banning, N.; Toze, S.; Mee, B. J. *Microbiology* **2003**, *149*, 47–55.

(17) Bard, A. J.; Faulkner, L. R. Electrochemical Methods Fundamentals and Applications, 2nd ed.; Harris, D., Ed.; John Wiley & Sons, Inc., 2001; pp 1–850.

(18) Barraud, N.; Hassett, D. J.; Hwang, S. H.; Rice, S. A.; Kjelleberg, S.; Webb, J. S. *J. Bacteriol.* **2006**, *188*, 7344–7353.

(19) Bassler, B. L.; Losick, R. *Cell* **2006**, *125*, 237–246.

(20) Beaudoin, T.; Yau, Y. C. W.; Stapleton, P. J.; Gong, Y.; Wang, P. W.; Guttman, D. S.; Waters, V. *npj Biofilms and Microbiomes* **2017**, *3*, 25–34.

(21) Beckman, J. S.; Koppenol, W. H. *Am. J. Physiol.* **1996**, *271*, C1424–C1437.

(22) Bedioui, F.; Griveau, S. *Electroanalysis* **2012**, 25, 587–600.

(23) Bedrossian, C. W. M.; Greenberg, S. D.; Singer, D. B.; Hansen, J. J.; Rosenberg, H. S. *Hum. Pathol.* **1976**, 7, 195–204.

(24) Bellin, D. L.; Sakhtah, H.; Rosenstein, J. K.; Levine, P. M.; Thimot, J.; Emmett, K.; Dietrich, L. E. P.; Shepard, K. L. *Nat. Commun*. **2014**, *5*, 3256–3266.

(25) Bellin, D. L.; Sakhtah, H.; Zhang, Y.; Price-Whelan, A.; Dietrich, L. E. P.; Shepard, K. L. *Nat. Commun.* **2016**, *7*, 10535–10544.

(26) Bergen, G. A.; Shelhamer, J. H. *Infect Dis Clin North Am* **1996**, *10*, 297–325.

(27) Bergeron, A. C.; Seman, B. G.; Hammond, J. H.; Archambault, L. S.; Hogan, D. A.; Wheeler, R. T. *Infect. Immun*. **2017**, *85*, 340–358.

(28) Bertesteanu, S.; Triaridis, S.; Stankovic, M.; Lazar, V.; Chifiriuc, M. C.; Vlad, M.; Grigore, R. *International Journal of Pharmaceutics* **2014**, *463*, 119–126.

(29) Bogdan, C.; Röllinghoff, M.; Diefenbach, A. *Immunological Reviews* **2000**, *173*, 17–26.

(30) Bosire, E. M.; Rosenbaum, M. A. *Front. Microbiol*. **2017**, *8*, 5026–5037.

(31) Boucher, H. W.; Talbot, G. H.; Bradley, J. S.; Edwards, J. E.; Gilbert, D.; Rice, L. B.; Scheld, M.; Spellberg, B.; Bartlett, J. *Clin. Infect. Dis*. **2009**, *48*, 1–12.

(32) Bowler, P. G.; Duerden, B. I.; Armstrong, D. G. *Clinical Microbiology Reviews* **2001**, *14*, 244–269.

(33) Bozinovski, J.; Brien, J. F.; Marks, G. S.; Nakatsu, K. *Can. J. Physiol. Pharmacol*. **1994**, *72*, 746–752.

(34) Brown, F. O.; Finnerty, N. J.; Bolger, F. B.; Millar, J.; Lowry, J. P. *Anal Bioanal Chem* **2005**, *381*, 964–971.

(35) Buchan, B. W.; Ledeboer, N. A. *Clinical Microbiology Reviews* **2014**, *27*, 783–822.

(36) Buzid, A.; Reen, F. J.; Langsi, V. K.; Muimhneacháin, E. Ó.; O'Gara, F.; McGlacken, G. P.; Luong, J. H. T.; Glennon, J. D. *ChemElectroChem* **2017**, *4*, 533–541.

(37) Buzid, A.; Shang, F.; Reen, F. J.; Muimhneacháin, E. Ó.; Clarke, S. L.; Zhou, L.; Luong, J. H. T.; O'Gara, F.; McGlacken, G. P.; Glennon, J. D. *Sci. Rep*. **2016**, *6*, 30001–30009.

(38) Cappiello, A.; Famiglini, G.; Rossi, L.; Magnani, M. *Anal. Chem.* **1997**, *69*, 5136–5141.

(39) Cernat, A.; Tertis, M.; Gandouzi, I.; Bakhrouf, A.; Suciu, M.; Cristea, C. *Electrochemistry Communications* **2018**, *88*, 5–9.

(40) Chen, R.; Li, Y.; Huo, K.; Chu, P. K. *RSC Adv.* **2013**, *3*, 18698–18716.

(41) Chen, W.; Liu, X.-Y.; Qian, C.; Song, X.-N.; Li, W.-W.; Yu, H.-Q. *Biosens. Bioelectron.* **2015**, *64*, 25–29.

(42) Cho, J. C.; Tiedje, J. M. *Applied and Environmental Microbiology* **2001**, *67*, 3677–3682.

(43) Chu, W.; Zere, T. R.; Weber, M. M.; Wood, T. K.; Whiteley, M.; Hidalgo-Romano, B.; Valenzuela, E., Jr.; McLean, R. J. C. *Applied and Environmental Microbiology* **2011**, *78*, 411–419.

(44) Connell, J. L.; Kim, J.; Shear, J. B.; Bard, A. J.; Whiteley, M. *Proc Natl Acad Sci USA* **2014**, *111*, 18255–18260.

(45) Connell, J. L.; Ritschdorff, E. T.; Whiteley, M.; Shear, J. B. *Proc Natl Acad Sci USA* **2013**, *110*, 18380–18385.

(46) Cornforth, D. M.; Dees, J. L.; Ibberson, C. B.; Huse, H. K.; Mathiesen, I. H.; Kirketerp-Møller, K.; Wolcott, R. D.; Rumbaugh, K. P.; Bjarnsholt, T.; Whiteley, M. *Proc Natl Acad Sci USA* **2018**, *115*, E5125–E5134.

(47) Cremaschi, P. *The Journal of Chemical Physics* **1981**, *75*, 3944–3953.

(48) Cruickshank, C. N. D.; Lowbury, E. J. L. *Brit. J. Exp. Pathol*. **1953**, *34*, 1–6.

(49) Culotti, A.; Packman, A. I. *PLoS ONE* **2014**, *9*, e107186–e107189.

(50) Cutruzzolà, F.; Frankenberg-Dinkel, N. *J. Bacteriol.* **2015**, *198*, 55–65.

(51) Dang, X.; Hu, H.; Wang, S.; Hu, S. *Microchim Acta* **2014**, *182*, 455–467.

(52) Darch, S. E.; Kragh, K. N.; Abbott, E. A.; Bjarnsholt, T.; Bull, J. J.; Whiteley, M. *mBio* **2017**, *8*, 277–292.

(53) Darch, S. E.; McNally, A.; Harrison, F.; Corander, J.; Barr, H. L.; Paszkiewicz, K.; Holden, S.; Fogarty, A.; Crusz, S. A.; Diggle, S. P. *Sci. Rep.* **2015**, *5*, 7649–7661.

(54) Darch, S. E.; Simoska, O.; Fitzpatrick, M.; Barraza, J. P.; Stevenson, K. J.; Bonnecaze, R. T.; Shear, J. B.; Whiteley, M. *Proc Natl Acad Sci USA* **2018**, *115*, 4779–4789.

(55) Das, T.; Kutty, S. K.; Tavallaie, R.; Ibugo, A. I.; Panchompoo, J.; Sehar, S.; Aldous, L.; Yeung, A. W. S.; Thomas, S. R.; Kumar, N.; Gooding, J. J.; Manefield, M. *Sci. Rep.* **2015**, *5*, 71–79.

(56) Dauphin-Ducharme, P.; Arroyo-Currás, N.; Kurnik, M.; Ortega, G.; Li, H.; Plaxco, K. W. *Langmuir* **2017**, *33*, 4407–4413.

(57) DeLeon, S.; Clinton, A.; Fowler, H.; Everett, J.; Horswill, A. R.; Rumbaugh, K. P. *Infect. Immun.* **2014**, *82*, 4718–4728.

(58) Denervaud, V.; TuQuoc, P.; Blanc, D.; Favre-Bonte, S.; Krishnapillai, V.; Reimmann, C.; Haas, D.; van Delden, C. *J Clin Microbiol* **2004**, *42*, 554–562.

(59) Diederich, C.; Leypold, M.; Culka, M.; Weber, H. X. R.; Breinbauer, R.; Ullmann, G. M.; Blankenfeldt, W. *Sci. Rep*. **2017**, 1–13.

(60) Dietrich, L. E. P.; Price-Whelan, A.; Petersen, A.; Whiteley, M.; Newman, D. K. *Mol. Microbiol.* **2006**, *61*, 1308–1321.

(61) Do, H.; Kwon, S.-R.; Fu, K.; Morales-Soto, N.; Shrout, J. D.; Bohn, P. W. *Langmuir* **2019**, *35*, 7043–7049.

(62) Douterelo, I.; Jackson, M.; Solomon, C.; Boxall, J. *Appl Microbiol Biotechnol* **2015**, *100*, 3301–3311.

(63) Dröge, W. *Physiol Rev* **2002**, *82*, 47–95.

(64) Duay, J.; Elliott, J.; Shear, J. B.; Stevenson, K. J. *Anal. Chem*. **2015**, *87*, 10109–10116.

(65) Duay, J.; Goran, J. M.; Stevenson, K. J. *Anal. Chem*. **2014**, *86*, 11528–11532.

(66) Dye, C. Philos. Trans. R. Soc. Lond., B, *Biol. Sci.* **2014**, *369*, 20130426–20130435.

(67) El-Fouly, M. Z.; Sharaf, A. M.; Shahin, A. A. M.; El-Bialy, H. A.; Omara, A. M. A. *Journal of Radiation Research and Applied Sciences* **2015**, *8*, 36–48.

(68) Elliott, J.; Duay, J.; Simoska, O.; Shear, J. B.; Stevenson, K. J. *Anal. Chem*. **2017**, *89*, 1267–1274.

(69) Elliott, J.; Simoska, O.; Karasik, S.; Shear, J. B.; Stevenson, K. J. *Anal. Chem*. **2017**, *89*, 6285–6289.

(70) Emonet, S.; Shah, H. N.; Cherkaoui, A.; Schrenzel, J. *Clinical Microbiology and Infection* **2010**, *16*, 1604–1613.

(71) Feeney, R.; Kounaves, S. P. *Electroanalysis* **2000**, *12*, 677–684.

(72) Fergie, J. E.; Shema, S. J.; Lott, L.; Crawford, R.; Patrick, C. C. *Clin Infect Dis* **1994**, *18*, 390–394.

(73) Fetzer, A. F.; Werner, A. S.; Hagstrom, J. W. *Am. Rev. Respir. Dis.* **1967**, *96*, 1121–1130.

(74) Fick, R. B. *Chest*. **1989**, *96*, 158–164.

(75) Ford, P. C.; Wink, D. A.; Stanbury, D. M. *FEBS Lett*. **1993**, *326*, 1–3.

(76) Friedheim, E.; Michaelis, L. *J. Biol. Chem*. **1931**, *91*, 355–369.

(77) Gaines, J. M. *Microbiology* **2005**, *151*, 2263–2275.

(78) Gaines, J. M.; Carty, N. L.; Tiburzi, F.; Davinic, M.; Visca, P.; Colmer-Hamood, J. A.; Hamood, A. N. *Microbiology* **2007**, *153*, 4219–4233.

(79) Gandouzi, I.; Tertis, M.; Cernat, A.; Saidane-Mosbahi, D.; Ilea, A.; Cristea, C. *Materials* **2019**, *12*, 1180–1193.

(80) Garber, E. D. Ann. *N. Y. Acad. Sci*. **1960**, *88*, 1187–1194.

(81) Gardner, R. D.; Zhou, A.; Zufelt, N. A. *Sensor Actuat B-Chemical* **2009**, *136*, 177–185.

(82) Garthwaite, J. *Trends in Neurosciences* **1991**, *14*, 60–67.

(83) Ge, M.-C.; Kuo, A.-J.; Liu, K.-L.; Wen, Y.-H.; Chia, J.-H.; Chang, P.-Y.; Lee, M.-H.; Wu, T.-L.; Chang, S.-C.; Lu, J.-J. *J Microbiol Immunol Infect* **2017**, *50*, 662–668.

(84) Giacometti, A.; Cirioni, O.; Schimizzi, A. M.; Del Prete, M. S.; Barchiesi, F.; D'Errico, M. M.; Petrelli, E.; Scalise, G. *J Clin Microbiol* **2000**, *38*, 918–922.

(85) Glasser, N. R.; Kern, S. E.; Newman, D. K. *Mol. Microbiol*. **2014**, *92*, 399–412.

(86) Goldstein, S.; Czapski, G. *J. Am. Chem. Soc.* **1996**, *118*, 3419–3425.

(87) Goluch, E. D. *Trends Biotechnol* **2017**, *35*, 1125–1128.

(88) Griveau, S.; Bedioui, F. *Anal Bioanal Chem* **2013**, *405*, 3475–3488.

(89) Guo, J.; Lindner, E. *Anal. Chem.* **2009**, *81*, 130–138.

(90) Hall, S.; McDermott, C.; Anoopkumar-Dukie, S.; McFarland, A.; Forbes, A.; Perkins, A.; Davey, A.; Chess-Williams, R.; Kiefel, M.; Arora, D.; Grant, G. *Toxins* **2016**, *8*, 236–14.

(91) Hansford, G. S.; Holliman, F. G.; Herbert, R. B. *J. Chem. Soc., Perkin Trans*. *1* **1972**, 103–105.

(92) Hassett, D. J.; Charniga, L.; Bean, K.; Ohman, D. E.; Cohen, M. S. *Infect. Immun.* **1992**, *60*, 328–336.

(93) Hauser, A. R. *Nature Rev. Microbiol*. **2009**, *7*, 654–665.

(94) Hauser, A. R.; Jain, M.; Bar-Meir, M.; McColley, S. A. *Clinical Microbiology Reviews* **2011**, *24*, 29–70.

(95) Hendiani, S.; Pornour, M.; Kashef, N. *Photodiagnosis and Photodynamic Therapy* **2019**, *26*, 8–12.

(96) Henke, J. M.; Bassler, B. L. *Trends in Cell Biology* **2004**, *14*, 648–656.

(97) Ho, Y. P.; Reddy, P. M. *Clinical Chemistry* **2010**, 56, 525–536.

(98) Hood, S. J.; Kampouris, D. K.; Kadara, R. O.; Jenkinson, N.; del Campo, F. J.; Muñoz, F. X.; Banks, C. E. *Analyst* **2009**, *134*, 2301–2305.

(99) Hossain, S.; Nisbett, L.-M.; Boon, E. M. *Acc. Chem. Res.* **2017**, *50*, 1633–1639.

(100) Hou, T.-Y.; Chiang-Ni, C.; Teng, S.-H. *J Food Drug Anal* **2019**, *27*, 404–414.

(101) Hudu, S. A.; Alshrari, A. S.; Syahida, A.; Sekawi, Z. *J Clin Diagn Res* **2016**, *10*, DE01–DE05.

(102) Hunter, R. C.; Klepac-Ceraj, V.; Lorenzi, M. M.; Grotzinger, H.; Martin, T. R.; Newman, D. K. *Am J Respir Cell Mol Biol* **2012**, *47*, 738–745.

(103) Hussain, A. S.; Bozinovski, J.; Maurice, D. H.; McLaughlin, B. E.; Marks, G. S.; Brien, J. F.; Nakatsu, K. *Can. J. Physiol. Pharmacol*. **1997**, *75*, 398–406.

(104) ImQuest BioSciences. September 19, **2016**, pp 1–6.

(105) Ino, K.; Shiku, H.; Matsue, T. *Current Opinion in Electrochemistry* **2017**, *5*, 146–151.

(106) Ino, K.; Yamada, Y.; Kanno, Y.; Imai, S.; Shiku, H.; Matsue, T. *Sensor Actuat B-Chemical* **2016**, *234*, 201–208.

(107) Ivnitski, D.; Hamid, I. A.; Atanasov, P.; Wilkins, E.; Stricker, S. *Electroanalysis* **2000**, *12*, 317–325.

(108) Jarošová, R.; Mcclure, S. E.; Gajda, M.; Jović, M.; Girault, H. H.; Lesch, A.; Maiden, M.; Waters, C.; Swain, G. M. *Anal. Chem*. **2019**, *91*, 8835–8844.

(109) Jayaraman, S.; Joo, N. S.; Reitz, B.; Wine, J. J.; Verkman, A. S. *Proc Natl Acad Sci USA* **2001**, *98*, 8119–8123.

(110) Jayaseelan, S.; Ramaswamy, D.; Dharmaraj, S. *World J. Microbiol. Biotechnol.* **2014**, *30*, 1159–1168.

(111) Justino, C. I. L.; Duarte, A. C.; Rocha-Santos, T. A. P. *Trends in Analytical Chemistry* **2016**, 85, 36–60.

(112) Jyot, J.; Sonawane, A.; Wu, W.; Ramphal, R. *Mol. Microbiol.* **2007**, *63*, 1026–1038.

(113) Klevens, R. M.; Edwards, J. R.; Richards, C. L.; Horan, T. C.; Gaynes, R. P.; Pollock, D. A.; Cardo, D. M. *Public Health Rep* **2007**, *122*, 160–166.

(114) Koehne, J. E.; Marsh, M.; Boakye, A.; Douglas, B.; Kim, I. Y.; Chang, S.-Y.; Jang, D.-P.; Bennet, K. E.; Kimble, C.; Andrews, R.; Meyyappan, M.; Lee, K. H. *Analyst* **2011**, *136*, 1802–1805.

(115) Kokkinos, C.; Economou, A.; Prodromidis, M. I. *Trends in Analytical Chemistry* **2016**, *79*, 88–105.

(116) Koley, D.; Ramsey, M. M.; Bard, A. J.; Whiteley, M. *Proc. Natl. Acad. Sci. U.S.A.* **2011**, *108*, 19996–20001.

(117) Korgaonkar, A.; Trivedi, U.; Rumbaugh, K. P.; Whiteley, M. *Proc Natl Acad Sci USA* **2013**, *110*, 1059–1064.

(118) Kragh, K. N.; Alhede, M.; Jensen, P. Ø.; Moser, C.; Scheike, T.; Jacobsen, C. S.; Seier Poulsen, S.; Eickhardt-Sørensen, S. R.; Trøstrup, H.; Christoffersen, L.;

Hougen, H.-P.; Rickelt, L. F.; Kühl, M.; Høiby, N.; Bjarnsholt, T. *Infect. Immun.* **2014**, *82*, 4477–4486.

(119) Kruczek, C.; Wachtel, M.; Alabady, M. S.; Payton, P. R.; Colmer-Hamood, J. A.; Hamood, A. N. *Microbiology* **2012**, *158*, 353–367.

(120) Krásný, L.; Hynek, R.; Hochel, I. *Int. J. Mass Spectrom*. **2013**, *353*, 67–79.

(121) Kurosawa, H.; Utsunomiya, H.; Shiga, N.; Takahashi, A.; Ihara, M.; Ishibashi, M.; Nishimoto, M.; Watanabe, Z.; Abe, H.; Kumagai, J.; Terada, Y.; Igarashi, H.; Takahashi, T.; Fukui, A.; Suganuma, R.; Tachibana, M.; Yaegashi, N. *Hum. Reprod.* **2016**, *31*, 2321–2330.

(122) Kuss, S.; Amin, H. M. A.; Compton, R. G. *Chem. Asian J.* **2018**, *13*, 2758–2769.

(123) Landry, R. M.; An, D.; Hupp, J. T.; Singh, P. K.; Parsek, M. *R. Mol. Microbiol*. **2006**, *59*, 142–151.

(124) Lau, G. W.; Hassett, D. J.; Ran, H.; Kong, F. *Trends Mol. Med*. **2004**, *10*, 599–606.

(125) Lazcka, O.; Campo, F. J. D.; Muñoz, F. X. *Biosens. Bioelectron*. **2007**, *22*, 1205–1217.

(126) Lee, D.-H.; Koh, E.-H.; Choi, S.-R.; Kim, S. *Ann Lab Med* **2013**, *33*, 406–444.

(127) Lee, J.-H.; Lee, J. *FEMS Microbiol Rev* **2010**, *34*, 426–444.

(128) Lewis, R. S.; Deen, W. M. *Chem. Res. Toxicol*. **1994**, *7*, 568–574.

(129) Li, S.; Mou, Q.; Feng, N.; Leung, P. H. M. *Int. J. Electrochem. Sci*. **2018**, *13*, 3789–3798.

(130) Li, Y.-H.; Tian, X. *Sensors* **2012**, *12*, 2519–2538.

(131) Liang, H.; Duan, J.; Sibley, C. D.; Surette, M. G.; Duan, K. *J. Med. Microbiol*. **2011**, *60*, 22–34.

(132) Liu, Y.-C.; Zhao, J.; Wu, W.-L.; Yang, Z.-S. *Electrochimica Acta* **2007**, *52*, 4848–4852.

(133) Llor, C.; Bjerrum, L. *Ther Adv Drug Saf* **2014**, *5*, 229–241.

(134) Lyczak, J. B.; Cannon, C. L.; Pier, G. B. *Clinical Microbiology Reviews* **2002**, *15*, 194–222.

(135) Magill, S. S.; Edwards, J. R.; Bamberg, W.; Beldavs, Z. G.; Dumyati, G.; Kainer, M. A.; Lynfield, R.; Maloney, M.; McAllister-Hollod, L.; Nadle, J.; Ray, S. M.; Thompson, D. L.; Wilson, L. E.; Fridkin, S. K. *N Engl J Med* **2014**, *370*, 1198–1208.

(136) Mavrodi, D. V.; Blankenfeldt, W.; Thomashow, L. S. *Annu. Rev. Phytopathol*. **2006**, *44*, 417–445.

(137) Mavrodi, D. V.; Bonsall, R. F.; Delaney, S. M.; Soule, M. J.; Phillips, G.; Thomashow, L. S. *J. Bacteriol*. **2001**, *183*, 6454–6465.

(138) Mavrodi, D. V.; Peever, T. L.; Mavrodi, O. V.; Parejko, J. A.; Raaijmakers, J. M.; Lemanceau, P.; Mazurier, S.; Heide, L.; Blankenfeldt, W.; Weller, D. M.; Thomashow, L. S. *Applied and Environmental Microbiology* **2010**, *76*, 866–879.

(139) McKnight, T. E.; Melechko, A. V.; Fletcher, B. L.; Jones, S. W.; Hensley, D. K.; Peckys, D. B.; Griffin, G. D.; Simpson, M. L.; Ericson, M. N. *J. Phys. Chem. B* **2006**, *110*, 15317–15327.

(140) McLister, A.; McHugh, J.; Cundell, J.; Davis, *J. Adv. Mater*. **2016**, *28*, 5732–5737.

(141) Meadows, J. A.; Wargo, M. J. *Applied and Environmental Microbiology* **2013**, *79*, 3355–3363.

(142) Miescher, E. *Journal of Molecular Spectroscopy* **1978**, *69*, 281–293.

(143) Mikkelsen, H.; McMullan, R.; Filloux, A. *PLoS ONE* **2011**, *6*, e29113–e29117.

(144) Miller, M. B.; Bassler, B. L. *Annu. Rev. Microbiol*. **2003**, *55*, 165–199.

(145) Mirani, Z. A.; Fatima, A.; Urooj, S.; Aziz, M.; Khan, M. N.; Abbas, T. *Iran J Basic Med Sci* **2018**, *21*, 760–770.

(146) Mirceski, V.; Laborda, E.; Guziejewski, D.; Compton, R. G. *Anal. Chem.* **2013**, *85*, 5586–5594.

(147) Mocak, J.; Bond, A. M.; Mitchell, S.; Scollary, G. *Pure & Appl. Chem.* **1997**, *69*, 297–328.

(148) Monzó, J.; Insua, I.; Fernandez-Trillo, F.; Rodriguez, P. *Analyst* **2015**, *140*, 7116–7128.

(149) Morales, D. K.; Grahl, N.; Okegbe, C.; Dietrich, L. E. P.; Jacobs, N. J.; Hogan, D. A. *mBio* **2013**, *4*, e00526–e00538.

(150) Morales, D. K.; Jacobs, N. J.; Rajamani, S.; Krishnamurthy, M.; Cubillos-Ruiz, J. R.; Hogan, D. A. *Mol. Microbiol*. **2010**, *78*, 1379–1392.

(151) Moya, A.; Gabriel, G.; Villa, R.; del Campo, F. J. *Current Opinion in Electrochemistry* **2017**, *3*, 29–39.

(152) Muller, M. *Free Radical Biology and Medicine* **2006**, *41*, 1670–1677.

(153) Möker, N.; Dean, C. R.; Tao, J. *J. Bacteriol.* **2010**, *192*, 1946–1955.

(154) Nebling, E.; Grunwald, T.; Albers, J.; Schäfer, P.; Hintsche, R. *Anal. Chem*. **2004**, *76*, 689–696.

(155) Nisbett, L.-M.; Boon, E. M. *Biochemistry* **2016**, *55*, 4873–4884.

(156) Noto, M. J.; Burns, W. J.; Beavers, W. N.; Skaar, E. P. *J. Bacteriol.* **2017**, *199*, e00221-17.

(157) O'Brien, S.; Fothergill, J. L. *FEMS Microbiol Lett* **2017**, *364*, 850–860.

(158) O'Malley, Y. Q.; Reszka, K. J.; Britigan, B. E. *Free Radical Biology and Medicine* **2004**, *36*, 90–100.

(159) O'Toole, G.; Kaplan, H. B.; Kolter, R. *Annu. Rev. Microbiol.* **2000**, *54*, 49–79.

(160) Ohfuji, K.; Sato, N.; Hamada-Sato, N.; Kobayashi, T.; Imada, C.; Okuma, H.; Watanabe, E. *Biosens. Bioelectron.* **2004**, *19*, 1237–1244.

(161) Opperman, M. J.; Shachar-Hill, Y. *Metabolic Engineering* **2016**, *38*, 251–263.

(162) Orazi, G.; O'Toole, G. A. *mBio* **2017**, *8*, 3–17.

(163) Orozco, J.; Fernández-Sánchez, C.; Jiménez-Jorquera, C. *Sensors* **2010**, *10*, 475–490.

(164) Orwiler, B. Oscilloscope Vertical Amplifier Circuit Concepts © Tektronix **1969**, 1–467.

(165) Palmer, K. L.; Aye, L. M.; Whiteley, M. *J. Bacteriol*. **2007**, *189*, 8079–8087.

(166) Palmer, K. L.; Brown, S. A.; Whiteley, M. *J. Bacteriol*. **2007**, *189*, 4449–4455.

(167) Pandey, R.; Swamy, K. V.; Khetmalas, M. B. *IJBT* **2019**, *12*, 297–310.

(168) Paniel, N.; Baudart, J.; Hayat, A.; Barthelmebs, L. *Methods* **2013**, *64*, 229–240.

(169) Pariente, F.; Alonso, J. L.; Abrufia, H. D. *Journal of Electroanalytical Chemistry* **1994**, *379*, 191–197.

(170) Parsons, J. F.; Greenhagen, B. T.; Shi, K.; Calabrese, K.; Robinson, H.; Ladner, J. E. *Biochemistry* **2007**, *46*, 1821–1828.

(171) Patel, B. A.; Arundell, M.; Quek, R. G. W.; Harvey, S. L. R.; Ellis, I. R.; Florence, M. M.; Cass, A. E. G.; Schor, A. M.; O'Hare, D. *Anal Bioanal Chem* **2008**, *390*, 1379–1387.

(172) Phelan, V. V.; Fang, J.; Dorrestein, P. C. *J. Am. Soc. Mass Spectrom.* **2015**, *26*, 873–877.

(173) Pierson, L. S.; Pierson, E. A. *Appl Microbiol Biotechnol* **2010**, *86*, 1659–1670.

(174) Pogue, J. M.; Kaye, K. S.; Cohen, D. A.; Marchaim, D. *Clin. Microbiol. Infect*. **2015**, *21*, 302–312.

(175) Pons, S.; Fleischmann, M. *Anal. Chem*. **1987**, *59*, 1391A–1399A.

(176) Price-Whelan, A.; Dietrich, L. E. P.; Newman, D. K. *J. Bacteriol*. **2007**, *189*, 6372–6381.

(177) Propst, C.; Lubin, L. J. *Gen. Microbiol.* **1979**, *113*, 261–266.

(178) Pseudomonas Methods and Protocols, 1st ed.; Filloux, A., Ramos, J.-L., Eds.; Springer New York: New York, NY, 2014; pp 1–800.

(179) Radi, R. *Proc Natl Acad Sci USA* **2018**, *115*, 5839–5848.

(180) Rasouly, A.; Nudler, E. *Proc Natl Acad Sci USA* **2019**, *2*, 9696–9698.

(181) Recinos, D. A.; Sekedat, M. D.; Hernandez, A.; Cohen, T. S.; Sakhtah, H.; Prince, A. S.; Price-Whelan, A.; Dietrich, L. E. P. *Proc. Natl. Acad. Sci. USA* **2012**, *109*, 19420–19425.

(182) Reimer, Å. *Acta Otolaryngol*. **2009**, *120*, 86–88.

(183) Reyes, E. A. P.; Bale, M. J.; Cannon, W. H.; Matsen, J. M. *J Clin Microbiol* **1981**, *13*, 456–458.

(184) Ringen, L. M.; Drake, C. H. *J. Bacteriol.* **1952**, *64*, 841–845.

(185) Rohmer, L.; Hocquet, D.; Miller, S. I. *Trends Microbiol* **2011**, *19*, 341–348.

(186) Römling, U. *J Innate Immun* **2019**, *11*, 191–192.

(187) Rossi, E.; Falcone, M.; Molin, S.; Johansen, H. K. *Nat. Commun.* **2018**, *9*, 57–13.

(188) Ryder, C.; Byrd, M.; Wozniak, D. J. *Current Opinion in Microbiology* **2007**, *10*, 644–648.

(189) Santiveri, C. R.; Sismaet, H. J.; Kimani, M.; Goluch, E. D. *ChemistrySelect* **2018**, *3*, 2926–2930.

(190) Schiessl, K. T.; Hu, F.; Jo, J.; Nazia, S. Z.; Wang, B.; Price-Whelan, A.; Min, W.; Dietrich, L. E. P. *Nat. Commun.* **2019**, *10*, 762–772.

(191) Schleheck, D.; Barraud, N.; Klebensberger, J.; Webb, J. S.; McDougald, D.; Rice, S. A.; Kjelleberg, S. *PLoS ONE* **2009**, *4*, e5513–e5515.

(192) Seviour, T.; Doyle, L. E.; Lauw, S. J. L.; Hinks, J.; Rice, S. A.; Nesatyy, V. J.; Webster, R. D.; Kjelleberg, S.; Marsili, E. *Chem Comm* **2015**, *51*, 3789–3792.

(193) Shah, A.; Ullah, A.; Nosheen, E.; Rana, U. A.; Shakir, I.; Badshah, A.; Rehman, Z. U.; Hussain, H. Journal of the Electrochemical Society 2013, 160, H765–H769.

(194) Shahdordizadeh, M.; Taghdisi, S. M.; Ansari, N.; Langroodi, F. A.; Abnous, K.; Ramezani, M. *Sensor Actuat B-Chemical* **2017**, *241*, 619–635.

(195) Sharp, D.; Gladstone, P.; Smith, R. B.; Forsythe, S.; Davis, J. *Bioelectrochemistry* **2010**, *77*, 114–119.

(196) Simoska, O.; Sans, M.; Eberlin, L. S.; Shear, J. B.; Stevenson, K. J. *Biosens. Bioelectron.* **2019**, *142*, 111538.

(197) Simoska, O.; Sans, M.; Fitzpatrick, M. D.; Crittenden, C. M.; Eberlin, L. S.; Shear, J. B.; Stevenson, K. J. *ACS Sensors* **2019**, *4*, 170–179.

(198) Sismaet, H. J.; Pinto, A. J.; Goluch, E. D. *Biosens. Bioelectron*. **2017**, *97*, 65–69.

(199) Sismaet, H. J.; Webster, T. A.; Goluch, E. D. *Analyst* **2014**, *139*, 4241–4246.

(200) Smith, E. E.; Buckley, D. G.; Wu, Z.; Saenphimmachak, C.; Hoffman, L. R.; D'Argenio, D. A.; Miller, S. I.; Ramsey, B. W.; Speert, D. P.; Moskowitz, S. M.; Burns, J. L.; Kaul, R.; Olson, M. V. *Proc Natl Acad Sci USA* **2006**, *103*, 8487–8492.

(201) Son, M. S.; Matthews, W. J.; Kang, Y.; Nguyen, D. T.; Hoang, T. T. *Infect. Immun.* **2007**, *75*, 5313–5324.

(202) Sterling, H. J.; Batchelor, J. D.; Wemmer, D. E.; Williams, E. R. *J. Am. Soc. Mass Spectrom.* **2010**, *21*, 1045–1049.

(203) Stevens, A. M.; Schuster, M.; Rumbaugh, K. P. *J. Bacteriol.* **2012**, *194*, 2131–2141.

(204) Sullivan, N. L.; Tzeranis, D. S.; Wang, Y.; So, P. T. C.; Newman, D. *ACS Chem. Biol.* **2011**, *6*, 893–899.

(205) Sultana, S.; Shahidullah, A. H.; Islam, M. M.; Wasey, A. F. S. A.; Nahar, S. Malays. *J. Med. Biol. Res.* **2015**, *2*, 89–100.

(206) Swaminathan, B.; Feng, P. *Annu. Rev. Microbiol.* **1994**, *48*, 401–426.

(207) Takahashi, Y.; Zhou, Y.; Fukuma, T. *Current Opinion in Electrochemistry* **2017**, *5*, 121–125.

(208) Tang, Y.; Ali, Z.; Zou, J.; Jin, G.; Zhu, J.; Yang, J.; Dai, J. *RSC Adv*. **2017**, *7*, 51789–51800.

(209) Toledo, J. C., Jr.; Augusto, O. *Chem. Res. Toxicol*. **2012**, *25*, 975–989.

(210) Turkina, M. V.; Vikström, E. *J Innate Immun* **2019**, *11*, 263–279.

(211) Turner, K. H.; Wessel, A. K.; Palmer, G. C.; Murray, J. L.; Whiteley, M. *Proc Natl Acad Sci USA* **2015**, *112*, 4110–4115.

(212) Ventola, C. L. *P T*, **2015**, *40*, 344–352.

(213) Vukomanovic, D. V.; Zoutman, D. E.; Stone, J. A.; Marks, G. S.; Brien, J. F.; Nakatsu, K. *Biochem. J*. **1997**, *322*, 25–29.

(214) Walker, T. S. *Plant Physiol*. **2004**, *134*, 320–331.

(215) Wang, F.; Deng, X.; Wang, W.; Chen, Z. *J Solid State Electrochem* **2011**, *15*, 829–836.

(216) Warren, J. B.; Rashpal, L.; Rendell, N. B.; Taylor, G. W. *Biochem. J.* **1990**, *266*, 921–923.

(217) Watrous, J. D.; Dorrestein, P. C. *Nature Rev. Microbiol.* **2011**, *9*, 683–694.

(218) Watrous, J.; Roach, P.; Alexandrov, T.; Heath, B. S.; Yang, J. Y.; Kersten, R. D.; van der Voort, M.; Pogliano, K.; Gross, H.; Raaijmakers, J. M.; Moore, B. S.;

Laskin, J.; Bandeira, N.; Dorrestein, P. C. *Proc Natl Acad Sci USA* **2012**, *109*, E1743–E1752.

(219) Webster, T. A.; Goluch, E. D. *Lab Chip* **2012**, *12*, 5195–5197.

(220) Webster, T. A.; Sismaet, H. J.; Conte, J. L.; Chan, I.-P. J.; Goluch, E. D. *Biosens. Bioelectron.* **2014**, *60*, 265–270.

(221) Werner, E.; Roe, F.; Bugnicourt, A.; Franklin, M. J.; Heydorn, A.; Molin, S.; Pitts, B.; Stewart, P. S. *Applied and Environmental Microbiology* **2004**, *70*, 6188–6196.

(222) Wightman, R. *Anal. Chem.* **1981**, *53*, 1125A–1134A.

(223) Williams, D. E.; Boon, E. M. *J Innate Immun* **2018**, *11*, 205–215.

(224) Wilson, R.; Pitt, T.; Taylor, G.; Watson, D.; MacDermot, J.; Sykes, D.; Roberts, D.; Cole, P. *J. Clin. Invest.* **1987**, *79*, 221–229.

(225) Wilson, R.; Sykes, D. A.; Watson, D.; Rutman, A.; Taylor, G. W.; Cole, P. J. *Infect. Immun.* **1988**, *56*, 2515–1517.

(226) Wilson, R.; Sykes, D. A.; Watson, D.; Rutman, A.; Taylor, G. W.; Cole, P. J. *Infect. Immun.* **1988**, *56*, 2515–2517.

(227) Woods, D. E.; Iglewski, B. H. *Rev. Infect. Dis.* **1983**, *5*, S715–S722.

(228) Wu, X.; Siehnel, R. J.; Garudathri, J.; Staudinger, B. J.; Hisert, K. B.; Ozer, E. A.; Hauser, A. R.; Eng, J. K.; Manoil, C.; Singh, P. K.; Bruce, J. E. *Journal of Proteome Research* **2019**, *18*, 2601–2612.

(229) Xu, H.; Lin, W.; Xia, H.; Xu, S.; Li, Y.; Yao, H.; Bai, F.; Zhang, X.; Bai, Y.; Saris, P.; Qiao, M. *FEMS Microbiol Lett* **2006**, *253*, 103–109.

(230) Xu, N.; Ahuja, E. G.; Janning, P.; Mavrodi, D. V.; Thomashow, L. S.; Blankenfeldt, W. *Acta Crystallogr. D Biol. Crystallogr*. **2013**, *69*, 1403–1413.

(231) Xu, T.; Scafa, N.; Xu, L.-P.; Su, L.; Li, C.; Zhou, S.; Liu, Y.; Zhang, X. *Electroanalysis* **2014**, *26*, 449–468.

(232) Yakushenko, A.; Schnitker, J.; Wolfrum, B. *Anal. Chem*. **2012**, *84*, 4613–4617.

(233) Yang, L.; Haagensen, J. A. J.; Jelsbak, L.; Johansen, H. K.; Sternberg, C.; Hoiby, N.; Molin, S. *J. Bacteriol.* **2008**, *190*, 2767–2776.

(234) Yoon, S. S.; Hennigan, R. F.; Hilliard, G. M.; Ochsner, U. A.; Parvatiyar, K.; Kamani, M. C.; Allen, H. L.; DeKievit, T. R.; Gardner, P. R.; Schwab, U.; Rowe, J. J.; Iglewski, B. H.; McDermott, T. R.; Mason, R. P.; Wozniak, D. J.; Hancock, R. E. W.; Parsek, M. R.; Noah, T. L.; Boucher, R. C.; Hassett, D. J. *Dev. Cell* **2002**, *3*, 593–603.

(235) Zaugg, W. S. *J. Biol. Chem*. **1964**, *239*, 3964–3970.

(236) Zhang, Y.; Huang, L. *Microchim Acta* **2011**, *176*, 463–470.

(237) Zheng, H.; Kim, J.; Liew, M.; Yan, J. K.; Herrera, O.; Bok, J. W.; Kelleher, N. L.; Keller, N. P.; Wang, Y. *Curr Biol* **2015**, *25*, 29–37.

(238) Zhuang, J. C.; Wogan, G. N. *Proc Natl Acad Sci USA* **1997**, *94*, 11875–11880.

(239) Zoski, C. G. Handbook of Electrochemistry. Elsevier, **2006**.

Vita

Olja Simoska, the daughter of Svetislav Simoski and Maja Stefanovska-Simoska was born in Tetovo, Macedonia. After graduating from NOVA International High School in Skopje, Macedonia in 2011, she enrolled at Bard College in Annandale-on-Hudson, New York. She received her Bachelor Degree in Chemistry from Bard College in May 2015. She entered the Graduate School at The University of Texas at Austin in August 2015 to begin her graduate studies in Analytical Chemistry under the guidance of Prof. Keith J. Stevenson and Prof. Jason B. Shear.

Permanent email: osimoska@gmail.com

This dissertation was typed by the author.